1-1-2024

Elucidating the Mechanisms of Myosin II Force Feedback and Coordination in Actomyosin Ensembles

Omayma Alazzam

ELUCIDATING THE MECHANISMS OF MYOSIN II FORCE FEEDBACK AND COORDINATION IN ACTOMYOSIN ENSEMBLES

By

Omayma Alazzam

Dissertation Submitted to the Faculty of the

Graduate School of the University of Mississippi

in partial fulfillment of the requirements for the degree of

DOCTOR OF PHILOSOPHY

in

Engineering Science

with an emphasis in Chemical Engineering

May 2024

Oxford, Mississippi

ABSTRACT

This dissertation delves into the dynamics of myosin II motors within actomyosin networks, emphasizing their crucial role in muscle functionality and the broader implications for cardiovascular health. Given the critical involvement of myosin II in conditions such as hypertrophic cardiomyopathy (HCM) and heart failure, this research presented here is important for understanding such diseases at the molecular level. Through the use of fluorescence microscopy and optical tweezers, the study reveals novel insights into how myosin II generates force and coordinates within myosin ensembles—a key to grasping the mechanics of muscle contraction. Specifically, this work aimed to unravel the mechanisms of myosin II functionality in actomyosin ensembles and to assess how variations in the dynamics of motor proteins affect force production. We leveraged a novel assay that probes the complex interactions of myosin II within hierarchical structures with mechanical compliancy, allowing for more native-like measurements of force generation and the analysis of myosin ensemble behavior. Results reveal the significant impact of environmental stiffness and the number of engaged motors on the behavior of myosin II ensembles. The study sheds light on a sophisticated system of sensory force feedback among myosin motors, showing that force production results from the collective dynamics of the ensemble, rather than from the actions of individual motors. Additionally, it was discovered that changes in the environmental context and structure of the ensemble can significantly alter force output. This work advances understanding of muscle mechanics at the molecular level and how emergent biophysical properties of the cytoskeleton rely on intricate

feedback loops. By elucidating the principles of force generation and coordination within actomyosin networks, this research sets the stage for future studies aimed at understanding the details of the feedback loops, influences of mechanical environments on intracellular crosstalk, and creating targeted treatments for cardiovascular conditions linked to malfunctioning myosin II motors.

In loving memory of my mother, whose dreams and aspirations never left my side throughout this PhD journey. Her love and support remain etched in my heart, guiding me always. Inspired by your legacy, I built this for you and for the world.

ACKNOWLEDGMENTS

The journey of obtaining my Ph.D. has been a remarkable and transformative experience over the past several years. It's been filled with both challenges and triumphs, and I owe my success to the unwavering support and encouragement of several remarkable individuals.

First and foremost, I want to express my deep gratitude to my Ph.D. advisor. She has not only been a mentor but a pillar of strength throughout this academic journey. Her understanding of my family circumstances and her willingness to make my academic pursuits flexible enough to accommodate my role as a parent have been instrumental in reaching this point. She taught me how to build my self-confidence and persevere through the toughest of times. Without her cooperation and guidance, I would not have achieved this significant milestone.

Next, I want to extend my heartfelt thanks to my husband and children. Their constant love, understanding, and support have been the cornerstone of my academic journey. They've stood by me through the ups and downs, and this achievement is as much theirs as it is mine. To my family and friends back home, your unwavering support from a distance has been a source of great motivation, and I'm immensely grateful for your enduring belief in me.

I am indebted to my dedicated committee members who generously shared their valuable time and expertise despite their busy schedules. Your guidance, advice, and support have been invaluable in shaping my research and guiding me towards success.

To my fellow lab mates, you have not only been colleagues but a second family to me. Your support, camaraderie, and shared aspirations have created a nurturing and inspiring

environment. From sharing thoughts to indulging in delicious food, our journey together has been unforgettable.

In closing, I extend my heartfelt gratitude to all those who have played a role in this journey. Each of you has been an essential part of this achievement, and I am deeply thankful for your unwavering support, love, and encouragement. This accomplishment would not have been possible without you, and I look forward to continuing this journey with your continued support and belief in me.

TABLE OF CONTENTS

Page

Appendix

LIST OF FIGURES

CHAPTER 1

INTRODUCTION

1.1 Cardiovascular Disease and Its Molecular Foundations

Cardiovascular diseases (CVD) represent a major category of non-communicable diseases, significantly impacting global morbidity and mortality. This group includes a spectrum of conditions affecting the heart and blood vessels, notably coronary artery disease, which is a major cause of myocardial infarctions, cerebrovascular disease leading to strokes, hypertension, peripheral artery disease, rheumatic heart disease, congenital heart anomalies, and heart failure (*Heart Disease: Types, Causes, and Symptoms*, n.d.; Roth *et al*., 2020).

Numerous factors come together and contribute to the development of heart diseases. These factors include how our genes work, our daily habits, and the environment around us. Heart diseases encompass a range of health problems like blocked heart arteries, heart failure, irregular heartbeats, and issues with heart valves. These problems have a significant impact on public health. Despite significant efforts in improving medical diagnoses and treatments, heart disease remains a serious and enduring global health issue (*Heart Disease: Types, Causes, and Symptoms*, n.d.).

Heart disease stands out as a significant contributor to both illness and loss of life globally. Within the United States, it accounts for a considerable portion of yearly fatalities, with heart disease playing a role in around 23% of all reported deaths in 2020. This impact differs among

various demographic groups, underscoring the interplay of elements like age, gender, race, and lifestyle. Scientific investigations, including the influential Framingham Heart Study, have brought to light critical understandings of the risk factors and epidemiology of heart disease, revealing connections with lifestyle choices such as tobacco use, lack of physical activity, unhealthy eating habits, and obesity. Conditions like hypertension, diabetes, and hyperlipidemia have emerged as major contributors to the overall burden of the disease (*Heart Disease and Stroke Statistics—2023 Update: A Report From the American Heart Association | Circulation*, n.d.; *Sudden Death in Young People: Heart Problems Often Blamed - Mayo Clinic*, n.d.).

Heart failure is a specific condition that falls under the category of heart diseases, as illustrated in Figure 1.1(*Heart Failure - Are You at Risk?*, n.d.). It occurs when the heart is unable to pump blood effectively, leading to symptoms such as shortness of breath, fatigue, and fluid retention.

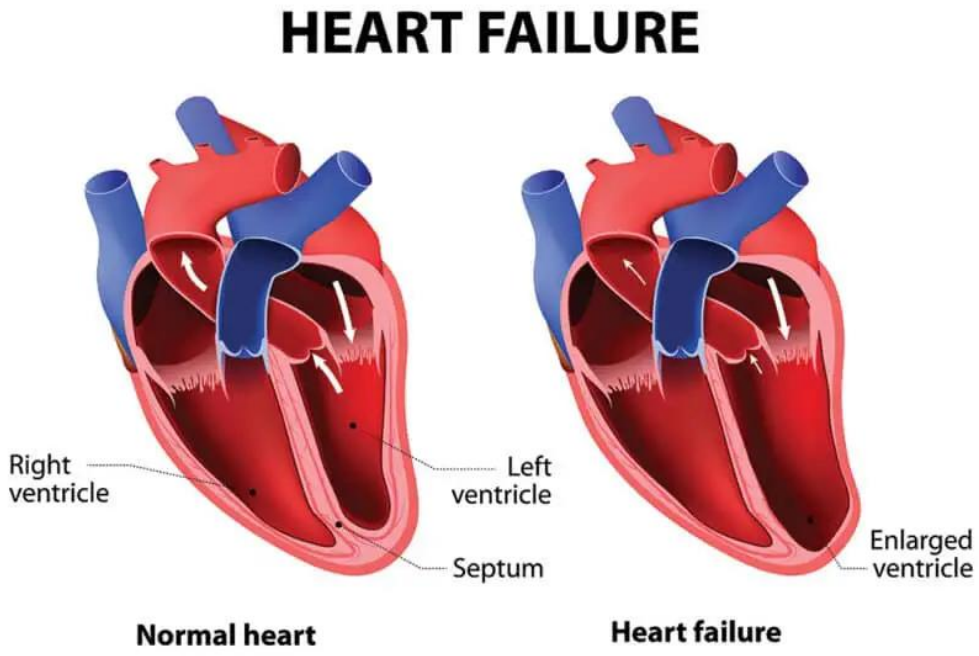

Figure 1.1: Comparative Anatomy of a Normal Heart and a Heart with Heart Failure. On the left, the normal heart shows well-proportioned chambers with a right ventricle and left ventricle separated by the septum. On the right, the heart with heart failure demonstrates an enlarged left ventricle with dilated chamber walls, indicative of the ventricular remodeling that occurs in heart failure. Such changes are associated with reduced cardiac function and impaired blood circulation. (Adapted from Just Heart Cardiovascular Group Inc., 2024).

In the United States, the prevalence of heart failure has been on a significant rise.(Chou & Chin, 2021; Teekakirikul *et al*., 2019)*Heart Failure*, n.d.; *Heart Failure - Symptoms and Causes*, n.d.) Between 2013 and 2016, approximately 6.2 million Americans suffered from heart failure, an increase from 5.7 million between 2009 and 2012. This represents an 8.77% increase. If current trends continue, the prevalence rate is projected to rise by 46%, potentially affecting more than 8 million Americans by 2030 (Glynn *et al*., 2021).

Hypertrophic Cardiomyopathy (HCM) is caused by the complex interaction between genetic and molecular factors that affect cardiac development and function. It has been identified that this hereditary cardiovascular condition is primarily caused by mutations in genes that encode proteins of the cardiac sarcomere, the fundamental contractile unit of heart cells (more in subsequent sections) (Chou & Chin, 2021; Teekakirikul *et al*., 2019). Research initiatives have been undertaken in the United States with the purpose of elucidating the inheritance patterns and clinical implications of genetic mutations associated with HCM. There is evidence that HCM is inherited autosomal dominantly, which means that an affected individual has a 50% chance of passing the mutated gene to their children (*Hypertrophic Cardiomyopathy*, 2016). A genetic test has become an essential component of the diagnosis of HCM, allowing for the early identification of patients at risk and facilitating informed decision-making regarding management and family screening (Ireland & Ho, 2024).

The management of heart conditions such as Hypertrophic Cardiomyopathy (HCM) and heart failure (HF) has traditionally focused on symptom management and slowing disease progression. These strategies, while important, do not specifically target the underlying mechanisms of the disease. Cardiomyopathy, fundamentally a disorder of abnormal cardiac contractility, calls for therapies that act directly on the cardiac muscle's contractile apparatus and its regulatory

mechanisms. In the United States, comprehensive strategies and interventions have been developed to prevent and treat heart disease. American Heart Association (AHA) is at the forefront of promoting heart health, promoting healthy lifestyles, and providing evidence-based guidelines for healthcare providers. The array of available treatment options has greatly expanded due to advances in medical technology, innovations in pharmaceuticals, and advancements in surgical techniques, ranging from medication regimens to minimally invasive procedures and complex cardiac surgeries.

A comprehensive approach to heart disease must focus on genetics, lifestyle choices, and environmental factors. Heart disease remains a critical health concern globally and in the United States. Public health campaigns, scientific research endeavors, and optimized clinical care are necessary to achieve this (Chou & Chin, 2021; Glynn *et al*., 2021; *Heart Failure*, n.d.; Spirito *et al*., 1997).

In the context of HCM, a major breakthrough in comprehending the disease came with the identification of its genetic foundation. A clinical observation and a pathological study provided the first insights into the genetic basis of HCM. The development of molecular genetics has, however, not been able to unravel the complex origins of HCM until the latter half of the 20th century. As early as the 1950s and 1960s, researchers like Dr. Donald Teare documented structural abnormalities of the heart muscle in individuals with HCM. These initial observations laid the groundwork for subsequent investigations into the genetic roots of the disorder. Scientists have been identifying genetic mutations associated with HCM as molecular biology and genetic sequencing techniques have evolved (Elliott & McKenna, 2008).

A key breakthrough was made in the 1980s when researchers identified mutations in genes encoding sarcomere proteins, particularly myosin and myosin-binding protein C. It has been

shown that these genetic mutations result in altered interactions between these proteins, which leads to impaired contractility of the heart muscle (Chou & Chin, 2021; Kawana *et al*., 2022; Woo *et al*., 2003). The discovery of these mutations revolutionized our understanding of HCM, providing a molecular framework to explain the observed cardiac structural and functional abnormalities.

1.1.1 Hypertrophic Cardiomyopathy (HCM)

Hypertrophic cardiomyopathy (HCM) is characterized by the thickening of the heart wall, a condition known as hypertrophy, which can significantly impair the heart's ability to pump blood efficiently. This thickening, often concentrated in the ventricular septum, results in a reduced volume within the heart chambers and can lead to a variety of symptoms, ranging from shortness of breath to sudden cardiac death. The detailed comparison of a normal heart anatomy and one exhibiting hypertrophic changes is illustrated in Figure 1.2 (*Hypertrophic Cardiomyopathy Center | Cleveland Clinic*, n.d.). This figure highlights the significant differences in the thickness of the heart wall, providing a visual representation of how these genetic mutations manifest physically within the heart structure. Genetic testing plays a pivotal role in the management of HCM by identifying mutations in various cardiac proteins, including myosin and actinin, which can predispose individuals to this condition. By understanding the specific genetic alterations present, clinicians can offer more personalized care strategies, aiming to mitigate the risk of complications and improve patient outcomes (Ireland & Ho, 2024; Kawana *et al*., 2022; Woo *et al*., 2003).

From a broader societal and health perspective, HCM poses considerable challenges. HCM is recognized as a leading cause of sudden cardiac death (SCD) in younger people. This is

particularly significant given that most cases of SCD due to HCM occur in previously undiagnosed individuals (Barrick & Greenberg, 2021; *Sudden Death in Young People: Heart Problems Often Blamed - Mayo Clinic*, n.d.). Consequently, it is critically important for the well-being of patients with HCM to be identified and treated with prompt action. Furthermore, the implications of managing patients with HCM reverberate through healthcare systems, requiring long-term care, medical surveillance, and potentially modifying treatment plans.

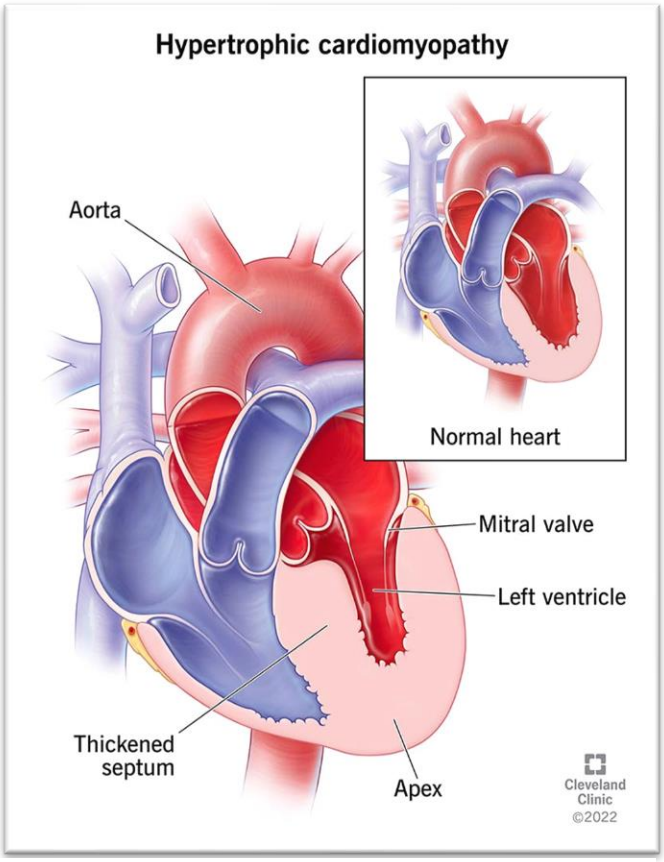

Figure 1.2: Anatomical Comparison of a Normal Heart and a Heart with Hypertrophic Cardiomyopathy. Cleveland Clinic. (2023, January23).

Given the hereditary nature of the disease, the psychosocial impacts on the persons diagnosed with the disease and their families can also significantly contribute to the health burdens on society as a whole (Zaiser *et al*., 2020).

The fundamental mechanics of cardiac muscle contraction are heavily dependent on the interaction between actin and myosin (more detail in Section 1.2). HCM develops due to irregularities in myosin II or mutations or malfunctions in actin-myosin interactions. Myosin motor proteins engage with actin filaments, forming cross-bridges. As a consequence of myosin II dynamics, these actin filaments slide, leading to force generation. This generated force results in the contractility of the heart muscles, facilitating effective blood pumping throughout the body

(Baldo *et al*., 2020a; Spudich, 2001; Woo *et al*., 2003).

In HCM, disruptions in the actin-myosin dynamics can lead to significant physiological alterations. Specific genetic mutations, especially in the myosin heavy chain gene (MYH7), can interfere with the interaction between myosin and actin. Such modifications can affect force generation kinetics, altering the intensity and duration of heart contractions, which can result in cardiac issues (Woo *et al*., 2003). Studies suggest that particular mutations in myosin II associated with HCM can alter force generation and relaxation dynamics. The details of these studies and results will be discussed later in the Introduction. Using experimental models, like mice genetically modified to express mutant myosin II down to single molecule-level studies, researchers have highlighted the relationship between abnormal myosin II behavior and the development of cardiac hypertrophy and contraction anomalies. This underscores the crucial role of myosin II in maintaining optimal heart function (Parker & Peckham, 2020; Teekakirikul *et al*., 2019; *β-Cardiac Myosin Hypertrophic Cardiomyopathy Mutations Release Sequestered Heads and Increase Enzymatic Activity | Nature Communications*, n.d.). Moreover, mutations can interfere with actin-myosin interactions, leading to complex cellular responses. Such disruptions can cause cellular changes such as increased cell size, alterations in sarcomere structures, and the development of interstitial fibrosis. These changes manifest as typical HCM features, including thickened heart walls and impaired diastolic relaxation (Maron & Maron, 2013).

There is a continued effort to decipher the exact molecular pathways by which myosin II mutations contribute to HCM. Emerging techniques in single-molecule imaging and biomechanics offer clarity on how certain mutations change myosin II's force properties and its engagement with actin. Such knowledge is pivotal for crafting therapies to normalize actin-myosin dynamics and mitigate HCM-related mutation effects (O. Y. Al Azzam *et al*., 2022;

Albert *et al*., 2014; Azzam *et al*., 2022; Baldo *et al*., 2020a; Guhathakurta *et al*., 2018; Ruegg *et al*., 2002).

1.1.2 Heart Failure

As for HCM, a deeper exploration at the molecular level reveals critical insights into the origin and mechanisms of heart failure. At this intricate level of analysis, it becomes evident that disruptions in cardiac myosin function are central to understanding the molecular basis of heart failure. Within the field of cardiomyopathy, a comprehensive understanding of cardiac myosin's mechanisms takes center stage. Cardiac myosin, a pivotal motor protein essential for muscle function and contraction, relies on the precise hydrolysis of adenosine triphosphate (ATP) within the ATP cycle. This cycle encompasses the binding, hydrolysis, and subsequent release of ATP, serving as the driving force behind the contractions crucial for effective blood pumping. However, when examining the context of heart failure, this fundamental ATP cycle can undergo significant disturbances (Barrick & Greenberg, 2021; Brunello *et al*., 2020; Nikitina *et al*., 2015). One significant consequence of such disruption is the inefficient utilization of ATP, resulting in suboptimal force generation during the power stroke of cardiac myosin. This deficiency often manifests as a reduction in the heart muscle's contractile capacity, a hallmark feature of heart failure. These disruptions in the ATP cycle can originate from various sources, including genetic mutations that impact both the structure and function of the myosin molecule itself. Moreover, alterations in the expression of different myosin isoforms or dysregulation of the myosin ATPase activity can further contribute to these inefficiencies. Consequently, individuals with heart failure often find themselves in a challenging scenario where the heart consumes energy (in the form of ATP) without generating the necessary contractile force, ultimately leading to an energy-

depleted state within the heart muscle cells (Barrick & Greenberg, 2021; Daniels *et al*., 2021; Tang *et al*., 2021).

In addition to the role of cardiac myosin, several other molecular-level factors come into play in the context of heart diseases. These factors encompass imbalances in calcium handling, oxidative stress, and disruptions in the intricate signaling pathways that regulate cardiac muscle contraction. Together, these complex molecular mechanisms provide a comprehensive understanding of the molecular underpinnings of heart failure, shedding light on potential avenues for therapeutic interventions and treatments (Doenst *et al*., 2013; Johnson *et al*., 2019; Liew & Dzau, 2004; Tsutsui *et al*., 2011).

1.1.3 Omecamtiv Mecarbil (OM): Cardiac myosin II modulator

Studies at the molecular level revealed the discovery of a drug that is used to treat heart failure by assessing its impact on cardiac myosin dynamics. This drug, known as Omecamtiv Mecarbil (OM), is a notable cardiac inotropic agent that has demonstrated its efficacy in improving cardiac function, especially in hearts affected by failure. It has garnered significant attention due to its unique mechanism of action and its potential benefits in addressing heart failure (Liu, n.d.; Malik *et al*., 2011; Teerlink *et al*., 2009).

OM is a small molecule with a distinctive approach to influencing cardiac myosin, the motor protein responsible for heart muscle contractions. In contrast to traditional heart failure medications, OM's mode of action does not primarily involve neurohormonal pathways or the excitation-contraction coupling process (Andrei & Iorgoveanu, 2014; Morgan *et al*., 2010). Instead, as illustrated in Figure 1.3, (Winkelmann *et al*., 2015) it binds to an allosteric site on the myosin protein, separate from the active site where ATP interacts, inducing a significant

conformational change in the protein's structure. This allosteric modulation results in the enhancement of force production and the extension of cardiac muscle contraction duration, effectively addressing the underlying contractile dysfunction commonly observed in heart failure (Auguin *et al*., 2023; Chakraborti *et al*., 2022b; Hashem *et al*., 2017).

When examining the mechanism of action of OM, the significance of its implications becomes apparent. By directly targeting the contractile apparatus of the heart, OM introduces a groundbreaking approach to treating heart failure, one that closely aligns with the fundamental pathology of the disease. It signifies a shift toward therapies that directly impact the contractile machinery and its regulators, potentially offering a treatment option tailored to the disease with fewer side effects than existing therapies (Chakraborti *et al*., 2022b; Malik *et al*., 2011; Morgan *et al*., 2010).

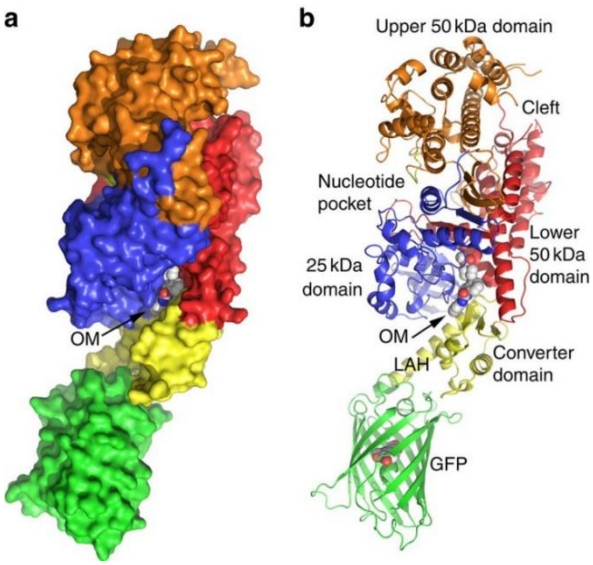

Figure 1.3: The structural organization of the human β-cardiac myosin motor domain (MD) when bound to OM.
(a) The space-filling model for the A chain of the OM-bound structure reveals the OM-binding site located between the N-terminal 25-K domain (residues 2–204; colored in blue) and the lower 50-K domain (residues 471–708; colored in red). The upper 50-K domain (residues 211–470; colored in orange) is delineated from the lower 50-K domain by the 'Cleft.' With no nucleotide present, the cleft is 'open,' and the lever arm extends, aligning with a near-rigour state. The converter domain (residues 709–777) and lever arm helix (LAH) (residues 778–787) are highlighted in yellow, and the GFP domain is in green.
(b) A ribbon model from the same perspective illustrates the OM-binding site deeply positioned within a narrow cleft between the 25-K and lower 50-K domains. The LAH that extends from the converter domain to the GFP domain is identified. The Apo cMD structure's conformation closely matches that of the OM-bound structure shown here, with a root mean square deviation (r.m.s.d.) of 1.14 Å for all 962 Cα atoms. Adapted from: Winkelmann DA *et al*, 2015 [*], Nature Publishing Group. License: https://creativecommons.org/licenses/by/4.0/

1.1.4 OM Discovery

The discovery of OM can be attributed to Bradley P. Morgan and his team's research at Cytokinetics, Inc. (Morgan *et al*., 2010). Their objective was to identify selective activators of cardiac myosin for treating systolic heart failure. They embarked on their journey with a poorly soluble nitro-aromatic compound (1) and, through systematic design and synthesis, developed potent, selective, and soluble myosin activators, eventually leading to the discovery of OM, referred to as compound 24 as illustrated in Figure 1.4. This compound stands out for its potential to treat systolic heart failure via intravenous and oral administration (Morgan *et al*., 2010). In this study, the emphasis has been on identifying compounds that activate the cardiac sarcomere by monitoring the rise in myosin ATPase activity. This critical aspect of the research was aimed at understanding how OM, the newly discovered molecule, influenced ATPase activity within the cardiac sarcomere. Figure 1.5 describes the effect of OM drug on the interactions between actin and myosin during ATP hydrolysis (Day *et al*., 2022).

The discovery of OM represents a significant advancement in the treatment of heart failure. Researchers found that OM binds directly to cardiac myosin, specifically at the site where the motor protein interacts with ATP, influencing the ATPase cycle crucial for muscle contraction. Consequently, the findings of Woody *et al.* highlight a paradoxical mechanism

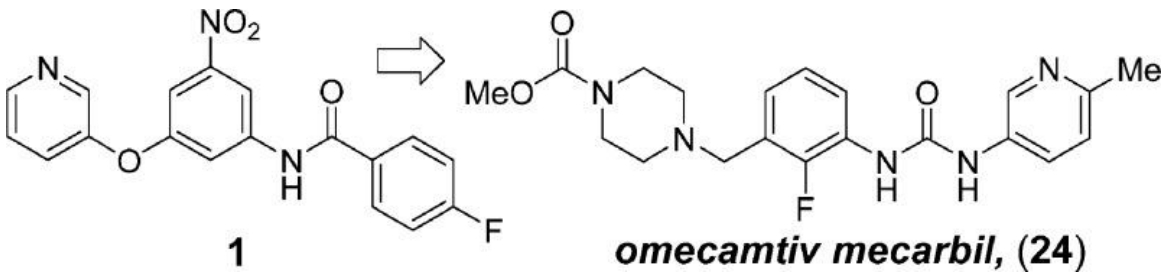

Figure 1.4: This figure outlines the development of the first selective cardiac myosin activator OM, from an initial poorly soluble compound (1) to the creation of omecamtiv mecarbil (24), a potent and soluble candidate now in clinical trials for systolic heart failure treatment. Adapted with permission from: Morgan, Bradley P *et al*. "Discovery of omecamtiv mecarbil the first, selective, small molecule activator of cardiac Myosin." ACS medicinal chemistry letters vol. 1,9 472-7. 20 Aug. 2010, doi:10.1021/ml100138q. Copyright {2024} American Chemical Society.

where OM prolongs the myosin-actin cross-bridge cycle and enhances cardiac contractility without a proportional increase in energy consumption. One remarkable aspect of OM is its effectiveness in enhancing cardiac function, particularly in hearts affected by failure. This is evident through substantial improvements in left ventricular fractional shortening and ejection fraction, both essential indicators of the heart's ability to pump blood efficiently—a function often compromised in heart failure (Woody *et al*., 2018).

Despite evidence supporting OM's enhancement of cardiac contractility, debates persist regarding its specific influence on cardiac myosin II dynamics. While some researchers posit OM as a myosin activator, others contend that, despite its overall positive effect on contraction, it acts as a myosin II inhibitor (Chakraborti *et al*., 2022b; Cleland *et al*., 2011; Hashem *et al*., 2017; Teerlink *et al*., 2021; Woody *et al*., 2018). This discourse, along with further discussions on the mechanisms of OM at the molecular level, will be further discussed in Chapter 6.

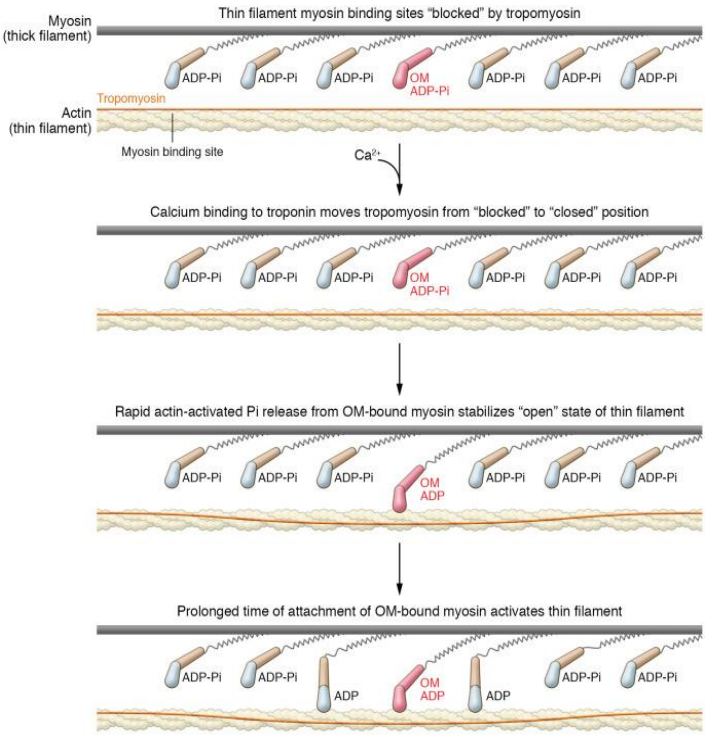

Figure 1.5: Enhancement of Myosin-Actin Interaction by OM Drug During ATP Hydrolysis: This diagram illustrates the molecular mechanism by which the drug OM (myosin activator) facilitates muscle contraction. Initially, the myosin binding sites on actin are obscured by tropomyosin. Upon calcium binding to troponin, tropomyosin is repositioned, revealing the binding sites. OM drug-bound myosin (highlighted in pink) then attaches to actin, and the rapid release of inorganic phosphate (Pi) from the OM-bound myosin complex stabilizes actin's "open" state. Prolonged binding of OM-modified myosin to actin leads to sustained activation of the thin filament, thereby enhancing muscle contractility. This figure is adapted from Day SM, *et, al* 2022 American Society for Clinical Investigation Copyright © 2024 American Society for Clinical Investigation ISSN: 0021-9738 (print), 1558-8238 (online)

OM is currently under clinical evaluation to determine its efficacy and safety in treating heart failure with reduced ejection fraction (HFrEF). Notably, it is a subject of investigation in the GALACTIC-HF trial, which seeks to understand its potential benefits in improving cardiac function and reducing adverse cardiovascular outcomes. This trial is pivotal in assessing the therapeutic value of OM, including its effects on heart failure symptoms, hospitalization rates, and overall survival. Furthermore, the trial places a strong emphasis on monitoring potential side effects, aiming to establish a comprehensive safety profile for OM. Through these efforts, the GALACTIC-HF trial is expected to illuminate the drug's mechanism of action, optimal dosage, and its place in the treatment landscape for heart failure (Teerlink *et al*., 2020)**.** The introduction of OM into the field of therapeutics adds a new dimension to heart failure treatment. It presents a novel approach that directly addresses the core issue in heart failure—the reduced contractility of the heart muscle. This targeted approach not only improves heart function but also holds promise for better patient outcomes by addressing the fundamental mechanics of the disease, rather than merely alleviating its symptoms.

1.2 Myosin Motor Protein

1.2.1 Motor Proteins

Motor proteins are a specialized class of proteins that convert chemical energy, usually derived from ATP hydrolysis, into mechanical work. These molecular engines play a crucial role in a multitude of cellular processes, including intracellular transport and cell division (Akhshi *et al*., 2014; Hartman & Spudich, 2012; Pollard, 2010). A key characteristic of many motor proteins is their processivity, which denotes the ability of these proteins to take multiple steps along a track (like actin or microtubules) without detaching. The duty ratio of a motor protein refers to the

fraction of its catalytic cycle during which it remains bound to the track; a duty ratio greater than 0.5 means the motor is often bound, supporting its processive nature (Cooper & Hausman, 2000; Hancock & Howard, 1998; Watanabe *et al*., 2008). Another critical parameter is the stall force, which is the force at which a motor protein's forward velocity becomes zero, essentially the maximum force it can exert without moving backward. Stepping refers to the discrete increments by which these proteins move along their tracks. The debate of "porter vs. rower" offers insight into how motor proteins operate: while a porter carries its cargo and moves itself along a track, a rower remains stationery and "rows" its cargo past. The power stroke, on the other hand, represents the force-generating conformational change during the protein's mechanochemical cycle (O. Al Azzam *et al*., 2021; “Porters versus Rowers,” 1993; Reinemann *et al*., 2018). Other vital aspects of motor protein function involve their adaptability in navigating cellular environments, responding to cellular signals, and working in teams to achieve the desired mechanical output. These proteins are not just simple machines but adaptive entities that can adjust their functions based on the cellular context (Alberts *et al*., 2002; Kruppa & Buss, 2021).

1.2.2 Myosin Motor Protein

Myosin motors are a diverse family of motor proteins essential for a variety of cellular activities, including intracellular transport, cell motility, and muscle contraction. These proteins interact with actin filaments, a core component of the cytoskeleton, to facilitate cellular movements (Guhathakurta *et al*., 2018). The structure of myosin motors, as illustrated in Figure 1.6, is both complex and fascinating, consisting of three main domains: the head, neck (or stalk), and tail. The head domain plays a dual role, engaging in ATP hydrolysis and interacting with actin filaments, driving the motor's movement. Meanwhile, the neck functions as a kind of lever,

amplifying the changes happening in the head for better efficiency. The tail, quite varied among different myosins, dictates the specific function a myosin motor will undertake within a cell. The core structure of myosins is defined by a motor domain at their amino-terminus, known as the 'head'. Yet, distinct variations can be identified at the carboxy-terminus, or the 'tail' domain. Some myosins also exhibit an extended amino-terminus. The composition of light chains, integral to the motor's functionality, differs among myosin types as shown in Figure 1.6 For instance, myosin V has a unique design with two heads and a tail specialized for cargo binding. This tail structure enables myosin V to move organelles and vesicles along actin filaments with remarkable continuity. In contrast, myosin II stands out with its long coiled-coil stalk, allowing it to assemble into thick filaments pivotal for muscle contraction. The absence of a cargo-binding domain in myosin II's tail underlines its primary function, which is different from the transport role of myosin V. One particularly significant member is myosin II. Notably, myosin II has a unique importance in humans due to its critical role in muscle contraction and heart function (Pollard, 2010; Spudich, 2001; Spudich *et al*., 1995).

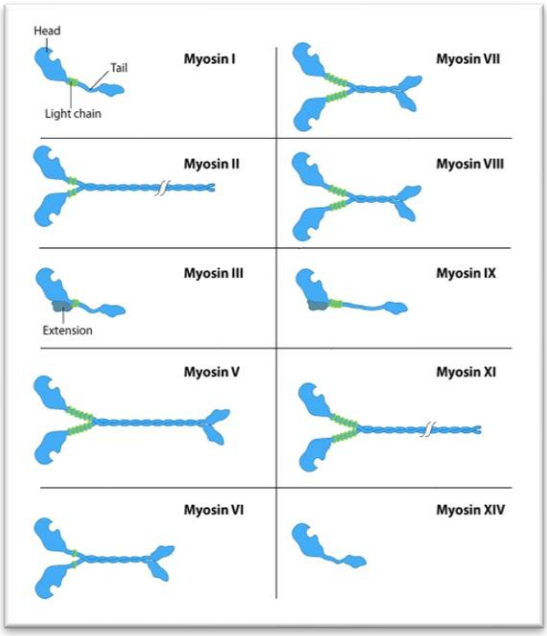

Figure 1.6: The figure highlights the variety within the myosin family. All myosins possess a 'head' for ATP and actin binding, but their tails, which determine specific cellular roles, differ significantly. For instance, myosin V takes larger steps on actin due to its additional light chains, enabling efficient cargo transport. In contrast, myosin II has the unique ability to form multiple contacts on actin, playing a role in muscle contraction. Intriguingly, select myosins, such as Nuclear Myosin I, even function within the cell nucleus. Adapted from: Varol, Onur. "Modal Analysis of Myosin II and Identification of Functionally Important Sites." (2012).

1.2.3 Myosin II Structure

The structural integrity of myosin II is delineated by several specialized domains as shown in Figure 1.7. Motor Domain (Head Domain): The motor domain is responsible for ATP hydrolysis, catalyzing the transduction of chemical energy into mechanical work, essential for the stepping of myosin along the actin filaments. Motor domain interact directly with binding cites a long actin filament. The hydrolytic activity leads to conformational alterations within the motor domain, facilitating the progressive movement along the actin filament, a critical component of muscle contraction dynamics (Kad *et al.*, 2005).

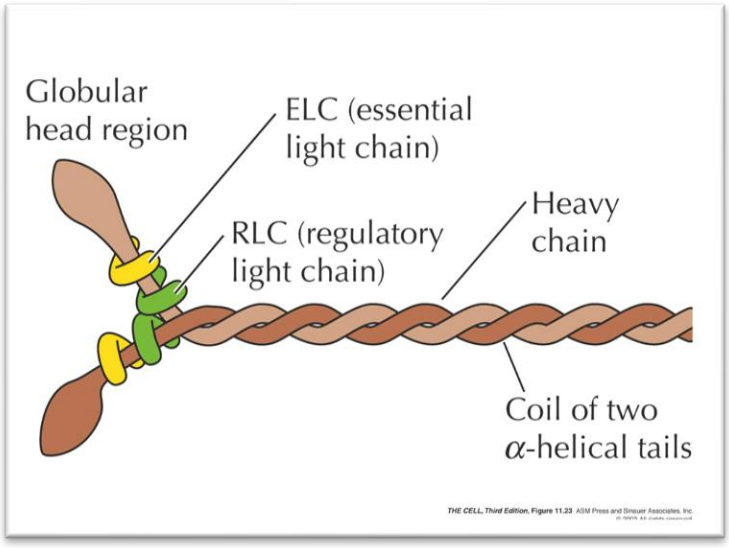

Figure 1.7: The structure of myosin II motor. Adopted from: Cooper, G. M. (2003). The Cell (3rd ed.). [Sinauer Associates].

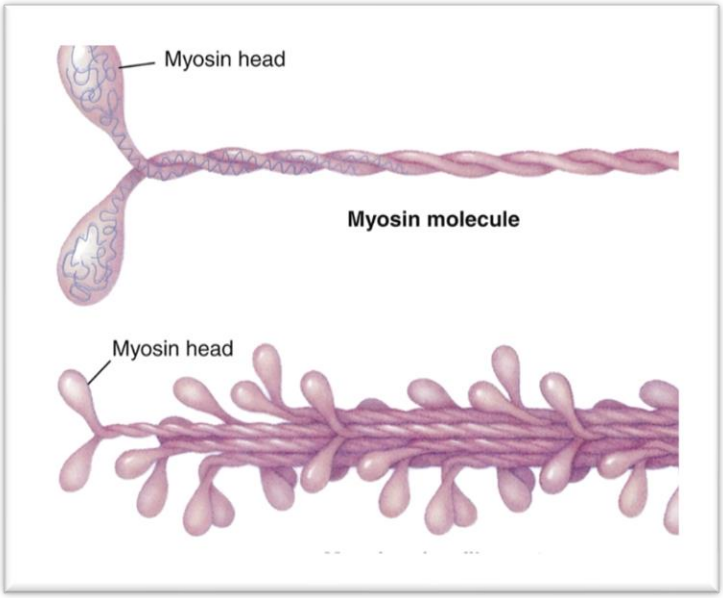

Figure 1.8: The aggregation of myosin motors into thick filaments. Adapted from: McCance & Huether, 2019(*)

Lever Arm (Neck Domain): Extending from the motor domain is the neck domain, functioning as a pivotal lever arm that modulates the movements of the motor domain. This segment is known to bind light chains and regulatory proteins, which play a significant role in modulating

the activity of myosin and directing its movement and its calcium ion sensitivity, thereby regulating muscle contraction (Fujita *et al*., 2019; Syamaladevi *et al*., 2012).

Tail Domain: The tail domain is responsible for the aggregation of myosin molecules into thick filaments. Its coiled-coil architecture is instrumental in the parallel alignment of multiple myosin II molecules, thus forming the structural core of the thick filament. This self-organizing feature is indispensable for the ordered architecture of muscle fibers (*10.2 Skeletal Muscle - Anatomy and Physiology | OpenStax*, n.d.)(Cooper, 2000).

The assembly of myosin II into thick filaments is a tightly regulated process. The coalescence of tail domains from individual myosin molecules results in an elongated, filamentous structure with protruding motor domains. Figure 1.8 illustrates the critical function of the myosin tail domain in the assembly of myosin motors into thick filaments. These thick filaments are strategically positioned in parallel with actin filaments, creating a periodic pattern integral for muscle contraction. The cross-bridges formed by the interaction of myosin heads with actin filaments, coupled with ATP-driven conformational changes, generate the forces necessary for muscle contraction (Ojima, 2019; Syamaladevi *et al*., 2012). Myosin II motors develop cross bridges with actin filaments, inducing muscles to contract through conformational changes in their mechanochemical cycles. As a muscle contraction regulator, myosin II has attracted considerable attention. Insights into its intricate function have been aided by single molecule studies, including optical trapping (Hilbert *et al*., 2013; Pollard, 2010; Spudich, 2001).

1.2.4 Myosin Mechanochemical Cycle

The mechanochemical cycle, powered by ATP hydrolysis, is a molecular process that converts chemical energy from ATP into mechanical work, driving movements in actin-myosin

networks. This cycle forms the basis of numerous cellular functions, ranging from muscle contraction to cellular motility. For decades, scientists have sought to unravel the complex interplay between the chemical reactions and mechanical motions of myosin II motor protein. As shown in Figure 1.9, ATP is hydrolyzed by myosin II to produce ADP (adenosine diphosphate) and inorganic phosphate. This hydrolysis triggers a conformational change in the myosin II head, positioning it for interaction with an actin filament. Once myosin is bound to actin, the release of the inorganic phosphate initiates the power stroke – a force-generating conformational change in myosin that drives movement along the actin filament. Subsequent ADP release allows a new ATP molecule to bind. This causes the myosin head to detach from actin and re-enter the cycle at another binding site (Baldo *et al*., 2020a; Johnson *et al*., 2019).

During the ATP cycle, myosin undergoes multiple conformational changes that dictate its binding strength to actin. When ATP binds to myosin, it causes the myosin head to detach from the actin, resulting in a low-affinity or "weak" binding state. This is often termed the "relaxed" state of the muscle. As ATP is hydrolyzed by myosin II to produce ADP and inorganic phosphate, the myosin head undergoes a conformational change, priming it for interaction with actin but still remains in a weakly bound state (Chakraborti *et al*., 2021). Upon ADP binding, myosin transitions to a "strong" binding state with increased affinity for actin, leading to the release of inorganic phosphate. This release triggers the "power stroke," a forceful change in myosin's shape that drives its movement along the actin filament, pulling the actin filament with it and characterizing this state by tight, strong binding. The subsequent release of ADP, while still in the strong binding state, allows a new ATP molecule to bind to myosin. Upon ATP binding, the affinity between myosin and actin drops, leading to the detachment of the myosin head from actin and transitioning it back to a weakly bound state. The hydrolysis of this new

ATP molecule re-cocks the myosin head, enabling it to initiate another round of interaction with the actin filament (Baldo *et al*., 2020a; Chakraborti *et al*., 2021; Kad *et al*., 2005). The mechanochemical cycle of myosin, while often described in terms of a singular myosin interacting with an actin filament, is inherently a multi-molecular event when considered in the physiological context of a cell. In the actin-myosin cross bridges, this cycle becomes a choreographed dance of multiple myosin molecules simultaneously walking on multiple actin filaments as depicted in the top-left corner of Figure 1.7 Numerous myosin heads, each at varying stages of their individual cycles, are interacting with actin filaments at any given moment. This creates a dynamic and synchronized movement where myosins collectively generate force and move along actin filaments. This simultaneous walking of many myosins along actin filaments ensures consistent force production and movement. It is akin to how multiple rowers in a boat synchronize their strokes to propel the boat forward efficiently. In the

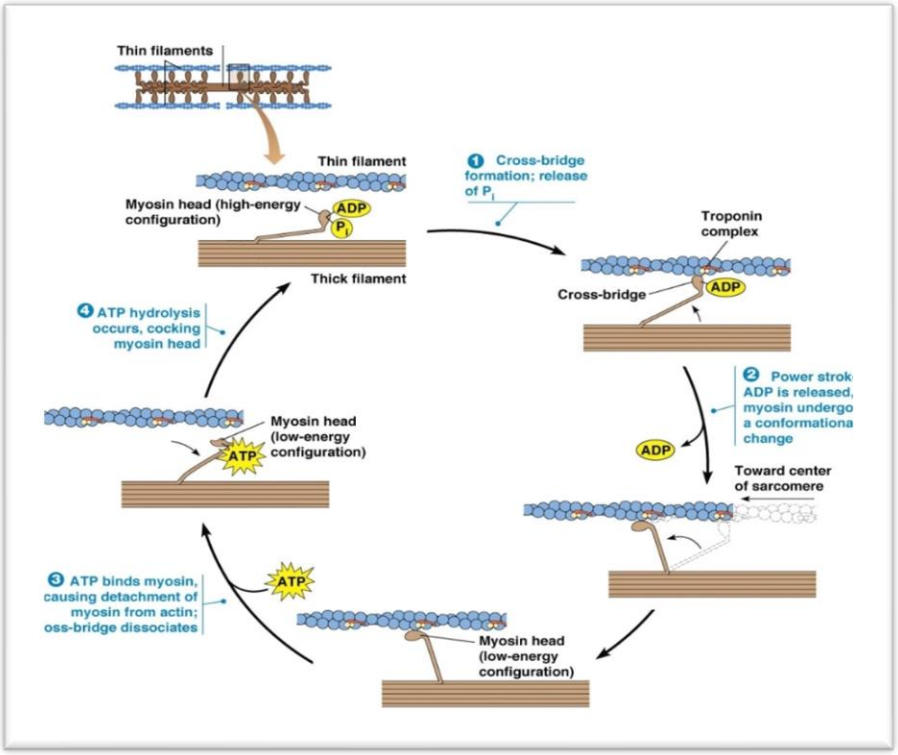

Figure 1.9: Contraction cycle of actin-myosin network through ATP hydrolysis. 1. Cross-bridge formation and release of Pi. 2. Myosin motor undergoes conformational change and takes a step toward the center of sarcomere when ADP is released. 3. ATP binds myosin, causing detachment from actin filament and cross-bridge dissociation. 4. ATP hydrolysis occurs, and the myosin head is cocked. Adapted from: Pearson Education Inc. 2012((*Create New Possibilities with Pearson. Start Learning Today.*, n.d.))

cell, this coordination ensures smooth muscle contraction and efficient intracellular transport. Furthermore, the efficiency and rate of these cycles can be modulated by various factors. For instance, different ionic concentrations and pH levels can influence the binding affinity of myosin to actin or the rate of ATP hydrolysis, thus affecting the overall cycle (Finer *et al*., 1994, 1995; Piazzesi *et al*., 2007; Yanagida *et al*., 2000).

1.2.5 Myosin II Single Molecule Properties

Single-molecule (SM) techniques are experimental methods that allow scientists to study the behavior and characteristics of individual molecules in isolation, rather than observing the averaged behavior of a group of molecules. These methods reveal unique details, offering deeper insights into molecular dynamics and interactions. By studying one molecule at a time, heterogeneous behaviors that are otherwise hidden in ensemble measurements come to the forefront. These studies reveal notable variability in step sizes, where individual molecules exhibit a range of movement lengths, and differences in force generation, with each motor potentially generating varying levels of force. Additionally, these studies uncover heterogeneity in binding and unbinding rates to filaments like actin, crucial for understanding motor efficiency and regulation (Finer *et al*.,

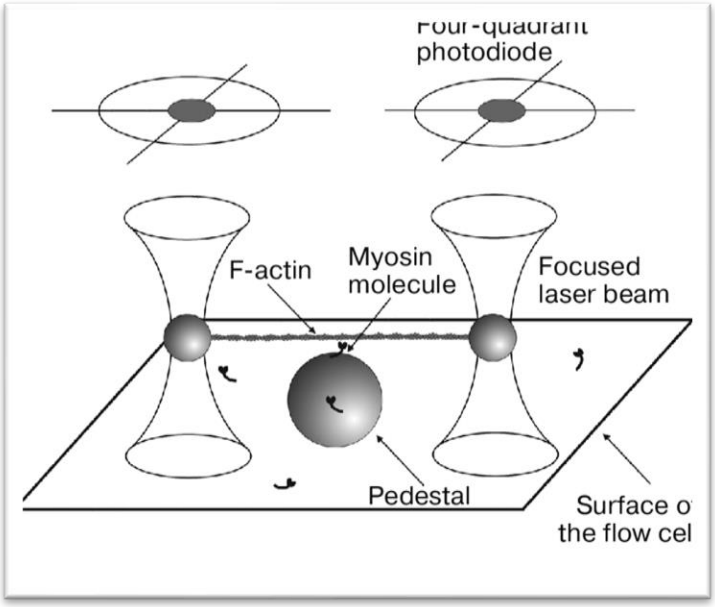

Figure 1.10: Investigation of the mechanics of single myosin molecule in actin–myosin network using optical tweezers. Adapted from: L. V. Nikitina et al., "Investigations of Molecular Mechanisms of Actin–Myosin Interactions in Cardiac Muscle," Biochemistry (Moscow), vol. 80, no. 13, pp. 1748-1763, Dec. 2015, doi: 10.1134/S0006297915130106

1995; Svoboda & Block, 1994b). There's also a noticeable diversity in the rates of ATP hydrolysis, the energy source for motor movement, indicating variations in motor speed and efficiency among individual molecules. Furthermore, conformational diversity is observed, with motors existing in multiple states, each potentially having unique functional properties. Interactions with regulatory proteins also vary among individual motors, influencing their activity and control. The lifetime and durability of each motor, key to understanding their role in long-term cellular functions, also differ (Rüegg *et al*., 2002). To probe myosin II dynamics at the molecular level, scientists developed protocols using optical trapping (more in Section 1.3). This tool, notable for its impressive sensitivity, measures forces as diminutive as piconewtons and movements down to the scale of nanometers (Ashkin, 1997; Kuo & Sheetz, 1993). Leveraging this precision, they observed individual myosin II motors interacting with actin filaments, providing clarity on specific motor features such as step size and stall force. Importantly, significant work by Finer *et al.* utilized optical trapping to dissect myosin II force generation at SM level (Ashkin, 1997; Kuo & Sheetz, 1993).

In contrast to the processive conventional kinesin-1 motor, which remains engaged with its microtubule track for the majority of its cycle, myosin II is non-processive. This behavior arises from myosin II's low duty ratio, preventing it from taking multiple steps without detaching from its track. Researchers modified the optical trapping assay used in a single motor-single filament orientation to include multiple motors, aiming to decipher myosin ensemble behavior (Mogilner, 2002; O'Connell *et al*., 2007). By employing the same principles of optical trapping used in single molecule orientations, a three-bead or dumbbell assay as shown in Figure 1.10, (Nikitina *et al*., 2015) was employed, with the bead surface coated in myosin motors. Within the framework of the three-bead assay, several key parameters of myosin motor performance were

elucidated from the literature. For instance, a study done by Finer *et al.* in 1994 demonstrated that a construct of myosin II, heavy meromyosin, executes steps on average of 11 nm. Moreover, the application of optical tweezers in the three-bead assay revealed myosin II generate force of 3-4 pN at the single molecule level (Finer *et al*., 1994). Such findings, derived specifically from the three-bead setup, have been instrumental in deepening our understanding of myosin's mechanical behavior in ensemble settings (Finer *et al*., 1994) (Debold *et al*., 2013; Kaya *et al*., 2017; Kaya & Higuchi, 2010; Walcott *et al*., 2012). An alternative approach involved coating a coverslip with motors and allowing them to slide actin filament held between two beads. These assay variations are discussed in more detail in the following section of the Introduction.

1.2.6 Myosin II Ensemble Properties and Force Feedback Mechanisms

Force feedback is fundamental for myosin function as it can modulate the detachment rate of the motor from actin and influence its stepping behavior. This feedback mechanism is especially critical for myosins working in teams, where the force exerted by one motor can impact the performance of its neighboring motors. Force feedback ensures that myosin motors can adapt to varying loads, optimizing their performance in dynamic cellular environments. Emphasizing the importance of force feedback in modulating myosin's detachment rate and stepping behavior, various investigations have underscored its pivotal role and the influence of the surrounding environment on the cumulative force produced by myosin II. Coupled with system compliance, this ensures optimal motor performance in dynamic cellular settings (Albert *et al*., 2014, 2014; Hilbert *et al*., 2013). Among these studies, Kaya *et al.* illuminated how low system stiffness could minimize the drag experienced by negatively strained myosins, especially when they are strategically positioned over an actin filament. The elastic portion of the myosin head is stretched

during active force production, reducing step size as load increases despite the working stroke remaining approximately constant. Step sizes of single myosin heads varied from 7 to 4 nm depending on load. Kaya *et al.* found that actin displacements reached 4 nm beyond 30 pN using the same assay orientation, this indicates that steps cannot be driven exclusively by single myosins but instead by potentially by multiple myosins working cooperatively, and the probability of coordinated force generation can be enhanced against high loads by using strain-dependent kinetics between force states, multiple power strokes, and high ATP concentration (Kaya *et al*., 2017; Kaya & Higuchi, 2010). Using a three-bead assay orientation, Walcott *et al.* observed that mechanical coupling between myosins causes differences between SM and ensemble by attaching multiple myosin motors to a coverslip-bound bead, thereby forming a small myosin ensemble that measured a smooth increase in force rather than individual binding events (Walcott *et al*., 2012).

In an attempt to investigate the effects of myosin II motor size on force generation and sliding speed, Hilbert *et al.* measured three distinct myosin group size-dependent motility regimes where above a critical length of AF, three distinct modes develop. Myosins attached to the AF increase gliding velocity when they are more abundant, and at lower myosin concentrations, the group effect disappears, suggesting that a minimal myosin concentration is required to achieve inter-myosin communication, as also observed by Stachowiak *et al.* within reconstituted actomyosin bundles, myosin II self-organizes (Hilbert *et al*., 2013).

Using the AF gliding assay, Stewart *et al.* discovered that velocity and ATPase activity depend on strain, and gliding velocity peaks with myosin binding sites on actin saturation, which challenges the conventional independent force model of muscle contraction that assumes AF sliding is limited by detachment of individual myosins from actin (Stewart *et al*., 2021a).

Similarly, Wagoner *et al.* purported that the amount of force felt by an individual motor will depend on the forces exerted by the other motors, giving rise to force-mediated motor cooperativity that affects the number of motors bound but also the order in which each motor performs its transitions; further, myosins have evolved to reduce filament backsliding to increase the speed and efficiency of muscle contraction (Wagoner & Dill, 2021).

In a previous study by Greenberg *et al*., it was demonstrated that myosin subfragment ADP release rate depends exponentially on applied load. Porcine myosin at saturating ATP released ADP in response to load. Moreover, cardiomyopathy-causing mutations and small molecule activators and inhibitors of cardiac myosin altered load-dependent cardiac S1 myosin detachment rates, suggesting that large-scale cardiac contractility can be controlled by tuning molecular level load-dependent kinetics (Greenberg & Moore, 2010; Sung *et al*., 2015).

Based on those studies, it is clear that myosin motor behavior varies between SM levels and teamwork based on the fact that it has to adapt to multiple types of environments and external loads. The feedback loop from the environment to the motor ensemble will also determine force output by altering motor communication and coordination in the form of force generation and duty ratio as a result of network stiffness, motor compliance, and the detection of number bound motors.

A recent study employing atomic force microscopy (AFM) was conducted that purported that there is not a cooperative effect in myosin II groups. However, their approach included rigidly coating actin filaments to a surface, which significantly limits the natural dynamics of actin-myosin interactions. The AFM-based study's confined attachment of actin filaments potentially neglects the essential dynamic interplay and cooperative behavior of myosin motors, and the rigid environment does not provide the necessary compliance to accurately replicate

sarcomere dynamics. A minimum cooperative action between myosin motors was observed, which is most likely resulted from the environmental constraints imposed on the actin filaments, rather than a real absence of cooperativity among myosin motors. The differences observed between the outcomes of the AFM study and our research highlight the importance of simulating a physiologically relevant environment to accurately study the complex mechanics of motor protein interactions (Matusovsky *et al*., 2023). In diseases like HCM, it is important to know how many myosin motors are attaching to actin at once. A deviation in this number can critically alter the force generation of myosin systems, and it is postulated to be a significant contributing factor to the hypercontractility often reported in HCM patients (Barrick & Greenberg, 2021; Daniels *et al*., 2021).

Understanding the role of bound motor numbers becomes even more crucial when considering the feedback loop from the environment to the motor ensemble. This feedback loop is not just a passive system responding to external stimuli. Instead, it actively shapes motor behavior, adjusting force generation and duty ratio in real-time. The interplay of factors, including the inherent stiffness of the cellular network, motor compliance, and the continuous detection and response to the number of bound motors, governs this dynamic system(O'Connell *et al*., 2007; Ruegg *et al*., 2002; Wagoner & Dill, 2021). Moreover, this system's sensitivity means that subtle changes in any of these parameters can lead to significant changes in motor output. For instance, increased motor binding might lead to a heightened force generation, which, in a condition like HCM, could exacerbate hypercontractility and further compromise cardiac function. This understanding has been a focal point in recent studies, emphasizing the importance of quantifying bound motors as a potential therapeutic target. Understanding the mechanisms by which myosin ensembles work together within higher complexity hierarchies

structures involving multiple myosin motors and actin filaments is vital for investigating actin myosin network synergy (Debold *et al*., 2013; O'Connell *et al*., 2007; Ruegg *et al*., 2002; Wagoner & Dill, 2021; Walcott *et al*., 2012).

1.3 Optical Tweezers

Optical trapping, commonly known as optical tweezers (OT), has emerged as a revolutionary tool that plays an essential role in exploring the domains of biophysics and cellular biology. Discovered by Arthur Ashkin in 1970, this method harnesses focused laser beams to capture and manipulate minuscule entities, encompassing biological entities such as cells or proteins (Ashkin *et al*., 1986; Finer *et al*., 1994; Schirber, 2018). The underlying principle of OT lies on the momentum of light. When a laser beam passes through a small, transparent object, such as a cell or a tiny bead, as shown in Figure 1.11, it refracts (bends). Due to the change in the light's momentum, a force is exerted on the object. This force tends to move the object to the center of the beam, effectively "trapping" it. The fundamental equation governing this is:

$$\boldsymbol{F} = \Delta(n^2) \qquad (1.1)$$

where F is the optical force and n is the refractive index of the medium. The gradient of the squared refractive index guarantees the object's attraction towards the focal point of the beam (Ashkin & Laboratories, n.d.; Shaevitz, 2006).

Calibrating OT is crucial for accurate measurements. Calibration ensures that readings taken during experiments are accurate, reliable, and can be replicated in other setups or labs. Calibration methods for optical tweezers vary depending on the specific

requirements of the experiment and the type of measurements being conducted. One common method is the power spectrum analysis, which involves analyzing the Brownian motion of the trapped bead as thermal fluctuations. By fitting the power spectrum of these fluctuations to the Lorentzian distribution, the trap stiffness (k) can be determined.

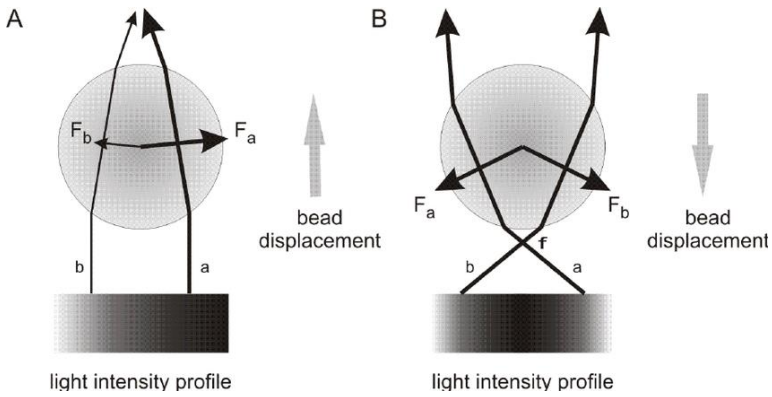

Figure 1.11: The principles behind optical trapping. A – 2D optical trap. A parallel beam of light interacts with a semi-transparent particle (e.g. polystyrene bead), which has a different refraction index than its surrounding: the ray of light with a higher intensity (a) gives rise to a stronger force (F a), which compensates the photon momentum change caused by refraction. The bead is pushed towards. Adapted from: Petelenz-Kurdziel, E. (2010). From cell populations to single cells-quantitative analysis of osmotic regulation in yeast.

This method is widely used due to its simplicity and the minimal requirement for external calibration standards. Another calibration method is the direct force measurement, where known forces are applied to the trapped object, often through the use of calibrated fluid flow or magnetic fields acting on magnetic beads. The displacement of the bead from the trap center in response to the applied force is measured, allowing for the direct calculation of trap stiffness. This method is advantageous for its directness but requires additional calibrated equipment. In Stokes' drag method, calibration is done by moving the trapped bead through a viscous fluid at known velocities and measuring the drag force exerted on the bead. According to Stokes' law, this force is proportional to the velocity and viscosity of the fluid, allowing for the calculation of trap stiffness. This method is particularly useful for calibrating optical tweezers that manipulate objects in fluid environments. Equipartition theorem method utilizes the equipartition theorem to allow for the determination of trap stiffness by measuring the variance in the bead's position

within the trap. According to this theorem, the thermal energy at equilibrium is equally distributed among all degrees of freedom, which relates the measured position variance to the trap stiffness. This method is beneficial for its straightforward application and does not require moving the sample or applying external forces. In interferometric methods, advanced calibration techniques utilized involve using interferometry to precisely measure the displacement of trapped particles. These methods can achieve extremely high spatial resolution, making them suitable for experiments requiring precise measurements of particle position and movement within the trap (Pérez-García *et al*., 2023; Rice & Fischer, n.d.).

Another method used for calibration is power spectrum method, the power spectrum method, which employs the Brownian motion-induced natural fluctuations of the bead in fluid. The calibration method assumes the system operates in a harmonic potential, meaning the restoring force acting on the trapped bead is proportional to its displacement from equilibrium. In an ideal system with a known fluid temperature and Boltzmann constant, we can estimate the trap stiffness by analyzing the bead's Brownian motion. However, the bead's behavior isn't simply characterized by its average displacement. To account for the bead's fluctuations at different frequencies, we utilize the power spectrum method. This involves measuring the bead's position with high-resolution techniques (e.g., quadrant photodiodes) and converting the time-series data into the frequency domain using the Fast Fourier Transform (FFT). This transformation reveals the spectral density, essentially the distribution of energy across different frequencies within the bead's movement. By analyzing the power spectrum, we can identify the corner frequency, a critical characteristic point where energy transfer through the system starts to diminish. This corner frequency, combined with theoretical models based on the bead properties and known drag coefficient, allows us to calculate the trap stiffness. The restoring force exerted

by an optical trap on a trapped bead behaves similarly to a spring, which means that the force increases proportionally to the displacement of the bead from its equilibrium position. This allows us to apply the concepts of spring constant and potential energy from Hooke's Law to understand the trap's basic behavior (Stilgoe *et al*., 2021).

Hooke's law is derived as followed:

The potential energy (U) in a spring system is given by:

$$U = \frac{1}{2} k_S (x - x_0)^2 \quad (1)$$

Where 'U' is the potential energy stored in a spring, k_s is the spring constant, x is the change in length, and x_0 is the equilibrium length, and x_i is the initial length of the spring, which is equal to x in this scenario.

Assume that:

$$x_0 = 0;\ x_i = x;\ x_f = x + dx \quad (2)$$

Here dx is a very small change in length. Now for the change in potential energy:

$$dU = U_f - U_i \quad (3)$$

Where U_f is the final potential energy, and U_i is the initial potential energy

Substituting in (2) to (3), we get:

$$dU = \frac{1}{2} k_s (x - x_0)^2 - \frac{1}{2} k_s x^2 \quad (4)$$

Expanding (4), we get:

$$dU = \frac{1}{2}k_s(x^2 + 2x\,dx + dx^2) - \frac{1}{2}k_s x^2 \qquad (5)$$

Simplifying (5), we get:

$$dU = k_s x\,dx + \frac{1}{2}k_s dx^2 \qquad (6)$$

If dx << 1, $dx^2 \rightarrow 0$ and we get:

$$dU = k_s x dx \qquad (7)$$

Now looking at the conservation of energy equation:

$$dE = d\mathrm{K} + dU = 0 \qquad (8)$$

Where K is the kinetic energy and E is the mechanical energy. Setting (8) equal to zero, we get:

$$d\mathrm{K} + \mathrm{K}xdx = 0 \tag{9}$$

Rearranging (9), we get:

$$d\mathrm{K} = -\mathrm{K}xdx \tag{10}$$

Now looking at the work-energy theorem:

$$d\mathrm{K} = \vec{F} \cdot d\vec{x} \tag{11}$$

Where $\vec{F}$ is the force vector and $d\vec{x}$ is the displacement vector, assuming the force vector and displacement vector are going in the same direction, $\theta=0$, and $cos\theta=1$, we get:

$$\vec{F} \cdot d\vec{x} = Fdxcos\theta = Fdx \tag{12}$$

Combining (10), (11), and (13), we get Hooke's Law where the spring constant k_s is also the trap stiffness k_{trap}:

$$F_{trap} = -k_{\mathrm{trap}}x \tag{13}$$

The calibration of optical tweezers through power spectrum analysis involves understanding the motion of a trapped particle and its interaction with the surrounding fluid. The motion of the particle can be described by the equation of motion under the influence of an optical trap and thermal fluctuations. The equation of motion for a trapped particle is given by: (*Optical Trapping*, n.d.).

$$m\frac{d^2x(t)}{dt^2} = -\gamma\frac{dx(t)}{dt} + k_{trap}x(t) + \xi(t) \quad (14)$$

where m is the mass of the particle, $x(t)$ its position as a function of time, γ the damping coefficient due to viscous drag, k_{trap} the trap stiffness, and $\xi(t)$ represents the thermal force acting on the particle due to Brownian motion.

Fourier Transform and Power Spectrum

To analyze the motion in the frequency domain, we apply the Fourier transform to both sides of the equation. The Fourier transform of a function $f(t)$ is given by:

$$F(\omega) = \int_{-\infty}^{\infty} f(t)e^{-i\omega t}\,dt, \quad (15)$$

where ω is the angular frequency.

Applying the Fourier transform to the equation of motion yields:

$$(-i\omega\gamma + k_{trap})X(\omega) = \Xi(\omega) \quad (16)$$

where $X(\omega)$ and $\Xi(\omega)$ are the Fourier transforms of $x(t)$ and $\xi(t)$, respectively.

The power spectrum $P(\omega)$ is defined as the square of the magnitude of $X(\omega)$, which gives us the power at a particular frequency ω. Through some algebraic manipulation, the power spectrum can be expressed as:

$$P(\omega) = \frac{|\omega|^2}{\omega^2\gamma^2 + {k_{trap}}^2} = \frac{2k_B T\gamma}{\omega^2\gamma^2 + {k_{trap}}^2} \quad (17)$$

where k_B is the Boltzmann constant and T the temperature. This equation reveals that the power spectrum of the trapped particle's motion has a Lorentzian shape with a corner frequency $\omega c = k_{trap}/\gamma$. The corner frequency ω_c is a critical parameter that can be directly measured from the power spectrum. Given ω_c, the trap stiffness k_{trap} can be calculated if the damping coefficient γ is known (which can be determined from the properties of the fluid and the size of the particle). The relationship is given by

$$k_{trap} = \gamma\omega_c \quad (18)$$

Analysis using OT does not stop at force measurements. Temporal displacements, stepping behaviors of motor proteins, and even changes in the rotational dynamics of trapped objects can be studied. Numerous studies, including those by Svoboda & Block (1994) and Neuman & Block (2004), have showcased the versatility of OT in probing the microscopic world. They underscore its ability to not only trap particles but also offer a dynamic framework for real-time examination of biological activities. Moreover, advancements in the field have led to innovations like holographic optical tweezers, which can trap and manipulate multiple particles simultaneously. This opens the door to studying interactions between several

biological entities in a controlled environment, further expanding the horizons of research (Neuman & Block, 2004; Svoboda & Block, 1994a; Woerdemann, 2012).

1.3.1 Optical Tweezers Assays Probe the Dynamics of Molecular Motors

In the field of biophysics, optical tweezers (OT) have risen as a crucial instrument, revealing the nuanced dynamics of motor proteins in real-time (Spudich *et al.*, 2011). Motor proteins navigate their paths by "walking" along specific tracks, such as actin filaments or microtubules. To observe the dynamics of motor proteins, scientists link small beads to motor proteins, making their minute actions visible in the diffraction-limited world. Following this attachment, the bead's movements are tracked using the laser beam in optical tweezers. As the motor protein travels, pulling the bead with it, this movement resists the confining force of the laser. This displacement of the bead over time provides a direct measure of the force exerted by the motor protein and its interactions. By monitoring the bead's position and changes, scientists can infer details about the protein's dynamics, such as step size, directionality, and binding characteristics (Finer *et al*., 1994; Kitamura *et al*., 1999; C. T. Murphy *et al*., 2001; Woerdemann, 2012).

OT assays have evolved from single-molecule studies to encompass a rich array of techniques that delve into motor protein dynamics. Figure 12. below illustrates this evolution, capturing the progression from basic single-molecule force measurements to the exploration of rower motors, non-processive behaviors, and multi-motor interactions. Each assay type offers unique insights, paving the way for a comprehensive understanding of motor protein mechanics and behaviors (O. Al Azzam *et al*., 2021).

OT experiments have relied on understanding that different motor types, like "porters" or "rowers", demand specific OT geometries for effective study. Early experiments, like those from Sheetz and Block labs, used OT to measure force generation by motor proteins (Chowdhury, 2014; Kuo & Sheetz, 1993; Svoboda & Block, 1994a). They innovatively utilized OT to measure force produced by the classical porter kinesin- 1's by employing a streptavidin coated bead bound to a biotinylated MT. The bead was displaced by a single kinesin attached to a coverslip

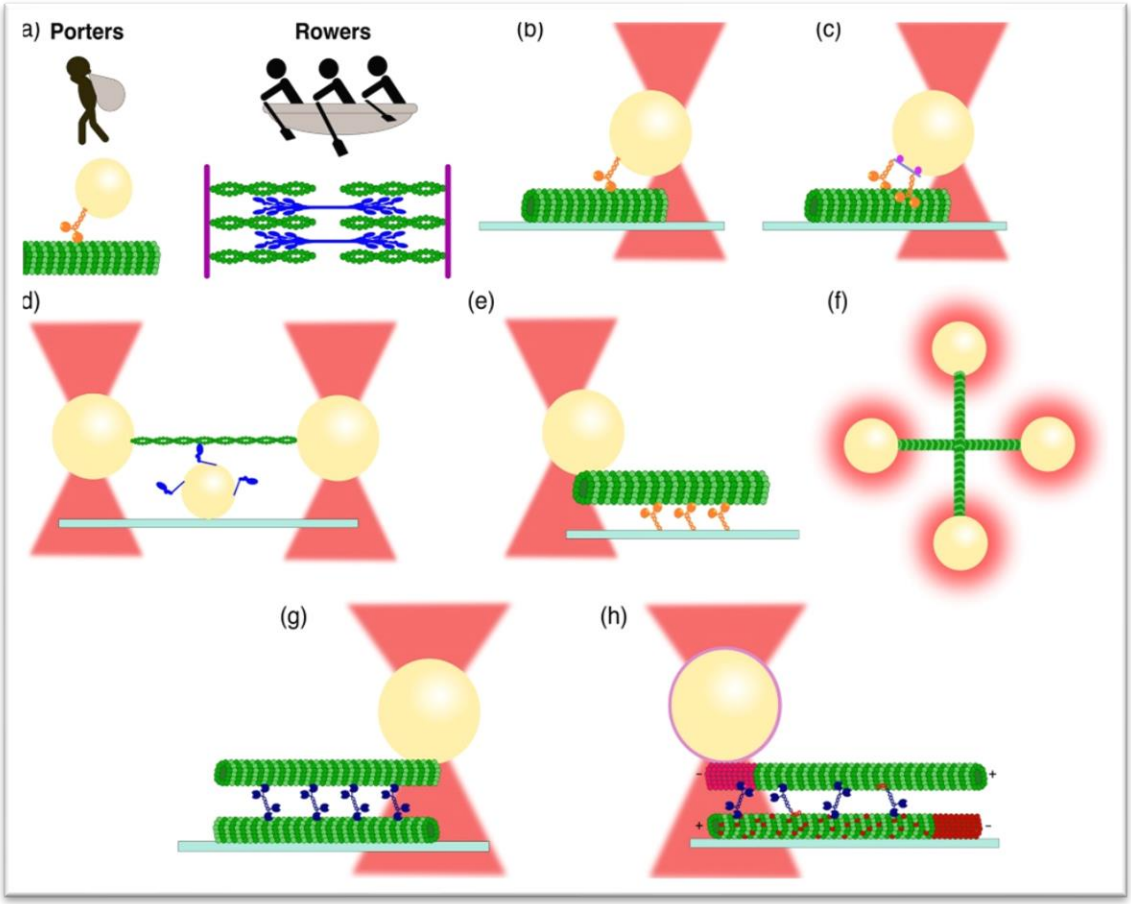

Figure 1.12: The diverse world of optical trapping motor assays encompasses: (a) Processive and nonprocessive motor distinctions, necessitating tailored assays. (b) Single molecule force measurements using trapped beads. (c) Single bead, single filament orientation for team motility study. (d) Three-bead assay for rower motor force analysis. (e) Adapted filament gliding assays. (f) Holographic optical trapping for 3D microtubule networks. (g) Crosslinked filament force measurement using "sandwich" assays. (h) Complex force measurements via customized filament labeling and multi-motor ensembles. Adapted from: Al Azzam et al., "Measuring force generation within reconstituted microtubule bundle assemblies using optical tweezers," Cytoskeleton, first published 29 May 2021 (https://doi.org/10.1002/cm.21678).

(Kuo & Sheetz, 1993). Later, this orientation was reversed by Svoboda *et al*., where the MT was bound to a coverslip and a kinesin motor was attached to a trapped bead. Upon the presence of ATP, the bead-bound kinesin initiates movement away from the center of the trap, navigating along the microtubule (MT) pathway. This action simultaneously extends the spring of the trap, resulting in an elevation of force. Both experimental setups have been extensively modified and utilized to explore the behaviors of kinesins and various other molecular motors, with particular emphasis on the configuration where the motor is bound to the bead (Svoboda & Block, 1994b, 1994a).

Challenges arise when examining rower motors, which often have low processivity – the ability to take successive steps on their track without dissociating ("Porters versus Rowers," 1993). Some motors, such as mitotic kinesin-5, kinesin-12, and kinesin-14, display a mix of motility behaviors, further complicating the categorization process. A solution to this challenge involves binding multiple motors to a bead to explore variations between individual versus team motility. DNA origami has even been used to precisely control motor spacing (O. Al Azzam *et al*., 2021; Furuta & Toyoshima, 2008; Reinemann *et al*., 2018). In a study conducted by Finer *et al.,* they introduced the "three-bead assay," also known as the "dumbbell assay." Utilizing two laser traps, this technique effectively examined non processive motors, such as myosin II, that disconnect after each movement (Finer *et al*., 1994).

While single-molecule orientations offer foundational insights, they often fall short in capturing the complexity of physiological systems. The predominant focus of many OT motor studies has been the interaction between a single motor and filament. This narrowed view does not fully reflect the physiologically relevant environments where motors operate. Consequently, there is an emergent demand for in vitro methodologies that closely replicate these physiological

settings. Some approaches, like the "gliding filament" assay, integrate multiple motors or filaments. In contrast, other techniques leverage fluorescence microscopy or computational modeling to delve deeper into the collective behaviors of motor assemblies (Albert *et al*., 2014; Barrick & Greenberg, 2021; Hilbert *et al*., 2013; Nikitina *et al*., 2015; Spudich, 2001; Sung *et al*., 2015).

1.4 Advancements in Motor Protein Dynamics Analysis Through Optical Tweezers

In order to address the challenges arising from traditional single-molecule (SM) studies and to attain a more physiologically relevant approach that offers deeper insights into system compliance, hierarchy, and motor coordination, this dissertation introduces a novel experimental paradigm. This innovative approach integrates the precision of optical trapping (OT) with the active in vitro assembly of cytoskeletal structures. Central to this methodology is the creation of a motor coordination-compliant environment that more accurately mimics the natural, dynamic conditions of muscle cells. This novel setup not only facilitates the study of myosin II ensemble force generation but also allows for a more comprehensive investigation of the intricate communication and coordination mechanisms among myosin motors within a compliant and hierarchically structured system. Through this advanced experimental design, the dissertation aims to bridge the gaps identified in traditional assays, providing a more thorough and nuanced understanding of myosin II dynamics and functionality. Within this approach, multiple motors are assembled into an ensemble configuration, facilitating their interaction within the ensemble while maintaining the ability to move freely between the multiple actin filaments during force generation. This design creates an environment that closely mimics muscle sarcomeres and prioritizes motor coordination within a compliant framework.

In this novel approach, actin-myosin-actin bundles were constructed using muscle

myosin II, rhodamine-labeled actin filaments at the bottom of the microscopic slide, and 488-labeled biotinylated actin filaments on top of the bundle. Successful bundle formation, characterized by colocalized actin filaments and myosin motors interacting in between, was confirmed through fluorescence visualization, demonstrating that the filaments were properly aligned, resulting in the successful modeling of the sandwich structure. The mechanics of myosin ensembles interacting between two actin filaments were measured for the first time using optical tweezers. This in vitro assay combined by optical tweezers was conducted to assess force generation, characterize the dynamics of myosin motors, and investigate how these dynamics influence force generation in interactions between actin-myosin bundles. Myosin-actin ensembles were assembled and connected to optically trapped microspheres to study the motility and force generated during interactions with actin-myosin bundles. The displacement of the trapped bead was monitored and correlated with force output, utilizing corner frequency-based calibrations. The resulting data were subjected to analysis using MATLAB to extract information regarding force magnitude and stepping behavior. Using this modular assay geometry, conditions that might influence myosin ensemble biophysical mechanics such as motor structure and cell environment conditions will directly be altered and investigated. Further, investigating force generation mechanisms through these actin–myosin ensembles have the potential to aid in modeling and understanding how large-scale cellular tasks, such as muscle contraction, propagate up from the molecular level.

BIBLIOGRAPHY

1.5 Bibliography

Akhshi, T. K., Wernike, D., & Piekny, A. (2014). Microtubules and actin crosstalk in cell migration and division. *Cytoskeleton*, *71*(1), 1–23.

Al Azzam, O., Trussell, C. L., & Reinemann, D. N. (2021). Measuring force generation within reconstituted microtubule bundle assemblies using optical tweezers. *Cytoskeleton*, *78*(3), 111–125. https://doi.org/10.1002/cm.21678

Al Azzam, O. Y., Watts, J. C., Reynolds, J. E., Davis, J. E., & Reinemann, D. N. (2022). Myosin II Adjusts Motility Properties and Regulates Force Production Based on Motor Environment. *Cellular and Molecular Bioengineering*, *15*(5), 451–465. https://doi.org/10.1007/s12195-022-00731-1

Albert, P. J., Erdmann, T., & Schwarz, U. S. (2014). Stochastic dynamics and mechanosensitivity of myosin II minifilaments. *New Journal of Physics*, *16*(9), 093019. https://doi.org/10.1088/1367-2630/16/9/093019

Alberts, B., Johnson, A., Lewis, J., Raff, M., Roberts, K., & Walter, P. (2002). Molecular Motors. In *Molecular Biology of the Cell. 4th edition*. Garland Science. https://www.ncbi.nlm.nih.gov/books/NBK26888/

Altman, D. (2013). Myosin Work and Motility: Mechanism. In G. C. K. Roberts (Ed.), *Encyclopedia of Biophysics* (pp. 1671–1679). Springer. https://doi.org/10.1007/978-3-642-16712-6_754

Andrei, S., & Iorgoveanu, C. (2014). New perspective in heart failure management: Could myosin activators be the answer? *Discoveries (Craiova, Romania)*, *2*(4), e33. https://doi.org/10.15190/d.2014.25

Ashkin, A. (1997). Optical trapping and manipulation of neutral particles using lasers.

Proceedings of the National Academy of Sciences of the United States of America, *94*(10), 4853–4860. https://doi.org/10.1073/pnas.94.10.4853

Ashkin, A., Dziedzic, J. M., Bjorkholm, J. E., & Chu, S. (1986). Observation of a single-beam gradient force optical trap for dielectric particles. *Optics Letters*, *11*(5), 288. https://doi.org/10.1364/ol.11.000288

Ashkin, A., & Laboratories, B. (n.d.). *Optical Tweezers and their Application to Biological Systems*.

Auguin, D., Robert-Paganin, J., Réty, S., Kikuti, C., David, A., Theumer, G., Schmidt, A. W., Knölker, H.-J., & Houdusse, A. (2023). Omecamtiv mecarbil and Mavacamten target the same myosin pocket despite antagonistic effects in heart contraction. *bioRxiv*, 2023.11.15.567213. https://doi.org/10.1101/2023.11.15.567213

Azzam, O. A., Watts, J. C., Reynolds, J. E., Davis, J. E., & Reinemann, D. N. (2022). Probing Myosin Ensemble Mechanics in Actin Filament Bundles Using Optical Tweezers. *JoVE (Journal of Visualized Experiments)*, *183*, e63672. https://doi.org/10.3791/63672

Baldo, A. P., Tardiff, J. C., & Schwartz, S. D. (2020a). Mechanochemical Function of Myosin II: Investigation into the Recovery Stroke and ATP Hydrolysis. *The Journal of Physical Chemistry. B*, *124*(45), 10014–10023. https://doi.org/10.1021/acs.jpcb.0c05762

Baldo, A. P., Tardiff, J. C., & Schwartz, S. D. (2020b). Mechanochemical Function of Myosin II: Investigation into the Recovery Stroke and ATP Hydrolysis. *The Journal of Physical Chemistry. B*, *124*(45), 10014–10023. https://doi.org/10.1021/acs.jpcb.0c05762

Barrick, S. K., & Greenberg, M. J. (2021). Cardiac myosin contraction and mechanotransduction in health and disease. *The Journal of Biological Chemistry*, *297*(5), 101297. https://doi.org/10.1016/j.jbc.2021.101297

Beeler, T. J., Wang, T., Gable, K., & Lee, S. (1985). Comparison of the rat microsomal Mg-ATPase of various tissues. *Archives of Biochemistry and Biophysics, 243*(2), 644–654. https://doi.org/10.1016/0003-9861(85)90542-9

Brunello, E., Fusi, L., Ghisleni, A., Park-Holohan, S.-J., Ovejero, J. G., Narayanan, T., & Irving, M. (2020). Myosin filament-based regulation of the dynamics of contraction in heart muscle. *Proceedings of the National Academy of Sciences, 117*(14), 8177–8186. https://doi.org/10.1073/pnas.1920632117

Burghardt, T. P., Yan Hu, J., & Ajtai, K. (2007). Myosin Dynamics on the Millisecond Time Scale. *Biophysical Chemistry, 131*(1–3), 15–28. https://doi.org/10.1016/j.bpc.2007.08.008

Chakraborti, A., Baldo, A. P., Tardiff, J. C., & Schwartz, S. D. (2021). Investigation of the Recovery Stroke and ATP Hydrolysis and Changes Caused Due to the Cardiomyopathic Point Mutations in Human Cardiac β Myosin. *The Journal of Physical Chemistry. B, 125*(24), 6513–6521. https://doi.org/10.1021/acs.jpcb.1c03144

Chakraborti, A., Tardiff, J. C., & Schwartz, S. D. (2022a). Insights into the Mechanism of the Cardiac Drug Omecamtiv Mecarbil─A Computational Study. *The Journal of Physical Chemistry. B, 126*(48), 10069–10082. https://doi.org/10.1021/acs.jpcb.2c06679

Chakraborti, A., Tardiff, J. C., & Schwartz, S. D. (2022b). Insights into the Mechanism of the Cardiac Drug Omecamtiv Mecarbil—A Computational Study. *The Journal of Physical Chemistry. B, 126*(48), 10069–10082. https://doi.org/10.1021/acs.jpcb.2c06679

Chakraborti, A., Tardiff, J. C., & Schwartz, S. D. (2023). Exploring the effect of myosin modulators on the ATP hydrolysis step of human cardiac beta myosin using transition path sampling. *Biophysical Journal, 122*(3), 259a. https://doi.org/10.1016/j.bpj.2022.11.1491

Chou, C., & Chin, M. T. (2021). Pathogenic Mechanisms of Hypertrophic Cardiomyopathy

beyond Sarcomere Dysfunction. *International Journal of Molecular Sciences*, *22*(16), 8933. https://doi.org/10.3390/ijms22168933

Chowdhury, D. (2014). Michaelis-Menten at 100 and allosterism at 50: Driving molecular motors in a hailstorm with noisy ATPase engines and allosteric transmission. *The FEBS Journal*, *281*(2), 601–611. https://doi.org/10.1111/febs.12596

Clark, K., Langeslag, M., Figdor, C. G., & van Leeuwen, F. N. (2007). Myosin II and mechanotransduction: A balancing act. *Trends in Cell Biology*, *17*(4), 178–186. https://doi.org/10.1016/j.tcb.2007.02.002

Cleland, J. G., Teerlink, J. R., Senior, R., Nifontov, E. M., Mc Murray, J. J., Lang, C. C., Tsyrlin, V. A., Greenberg, B. H., Mayet, J., Francis, D. P., Shaburishvili, T., Monaghan, M., Saltzberg, M., Neyses, L., Wasserman, S. M., Lee, J. H., Saikali, K. G., Clarke, C. P., Goldman, J. H., … Malik, F. I. (2011). The effects of the cardiac myosin activator, omecamtiv mecarbil, on cardiac function in systolic heart failure: A double-blind, placebo-controlled, crossover, dose-ranging phase 2 trial. *The Lancet*, *378*(9792), 676–683. https://doi.org/10.1016/S0140-6736(11)61126-4

Cooper, G. M., & Hausman, R. (2000). A molecular approach. *The Cell. 2nd Ed. Sunderland, MA: Sinauer Associates*.

Create new possibilities with Pearson. Start learning today. (n.d.). Retrieved March 22, 2024, from https://www.pearson.com/en-us.html

Cytokinetics' heart failure drug gets a thumbs-down from FDA. (n.d.). Retrieved March 26, 2024, from https://www.fiercepharma.com/pharma/fda-turns-down-cytokinetics-once-promising-heart-failure-drug-omecamtiv

Daniels, M. J., Fusi, L., Semsarian, C., & Naidu, S. S. (2021). Myosin Modulation in

Hypertrophic Cardiomyopathy and Systolic Heart Failure: Getting Inside the Engine. *Circulation*, *144*(10), 759–762. https://doi.org/10.1161/CIRCULATIONAHA.121.056324

Day, S. M., Tardiff, J. C., & Ostap, E. M. (2022). Myosin modulators: Emerging approaches for the treatment of cardiomyopathies and heart failure. *The Journal of Clinical Investigation*, *132*(5). https://doi.org/10.1172/JCI148557

Debold, E. P., Walcott, S., Woodward, M., & Turner, M. A. (2013). Direct observation of phosphate inhibiting the force-generating capacity of a miniensemble of Myosin molecules. *Biophysical Journal*, *105*(10), 2374–2384. https://doi.org/10.1016/j.bpj.2013.09.046

Doenst, T., Nguyen, T. D., & Abel, E. D. (2013). Cardiac Metabolism in Heart Failure—Implications beyond ATP production. *Circulation Research*, *113*(6), 709–724. https://doi.org/10.1161/CIRCRESAHA.113.300376

Doran, M. H., & Lehman, W. (2021). The Central Role of the F-Actin Surface in Myosin Force Generation. *Biology*, *10*(12), 1221. https://doi.org/10.3390/biology10121221

Dulyaninova, N. G., & Bresnick, A. R. (2013). The heavy chain has its day. *Bioarchitecture*, *3*(4), 77–85. https://doi.org/10.4161/bioa.26133

El Hadi, H., Freund, A., Desch, S., Thiele, H., & Majunke, N. (2023). Hypertrophic, Dilated, and Arrhythmogenic Cardiomyopathy: Where Are We? *Biomedicines*, *11*(2), 524. https://doi.org/10.3390/biomedicines11020524

Elliott, P., & McKenna, W. (2008). Hypertrophic cardiomyopathy: A 50th anniversary. *Heart*, *94*(10), 1247–1248. https://doi.org/10.1136/hrt.2008.154344

Felker, G. M., Solomon, S. D., Claggett, B., Diaz, R., McMurray, J. J. V., Metra, M., Anand, I., Crespo-Leiro, M. G., Dahlström, U., Goncalvesova, E., Howlett, J. G., MacDonald, P., Parkhomenko, A., Tomcsányi, J., Abbasi, S. A., Heitner, S. B., Hucko, T., Kupfer, S., Malik,

F. I., & Teerlink, J. R. (2022). Assessment of Omecamtiv Mecarbil for the Treatment of Patients With Severe Heart Failure. *JAMA Cardiology*, *7*(1), 26–34. https://doi.org/10.1001/jamacardio.2021.4027

Finer, J. T., Mehta, A. D., & Spudich, J. A. (1995). Characterization of single actin-myosin interactions. *Biophysical Journal*, *68*(4 Suppl), 291S-296S; discussion 296S-297S.

Finer, J. T., Simmons, R. M., & Spudich, J. A. (1994). Single myosin molecule mechanics: Piconewton forces and nanometre steps. *Nature*, *368*(6467), 113–119. https://doi.org/10.1038/368113a0

Fujita, K., Ohmachi, M., Ikezaki, K., Yanagida, T., & Iwaki, M. (2019). Direct visualization of human myosin II force generation using DNA origami-based thick filaments. *Communications Biology*, *2*(1), 1–11. https://doi.org/10.1038/s42003-019-0683-0

Furuta, K., & Toyoshima, Y. Y. (2008). Minus-end-directed motor Ncd exhibits processive movement that is enhanced by microtubule bundling in vitro. *Current Biology: CB*, *18*(2), 152–157. https://doi.org/10.1016/j.cub.2007.12.056

Glynn, P., Ning, H., Bavishi, A., Mehta, P. P., Shah, S., Yancy, C., Lloyd-Jones, D. M., & Khan, S. S. (2021). Heart Failure Risk Distribution and Trends in the United States Population, NHANES 1999–2016. *The American Journal of Medicine*, *134*(3), e153–e164. https://doi.org/10.1016/j.amjmed.2020.07.025

Gordon, A. M., Regnier, M., & Homsher, E. (2001). Skeletal and Cardiac Muscle Contractile Activation: Tropomyosin "Rocks and Rolls." *Physiology*, *16*(2), 49–55. https://doi.org/10.1152/physiologyonline.2001.16.2.49

Greenberg, M. J., & Moore, J. R. (2010). The molecular basis of frictional loads in the in vitro motility assay with applications to the study of the loaded mechanochemistry of molecular

motors. *Cytoskeleton (Hoboken, N.J.)*, *67*(5), 273–285. https://doi.org/10.1002/cm.20441

Guhathakurta, P., Prochniewicz, E., & Thomas, D. D. (2018). Actin-Myosin Interaction: Structure, Function and Drug Discovery. *International Journal of Molecular Sciences*, *19*(9), 2628. https://doi.org/10.3390/ijms19092628

Hancock, W. O., & Howard, J. (1998). Processivity of the motor protein kinesin requires two heads. *The Journal of Cell Biology*, *140*(6), 1395–1405.

Hartman, M. A., & Spudich, J. A. (2012). The myosin superfamily at a glance. *Journal of Cell Science*, *125*(7), 1627–1632.

Hashem, S., Tiberti, M., & Fornili, A. (2017). Allosteric modulation of cardiac myosin dynamics by omecamtiv mecarbil. *PLOS Computational Biology*, *13*(11), e1005826. https://doi.org/10.1371/journal.pcbi.1005826

Heart Disease and Stroke Statistics—2023 Update: A Report From the American Heart Association | Circulation. (n.d.). Retrieved March 25, 2024, from https://www.ahajournals.org/doi/10.1161/CIR.0000000000001123

Heart Disease: Types, Causes, and Symptoms. (n.d.). Retrieved March 25, 2024, from https://www.webmd.com/heart-disease/heart-disease-types-causes-symptoms

Heart failure: Symptoms, causes, diagnosis and treatments. (n.d.). Retrieved March 25, 2024, from https://www.msn.com/en-us/health/condition/in-heart-failure/in-heart-failure

Heart Failure—Are you at risk?: Just Heart Cardiovascular Group Inc.: Cardiologists. (n.d.). Retrieved March 25, 2024, from https://www.myjustheart.com/blog/heart-failure-are-you-at-risk

Heart failure—Symptoms and causes. (n.d.). Mayo Clinic. Retrieved March 25, 2024, from https://www.mayoclinic.org/diseases-conditions/heart-failure/symptoms-causes/syc-

20373142

Hilbert, L., Cumarasamy, S., Zitouni, N. B., Mackey, M. C., & Lauzon, A.-M. (2013). The kinetics of mechanically coupled myosins exhibit group size-dependent regimes. *Biophysical Journal*, *105*(6), 1466–1474.

Houdusse, A., & Sweeney, H. L. (2016). How myosin generates force on actin filaments. *Trends in Biochemical Sciences*, *41*(12), 989–997. https://doi.org/10.1016/j.tibs.2016.09.006

Https://www.aasavariclinic.com/latest-update/heart-failure-is-a-m/15. (n.d.). Retrieved March 25, 2024, from https://www.aasavariclinic.com/latest-update/heart-failure-is-a-m/15

Hypertrophic Cardiomyopathy Center | Cleveland Clinic. (n.d.). Retrieved March 25, 2024, from https://my.clevelandclinic.org/departments/heart/depts/hypertrophic-cardiomyopathy

Hypertrophic cardiomyopathy: Who has an inherited risk? (2016, July 12). Harvard Health. https://www.health.harvard.edu/heart-health/hypertrophic-cardiomyopathy-who-has-an-inherited-risk

Ireland, C. G., & Ho, C. Y. (2024). Genetic Testing in Hypertrophic Cardiomyopathy. *American Journal of Cardiology*, *212*, S4–S13. https://doi.org/10.1016/j.amjcard.2023.10.032

Irving, M., Piazzesi, G., Lucii, L., Sun, Y.-B., Harford, J. J., Dobbie, I. M., Ferenczi, M. A., Reconditi, M., & Lombardi, V. (2000). Conformation of the myosin motor during force generation in skeletal muscle. *Nature Structural Biology*, *7*(6), 482–485. https://doi.org/10.1038/75890

Ishikawa, R. (2007). Actin, Actin-binding Proteins and Myosins in Nervous System. In A. Lajtha & N. Banik (Eds.), *Handbook of Neurochemistry and Molecular Neurobiology: Neural Protein Metabolism and Function* (pp. 223–242). Springer US. https://doi.org/10.1007/978-0-387-30379-6_6

Itakura, S., Yamakawa, H., Toyoshima, Y. Y., Ishijima, A., Kojima, T., Harada, Y., Yanagida, T., Wakabayashi, T., & Sutoh, K. (1993). Force-Generating Domain of Myosin Motor. *Biochemical and Biophysical Research Communications*, *196*(3), 1504–1510. https://doi.org/10.1006/bbrc.1993.2422

Johnson, C. A., Walklate, J., Svicevic, M., Mijailovich, S. M., Vera, C., Karabina, A., Leinwand, L. A., & Geeves, M. A. (2019). The ATPase cycle of human muscle myosin II isoforms: Adaptation of a single mechanochemical cycle for different physiological roles. *The Journal of Biological Chemistry*, *294*(39), 14267–14278. https://doi.org/10.1074/jbc.RA119.009825

Kad, N. M., Kim, S., Warshaw, D. M., VanBuren, P., & Baker, J. E. (2005). Single-myosin crossbridge interactions with actin filaments regulated by troponin-tropomyosin. *Proceedings of the National Academy of Sciences*, *102*(47), 16990–16995.

Kawana, M., Spudich, J. A., & Ruppel, K. M. (2022). Hypertrophic cardiomyopathy: Mutations to mechanisms to therapies. *Frontiers in Physiology*, *13*. https://doi.org/10.3389/fphys.2022.975076

Kaya, M., & Higuchi, H. (2010). Nonlinear elasticity and an 8-nm working stroke of single myosin molecules in myofilaments. *Science (New York, N.Y.)*, *329*(5992), 686–689. https://doi.org/10.1126/science.1191484

Kaya, M., Tani, Y., Washio, T., Hisada, T., & Higuchi, H. (2017). Coordinated force generation of skeletal myosins in myofilaments through motor coupling. *Nature Communications*, *8*, 16036. https://doi.org/10.1038/ncomms16036

Kitamura, K., Tokunaga, M., Iwane, A. H., & Yanagida, T. (1999). A single myosin head moves along an actin filament with regular steps of 5.3 nanometres. *Nature*, *397*(6715), 129–134. https://doi.org/10.1038/16403

KOHAMA, K. (2016). Calcium inhibition as an intracellular signal for actin–myosin interaction. *Proceedings of the Japan Academy. Series B, Physical and Biological Sciences*, *92*(10), 478–498. https://doi.org/10.2183/pjab.92.478

Korn, E. D. (2000). Coevolution of head, neck, and tail domains of myosin heavy chains. *Proceedings of the National Academy of Sciences of the United States of America*, *97*(23), 12559–12564.

Kruppa, A. J., & Buss, F. (2021). Motor proteins at the mitochondria–cytoskeleton interface. *Journal of Cell Science*, *134*(7), jcs226084. https://doi.org/10.1242/jcs.226084

Kuo, S. C., & Sheetz, M. P. (1993). Force of single kinesin molecules measured with optical tweezers. *Science (New York, N.Y.)*, *260*(5105), 232–234. https://doi.org/10.1126/science.8469975

Liew, C.-C., & Dzau, V. J. (2004). Molecular genetics and genomics of heart failure. *Nature Reviews Genetics*, *5*(11), 811–825. https://doi.org/10.1038/nrg1470

Liu, L. C. Y. (n.d.). *Novel Therapies in Heart Failure*.

Lőrinczy, D., & Belagyi, J. (2000). Functional and structural differences in skeletal and cardiac myosins. A molecular dynamic approach. *Thermochimica Acta*, *343*(1), 27–33. https://doi.org/10.1016/S0040-6031(99)00361-5

Malik, F. I., Hartman, J. J., Elias, K. A., Morgan, B. P., Rodriguez, H., Brejc, K., Anderson, R. L., Sueoka, S. H., Lee, K. H., Finer, J. T., Sakowicz, R., Baliga, R., Cox, D. R., Garard, M., Godinez, G., Kawas, R., Kraynack, E., Lenzi, D., Lu, P. P., … Morgans, D. J. (2011). Cardiac myosin activation: A potential therapeutic approach for systolic heart failure. *Science (New York, N.Y.)*, *331*(6023), 1439–1443. https://doi.org/10.1126/science.1200113

Maron, B. J., & Maron, M. S. (2013). Hypertrophic cardiomyopathy. *Lancet (London, England)*,

381(9862), 242–255. https://doi.org/10.1016/S0140-6736(12)60397-3

Matusovsky, O. S., Månsson, A., & Rassier, D. E. (2023). Cooperativity of myosin II motors in the non-regulated and regulated thin filaments investigated with high-speed AFM. *Journal of General Physiology*, *155*(3), e202213190. https://doi.org/10.1085/jgp.202213190

McNamara, J. W., Li, A., dos Remedios, C. G., & Cooke, R. (2014). The role of super-relaxed myosin in skeletal and cardiac muscle. *Biophysical Reviews*, *7*(1), 5–14. https://doi.org/10.1007/s12551-014-0151-5

Means, A. R. (1988). Molecular Mechanisms of Action of Calmodulin. In J. H. Clark (Ed.), *Proceedings of the 1987 Laurentian Hormone Conference* (Vol. 44, pp. 223–262). Academic Press. https://doi.org/10.1016/B978-0-12-571144-9.50012-0

Mogilner, A. (2002). Mechanics of Motor Proteins and the Cytoskeleton. *Physics Today*, *55*(3), 63–64. https://doi.org/10.1063/1.1472396

Moraczewska, J., Sliwińska, M., & Redowicz, M. J. (2012). [Calcium ions in the regulation of acto-myosin interactions]. *Postepy Biochemii*, *58*(4), 437–451.

Morgan, B. P., Muci, A., Lu, P.-P., Qian, X., Tochimoto, T., Smith, W. W., Garard, M., Kraynack, E., Collibee, S., Suehiro, I., Tomasi, A., Valdez, S. C., Wang, W., Jiang, H., Hartman, J., Rodriguez, H. M., Kawas, R., Sylvester, S., Elias, K. A., … Morgans, D. J. (2010). Discovery of omecamtiv mecarbil the first, selective, small molecule activator of cardiac Myosin. *ACS Medicinal Chemistry Letters*, *1*(9), 472–477. https://doi.org/10.1021/ml100138q

Murphy, C. T., Rock, R. S., & Spudich, J. A. (2001). A myosin II mutation uncouples ATPase activity from motility and shortens step size. *Nature Cell Biology*, *3*(3), 311–315. https://doi.org/10.1038/35060110

Murphy, R. A., Walker, J. S., & Strauss, J. D. (1997). Myosin Isoforms and Functional Diversity in Vertebrate Smooth Muscle. *Comparative Biochemistry and Physiology Part B: Biochemistry and Molecular Biology*, *117*(1), 51–60. https://doi.org/10.1016/S0305-0491(96)00314-8

Myung, S.-K., Kim, H.-B., Lee, Y.-J., Choi, Y.-J., & Oh, S.-W. (2021). Calcium Supplements and Risk of Cardiovascular Disease: A Meta-Analysis of Clinical Trials. *Nutrients*, *13*(2), 368. https://doi.org/10.3390/nu13020368

Nagy, L., Kovács, Á., Bódi, B., Pásztor, E. T., Fülöp, G. Á., Tóth, A., Édes, I., & Papp, Z. (2015). The novel cardiac myosin activator omecamtiv mecarbil increases the calcium sensitivity of force production in isolated cardiomyocytes and skeletal muscle fibres of the rat. *British Journal of Pharmacology*, *172*(18), 4506–4518. https://doi.org/10.1111/bph.13235

Neuman, K. C., & Block, S. M. (2004). Optical trapping. *The Review of Scientific Instruments*, *75*(9), 2787–2809. https://doi.org/10.1063/1.1785844

Nikitina, L. V., Kopylova, G. V., Shchepkin, D. V., Nabiev, S. R., & Bershitsky, S. Y. (2015). Investigations of Molecular Mechanisms of Actin-Myosin Interactions in Cardiac Muscle. *Biochemistry. Biokhimiia*, *80*(13), 1748–1763. https://doi.org/10.1134/S0006297915130106

O'Connell, C. B., Tyska, M. J., & Mooseker, M. S. (2007). Myosin at work: Motor adaptations for a variety of cellular functions. *Biochimica et Biophysica Acta (BBA) - Molecular Cell Research*, *1773*(5), 615–630. https://doi.org/10.1016/j.bbamcr.2006.06.012

Ojima, K. (2019). Myosin: Formation and maintenance of thick filaments. *Animal Science Journal = Nihon Chikusan Gakkaiho*, *90*(7), 801–807. https://doi.org/10.1111/asj.13226

Optical Trapping. (n.d.). Retrieved March 25, 2024, from

https://advlabs.aapt.org/items/detail.cfm?ID=13735

Parker, F., & Peckham, M. (2020). Disease mutations in striated muscle myosins. *Biophysical Reviews*, *12*(4), 887–894. https://doi.org/10.1007/s12551-020-00721-5

(PDF) Molecular Mechanism of Mg-ATPase Activity. (n.d.). Retrieved March 26, 2024, from https://www.researchgate.net/publication/270650202_Molecular_Mechanism_of_Mg-ATPase_Activity

Pérez-García, L., Selin, M., Ciarlo, A., Magazzù, A., Pesce, G., Sasso, A., Volpe, G., Pérez Castillo, I., & Arzola, A. V. (2023). Optimal calibration of optical tweezers with arbitrary integration time and sampling frequencies: A general framework [Invited]. *Biomedical Optics Express*, *14*(12), 6442–6469. https://doi.org/10.1364/BOE.495468

Pette, D., & Staron, R. S. (2000). Myosin isoforms, muscle fiber types, and transitions. *Microscopy Research and Technique*, *50*(6), 500–509. https://doi.org/10.1002/1097-0029(20000915)50:6<500::AID-JEMT7>3.0.CO;2-7

Piazzesi, G., Reconditi, M., Linari, M., Lucii, L., Bianco, P., Brunello, E., Decostre, V., Stewart, A., Gore, D. B., Irving, T. C., Irving, M., & Lombardi, V. (2007). Skeletal muscle performance determined by modulation of number of myosin motors rather than motor force or stroke size. *Cell*, *131*(4), 784–795. https://doi.org/10.1016/j.cell.2007.09.045

Planelles-Herrero, V. J., Hartman, J. J., Robert-Paganin, J., Malik, F. I., & Houdusse, A. (2017). Mechanistic and structural basis for activation of cardiac myosin force production by omecamtiv mecarbil. *Nature Communications*, *8*(1), 190. https://doi.org/10.1038/s41467-017-00176-5

Pollard, T. D. (2010). Mechanics of cytokinesis in eukaryotes. *Current Opinion in Cell Biology*, *22*(1), 50–56.

Porters versus rowers: A unified stochastic model of motor proteins. (1993). *The Journal of Cell Biology*, *121*(6), 1357–1368.

Rayment, I., Rypniewski, W. R., Schmidt-Bäse, K., Smith, R., Tomchick, D. R., Benning, M. M., Winkelmann, D. A., Wesenberg, G., & Holden, H. M. (1993). Three-dimensional structure of myosin subfragment-1: A molecular motor. *Science (New York, N.Y.)*, *261*(5117), 50–58. https://doi.org/10.1126/science.8316857

Reinemann, D. N., Norris, S. R., Ohi, R., & Lang, M. J. (2018). Processive Kinesin-14 HSET Exhibits Directional Flexibility Depending on Motor Traffic. *Current Biology*, *28*(14), 2356-2362.e5. https://doi.org/10.1016/j.cub.2018.06.055

Rice, A., & Fischer, R. (n.d.). *Calibration of Optical Tweezers*.

Roth, G. A., Mensah, G. A., Johnson, C. O., Addolorato, G., Ammirati, E., Baddour, L. M., Barengo, N. C., Beaton, A. Z., Benjamin, E. J., Benziger, C. P., Bonny, A., Brauer, M., Brodmann, M., Cahill, T. J., Carapetis, J., Catapano, A. L., Chugh, S. S., Cooper, L. T., Coresh, J., … Fuster, V. (2020). Global Burden of Cardiovascular Diseases and Risk Factors, 1990–2019. *Journal of the American College of Cardiology*, *76*(25), 2982–3021. https://doi.org/10.1016/j.jacc.2020.11.010

Ruegg, C., Veigel, C., Molloy, J. E., Schmitz, S., Sparrow, J. C., & Fink, R. H. A. (2002). Molecular motors: Force and movement generated by single myosin II molecules. *News in Physiological Sciences*, *17*, 213–218. https://doi.org/10.1152/nips.01389.2002

Rüegg, C., Veigel, C., Molloy, J. E., Schmitz, S., Sparrow, J. C., & Fink, R. H. A. (2002). Molecular motors: Force and movement generated by single myosin II molecules. *News in Physiological Sciences: An International Journal of Physiology Produced Jointly by the International Union of Physiological Sciences and the American Physiological Society*, *17*,

213–218. https://doi.org/10.1152/nips.01389.2002

Schirber, M. (2018). Nobel Prize—Lasers as Tools. *Physics*, *11*, 100. https://doi.org/10.1103/PhysRevLett.24.156

Shaevitz, J. (2006). *A Practical Guide to Optical Trapping*. https://www.semanticscholar.org/paper/A-Practical-Guide-to-Optical-Trapping-Shaevitz/d28a1af8ba1550ed69c28a13a385be58765bb867

Sitbon, Y. H., Yadav, S., Kazmierczak, K., & Cordary, D. S. (2020). Insights into myosin regulatory and essential light chains: A focus on their roles in cardiac and skeletal muscle function, development and disease. *Journal of Muscle Research and Cell Motility*, *41*(4), 313–327. https://doi.org/10.1007/s10974-019-09517-x

Sliding Filament Theory, Sarcomere, Muscle Contraction, Myosin | Learn Science at Scitable. (n.d.). Retrieved March 26, 2024, from https://www.nature.com/scitable/topicpage/the-sliding-filament-theory-of-muscle-contraction-14567666/

Spirito, P., Seidman, C. E., McKenna, W. J., & Maron, B. J. (1997). The management of hypertrophic cardiomyopathy. *The New England Journal of Medicine*, *336*(11), 775–785. https://doi.org/10.1056/NEJM199703133361107

Spudich, J. A. (2001). The myosin swinging cross-bridge model. *Nature Reviews Molecular Cell Biology*, *2*(5), 387–392.

Spudich, J. A., Finer, J., Simmons, B., Ruppel, K., Patterson, B., & Uyeda, T. (1995). Myosin structure and function. *Cold Spring Harbor Symposia on Quantitative Biology*, *60*, 783–791.

Spudich, J. A., Rice, S. E., Rock, R. S., Purcell, T. J., & Warrick, H. M. (2011). Optical Traps to Study Properties of Molecular Motors. *Cold Spring Harbor Protocols*, *2011*(11), 1305–1318. https://doi.org/10.1101/pdb.top066662

Squire, J. (2019). Special Issue: The Actin-Myosin Interaction in Muscle: Background and Overview. *International Journal of Molecular Sciences*, *20*(22), 5715. https://doi.org/10.3390/ijms20225715

Stevens, H. M., Azzam, O. A., & Reinemann, D. N. (2024). Effects of a cardiac myosin activator on actin-myosin ensemble coordination. *Biophysical Journal*, *123*(3), 540a. https://doi.org/10.1016/j.bpj.2023.11.3268

Stewart, T. J., Jackson, D. R., Smith, R. D., Shannon, S. F., Cremo, C. R., & Baker, J. E. (2013). Actin Sliding Velocities are Influenced by the Driving Forces of Actin-Myosin Binding. *Cellular and Molecular Bioengineering*, *6*(1), 26–37. https://doi.org/10.1007/s12195-013-0274-y

Stewart, T. J., Murthy, V., Dugan, S. P., & Baker, J. E. (2021a). Velocity of myosin-based actin sliding depends on attachment and detachment kinetics and reaches a maximum when myosin-binding sites on actin saturate. *The Journal of Biological Chemistry*, *297*(5), 101178. https://doi.org/10.1016/j.jbc.2021.101178

Stewart, T. J., Murthy, V., Dugan, S. P., & Baker, J. E. (2021b). Velocity of myosin-based actin sliding depends on attachment and detachment kinetics and reaches a maximum when myosin-binding sites on actin saturate. *The Journal of Biological Chemistry*, *297*(5), 101178. https://doi.org/10.1016/j.jbc.2021.101178

Stilgoe, A. B., Armstrong, D. J., & Rubinsztein-Dunlop, H. (2021). Enhanced Signal-to-Noise and Fast Calibration of Optical Tweezers Using Single Trapping Events. *Micromachines*, *12*(5), 570. https://doi.org/10.3390/mi12050570

Sudden death in young people: Heart problems often blamed—Mayo Clinic. (n.d.). Retrieved March 25, 2024, from https://www.mayoclinic.org/diseases-conditions/sudden-cardiac-

arrest/in-depth/sudden-death/art-20047571

Sung, J., Nag, S., Mortensen, K. I., Vestergaard, C. L., Sutton, S., Ruppel, K., Flyvbjerg, H., & Spudich, J. A. (2015). Harmonic force spectroscopy measures load-dependent kinetics of individual human β-cardiac myosin molecules. *Nature Communications*, *6*, 7931. https://doi.org/10.1038/ncomms8931

Svoboda, K., & Block, S. M. (1994a). Biological applications of optical forces. *Annual Review of Biophysics and Biomolecular Structure*, *23*, 247–285. https://doi.org/10.1146/annurev.bb.23.060194.001335

Svoboda, K., & Block, S. M. (1994b). Force and velocity measured for single kinesin molecules. *Cell*, *77*(5), 773–784. https://doi.org/10.1016/0092-8674(94)90060-4

Swenson, A. M., Tang, W., Blair, C. A., Fetrow, C. M., Unrath, W. C., Previs, M. J., Campbell, K. S., & Yengo, C. M. (2017). Omecamtiv Mecarbil Enhances the Duty Ratio of Human β-Cardiac Myosin Resulting in Increased Calcium Sensitivity and Slowed Force Development in Cardiac Muscle*. *Journal of Biological Chemistry*, *292*(9), 3768–3778. https://doi.org/10.1074/jbc.M116.748780

Syamaladevi, D. P., Spudich, J. A., & Sowdhamini, R. (2012). Structural and Functional Insights on the Myosin Superfamily. *Bioinformatics and Biology Insights*, *6*, 11–21. https://doi.org/10.4137/BBI.S8451

Tang, W., Ge, J., Unrath, W. C., Desetty, R., & Yengo, C. M. (2021). Cardiomyopathy mutations impact the actin-activated power stroke of human cardiac myosin. *Biophysical Journal*, *120*(11), 2222–2236. https://doi.org/10.1016/j.bpj.2021.04.007

Teekakirikul, P., Zhu, W., Huang, H. C., & Fung, E. (2019). Hypertrophic Cardiomyopathy: An Overview of Genetics and Management. *Biomolecules*, *9*(12), 878.

https://doi.org/10.3390/biom9120878

Teerlink, J. R., Diaz, R., Felker, G. M., McMurray, J. J. V., Metra, M., Solomon, S. D., Adams, K. F., Anand, I., Arias-Mendoza, A., Biering-Sørensen, T., Böhm, M., Bonderman, D., Cleland, J. G. F., Corbalan, R., Crespo-Leiro, M. G., Dahlström, U., Echeverria Correa, L. E., Fang, J. C., Filippatos, G., … GALACTIC-HF Investigators. (2020). Omecamtiv mecarbil in chronic heart failure with reduced ejection fraction: GALACTIC-HF baseline characteristics and comparison with contemporary clinical trials. *European Journal of Heart Failure*, *22*(11), 2160–2171. https://doi.org/10.1002/ejhf.2015

Teerlink, J. R., Diaz, R., Felker, G. M., McMurray, J. J. V., Metra, M., Solomon, S. D., Adams, K. F., Anand, I., Arias-Mendoza, A., Biering-Sørensen, T., Böhm, M., Bonderman, D., Cleland, J. G. F., Corbalan, R., Crespo-Leiro, M. G., Dahlström, U., Echeverria, L. E., Fang, J. C., Filippatos, G., … Kurtz, C. E. (2021). Cardiac Myosin Activation with Omecamtiv Mecarbil in Systolic Heart Failure. *New England Journal of Medicine*, *384*(2), 105–116. https://doi.org/10.1056/NEJMoa2025797

Teerlink, J. R., Metra, M., Zacà, V., Sabbah, H. N., Cotter, G., Gheorghiade, M., & Cas, L. D. (2009). Agents with inotropic properties for the management of acute heart failure syndromes. Traditional agents and beyond. *Heart Failure Reviews*, *14*(4), 243–253. https://doi.org/10.1007/s10741-009-9153-y

The myosin II coiled-coil domain atomic structure in its native environment | PNAS. (n.d.). Retrieved March 26, 2024, from https://www.pnas.org/doi/10.1073/pnas.2024151118

Thomas, D. D., & Roopnarine, O. (2002). An Overview of the Actin-Myosin Interaction. *Results and Problems in Cell Differentiation*, *36*, 1–5. https://doi.org/10.1007/978-3-540-46558-4_1

Thoresen, T., Lenz, M., & Gardel, M. L. (2013). Thick filament length and isoform composition

determine self-organized contractile units in actomyosin bundles. *Biophysical Journal*, *104*(3), 655–665. https://doi.org/10.1016/j.bpj.2012.12.042

Tsutsui, H., Kinugawa, S., & Matsushima, S. (2011). Oxidative stress and heart failure. *American Journal of Physiology. Heart and Circulatory Physiology*, *301*(6), H2181-2190. https://doi.org/10.1152/ajpheart.00554.2011

Tu, M. K., Levin, J. B., Hamilton, A. M., & Borodinsky, L. N. (2016). Calcium signaling in skeletal muscle development, maintenance and regeneration. *Cell Calcium*, *59*(2–3), 91–97. https://doi.org/10.1016/j.ceca.2016.02.005

Types of heart failure. (2018). In *InformedHealth.org [Internet]*. Institute for Quality and Efficiency in Health Care (IQWiG). https://www.ncbi.nlm.nih.gov/books/NBK481485/

Unconventional Myosins: How Regulation Meets Function—PMC. (n.d.). Retrieved March 26, 2024, from https://www.ncbi.nlm.nih.gov/pmc/articles/PMC6981383/

Viswanathan, M. C., Schmidt, W., Franz, P., Rynkiewicz, M. J., Newhard, C. S., Madan, A., Lehman, W., Swank, D. M., Preller, M., & Cammarato, A. (2020). A role for actin flexibility in thin filament-mediated contractile regulation and myopathy. *Nature Communications*, *11*(1), 2417. https://doi.org/10.1038/s41467-020-15922-5

Wagner, P. D., & Giniger, E. (1981). Calcium-sensitive binding of heavy meromyosin to regulated actin in the presence of ATP. *Journal of Biological Chemistry*, *256*(24), 12647–12650. https://doi.org/10.1016/S0021-9258(18)42941-9

Wagoner, J. A., & Dill, K. A. (2021). Evolution of mechanical cooperativity among myosin II motors. *Proceedings of the National Academy of Sciences of the United States of America*, *118*(20), e2101871118. https://doi.org/10.1073/pnas.2101871118

Wakabayashi, T., & Ebashi, S. (1968). Reversible change in physical state of troponin induced

by calcium ion. *Journal of Biochemistry*, *64*(5), 731–732. https://doi.org/10.1093/oxfordjournals.jbchem.a128955

Walcott, S., Fagnant, P. M., Trybus, K. M., & Warshaw, D. M. (2009). Smooth Muscle Heavy Meromyosin Phosphorylated on One of Its Two Heads Supports Force and Motion *. *Journal of Biological Chemistry*, *284*(27), 18244–18251. https://doi.org/10.1074/jbc.M109.003293

Walcott, S., Warshaw, D. M., & Debold, E. P. (2012). Mechanical coupling between myosin molecules causes differences between ensemble and single-molecule measurements. *Biophysical Journal*, *103*(3), 501–510. https://doi.org/10.1016/j.bpj.2012.06.031

Watanabe, S., Watanabe, T. M., Sato, O., Awata, J., Homma, K., Umeki, N., Higuchi, H., Ikebe, R., & Ikebe, M. (2008). Human Myosin Vc Is a Low Duty Ratio Nonprocessive Motor. *The Journal of Biological Chemistry*, *283*(16), 10581–10592. https://doi.org/10.1074/jbc.M707657200

Wegner, A. (1976). Head to tail polymerization of actin. *Journal of Molecular Biology*, *108*(1), 139–150. https://doi.org/10.1016/S0022-2836(76)80100-3

Winkelmann, E. R., Dallazen, F., Bronzatti, A. B. S., Lorenzoni, J. C. W., & Windmöller, P. (2015). Analysis of steps adapted protocol in cardiac rehabilitation in the hospital phase. *Revista Brasileira De Cirurgia Cardiovascular: Orgao Oficial Da Sociedade Brasileira De Cirurgia Cardiovascular*, *30*(1), 40–48. https://doi.org/10.5935/1678-9741.20140048

Woerdemann, M. (2012). Introduction to Optical Trapping. In M. Wördemann (Ed.), *Structured Light Fields: Applications in Optical Trapping, Manipulation, and Organisation* (pp. 5–26). Springer. https://doi.org/10.1007/978-3-642-29323-8_2

Woo, A., Rakowski, H., Liew, J. C., Zhao, M.-S., Liew, C.-C., Parker, T. G., Zeller, M., Wigle, E. D., & Sole, M. J. (2003). Mutations of the β myosin heavy chain gene in hypertrophic

cardiomyopathy: Critical functional sites determine prognosis. *Heart*, *89*(10), 1179–1185.

Woody, M. S., Greenberg, M. J., Barua, B., Winkelmann, D. A., Goldman, Y. E., & Ostap, E. M. (2018). Positive cardiac inotrope omecamtiv mecarbil activates muscle despite suppressing the myosin working stroke. *Nature Communications*, *9*(1), 3838. https://doi.org/10.1038/s41467-018-06193-2

Yanagida, T., Esaki, S., Iwane, A. H., Inoue, Y., Ishijima, A., Kitamura, K., Tanaka, H., & Tokunaga, M. (2000). Single-motor mechanics and models of the myosin motor. *Philosophical Transactions of the Royal Society of London. Series B, Biological Sciences*, *355*(1396), 441–447. https://doi.org/10.1098/rstb.2000.0585

Yang, C.-F., & Tsai, W.-C. (2021). Calmodulin: The switch button of calcium signaling. *Tzu-Chi Medical Journal*, *34*(1), 15–22. https://doi.org/10.4103/tcmj.tcmj_285_20

Zaiser, E., Sehnert, A. J., Duenas, A., Saberi, S., Brookes, E., & Reaney, M. (2020). Patient experiences with hypertrophic cardiomyopathy: A conceptual model of symptoms and impacts on quality of life. *Journal of Patient-Reported Outcomes*, *4*(1), 102. https://doi.org/10.1186/s41687-020-00269-8

Zhang, Y., Fu, W., Liu, D., Chen, X., & Zhou, P. (2024). Deciphering the thick filaments assembly behavior of myosin as affected by enzymatic deamidation. *Food Chemistry*, *433*, 137385. https://doi.org/10.1016/j.foodchem.2023.137385

β-Cardiac myosin hypertrophic cardiomyopathy mutations release sequestered heads and increase enzymatic activity | Nature Communications. (n.d.). Retrieved March 25, 2024, from https://www.nature.com/articles/s41467-019-10555-9

CHAPTER 2

MEASURING FORCE GENERATION WITHIN RECONSTITUTED MICROTUBULE BUNDLE ASSEMBLIES USING OPTICAL TWEEZERS

*This chapter is adapted from Omayma Al Azzam, Cameron Lee Trussell, Dana N. Reinemann, "Measuring force generation within reconstituted microtubule bundle assemblies using optical tweezers". Cytoskeleton, 78(3), 111-125. Reproduced with permission from John Wiley and Sons, license number: 5734241007474

2.1 Summary

Kinesins and microtubule associated proteins (MAPs) are critical to sustain life, facilitating cargo transport, cell division, and motility. To interrogate the mechanistic underpinnings of their function, these microtubule-based motors and proteins have been studied extensively at the single molecule level. However, a long-standing issue in the single molecule biophysics field has been how to investigate motors and associated proteins within a physiologically relevant environment in vitro. While the one motor/one filament orientation of a traditional optical trapping assay has revolutionized our knowledge of motor protein mechanics, this reductionist geometry does not reflect the structural hierarchy in which many motors work within the cellular environment. Here, we review approaches that combine the precision of optical tweezers with reconstituted ensemble systems of microtubules, MAPs, and kinesins to understand how each of these unique elements work together to perform large scale cellular tasks, such as but not limited

to building the mitotic spindle. Not only did these studies develop novel techniques forinvestigating motor proteins in vitro, but they also illuminate ensemble filament and motor synergy that helps bridge the mechanistic knowledge gap between previous single molecule and cell level studies.

2.2 Introduction

A Microtubule (MT)-based motors and associated binding proteins are essential players in large scale cellular tasks, such as mitosis, cargo transport, and cell motility (Hirokawa, Noda, Tanaka, & Niwa, 2009). While the kinesin family of motors has a conserved ATPase domain, their remaining structural features distinguish each motor's unique function; these structure–function relationships have been reviewed extensively (Block, 2007; L. S. Goldstein, 2001; L. S. B. Goldstein & Philp, 1999; Gross, 2004; Hirokawa, 1998; Hirokawa *et al.*, 2009; Hirokawa & Takemura, 2004; Jon Kull & Endow, 2013; Kolomeisky & Fisher, 2007; Marx, Hoenger, & Mandelkow, 2009; Miki, Okada, & Hirokawa, 2005; Rath & Kozielski, 2012; Vale & Fletterick, 1997; Wordeman, 2010). A defining characteristic of kinesins that is highly influenced by its structure is force generation capacity, which yields the family-specific functions of kinesins. For instance, the terms “porters” and “rowers” have been used to describe highly processive kinesin-1 and less processive mitotic kinesins, respectively, where porters carry intracellular cargo over long distances and rowers work together to remain in contact with their track to facilitate sliding (Figure 1a; Chowdhury, 2014; Leibler & Huse, 1993). However, as we continue to attain higher resolution structures and force generation profiles of motors using both experimental methods and computational approaches, we realize that the boundaries of these two motor classes can become blurred, as

with mitotic kinesin-12 Kif15 and kinesin-14 HSET that exhibit a combination of nonprocessive and processive properties (Reinemann *et al.*, 2017; Reinemann, Norris, Ohi, & Lang, 2018). Kinesins, such as these that are not true porters or rowers, work between bundled MTs, and warrant further study to understand the nuanced influence of their structural features on cyto- skeletal function. However, the question arises regarding how to approach, execute, and analyze such studies of "nontraditional" kinesins that work in teams. Within the last decade, innovative optical trapping (OT) methodologies have emerged that have begun to address long-standing issues within the single molecule (SM) biophysics field: (1) how to study these nontraditional motors and (2) how to investigate force generation by motor teams within a physiologically relevant environment. Here, we review studies of reconstituted ensemble systems of multiple MTs, kinesins, and microtubule associated proteins (MAPs) using OT whose goal is to better understand how these proteins work together at the molecular level to perform large scale cellular tasks, such as building the mitotic spindle. SM techniques, such as fluorescence and OT, have revolutionized the way we approach interrogating and understanding the force generating properties of motor proteins (Ashkin, 1992; Duke, 1999; Finer, Simmons, & Spudich, 1994; Kitamura, Tokunaga, Iwane, & Yanagida, 1999; Kuo & Sheetz, 1993; Mehta *et al.*, 1999; Molloy, Burns, Kendrick-Jones, *et al.*, 1995; Molloy, Burns, Sparrow, *et al.*, 1995; Palliter, Tyska, Haeberle, & Alpert, 2000; Ruegg *et al.*, 2002; Svoboda & Block, 1994; Svoboda, Schmidt, Schnapp, & Block, 1993; Takagi, Homsher, Goldman, & Shuman, 2006; Tyska *et al.*, 1999, 2000; Matthew J. Tyska & Warshaw, 2002; Veigel, Molloy, Schmitz, & Kendrick-Jones, 2003). Measurements yield information overshadowed in bulk experiments, such as bond lifetimes, dissociation kinetics, step sizes, dwell times, and stall forces, among others, with

piconewton force and nanometer displacement resolution. (Neuman & Block, 2004) In OT assays, a micron-sized bead functions as a handle to examine SMs and is trapped by a tightly focused laser beam which acts as a Hookean spring. Displacements are then translated into force measurements via trap stiffness calibrations. (Ashkin, 1992; Neuman & Block, 2004) OT has been used to investigate both porter and rower type motors, but certain assay orientations are limited on the mechanistic information that can be gained due to the nature of the interrogated motor's motility. Therefore, to understand the capabilities and limitations of motor-based OT approaches, we need to review the evolution of these motor-filament assays and how they have been adapted to study single motors, motor teams, and motors across the processivity spectrum.

2.3 Historical Overview of Motors Assay

2.3.1 Single Molecule Assays

The evolution of the multi-motor, multi-filament OT experiment is founded on the realization that the motility properties of motors, for instance whether they are porters or rowers, will dictate the necessary OT geometry required for productive study. Therefore, it is important to review how kinesin OT assays have transformed over the years. The earliest measurements of the classical porter kinesin- 1's force generation using optical tweezers came from the Sheetz and Block labs. Kuo and Sheetz used OT to measure force produced through a streptavidin coated bead bound to a biotinylated MT and was displaced by a single kinesin attached to a coverslip (Figure 2.1; Kuo & Sheetz, 1993). Svoboda *et al.* reversed the orientation, where the MT was bound to a coverslip and a kinesin motor was attached to a trapped bead (Figure 2.1b; Svoboda *et al.,* 1993). In the presence of ATP, the kinesin

attached to the bead would “walk” from the trap center along the MT track, concomitantly stretching the trap spring and increasing force. Both assay orientations have been adapted and customized to study kinesins and other molecular motors, especially the latter bead with bound motor orientation.

Problems arise when investigating rowers or motors that do not fit either motility category as SMs. Here, rower motors have low or no processivity, or ability to take several steps along its track without dissociating, which would make trapping measurements using the bead with bound motor geometry challenging at best. However, the concept of a motor as processive and nonprocessive should not necessarily be a rigid classification either. Some motors, such as mitotic kinesin-5, kinesin-12, and kinesin-14, exhibit hybrid motility properties. Kinesin-5 and kinesin-14 have been previously classified as nonprocessive at the SM level but are able to slide MTs within the spindle(Crevel, Lockhart, & Cross, 1997; DeCastro, Ho, & Stewart, 1999; Foster & Gilbert, 2000); yet, additional studies have demonstrated that single Eg5 and HSET motors can take multiple steps along a MT before dissociating.(Reinemann *et al.*, 2018; Shimamoto, Forth, & Kapoor, 2015; Valentine, Fordyce, Krzysiak, Gilbert, & Block, 2006) Those motility properties, including maximum generated force, attachment time, and stepping coordination, change even further when working in motor teams.(Furuta *et al.*, 2013; Furuta & Toyoshima, 2008; Reinemann *et al.*, 2018, 2017; Shimamoto *et al.*, 2015) Therefore, processivity should be viewed as a spectrum, where classical porters would be on the high end, and classical rowers would be on the low end. Understanding where the motor may lie on that spectrum will aid in justifying an analytical technique or assay geometry that will thus provide informative behavioral and mechanistic data.

To combat this using OT, one approach is to bind multiple motors to a bead to interrogate whether SM versus team motility differs (Figure 2.1c). Motors can be bound nonspecifically using a high concentration of motor during an incubation step. Recently, more defined geometries have been implemented using nanotools like DNA origami to bind motors at user-defined intervals to investigate how this spacing affects team motility (Furuta *et al.,* 2013). On the other hand, in order to study rower motors at the SM level, a seminal study by Finer *et al.* (1994) employed OT using a different assay orientation. Muscle myosin II is a classic example of a rower motor protein that works in teams to contract actin filaments (AFs) within a sarcomere but is non- processive at the SM level. Myosin II detaches from the AF after every stroke, making the conventional motor-bound bead OT assay approach ineffective. Therefore, Finer and co-works developed a new experimental geometry where a "three-bead assay" or "dumbbell assay" was utilized (Figure 2.1d; Finer *et al.,* 1994). Here, two laser traps are used to suspend an AF over myosin motors sparsely distributed on a bead stuck to the coverslip surface. By immobilizing the non- processive motor on a bead, myosin will not have the opportunity to diffuse away after it has completed its power stroke, and the AF will still be within crossbridge-forming range for the next ATP cycle. Force generation by the motor is then recorded through displacements of the AF within the trap. Discrete power strokes by myosin were measured to produce around 11 nm of movement and 3–4 pN of force per ATP hydrolysis. (Finer *et al.,* 1994).

Variations on the three-bead SM experiment have been extended to other molecular motors, including nonconventional kinesins, in order to accommodate their lack of traditional processivity (Duke, 1999; Kitamura *et al.,* 1999; Mehta *et al.,* 1999; Molloy, Burns, Kendrick-Jones, *et al.,* 1995; Molloy, Burns, Sparrow, *et al.,* 1995; Takagi *et al.,* 2006; M. J.

Tyska *et al.,* 2000; M J Tyska *et al.,* 1999; Veigel *et al.,* 2003). However, regardless of orientation, most OT motor investigations to date involve a single motor interacting with a single filament. While these studies have revolutionized our under- standing of molecular motor mechanics, the reductionist single motor/single filament geometry does not necessarily recapitulate the architecture or complexity of the in vivo environment in which the motor functions. For example, mitotic kinesins work together as multi-motor teams between two MTs within the bipolar spindle.

A prevalent challenge for biophysicists is reconstituting a motor- filament environment that reflects physiological function by having enough systematic components to obtain specific and meaningful data but not so many that the system is too complicated to study as one entity. (Dogterom & Koenderink, 2019; Elting & Spudich, 2012) To combat this, other in vitro assay orientations, involving OT and not, have been explored. Assay alterations include adding multiple motors, multiple filaments, or a combination of both.

2.3.2 Multi-Motor Assays

An example of incorporating multiple motors in vitro is the “gliding fil- ament” assay, which is a multi-motor variant of the Kuo and Sheetz study mentioned earlier. Here, multiple motors are bound to a cover- slip surface, and addition of filaments in the presence of ATP results in their sliding, akin to crowd surfing at a concert. This orientation for kinesin and MTs has been probed by both total internal reflection fluorescence (TIRF) microscopy (standard practice in many motor studies) and OT assays (Fallesen, Roostalu, Duellberg, Pruessner, & Surrey, 2017; Reinemann *et al.,* 2017), where the trapped bead is attached to the gliding filament, and force generation is measured (Figure 2.1e). In addition, multiple

filaments have been assembled in the form of three-dimensional microtubule intersections using holo- graphic OT (Figure 2.1f) and bundles, or filament-motor-filament "sandwiches," using conventional OT and TIRF microscopy (Figure 1g; Bergman, Osunbayo, & Vershinin, 2015; Bergman *et al.*, 2018). In the latter case, through staged introduction and incubation steps, filaments are adhered to the coverslip surface (the substrate filament), and subsequently, motors bind the substrate filament and crosslink the top or cargo filament. In the context of kinesin and MTs, fluorescence bundle assays have been assembled and investigated to under- stand the motility and crosslinking effects of both mitotic kinesins and MAPs (Braun, Drummond, Cross, & Mcainsh, 2009; Braun *et al.*, 2011, 2017; Britto *et al.*, 2016; Dogterom & Surrey, 2013; Drechsler & Mcainsh, 2016; Drechsler, McHugh, Singleton, Carter, & McAinsh, 2014; Fink *et al.*, 2009; Forth & Kapoor, 2017; Furuta *et al.*, 2013; Gerson-Gurwitz *et al.*, 2011; Gicking, Qiu, & Hancock, 2018; Hentrich & Surrey, 2010; Hepperla *et al.*, 2014; Kapitein, Janson, *et al.*, 2008; Kapitein, Kwok, *et al.*, 2008; Kapitein *et al.*, 2005; Molodtsov *et al.*, 2016; Popchock *et al.*, 2017; Reinemann *et al.*, 2017; Roos, UμLer, Gräter, Surrey, & Spatz, 2005; Roostalu *et al.*, 2011; SturgiμL *et al.*, 2014; SturgiμL, Norris, Guo, & Ohi, 2016; Su *et al.*, 2013; Subramanian *et al.*, 2010; Tanenbaum, Vale, & McKenney, 2013; Tao *et al.*, 2006; van den Wildenberg *et al.*, 2008; Weinger, Qiu, & Yang, 2011; Wijeratne & Subramanian, 2018). These TIRF assays have revealed important insight into properties of motor ensembles, such as bundling propensity, velocity, and effects of filament architecture, such as bundle polarity. In complex environments like the mitotic spindle, microtubules are in both parallel and anti- parallel orientations, and activity in such environments reveals unique location-specific roles that motors play to build the spindle and balance forces. Behaviors of kinesin-MT bundles have also been investigated

computationally, especially to shed light on motor cooperativity that accomplishes force generation and thus cargo movement (Blackwell *et al.,* 2017; Chowdhury & Ghanti, 2020; Edellaier *et al.,* 2020; Kapoor, Hirst, Hentschel, Preibisch, & Reber, 2019; Lera- Ramirez & Nédélec, 2019; Prelogovic, Winters, Milas, Tolic, & Pavin, 2019; Sherin, Farwa, Sohail, Li, & Bég, 2018; Uçar & Lipowsky, 2019; Winters *et al.,* 2019; Zemel & Mogilner, 2009; Ziebert, Vershinin, Gross, & Aranson, 2009). Using this approach, the- orists and experimentalists are able to work together to reconcile to what degree motors are synergistically coupled and how their structural features facilitate the experimental results obtained.

Experiments that incorporate both MT architectural hierarchy and OT have unveiled new assay approaches and mechanistic information about kinesin and MAP ensembles (Figure 2.1h; Bodrug *et al.,* 2020; Fallesen *et al.*, 2017; Forth, Hsia, Shimamoto, & Kapoor, 2014; Gaska, Armstrong, Alfieri, & Forth, 2020; Laan, Husson, Munteanu, Kerssemakers, & Dogterom, 2008; Lansky *et al.*, 2015; Lüdecke, Seidel, Braun, & Diez, 2018; Reinemann *et al.*, 2018, 2017; Shimamoto *et al.,* 2015; Shimamoto & Kapoor, 2018). These experiments push the boundaries of the motor biophysics field by combining OT, which possesses the precision and resolution to study single motor mechanics, with a more physiologically relevant environment for motors that work in complex environments, like the mitotic spindle, and may not necessarily fit entirely in the “porter” or “rower” categories. Further, it is important to understand the construction of multi-motor assay geometry in order to be able to analyze the force generation of such geometries, the number of interacting motors, and how the force propagates throughout the system. This multi-motor, multi-filament approach allows for custom-building the local cytoskeletal environment through including staged

introduction and timely incubations, polarity marking, fluorescence protein labeling, probing protein ensembles of various sizes and composition, and incorporating multiple types of kinesins and MAPs. Here, we review such studies, analyze the techniques utilized to construct each OT-bundle assay, and what mechanistic information can be extracted in each case.

2.4 Probing Microtubule Bundle Forces in Microfabricated Devices

MTs can generate pushing and pulling forces without the assistance of motors or MAPs due to their constant switching between growing and shrinking states, referred to as dynamic instability (Mitchison & Kirschner, 1984). Individual MTs have been analyzed in vitro to evaluate- ate how force affects assembly dynamics, where growth velocity decreases and catastrophe rate increases as the force on the end of the MT increases (Dogterom & Yurke, 1997; Janson, De Dood, & Dogterom, 2003). However, MTs do not operate in isolation in vivo. Specifically, during mitosis, multi-filament bundles of kinetochore MTs are formed that are parallel in orientation and bind chromosomes (Walczak & Heald, 2008). Here, parallel refers to alignment of the MTs' plus and minus ends. As the chromosomes are initially bound and then pulled toward the spindle poles during anaphase, the MT bundles experience pushing and pulling forces, respectively, where dynamic instability is thought to contribute. Therefore, Laan *et al.* (2008) asked how much force a growing bundle of parallel MTs can generate. The authors used OT to track the dynamics of a MT bundle, where growing MTs polymerize tubulin and push against a microfabricated, rigid barrier (Figure 2.2a).

The authors used a time-shared optical tweezers set up that allowed them to measure

the forces and dynamics of MTs growing from an axoneme, which is naturally polarity aligned, against a wall. (Laan *et al.*, 2008) The time-shared "keyhole" trap allows one strong trap, or point trap, to hold the bead while multiple shallow traps form a line trap to limit the axoneme's movement. To perform the force measurements, a flow system was created that included microfabricated chambers made from clean coverslips using SU-8 negative tone photoresist to produce a 7 μm thick layer. After steps of baking and UV exposure, 7 μm high chambers of 40 x 80 μm separated by 20 μm wide walls were formed. Once incorporated into the flow system, a series of blocking steps were performed with agarose and BSA solutions. Then, axonemes and beads were added to the flow system, where a bead was trapped with the point trap, and an axoneme was captured with a line trap and stuck to the bead. The axoneme bound bead was then positioned close or pressed against one of the fabricated walls to keep the MTs short and prevent them from buckling (Figure 2.2b). Tubulin was added to the flow system to initiate MT growth, and force measurements by the bundle were measured by the trapped bead. Using this approach, Laan *et al.* (2008) measured force generated by the growing MT bundles and did so under a variety of nucleotide (GTP vs. GMPCPP) and tubulin concentration (10 and 25 μM) conditions (Figure 2.2c–e). In Figure 2.2c, force is measured as tubulin is incorporated into the MT bundles with a tubulin concentration of 25 μM in the presence of GTP. They were able to distinguish between plus and minus end growth due to plus ends growing faster and experiencing catastrophes. Traces were obtained from the polymerizing MTs pushing against the microfabricated wall and revealed that growing parallel MT bundle force generation is a linear addition of single MT maximum forces. As shown in Figure 2.2c, the authors observed the force generated by a single MT polymerizing and correlated that force to the maximum force generated when the all of the

MTs in the bundle were polymerizing together. As bundle force rate depends on polymerization rate, lowering the free tubulin concentration to 10 μM resulted in catastrophes occurring before maximum forces were reached (Figure 2.2d). Using GMPCPP instead of GTP to inhibit catastrophe restored the linear addition of individual MT forces (Figure 2.2e). Experiments in this paper were limited to a smaller than maximum force range due to the MT bundle construct getting stuck to the chamber wall. However, with further optimization, this approach could be utilized in conjunction with motor ensembles, such as dynein, that drive axoneme movement in systems like cilia and flagella, as well as using the time-shared OT to control larger and more extended synthetic MT-kinesin systems.

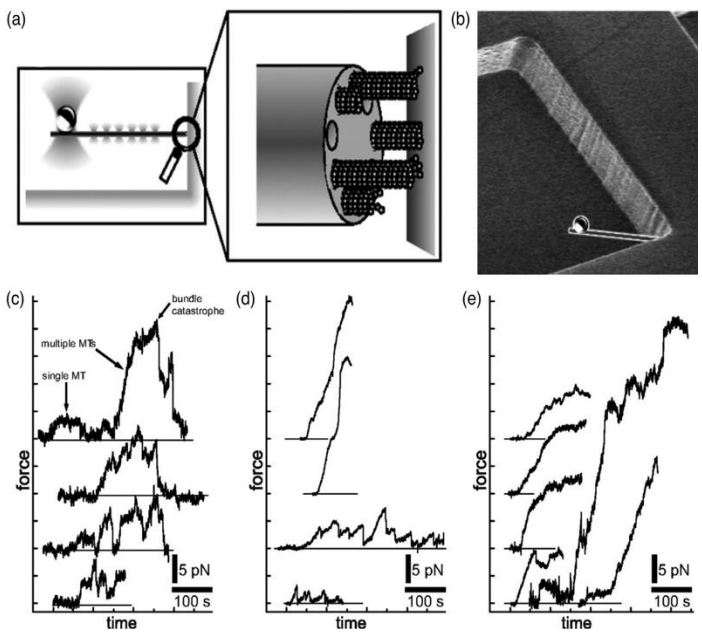

Figure 2.2: Force generation by growing MT bundles. (a) Assay setup of a MT bundle growing from an axoneme against a microfabricated wall. The axoneme bound bead is trapped in the strong point trap, and the time-shared line trap holds the MT bundle in place. (b) Scanning electron micrograph of a microchamber that is used as a rigid barrier. A schematic of the trapped bead and bundle is overlaid. (c) Force generation as a function of time of growing MTs in the axoneme bundle at a tubulin concentration of 25 μM in the presence of GTP. (d) Force traces of the growing MT bundle at a tubulin concentration of 10 μM. (e) Force traces at a tubulin concentration of 10 μM but in the presence of GMPCPP. Adapted from Laan *et al.* (2008), PNAS. Copyright 2008 National Academy of Sciences

2.5 Measuring MAP Mechanics in Microtubule Bundles

During the process of cell division, the cytoskeleton goes through many conformational changes that require mechanical force to accomplish the large rearrangements necessary for each phase, including formation of the mitotic spindle. (Walczak & Heald, 2008; Wordeman,

2010) There are two main categories of forces that con- tribute here, termed active and passive forces by Forth and Kapoor (2017). Active force is generated, in part, by assembly and dis- assembly mechanics of MTs with the aid of motor proteins and is essential for transporting cargos inside the cell during division, in addition to facilitating MT sliding to separate centrosomes and segregate chromosomes to form two daughter cells. For example, calculations based on the size and speed of chromosomes moving through a vis- cous environment suggest that it would require only approximately 0.1 pN to move chromosomes, but Nicklas showed that the spindle machinery can generate up to 700 pN before chromosome motion stalled (Forth & Kapoor, 2017; Nicklas, 1983, 1988). The active forces generated by spindle machinery and motor proteins need to be balanced and overcome by an opposite force, or passive forces, such as elastic forces, frictional resistance, and viscous drag (Forth & Kapoor, 2017). Crosslinkers are nonenzymatic molecules that diffuse between or statically connect two cytoskeletal filaments. They are capable of generating frictional resistance against active forces and help maintain the structural integrity of higher order cytoskeletal assemblies. Thus, crosslinkers are critical in describing the mechanics of MT networks as their binding can disrupt MT sliding and therefore generate resistive forces that control the direction and magnitude of sliding (Lansky *et al.*, 2015). Forth *et al.* investigated mitotic MAPs EB1, PRC1, and NuMA using a combined OT and TIRF approach to understand how active forces influence MAP behavior (Forth *et al.*, 2014). OT were used to pull each MAP along the MT lattice in a traditional SM assay orientation. PRC1-MT binding was found to be symmetric under load with respect to filament polarity, while NuMA and EB1 MT binding were asymmetric. (Forth *et al.*, 2014) In order to test whether frictional asymmetry can lead to directional movement in MT networks, the authors needed to analyze

NuMA-MT interactions in MT “sandwiches” or “bundles” rather than just as a single MAP acting on a single MT. To accomplish this, the authors developed a dimerized construct NuMA-Bonsai-Tail-GFP II that was capable of crosslinking MTs while retaining the frictional asymmetry found as a monomer (Figure 2.3a). The directionally-dependent behavior of dimerized NuMA-Bonsai-tail II-GFP in MT bundles were analyzed using optical tweezers by applying load on the polarity-marked MT system. A bead bound with rigor kinesin was attached to the end of the top, free MT, and high trap stiffness was used (0.2 pN/nm) to trap the bead while the stage and thus bottom MT underwent continuous sinusoidal oscillation (Figure 2.3a). By combining OT with TIRF, the authors were able to observe the movement of NuMA-Bonsai-tail II-GFP toward MT minus ends when in a parallel configuration only, and anti-parallel sandwiches did not facilitate MAP clustering (Figure 2.3a). Moreover, the magnitude of the oscillation was proportional to the speed of NuMA motion in parallel microtubule bundles (Forth *et al.*, 2014). Therefore, using the combined microtubule bundle OT assay, the authors were able to determine that different nonmotor MAPs exhibit unique frictional resistance based on hierarchical MT geometry and force application.

In a similar assay setup, Lansky *et al.* (2015) demonstrated the role of Ase1, the S. pombe analog of PRC1, in generating directed mechanical forces as diffusible microtubule crosslinkers confined between two partially overlapping microtubules in vitro (Figure 2.3b). Experimental work was performed by first preparing MT overlaps by immobilizing dimly-rhodamine-labeled MTs on a coverslip termed the “template” MT. Next, Ase1 with a GFP tag was added and incubated to allow binding to the immobilized MTs. Bright rhodamine-labeled “transport” microtubules were flushed into the flow cell where immobilized template

microtubules were bound to Ase1, also washing out any unbound Ase1 in solution. Hydrodynamic flow of assay buffer was then performed on the flow cell to allow the sliding of transport microtubule along the template MTs. TIRF was used to visualize the entropic expansion caused by friction forces generated by Ase1 and to determine how it would affect the sliding of partially overlapping MTs. Results from TIRF imaging revealed that the crosslinkers do not leave the regions they were initially bound to before the movement of the MTs. This is due to the high affinity of crosslinkers for the over- lapping MTs. Upon MT sliding, Ase1 crosslinkers became more con- fined in the overlaps, and when induced sliding from hydrodynamic flow ceased, Ase1 expansion caused directed MT sliding. Further, Ase1 crosslinkers distributed themselves evenly within the overlaps (Lansky *et al.*, 2015). Optical tweezers were used to measure the force generated by Ase1 crosslinkers due to this "entropic expansion" (Figure 2.3b; Lansky *et al.*, 2015). Template and transport MT overlaps

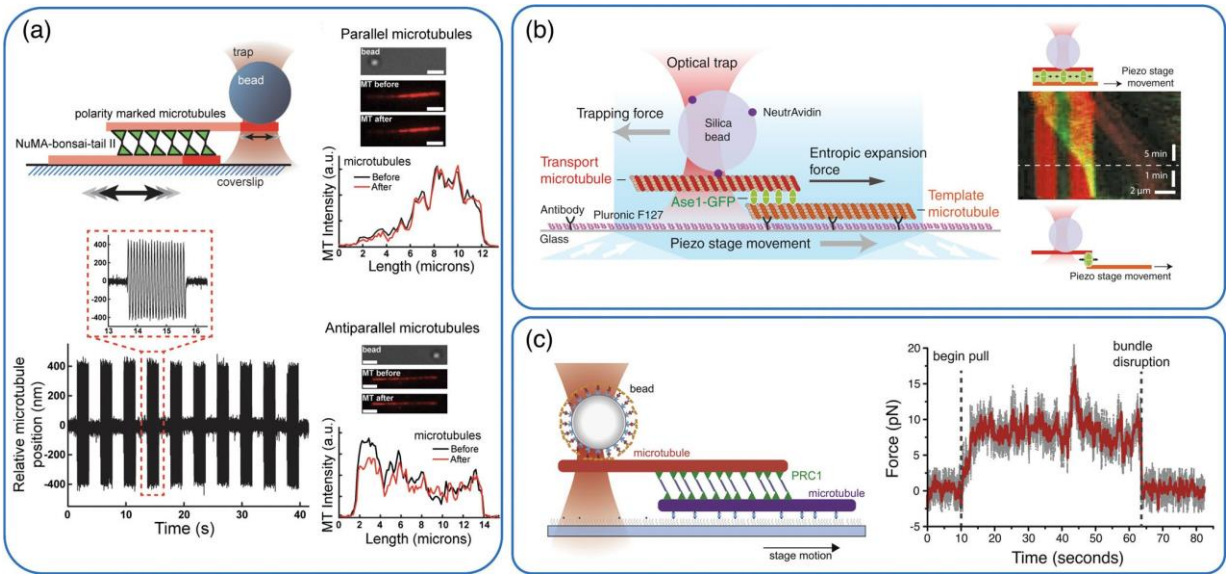

Figure 2.3: Nonmotor MAPs generate force in MT bundles. (a) Assembled polarity-marked MT bundles with NuMA "sandwiched" between were probed using OT. Upon oscillating the stage, NuMA moved toward MT minus ends in parallel MTs while showing no transport preference in anti-parallel MT bundles. Adapted from Forth et al. (2014), *Cell*. (b) OT is used to probe the entropic forces of nonmotor MAP Ase-1 within MT overlaps. As Ase-1 is able to diffuse within the overlap, entropic expansion facilitates MT sliding, generating forces in the pN range. Adapted from Lansky et al. (2015), *Cell*. (c) Sliding of MTs crosslinked by mitotic PRC1 results in resistive forces and sliding within MT overlaps. Adapted from Gaska et al. (2020), *Developmental Cell*. Reproduced with permission from Elsevier under licenses 4958850791490, 4958850073143, and 4958850683308, respectively

were assembled in a similar manner, except the transport MT was biotinylated and a Neutravidin bead was added in the last Ase1-absent flow step. The bead was trapped and attached to the transport MT. A piezo translation stage moved the template MT in the same axis with respect to the transport MT held in a fixed position by the trap to compact the Ase1 proteins. After each stage step, the system was allowed to equilibrate before measuring force. Results showed that the entropic expansion of Ase1 generated forces that are in the pico-newton range, which suggests that those forces are on the same scale as forces generated by molecular motors and could be of importance for balancing forces inside the cell. Kinesin-14 molecular motors were employed with partially overlapping MTs to prove this finding. The results showed that with the addition of Ase1, the direction of MT sliding caused by the kinesin-14 motor molecule was reversed. Through using the bundled MT assay with the optical trap and piezo stage, the authors were able to demonstrate that the force generated by nonmotor Ase1 is on the same scale as the force generated by mitotic motors, better putting these crosslinkers into context within spindle force balance (Lansky *et al.*, 2015).

PRC1, like Ase1, has a high affinity to crosslink antiparallel microtubules. Gaska *et al.* (2020) investigated PRC1 mechanics in MT bundles, utilizing optical tweezers and TIRF microscopy to control MT sliding motions, quantify resistive forces generated by PRC1 crosslinkers, and observe PRC1 distribution within the overlaps simultaneously (Figure 3c). First, PRC1-mediated MT bundles with various overlap lengths and concentrations of PRC1 molecules in the overlap were made by immobilizing biotinylated MTs containing HiLyte-647 on a passivated coverslip by neutravidin. Next, GFP-PRC1 and rhodamine-labeled MTs were added into the sample chamber to form a MT bundle. For OT measurements, beads were coated with truncated kinesin-1 and introduced to bind the top rhodamine-labeled

microtubule. MT sliding was performed to induce force on the PRC1 bundle ensemble by trapping the bead bound to the top MT and moving the sample stage at a fixed velocity parallel to the microtubule bundle axis to control filament separation. TIRF was used to image each of the moving and the trapped microtubules and PRC1. Results revealed that PRC1-crosslinked microtubules pairs generate passive force specifically as viscous resistance that acts like a mechanical dashpot during MT sliding (Figure 2.3c). This viscous force showed linear dependence on MT sliding velocity and number of PRC1 crosslinkers molecules (Gaska *et al.,* 2020). On the other hand, no change of viscous force with MT overlap length nor density of PRC1 was observed. Overall, these studies performed on nonmotor MT crosslinkers demonstrated how force generating behavior of these molecules deviates with respect to filament polarity and sliding, and these behaviors are well-captured using the MT bundle OT assay. These results have strong implications for the roles MAPs play in balancing forces and maintaining structural integrity within the MT cytoskeleton, revealing that they have unique properties outside of static crosslinking.

2.6 Force Generation by Mitotic Kinesin Teams in Microtubule Bundles

2.6.1 Kinesin-5

Molecular motors play an important role in regulating the mitotic spindle by generating pulling and pushing forces that control the sliding motion of adjacent MTs and therefore yield the proper bipolar structure for faithful segregation of chromosomes (Wordeman, 2010). One of the main contributors in the assembly of MT-based metaphase spindle is kinesin-5 (Mann & Wadsworth, 2019; Sawin, LeGuellec, Philippe, & Mitchison, 1992). Kinesin-5 is a conserved homotetrameric motor protein that has two motor domains at each

end of a central stalk, giving kinesin-5 the ability to crosslink and slide two MTs of kinesin-5 toward the plus ends of each MT causes them to push apart (Kapitein, Kwok, *et al.*, 2008; Kapitein *et al.*, 2005). On the other hand, when in parallel MT geometries, kinesin-5 is able to act as a brake, regulating the speed of sliding (Shimamoto *et al.*, 2015). Kinesin-5 has also been classified to have both processive and nonprocessive qualities, not allowing it fit well in either the porter or rower motility categories (Crevel *et al.*, 1997; Valentine *et al.*, 2006). Therefore, to determine how kinesin-5 facilitates differing force generating mechanisms within MT overlaps, Shimamoto *et al.* analyzed kinesin-5 ensembles in crosslinked, over-lapping MTs using OT combined with fluorescence (Figure 2.4a). To understand the capabilities of this assay setup, we will review the experimental methods used to construct each experiment. When kinesin-5 crosslinks antiparallel over- lapped MTs, the stepping setup, termed a mini-spindle, was employed to analyze force generation by kinesin-5 measurements were carried out using optical tweezers which controlled filament orientation, sliding speed, and overlap length to measure force generation. Nonbiotinylated and biotinylated MTs were assembled onto a glass coverslip which was precoated by polyethylene glycol to prevent sub- sequent nonspecific binding. The assay was made as a sandwich where the MTs were prepared on top of each other to mimic a bundled shape. Recombinant GFP-tagged full-length Xenopus kinesin-5 motor was used to crosslink the overlapped MTs. TIRF was employed to detect the regions of the overlap and kinesin-5 location, while at the same time, the optical trap controlled the overlap length and sliding speed and measured the force generated with changing these fac- tors. A trapped bead was attached to the free end of the nonbiotinylated MT to measure sliding forces (Figure 2.4a). As kinesin-5 mediated bundles would preferentially form and move within the anti- parallel

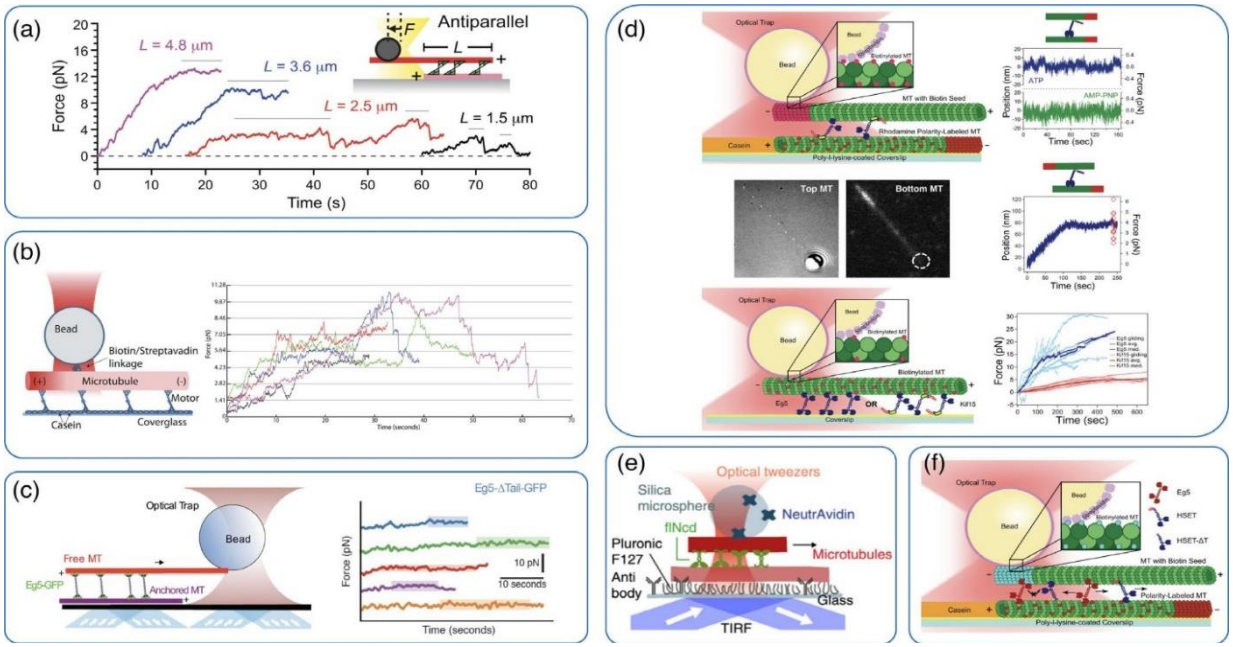

Figure 2.4: Deducing ensemble force generation by kinesins using optical tweezers. (a) Ensembles of kinesin-5 "sandwiched" between two differently fluorescently labeled MTs. Adapted from Shimamoto *et al.* (2015), Developmental Cell. (b) Budding yeast kinesin-5 Cin8 produces forces similar to that of Eg5 in both the plus and minus end direction, and directionality of sliding was not affected by hindering loads up to the ensemble stall force. Adapted from Fallesen *et al.* (2017), Biophysical Journal. (c) Using the same experimental set-up from Figure 4a, authors determine that the kinesin-5 tail domain is essential for producing pushing forces in the OT assay. Adapted from Bodrug *et al.* (2020), eLife. (d) Polarity-marked MTs were used to construct kinesin-12 Kif15 bundles. Kif15 groups selectively generate force within anti-parallel MT bundles, facilitating a backup mechanism for kinesin-5 Eg5-based mitotic spindle assembly. Using a combined OT-MT gliding assay, force generation by ensembles of Eg5 increase with motor concentration, as found by Shimamoto *et al.* However, Kif15 ensembles do not generate force beyond that of around the single molecule stall force, supporting a force-feedback mechanism for collective force generation. Adapted from Reinemann *et al.* (2017), Current Biology. (e) Kinesin-14 Ncd motors within anti-parallel MT overlaps are only diffusively anchored, generating sub-pN ensemble forces. Adapted from Lüdecke *et al.* (2018), Nature Communications. (f) Kinesin-14 HSET ensembles generates force within anti-parallel MT bundles, but parallel bundles remain static. Although HSET ensembles generate substantially less force than equivalent Eg5 ensembles, at a 1:1 ratio, HSET acts as a force brake against Eg5 in MT bundles. Adapted from Reinemann *et al.* (2018), Current Biology. Reproduced with permission under licenses 4958880042845, 4958880270622, and 4958890115250, open access policies, and Creative Commons Attribution License CC-BY

orientation, in order to get measurements in parallel MT bundles, the trapped bead attached to the top MT of a moving bundle was flipped around to the opposite side in order form a parallel MT bundle.(Shimamoto *et al.*, 2015; Shimamoto & Kapoor, 2018) Results revealed that a group of kinesin-5s acting between two antiparallel MTs can push those MTs apart by generating force that scales with the overlap length and number of motors (Figure 2.4a; Shimamoto *et al.*, 2015). The traces have an initial force ramp that is followed by a plateau that is achieved either through crowding, maximum force generated by the system, or both,

and this maximum force decreases as the MT overlap length decreases due to fewer motors present (Figure2.4a). Further, kinesin-5 acts as a “brake-like” resistance against relative microtubule sliding in both parallel and anti-parallel orientations. This behavior was observed when the template MT was moved with the piezostage at low speed (20 nm/s), and the magnitude of the generated pushing force that assisted MT sliding was proportional with the overlap length. On the other hand, faster relative sliding velocities (200 nm/s) opposed filament sliding. Thus, these kinesin-5 ensemble measurements between two MTs using OT illuminated how when working concertedly, the motors can read local structural and concentration cues that result in a specific mechanical output, which has important implications for force regulation within the mitotic spindle (Shimamoto *et al.,* 2015). Kinesin-5 motors were originally described as unidirectional plus- end-directed motors, whether as SMs or in ensembles (Fallesen *et al.,* 2017). Kinesin-5 family members from budding yeast (Cin8 and Kip1) and fission yeast (Cut7) have since been found to have the ability to move toward the MT plus and minus ends (Singh, Pandey, Al- Bassam, & Gheber, 2018). Fallesen *et al.* (2017) elucidate whether the mechanism of minus-end-directed motility in kinesin-5 is similar to that of the known plus-end-directed motility mechanism. In doing so, force spectroscopy was used to measure both the plus and minus end forces that ensembles of purified budding yeast kinesin-5 Cin8 pro- duce in microtubule gliding assays (Fallesen *et al.,* 2017).

A combined optical tweezers and microtubule gliding assay (Figure 2.4b) was assembled by first adding motility buffer into a prepared flow chamber (Fallesen *et al.,* 2017). After Cin8-mGFP addition and incubation, polarity-marked biotinylated microtubules were then added to the flow cell followed by an incubation and wash step. Finally, a dilute

streptavidin bead was added to act as the optical handle on the gliding MT. The force spectroscopy experiments were conducted by capturing a calibrated streptavidin-coated bead and moving it into contact with the lagging end of a biotinylated polarity-marked MT so that the motors pull the bead out of the trap. Fluorescence imaging was used to determine the gliding direction of the MT. OT measurements demonstrated that the bidirectional kinesin-5 Cin8 of budding yeast is capable of producing piconewton forces that are similar in magnitude in both directions of movement. These results are similar to assay performed with Eg5 in Figure 2.4a minus the ability to generate force toward the MT minus-end direction. Thus, minus-end directed motion may follow a conventional mechanism similar to that of plus-end directed motion. Also, Cin8 force production was shown to have a linear relationship with motor number, as was also found with Eg5, which indicates that additive force production is a conserved property of kinesin-5 motors (Fallesen *et al.,* 2017; Shimamoto *et al.,* 2015). This result could imply a functional requirement for spindle assembly and elongation during cell division. However, this linearity, as well as the magnitude of SM force produced by Cin8 and Eg5, are conserved properties of kinesin 5-motors but are not seen in all members of the kinesin family. Moreover, each kinesin-5 consists of twin tail and twin motor domains originating from two sets of antiparallel folded dimeric subunits that emerge in close proximity at each end of the bipolar homotetramer (Bodrug *et al.,* 2020). In order to investigate the dependence of this tail domain on kinesin-5 ensemble force production, Bodrug *et al.* employed a similar experimental setup to Figure 2.4a where force generated by kinesin-5s without their tail domains is measured in motor ensembles between two MTs (Figure 2.4c; Bodrug *et al.,* 2020; Shimamoto *et al.,* 2015) MT-kinesin- 5-MT sandwiches or bundles were formed in vitro, and force measurements by the

motor-MT system were obtained through the top MT bound to an optically trapped bead. Upon removal of the kinesin-5 tail domain, MT sliding events generated weak forces (Figure 2.4c) compared to the linear dependence of motor number on force generation with wild type kinesin-5 (Figure 2.4a). Further analysis revealed that the tail has a powerful role in down-regulating microtubule-activated ATP hydrolysis by assisting the capture of the nucleotide-free or ADP state. Also, the tail's presence helped stabilize a unique conformation of the motor N-terminal subdomain by facilitating the opening of its active site. Full-length kinesin-5 motors demonstrated relatively slow motility, likely to help maintain the spindle's integrity and avoid rupture of microtubules during sliding. Kinesin-5 motors also cluster together along the MT tracks, whereas tail-less motors exhibited high speed motility and no clustering. All together, these findings revealed that the tail domain of kinesin-5 has a significant impact on kinesin-5 ensemble mechanics within anti-parallel MT overlaps through tuning the motor's mechanochemical cycle, which in turn regulates assembly and force balance within the spindle (Bodrug *et al.*, 2020).

2.6.2 Kinesin-12

The kinesin-12 Kif15 acts as a redundant back-up mechanism for centrosome separation during spindle assembly when Eg5 has been inhibited by drugs (Reinemann *et al.*, 2017; Sturgill *et al.*, 2014, 2016; Sturgill & Ohi, 2013). However, Kif15 and Eg5 have different structures, where Kif15 contains motor heads, a second nonmotor MT binding site, and an inhibitory tail, and Kif15 has a smaller SM stall force than Eg5 (Reinemann *et al.*, 2017; Sturgill *et al.*, 2014, 2016; Sturgill & Ohi, 2013). These disparities then beg the question of how Kif15 is able to efficiently rescue spindle assembly. To answer this, Reinemann *et al.*

devised an OT assay to investigate Kif15 as an ensemble of motors between two MTs, as they would function physiologically in the spindle (Reinemann *et al.*, 2017). The assay was assembled using polarity marked MTs to determine MT bundle orientation. As Kif15 is plus end directed, contains a second MT binding site, as has the ability to change locations from parallel-oriented kinetochore MTs to anti-parallel interpolar MTs upon Eg5 inhibition, they hypothesized that force generation mechanisms would differ in these MT geometries.(Reinemann *et al.*, 2017) The bottom or template MT was polarity marked using fluorescently labeled tubulin, where GMPCPP seeds were brightly fluorescent and indicated the minus end, and dimmer elongations from polymerization marked the plus end (Figure 2.4d, top). The top or cargo MT was polarity marked using biotinylated GMPCPP seeds for the minus end and non-labeled elongations for the plus end. Streptavidin beads were utilized to facilitate only binding the minus end of the cargo MT. Therefore, by knowing the location of the trapped streptavidin bead and visualizing the relative location of the bright minus end seed of the template MT using fluorescence, the bundle was identified as parallel or anti-parallel in orientation (Reinemann *et al.*, 2017).

The MT bundle assay was assembled from the bottom up. First, template polarity marked MTs were added to a flow cell, incubated, and washed with casein to prevent nonspecific binding of motor. A combination of Kif15, biotin-marked cargo MTs, and streptavidin beads were then added to facilitate bundling of MTs by Kif15. A bead would then be trapped in solution, calibrated, and lowered to a MT bundle identified by differential interference contrast (DIC) imaging on the surface. Upon binding the bundle, polarity orientation was verified using fluorescence and the relative location of the trapped bead. Force generated by the Kif15 ensemble was then measured via displacement of the bead

attached to the cargo MT from the trap center. The authors determined that Kif15 slides antiparallel MTs apart while parallel bundles remain stationary. This is reflective of the location- specific roles that Kif15 plays in the spindle: static MT crosslinker/force regulator under physiological conditions (parallel kinetochore MTs) and active MT slider under drugged conditions (anti-parallel interpolar MTs; Reinemann *et al.*, 2017). The authors wanted to further dive into the ensemble behavior of Kif15. As demonstrated by Shimamoto *et al.* (2015), Eg5 has an additive, linear dependence of force generation with respect to motor concentration. To determine if this was the case for Kif15, Reinemann *et al.* (2017) adapted a combined MT gliding/OT assay for both Eg5 and Kif15 where motor is bound to the coverslip surface and glides a biotinylated MT for attachment of a streptavidin bead. After a bead was trapped in solution, it was lowered to the flow cell surface to a gliding MT. In the case of Eg5, their results corroborated those from Shimamoto *et al.*, indicating that as the concentration of Eg5 increased, the force generated increased accordingly. However, at even higher surface concentrations than used for Eg5, ensembles of Kif15 would not generate force above that of the SM stall force, indicating a level of force feedback within these motor-filament systems (Figure 2.4d, bottom). Therefore, the modularity of the MT bundle OT assay allowed the authors to determine how Kif15 motors function in different hierarchical MT environments, as they would exist within the spindle, but also allowed for comparison to its relevant partner Eg5 that it supports as a mitotic backup to differentiate how spindle assembly might occur under physiological versus chemotherapy drugged conditions.

2.6.3 Kinesin-14

The kinesin-14 family also aids in regulating force within the spindle, with the distinction that kinesin-14s move toward the minus-end of MTs (Fink *et al.,* 2009; Furuta & Toyoshima, 2008; Mountain *et al.,* 1999; Norris *et al.,* 2018; Pechatnikova & Taylor, 1999). Kinesin-14 motors, such as Ncd, each interact with crosslinked MTs in two ways: through the low-processive motor domains and diffusive tail domains. The tail domains' influence on the protein's performance is not yet understood. Therefore, Lüdecke *et al.* (2018) determine whether velocity and force produced by Ncd is governed by the tail domain-mediated diffusive anchorage of the motors to MTs. Their approach was to use a kinesin-MT bundle assay combined with OT (Figure 2.4e), very similar to the assay constructions previously dis- cussed for kinesin-5 and kinesin-12. To assemble the bundle assay, anti-SNAP antibodies were bound to diphenyldimethoxysilane (DDS)- functionalized coverslips in a flow cell. Using Pluronic F127, the sur- face was then passivated before Ncd tail motors in ATP buffer were injected into the chamber. Finally, the chamber was washed, and MTs were added. For experiments using crosslinked microtubules, anti- digoxigenin antibodies were first allowed to bind to the DDS- functionalized coverslips before the surfaces were blocked with Pluronic F127. Digoxigenated dimly-cy5-labeled microtubules were then added to the chamber and allowed to bind to the surface- immobilized antibodies. Next, Ncd in ADP buffer was added and allowed to bind MTs, followed by biotinylated, brightly-cy5-labeled MTs were then added to the chamber to form microtubule pairs. Finally, the buffer was replaced with ATP buffer. For the optical tweezer experiments, the ATP buffer was supplemented with NeutrAvidin- functionalized silica microspheres. (Lüdecke *et al.,* 2018).

For force measurements of MTs driven by diffusively anchored Ncd motors

crosslinked to surface-immobilized MTs, a trapped and calibrated microsphere was lowered directly on top of the moving MT. Bead movement relative to the surface-immobilized template MT was used to measure the force-velocity relationship by setting a constant force and monitoring the velocity or vice versa. The study showed that statically anchored Ncd motors transport microtubules faster and with greater force than diffusibly anchored Ncd motors, suggesting that anchoring of the tail domain regulates the force trans- mission between microtubules in motion.(Lüdecke *et al.,* 2018) Thus, the inefficient force production of kinesin-14 may be due to tail diffusion on the MT surface, and the role of kinesin-14 in sliding MTs may be due to both sliding nucleated microtubules that are otherwise untethered to the spindle poles while also crosslinking antiparallel microtubules.

However, kinesin-14s typically do not work alone within the spindle (Norris *et al.,* 2018; Reinemann *et al.,* 2018). Kinesin-14 has been proposed to oppose kinesin-5 and aid in maintaining force balance during division, but how these motors are able to accomplish this task is not clear (Fink *et al.,* 2009; Gicking *et al.,* 2018; Hepperla *et al.,* 2014; Norris *et al.,* 2018; Peterman & Scholey, 2009). Kinesin- 14 Ncd has been reported to be nonprocessive, and as demonstrated by Ludecke *et al.* and others, relies, at least in part, by the tail's diffusion (Braun *et al.,* 2017; Lüdecke *et al.,* 2018). On the other hand, kinesin-5 generates a 5 pN stall force and exhibits a level of processivity (Valentine *et al.,* 2006). Therefore, how a seemingly substantially weaker motor like kinesin-14 effectively opposes and resists force generated by kinesin-5 was not well understood. Ensembles of kinesin-14s on beads have been shown to produce processive motility and substantial force generation, which is markedly different from their SM properties (Furuta *et al.,* 2013; Norris *et al.,* 2018). However, how these motors work together between two MTs to resist kinesin-5 in not clear.

Reinemann *et al.* (2018) examined this question using the bundled MT assay and incorporate a mixed motor ensemble of kinesin-14 HSET and kinesin-5 Eg5 (Figure 2.4f). Bundles were assembled similarly to the Kif15 study except varying concentration ratios of Eg5 to HSET were introduced. Interestingly, even though Eg5 is notably stronger than HSET, HSET seems to dictate bundle force and velocity, serving as a force brake against Eg5 in bundles. Additionally, by noting the polarity of the bundle and the direction of cargo MT transport, the authors observed that when in bundles with Eg5, HSET's directionality is compliant, adopting the overall plus end directional movement facilitated by Eg5 while still resisting overall force production. These unique characteristics that were discovered using the multi- motor, multi-filament OT approach provide insight as to why kinesin- 14 overexpression causes spindle elongation as oppose to collapse and how HSET adopts specific properties in varied conditions: weak force production and motility as SMs, very processive in small groups, and resistive in mixed motor ensembles. (Furuta *et al.*, 2013; Norris *et al.*, 2018; Reinemann *et al.*, 2018).

2.7 Outlook

Here, we review novel approaches of incorporating microtubule structural hierarchy, MAPs, and motors into OT assays in order to deter- mine ensemble properties of motors that may not necessarily fall in the porter or rower motility categories. We included many of the experimental details to convey how these assays are currently constructed and demonstrate that understanding assay geometry has implications for interpreting mechanistic results. By incorporating MT hierarchy in OT experiments, motor biophysicists are able to extract information regarding ensemble force generation dynamics of kinesins and MAPs that would

otherwise be difficult to investigate using conventional methods. Using this approach, the influence of cooperativity and communication between motors or MAPs themselves, as well as through the motor-filament connection, on ensemble performance can be captured as opposed to having motors spaced out on a rigid coverslip or bead surface where that communication is likely dampened. Further, the influence of changes made at the molecular level on cytoskeletal system synergy are directly measured, and the modular nature of the assays opens exciting doors for the field. By taking advantage of the fact that individual cytoskeleton proteins and filaments are routinely isolated and/or polymerized on the bench or purchased from commercial sources, we can treat these elements like LEGOs, custom-building cytoskeletal architectures in a stepwise manner and inter- changing the "building blocks" as needed, with the goal of ultimately understanding how these alterations propagate up to system level force generation.

While innovative, these approaches have room for expansion and increased complexity. The studies reviewed here are confined to the surface of the flow cell's coverslip, immobilizing one of the bundled MTs and thus lessening the potential dynamic influence from the bot- tom half of the system. These assays are also the foundation for approaching higher levels of complexity in in vitro reconstitution. Mixed motor and crosslinker assays would be beneficial in elucidating the force balance in higher order structures like the mitotic spindle, including the MAPs and kinesins discussed in this review. However, structural hierarchy also is not confined to the MT cytoskeleton. Actin assemblies also have critical roles in essential processes like muscle contraction, cell division, and cell motility.(Huxley, 2004; Mandato, Benink, & Bement, 2000) Further, traditionally, the MT and actin cyto-skeleton have been evaluated separately in in vitro assays. Yet, it is becoming clear that

actin-MT crosstalk should be evaluated more ardently with increasing evidence of direct, coordinated relationships, and OT cytoskeletal hierarchical assays provide a unique platform to investigate the synergy of the molecular linkages that connect these structurally distinct filaments (Dogterom & Koenderink, 2019; Even- Ram *et al.*, 2007; Mandato *et al.*, 2000; Pimm & Henty-Ridilla, 2021). MTs consist of multiple protofilaments that form a tube and have a higher persistence length than helical AFs (Sept, Baker, & McCammon, 2009; Steffen, Smith, Simmons, & Sleep, 2001). The differences in pliability of not only the filaments, but also the crosslinkers that connect them, will surely influence the tension and compression forces that propagate throughout the system and thus the resulting ensemble force generation.(Bouck, Joglekar, & Bloom, 2008; Kim, 2015; MurreμL & Gardel, 2012) In addition, dynein is another MT motor protein that could be incorporated into these hierarchical OT assays to investigate their group dynamics on single and multi- filament complexes. Minus-end directed dynein works to transport cargo with the dynactin complex and facilitate large-scale motion in structures like cilia and flagella. (T. J. Mitchison & Mitchison, 2010; Waterman-Storer *et al.*, 1997) These large-scale complexes and multi-motor axon models could then be constructed and interrogated using the combined MT bundle OT approach outlined above.(Mallik, Carter, Lex, King, & Gross, 2004; Sims & Xie, 2009; Waterman-Storer *et al.*, 1997)

Further, new OT techniques and technology continue to emerge that have the ability to push these bundle assays to higher resolution. Recently, ~70 nm diameter germanium nanospheres were employed to interrogate the mechanics of a single kinesin-1 motor interacting with a microtubule in order to enhance the spatiotemporal resolution that can be limited by using traditional micron-sized beads (Sudhakar *et al.*, 2021). Sudhakar *et al.*

(2021) observed 4 nm center-of-mass motor steps with alternating force dependence scaling with dwell time, and detachment was not observed at maximum force but switched to a weakly bound state. Thus, utilizing micron-sized beads as motor probes may actually be hiding pieces of the mechanistic puzzles that the field has been trying to solve for the last few decades.

In summary, combining OT with in vitro MT hierarchy and kinesin ensembles has yielded a novel approach for investigating higher order mechanics of the cytoskeleton. Force measurements of kinesin and MAP teams reveal that ensemble mechanics are not necessarily the sum of the SM properties, and motor/MAP/filament communication and cooperativity dictate concerted force generation. As biochemists and biophysicists work toward grand challenges like building a syn thetic cell or even building minimal working subsystems like a spindle or sarcomere, they can utilize such methods to grasp the physical basis of each building block so that we can understand how they each contribute to overall system function.

BIBLIOGRAPHY

2.8 Bibliography

Ashkin, A. (1992). Forces of a single-beam gradient laser trap on a dielectric sphere in the optics regime. Biophysical Journal, 61(2), 569–582. https://doi.org/10.1016/S0006 3495(92)81860-X

Bergman, J., Osunbayo, O., & Vershinin, M. (2015). Constructing 3D micro- tubule networks using holographic optical trapping. Scientific Reports, 5(September), 1–10. https://doi.org/10.1038/srep18085

Bergman, J. P., Bovyn, M. J., Doval, F. F., Sharma, A., Gudheti, M. V., Gross, S. P., … Vershinin, M. D. (2018). Cargo navigation across 3D microtubule intersections. Proceedings of the National Academy of Sci- ences of the United States of America, 115(3), 537–542. https://doi. org/10.1073/pnas.1707936115

Blackwell, R., EdeµLaier, C., Sweezy-Schindler, O., Lamson, A., Gergely, Z. R., O'Toole, E., …

Betterton, M. D. (2017). Physical determinants of bipolar mitotic spindle assembly and stability in fission yeast. Science Advances, 3(1), e1601603 https://doi.org/10.1126/sciadv.1601603.

Block, S. M. (2007). Kinesin motor mechanics: Binding, stepping, tracking, gating, and limping. Biophysical Journal, 92(9), 2986–2995. https://doi. org/10.1529/biophysj.106.100677

Bodrug, T., Wilson-Kubalek, E., Nithianantham, S., Thompson, A. F., Alfieri, A., Gaska, I., Al-Bassam, J. (2020). The kinesin-5 tail domain directly modulates the mechanochemical cycle of the motor domain for anti-parallel microtubule sliding. ELife, 9, 1–36. https://doi. org/10.7554/eLife.51131

Bouck, D. C., Joglekar, A. P., & Bloom, K. S. (2008). Design features of a mitotic spindle: Balancing tension and compression at a single microtubule kinetochore interface in

budding yeast. Annual Review of Genetics, 42, 335–359. https://doi.org/10.1146/annurev.genet.42.110807. 091620

Braun, M., Drummond, D. R., Cross, R. A., & Mcainsh, A. D. (2009). The kinesin-14 Klp2 organizes microtubules into parallel bundles by an ATP-dependent sorting mechanism. Nature Cell Biology, 11(6), 724– 730. https://doi.org/10.1038/ncb1878

Braun, M., Lansky, Z., Fink, G., Ruhnow, F., Diez, S., & Janson, M. E. (2011). Adaptive braking by Ase1 prevents overlapping microtubules from sliding completely apart. Nature Cell Biology, 13(10), 1259–1264. https://doi.org/10.1038/ncb2323

Braun, M., Lansky, Z., Szuba, A., Schwarz, F. W., Mitra, A., Gao, M., … Diez, S. (2017). Changes in microtubule overlap length regulate kinesin-14-driven microtubule sliding. Nature Chemical Biology, 13, 1245–1252. https://doi.org/10.1038/nchembio.2495

Britto, M., Goulet, A., Rizvi, S., Von Loeffelholz, O., Moores, C. A., & Cross, R. A. (2016). Schizosaccharomyces pombe kinesin-5 switches direction using a steric blocking mechanism. Proceedings of the National Academy of Sciences of the United States of America, 113(47), E7483– E7489. https://doi.org/10.1073/pnas.1611581113

Chowdhury, D. (2014). Michaelis–Menten at 100 and allosterism at 50: Driving molecular motors in a hailstorm with noisy ATPase engines and allosteric transmission. FEBS Journal, 281(2), 601–611. https://doi. org/10.1111/febs.12596

Chowdhury, D., & Ghanti, D. (2020). Soft mechano-chemistry of molecular hubs in mitotic spindle: Biomechanics and mechanical proofreading at microtubule ends. Journal of Physics Condensed Matter, 32(28), 284001. https://doi.org/10.1088/1361-648X/ab7cc5

Crevel, I. M., Lockhart, A., & Cross, R. A. (1997). Kinetic evidence for low chemical processivity in ncd and Eg5. Journal of Molecular Biology, 273 (1), 160–170.

https://doi.org/10.1006/jmbi.1997.1319

DeCastro, M. J., Ho, C. H., & Stewart, R. J. (1999). Motility of dimeric Ncd on a metal-chelating surfactant: Evidence that Ncd is not processive. Biochemistry, 38(16), 5076–5081. https://doi.org/10.1021/bi9829175

Dogterom, M., & Koenderink, G. H. (2019). Actin – Microtubule crosstalk in cell biology. Nature Reviews Molecular Cell Biology, 20(1), 38–54.

Dogterom, M., & Surrey, T. (2013). Microtubule organization in vitro. Cur- rent Opinion in Cell Biology, 25(1), 23–29. https://doi.org/10.1016/j. ceb.2012.12.002

Dogterom, M., & Yurke, B. (1997). Measurement of the force-velocity relation for growing microtubules. Science, 278(5339), 856–860. https:// oi.org/10.1126/science.278.5339.856

Drechsler, H., & Mcainsh, A. D. (2016). Kinesin-12 motors cooperate to suppress microtubule catastrophes and drive the formation of parallel microtubule bundles. Proceedings of the National Academy of Sciences of the United States of America, 113, E1635–E1644. https://doi.org/ 10.1073/pnas.1516370113

Drechsler, H., McHugh, T., Singleton, M. R., Carter, N. J., & McAinsh, A. D. (2014). The Kinesin-12 Kif15 is a processive track-switching tetramer. ELife, 3, e01724. https://doi.org/10.7554/eLife.01724

Duke, T. A. J. (1999). Molecular model of muscle contraction. Proceedings of the National Academy of Sciences of the United States of America, 96 (6), 2770–2775. https://doi.org/10.1073/pnas.96.6.2770

Edellaier, C. J., Lamson, A. R., Gergely, Z. R., Ansari, S., Blackwell, R., Richard McIntosh, J., Betterton, M. D. (2020). Mechanisms of chromosome biorientation and bipolar spindle assembly analyzed by computational modeling. ELife, 9, 1–48.

https://doi.org/10.7554/eLife. 48787

Elting, M. W., & Spudich, J. A. (2012). Future challenges in single-molecule fluorescence and laser trap approaches to studies of molecular motors. Developmental Cell, 23(6), 1084–1091. https://doi.org/10.1016/j. devcel.2012.10.002

Even-Ram, S., Doyle, A. D., Conti, M. A., Matsumoto, K., Adelstein, R. S., & Yamada, K. M. (2007). Myosin IIA regulates cell motility and actomyosin-microtubule crosstalk. Nature Cell Biology, 9(3), 299–309. https://doi.org/10.1038/ncb1540

Fallesen, T., Roostalu, J., Duellberg, C., Pruessner, G., & Surrey, T. (2017). Ensembles of bidirectional Kinesin Cin8 produce additive forces in both directions of movement. Biophysical Journal, 113(9), 2055–2067. https://doi.org/10.1016/j.bpj.2017.09.006

Finer, J. T., Simmons, R. M., & Spudich, J. a. (1994). Single myosin molecule mechanics: Piconewton forces and nanometre steps. Nature, 368 (6467), 113–119. https://doi.org/10.1038/368113a0

Fink, G., Hajdo, L., Skowronek, K. J., Reuther, C., Kasprzak, A. A., & Diez, S. (2009). The mitotic kinesin-14 Ncd drives directional microtubule – Microtubule sliding. Nature Cell Biology, 11(6), 717–723. https://doi. org/10.1038/ncb1877

Forth, S., Hsia, K. C., Shimamoto, Y., & Kapoor, T. M. (2014). Asymmetric friction of nonmotor MAPs can lead to their directional motion in active microtubule networks. Cell, 157(2), 420–432. https://doi.org/ 10.1016/j.cell.2014.02.018

Forth, S., & Kapoor, T. M. (2017). The mechanics of microtubule networks in cell division. Journal of Cell Biology, 216(6), 1525–1531. https://doi. org/10.1083/jcb.201612064

Foster, K. A., & Gilbert, S. P. (2000). Kinetic studies of dimeric Ncd: Evi- dence that Ncd is not processive. Biochemistry, 39(7), 1784–1791. https://doi.org/10.1021/bi991500b

Furuta, K., Furuta, A., Toyoshima, Y. Y., Amino, M., Oiwa, K., & Kojima, H. (2013). Measuring collective transport by defined numbers of processive and nonprocessive kinesin motors. Proceedings of the National Academy of Sciences of the United States of America, 110(2), 501–506. https://doi.org/10.1073/pnas.1201390110

Furuta, K., & Toyoshima, Y. Y. (2008). Minus-end-directed motor Ncd exhibits Processive movement that is enhanced by microtubule bun- dling in vitro. Current Biology, 18(2), 152–157. https://doi.org/10. 1016/j.cub.2007.12.056

Gaska, I., Armstrong, M., Alfieri, A., & Forth, S. (2020). The mitotic crosslinking protein PRC1 acts as a mechanical dashpot to resist microtubule sliding. Developmental Cell, 54, 367–378. https://doi.org/ 10.1016/j.devcel.2020.06.017

Gerson-Gurwitz, A., Thiede, C., Movshovich, N., Fridman, V., Podolskaya, M., Danieli, T.,Gheber, L. (2011). Directionality of individual kinesin-5 Cin8 motors is modulated by loop 8, ionic strength and microtubule geometry. EMBO Journal, 30(24), 4942–4954. https://doi.org/10.1038/emboj.2011.403

Gicking, A. M., Qiu, W., & Hancock, W. O. (2018). Mitotic kinesins in action: Diffusive searching, directional switching, and ensemble coor- dination. Molecular Biology of the Cell, 29(10), 1153–1156. https://doi. org/10.1091/mbc.E17-10-0612

Goldstein, L. S. (2001). Kinesin molecular motors: Transport pathways, receptors, and human disease. Proc Natl Acad Sci U S A, 98(13), 6999– 7003. https://doi.org/10.1073/pnas.111145298

Goldstein, L. S. B., & Philp, A. V. (1999). The road less traveled: Emerging principles of kinesin motor utilization. Annual Review of Cell and Devel- opmental Biology, 15, 141–183. https://doi.org/10.1146/annurev. cellbio.15.1.141

Gross, S. P. (2004). Hither and yon: A review of bi-directional microtubule- based transport. Physical Biology, 1(2), 1–11. https://doi.org/10.1088/ 1478-3967/1/2/R01

Hentrich, C., & Surrey, T. (2010). Microtubule organization by the antago- nistic mitotic motors kinesin-5 and kinesin-14. Journal of Cell Biology, 189(3), 465–480. https://doi.org/10.1083/jcb.200910125

Hepperla, A. J., Willey, P. T., Coombes, C. E., Schuster, B. M., Gerami- Nejad, M., McClellan, M., … Gardner, M. K. (2014). Minus-end-directed kinesin-14 motors align antiparallel microtubules to control metaphase spindle length. Developmental Cell, 31(1), 61–72. https://doi.org/10. 1016/j.devcel.2014.07.023

Hirokawa, N. (1998). Kinesin and dynein superfamily proteins and the mechanism of organelle transport. Science, 279(5350), 519–526. https://doi.org/10.1126/science.279.5350.519

Hirokawa, N., Noda, Y., Tanaka, Y., & Niwa, S. (2009). Kinesin superfamily motor proteins and intracellular transport. Nature Reviews. Molecular Cell Biology., 10, 682–696. https://doi.org/10.1038/nrm2774

Hirokawa, N., & Takemura, R. (2004). Molecular motors in neuronal development, intracellular transport and diseases. Current Opinion in Neuro- biology, 14(5), 564–573. https://doi.org/10.1016/j.conb.2004.08.011

Huxley, H. E. (2004). Fifty years of muscle and the sliding filament hypothesis. European Journal of Biochemistry, 271(8), 1403–1415. https://doi. org/10.1111/j.1432-1033.2004.04044.x

Janson, M. E., De Dood, M. E., & Dogterom, M. (2003). Dynamic instability of microtubules is regulated by force. Journal of Cell Biology, 161(6), 1029–1034. https://doi.org/10.1083/jcb.200301147

Jon Kull, F., & Endow, S. A. (2013). Force generation by kinesin and myosin cytoskeletal motor proteins. Journal of Cell Science, 126(1), 9–19. https://doi.org/10.1242/jcs.103911

Kapitein, L. C., Janson, M. E., van den Wildenberg, S. M. J. L., Hoogenraad, C. C., Schmidt, C. F., & Peterman, E. J. G. (2008). Micro- tubule-driven Multimerization recruits ase1p onto overlapping microtubules. Current Biology, 18(21), 1713–1717. https://doi.org/10. 1016/j.cub.2008.09.046

Kapitein, L. C., Kwok, B. H., Weinger, J. S., Schmidt, C. F., Kapoor, T. M., & Peterman, E. J. G. (2008). Microtubule cross-linking triggers the direc- tional motility of kinesin-5. Journal of Cell Biology, 182(3), 421–428. https://doi.org/10.1083/jcb.200801145

Kapitein, L. C., Peterman, E. J. G., Kwok, B. H., Kim, J. H., Kapoor, T. M., & Schmidt, C. F. (2005). The bipolar mitotic kinesin Eg5 moves on both microtubules that it crosslinks. Nature, 435(7038), 114–118. https:// doi.org/10.1038/nature03503

Kapoor, V., Hirst, W. G., Hentschel, C., Preibisch, S., & Reber, S. (2019). MTrack: Automated detection, tracking, and analysis of dynamic microtubules. Scientific Reports, 9(1), 1–12. https://doi.org/10.1038/ s41598-018-37767-1

Kim, T. (2015). Determinants of contractile forces generated in disorganized actomyosin bundles. Biomechanics and Modeling in Mechanobiology, 14 (2), 345–355. https://doi.org/10.1007/s10237-014-0608-2

Kitamura, K., Tokunaga, M., Iwane, A. H., & Yanagida, T. (1999). A single myosin read moves along an Actin filament with regular steps of simi- lar to 5.5 nm. Biophysical Journal, 76(1), A36–A36.

Kolomeisky, A. B., & Fisher, M. E. (2007). Molecular motors: A theorist's perspective. Annual Review of Physical Chemistry, 58(February 2007), 675–695.

https://doi.org/10.1146/annurev.physchem.58.032806.
104532

Kuo, S. C., & Sheetz, M. P. (1993). Force of single Kinesin molecules mea- sured with optical tweezers. Science, 260(5105), 232–234.

Laan, L., Husson, J., Munteanu, E. L., Kerssemakers, J. W. J., & Dogterom, M. (2008). Force-generation and dynamic instability of microtubule bundles. Proceedings of the National Academy of Sciences of the United States of America, 105(26), 8920–8925. https://doi.org/ 10.1073/pnas.0710311105

Lansky, Z., Braun, M., Lüdecke, A., Schlierf, M., Ten Wolde, P. R., Janson, M. E., & Diez, S. (2015). Diffusible crosslinkers generate directed forces in microtubule networks. Cell, 160(6), 1159–1168. https://doi.org/10.1016/j.cell.2015.01.051

Leibler, S., & Huse, D. A. (1993). Porters versus rowers: A unified stochas- tic model of motor proteins. Journal of Cell Biology, 121(6), 1357– 1368. https://doi.org/10.1083/jcb.121.6.1357

Lera-Ramirez, M., & Nédélec, F. J. (2019). Theory of antiparallel microtu- bule overlap stabilization by motors and diffusible crosslinkers. Cyto- skeleton, 76(11–12), 600–610. https://doi.org/10.1002/cm.21574

Lüdecke, A., Seidel, A., Braun, M., & Diez, S. (2018). Diffusive tail anchor- age determines velocity and force produced by kinesin-14 between crosslinked microtubules. Nature Communications, 9(1), 2214. https:// doi.org/10.1038/s41467-018-04656-0

Mallik, R., Carter, B. C., Lex, S. A., King, S. J., & Gross, S. P. (2004). Cyto- plasmic dynein functions as a gear in response to load. Nature, 427 (6975), 649–652. https://doi.org/10.1038/nature02293

Mandato, C. A., Benink, H. A., & Bement, W. M. (2000). Microtubule- actomyosin interactions in cortical flow and cytokinesis. Cell Motility and the Cytoskeleton, 45(2), 87–92. https://doi.org/10.1002/(SICI) 1,097-0169(200002)45:2<87::AID-CM1>3.0.CO;2–0

Mann, B. J., & Wadsworth, P. (2019). Kinesin-5 regulation and function in mitosis. Trends in Cell Biology, 29(1), 66–79. https://doi.org/10.1016/j. tcb.2018.08.004

Marx, A., Hoenger, A., & Mandelkow, E. (2009). Structures of kinesin motor proteins. Cell Motility and the Cytoskeleton, 66(11), 958–966. https://doi.org/10.1002/cm.20392

Mehta, A. D., Rock, R. S., Rief, M., Spudich, J. A., Mooseker, M. S., & Cheney, R. E. (1999). Myosin-V is a processive Actin-based motor. Nature, 400(6744), 590–593. https://doi.org/10.1038/23072

Miki, H., Okada, Y., & Hirokawa, N. (2005). Analysis of the kinesin super- family: Insights into structure and function. Trends in Cell Biology, 15, 467–476. https://doi.org/10.1016/j.tcb.2005.07.006

Mitchison, T. J., & Mitchison, H. M. (2010). How cilia beat. Nature, 463(7279), 308–309. https://doi.org/10.1038/463308a

Mitchison, T. J., & Kirschner, M. (1984). Dynamic instability of microtubule growth. Nature, 312(15), 237–242.

Molloy, J. E., Burns, J. E., Kendrick-Jones, B., Tregear, R. T., & White, D. C. S. (1995). Movement and force produced by a single myosin head. Nature, 378(6553), 209–212. https://doi.org/10.1038/378209a0

Molloy, J. E., Burns, J. E., Sparrow, J. C., Tregear, R. T., Kendrick- Jones, J., & White, D. C. (1995). Single-molecule mechanics of heavy meromyosin and S1 interacting with rabbit or drosophila actins using optical tweezers. Biophysical Journal, 68(4 Suppl), 298S–

303S; 303S- 305S. Retrieved from http://www.ncbi.nll.nih.gov/pubmed/7787095

Molodtsov, M. I., Mieck, C., Dobbelaere, J., Dammermann, A.,Westermann, S., & Vaziri, A. (2016). A force-induced directional switch of a molecular motor enables parallel microtubule bundle formation. Cell, 167(2), 539–552. https://doi.org/10.1016/j.cell.2016.09.029

Mountain, V., Simerly, C., Howard, L., Ando, A., Schatten, G., & Compton, D. A. (1999). The Kinesin-related protein, HSET, opposes the activity of Eg5 and Cross-links microtubules in the mammalian mitotic spindle. Journal of Cell Biology, 147(2), 351–365.

Murrell, M. P., & Gardel, M. L. (2012). F-actin buckling coordinates con- tractility and severing in a biomimetic actomyosin cortex. Proceedings of the National Academy of Sciences of the United States of America, 109(51), 20820–20825. https://doi.org/10.1073/pnas.1214753109

Neuman, K. C., & Block, S. M. (2004). Optical trapping. Review of Scientific Instruments, 75(9), 2787–2809. https://doi.org/10.1063/1.1785844

Nicklas, R. B. (1983). Measurements of the force produced by the mitotic spindle in anaphase. Journal of Cell Biology, 97(2), 542–548. https:// doi.org/10.1083/jcb.97.2.542

Nicklas, R. B. (1988). The forces that move chromosomes in mitosis. Annual Review of Biophysics and Biophysical Chemistry, 17(14), 431–449. https://doi.org/10.1146/annurev.bb.17.060188.002243

Norris, S. R., Jung, S., Singh, P., Strothman, C. E., Erwin, A. L., Ohi, M. D., … Ohi, R. (2018). Microtubule minus-end aster organization is driven by processive HSET-tubulin clusters. Nature Communications, 9, 1–14.

Palliter, K. A., Tyska, M. J., Haeberle, J. R., & Alpert, N. R. (2000). R403Q and L908V mutant

β-cardiac myosin from patients with familial hyper- trophic cardiomyopathy exhibit enhanced mechanical performance at the single molecule level. Journal of Muscle Research and Cell Motility, 21, 609–620. https://doi.org/10.1023/a:1005678905119

Pechatnikova, E., & Taylor, E. W. (1999). Kinetics processivity and the direction of motion of Ncd. Biophysical Journal, 77(2), 1003–1016. https://doi.org/10.1016/S0006-3495(99)76951-1

Peterman, E. J. G., & Scholey, J. M. (2009). Mitotic microtubule cros- slinkers: Insights from mechanistic studies. Current Biology, 19(23), R1089–R1094. https://doi.org/10.1016/j.cub.2009.10.047

Pimm, M. L., & Henty-Ridilla, J. L. (2021). New twists in actin—Microtubule interactions. Molecular Biology of the Cell, 32, 211–217. https://doi. org/10.1091/mbc.E19-09-0491

Popchock, A. R., Tseng, K. F., Wang, P., Karplus, P. A., Xiang, X., & Qiu, W. (2017). The mitotic kinesin-14 KlpA contains a context-dependent directionality switch. Nature Communications, 8, 1–9. https://doi.org/ 10.1038/ncomms13999

Prelogovic, M., Winters, L., Milas, A., Tolic, I. M., & Pavin, N. (2019). Pivot- and-bond model explains microtubule bundle formation. Physical Review E - Statistical, Nonlinear, and Soft Matter Physics, 100(1), 012403.

Rath, O., & Kozielski, F. (2012). Kinesins and cancer. Nature Reviews Can- cer, 12(8), 527–539. https://doi.org/10.1038/nrc3310

Reinemann, D. N., Norris, S. R., Ohi, R., & Lang, M. J. (2018). Processive Kinesin-14 HSET exhibits directional flexibility depending on motor traffic. Current Biology, 28(14), 2356–2362 https://doi.org/10.1016/j. cub.2018.06.055

Reinemann, D. N., Sturgill, E. G., Das, D. K., Degen, M. S., Vörös, Z., Hwang, W., …

Lang, M. J. (2017). Collective force regulation in anti- parallel microtubule gliding by dimeric Kif15 Kinesin motors. Current Biology, 27(18), 2810–2820. https://doi.org/10.1016/j.cub.2017.08.018

Roos, W., Uller, J., Gräter, S., Surrey, T., & Spatz, J. P. (2005). Microtubule gliding and cross-linked microtubule networks on micropillar inter- faces. Nano Letters, 5(12), 2630–2634. https://doi.org/10.1021/ nl051865j

Roostalu, J., Hentrich, C., Bieling, P., TeμLey, I. A., Schiebel, E., & Surrey, T. (2011). Directional switching of the kinesin Cin8 through motor cou- pling. Science, 332(6025), 94–99. https://doi.org/10.1126/science.1199945

Ruegg, C., Veigel, C., Molloy, J. E., Schmitz, S., Sparrow, J. C., & Fink, R. H. A. (2002). Molecular motors: Force and movement gener- ated by single myosin II molecules. Physiology, 17(5), 213–218. https://doi.org/10.1152/nips.01389.2002

Sawin, K. E., LeGuellec, K., Philippe, M., & Mitchison, T. J. (1992). Mitotic spindle organization by a plus-end-directed microtubule motor. Nature, 359(6395), 540–543. https://doi.org/10.1038/359540a0

Sept, D., Baker, N. A., & McCammon, J. A. (2009). The physical basis of microtubule structure and stability. Protein Science, 12(10), 2257– 2261. https://doi.org/10.1110/ps.03187503

Sherin, L., Farwa, S., Sohail, A., Li, Z., & Bég, O. A. (2018). Cancer drug ther- apy and stochastic modeling of “nano-motors”. International Journal of Nanomedicine, 13, 6429–6440. https://doi.org/10.2147/IJN.S168780

Shimamoto, Y., Forth, S., & Kapoor, T. M. (2015). Measuring pushing and braking forces generated by ensembles of Kinesin-5 crosslinking two microtubules. Developmental Cell, 34(6), 669–681. https://doi.org/10. 1016/j.devcel.2015.08.017

Shimamoto, Y., & Kapoor, T. M. (2018). Analyzing the micromechanics of the cell division apparatus. Methods in Cell Biology, 145, 173–190. https://doi.org/10.1016/bs.mcb.2018.03.022.Analyzing

Sims, P. A., & Xie, X. S. (2009). Probing dynein and Kinesin stepping with mechanical manipulation in a living cell. ChemPhysChem, 10(9–10), 1511–1516.

Singh, S. K., Pandey, H., Al-Bassam, J., & Gheber, L. (2018). Bidirectional motility of kinesin-5 motor proteins: Structural determinants, cumulative functions and physiological roles. Cellular and Molecular Life Sciences, 75(10), 1757–1771. https://doi.org/10.1007/s00018-018-2754-7

Steffen, W., Smith, D., Simmons, R., & Sleep, J. (2001). Mapping the Actin filament with myosin. Proceedings of the National Academy of Sciences of the United States of America, 98(26), 14949–14954. https://doi.org/ 10.1073/pnas.261560698

Sturgill, E. G., Das, D. K., Takizawa, Y., Shin, Y., Collier, S. E., Ohi, M. D., … Ohi, R. (2014). Report Kinesin-12 Kif15 targets kinetochore fibers through an intrinsic two-step mechanism. Current Biology, 24, 2307– 2313. https://doi.org/10.1016/j.cub.2014.08.022

Sturgill, E. G., Norris, S. R., Guo, Y., & Ohi, R. (2016). Kinesin-5 inhibitor resistance is driven by kinesin-12. Journal of Cell Biology, 213(2), 213–227. https://doi.org/10.1083/jcb.201507036

Sturgill, E. G., & Ohi, R. (2013). Kinesin-12 differentially affects spindle assembly depending on its microtubule substrate. Current Biology, 23 (14), 1280–1290. https://doi.org/10.1016/j.cub.2013.05.043

Su, X., Arellano-santoyo, H., Portran, D., Gaillard, J., Vantard, M., Thery, M., & Pellan, D. (2013). Microtubule-sliding activity of a kinesin-8 promotes spindle assembly and

spindle-length control. Nature Cell Biology, 15(8), 948–957. https://doi.org/10.1038/ncb2801

Subramanian, R., Wilson-Kubalek, E. M., Arthur, C. P., Bick, M. J., CampbeμL, E. A., Darst, S. A.,Kapoor, T. M. (2010). Insights into anti- parallel microtubule crosslinking by PRC1, a conserved nonmotor microtubule binding protein. Cell, 142(3), 433–443. https://doi.org/10. 1016/j.cell.2010.07.012

Sudhakar, S., Kazem, M., Tobias, A., Jachowski, J., Bugiel, M., Jannasch, A., & Schäffer, E. (2021). Germanium nanospheres for ultraresolution picotensiometry of kinesin motors. Science, 371(6530), eabd9944. https://doi.org/10.1126/science.abd9944

Svoboda, K., & Block, S. M. (1994). Force and velocity measured for single kinesin molecules. Cell, 77(5), 773–784. https://doi.org/10.1016/ 0092-8674(94)90060-4

Svoboda, K., Schmidt, C. F., Schnapp, B. J., & Block, S. M. (1993). Direct observation of Kinesin stepping by optical trapping interferometry. Nature, 365, 721–727. https://doi.org/10.1038/365721a0

Takagi, Y., Homsher, E. E., Goldman, Y. E., & Shuman, H. (2006). Force gen- eration in single conventional actomyosin complexes under high dynamic load. Biophysical Journal, 90(4), 1295–1307. https://doi.org/ 10.1529/biophysj.105.068429

Tanenbaum, M. E., Vale, R. D., & McKenney, R. J. (2013). Cytoplasmic dynein crosslinks and slides anti-parallel microtubules using its two motor domains. ELife, 2013(2), 1–20. https://doi.org/10.7554/eLife.00943

Tao, L., Mogilner, A., Civelekoglu-Scholey, G., WoμμLan, R., Evans, J., Stahlberg, H., & Scholey, J. M. (2006). A homotetrameric Kinesin-5, KLP61F, bundles microtubules and

antagonizes Ncd in motility assays. Current Biology, 16(23), 2293–2302. https://doi.org/10.1016/j.cub.2006.09.064

Tyska, M. J., Dupuis, D. E., Guilford, W. H., Patlak, J. B., Waller, G. S., Trybus, K. M., … Lowey, S. (1999). Two heads of myosin are better than one for generating force and motion. Proceedings of the National Academy of Sciences of the United States of America, 96(8), 4402–4407. https://doi.org/10.1073/pnas.96.8.4402

Tyska, M. J., Hayes, E., Giewat, M., Seidman, C. E., Seidman, J. G., & Warshaw, D. M. (2000). Single-molecule mechanics of R403Q cardiac myosin isolated from the mouse model of familial hypertrophic cardio- myopathy. Circulation Research, 86(7), 737–744. https://doi.org/10. 1161/01.RES.86.7.737

Tyska, M. J., & Warshaw, D. M. (2002). The myosin power stroke. Cell Motility and the Cytoskeleton, 51(1), 1–15. https://doi.org/10.1002/ cm.10014

Uçar, M. C., & Lipowsky, R. (2019). Force sharing and force generation by two teams of elastically coupled molecular motors. Scientific Reports, 9 (1), 1–13. https://doi.org/10.1038/s41598-018-37126-0

Vale, R. D., & Fletterick, R. J. (1997). The design plan of kinesin motors. Annual Review of Cell and Developmental Biology, 13, 745–777. https:// doi.org/10.1146/annurev.cellbio.13.1.745

Valentine, M. T., Fordyce, P. M., Krzysiak, T. C., Gilbert, S. P., & Block, S. M. (2006). Individual dimers of the mitotic kinesin motor Eg5 step processively and support substantial loads in vitro. Nature Cell Biology, 8(5), 470–476. https://doi.org/10.1038/ncb1394

Van den Wildenberg, S. M. J. L., Tao, L., Kapitein, L. C., Schmidt, C. F., Scholey, J. M., &

Peterman, E. J. G. (2008). The Homotetrameric Kinesin-5 KLP61F preferentially crosslinks microtubules into antiparal- lel orientations. Current Biology, 18(23), 1860–1864. https://doi.org/ 10.1016/j.cub.2008.10.026

Veigel, C., Molloy, J. E., Schmitz, S., & Kendrick-Jones, J. (2003). Load- dependent kinetics of force production by smooth muscle myosin measured with optical tweezers. Nature Cell Biology, 5(11), 980–986. https://doi.org/10.1038/ncb1060

Walczak, C. E., & Heald, R. (2008). Mechanisms of mitotic spindle assembly and function. International Review of Cytology, 265, 111–158. https:// doi.org/10.1016/S0074-7696(07)65003-7

Waterman-Storer, C. M., Karki, S. B., Kuznetsov, S. A., Tabb, J. S., Weiss, D. G., Langford, G. M., & Holzbaur, E. L. F. (1997). The interaction between cytoplasmic dynein and dynactin is required for fast axo- nal transport. Proceedings of the National Academy of Sciences of the United States of America, 94(22), 12180–12185. https://doi.org/10. 1073/pnas.94.22.12180

Weinger, J. S., Qiu, M., & Yang, G. (2011). Report a nonmotor microtubule bind- ing site in Kinesin-5 is required for filament crosslinking and sliding. Current Biology, 21(2), 154–160. https://doi.org/10.1016/j.cub.2010.12.038

Wijeratne, S., & Subramanian, R. (2018). Geometry of antiparallel microtu- bule bundles regulates relative sliding and stalling by PRC1 and kif4A. ELife, 7, 1–28. https://doi.org/10.7554/eLife.32595

Winters, L., Ban, I., Prelogovi c, M., Kalinina, I., Pavin, N., & Toli c, I. M. (2019). Pivoting of microtubules driven by minus-end-directed motors leads to spindle assembly. BMC Biology, 17(1), 1–18. https://doi.org/ 10.1186/s12915-019-0656-2

Wordeman, L. (2010). How kinesin motor proteins drive mitotic spindle function: Lessons from molecular assays. Seminars in Cell and Develop- mental Biology, 21, 260–268. https://doi.org/10.1016/j.semcdb.2010.01.018

Zemel, A., & Mogilner, A. (2009). Motor-induced sliding of microtubule and Actin bundles. Physical Chemistry Chemical Physics, 11(24), 4821– 4833. https://doi.org/10.1039/b901646e

Ziebert, F., Vershinin, M., Gross, S. P., & Aranson, I. S. (2009). Collective alignment of polar filaments by molecular motors. European Physical Journal E, 28(4), 401–409. https://doi.org/10.1140/epje/i2008-10434-0

CHAPTER 3

PROBING MYOSIN ENSEMBLE MECHANICS IN ACTIN FILAMENT BUNDLES USING OPTICAL TWEEZERS

*This chapter is adapted from Omayma Al Azzam, Janie C. Watts, Justin E. Reynolds, Juliana E. Davis, Dana N. Reinemann, "Probing Myosin Ensemble Mechanics in Actin Filament Bundles Using Optical Tweezers". J. Vis. Exp. (183), e63672, doi:10.3791/63672 (2022). Reproduced with permission by JoVE's author license agreement.

3.1 Summary

Myosins are motor proteins that hydrolyze ATP to step along actin filament (AF) tracks and are essential in cellular processes such as motility and muscle contraction. To understand their force-generating mechanisms, myosin II has been investigated both at the single-molecule (SM) level and as teams of motors *in vitro* using biophysical methods such as optical trapping.

These studies showed that myosin force-generating behavior can differ greatly when moving from the single-molecule level in a three-bead arrangement to groups of motors working together on a rigid bead or coverslip surface in a gliding arrangement. However, these assay constructions do not permit evaluating the group dynamics of myosin within viscoelastic structural hierarchy as they would within a cell. We have developed a method using optical tweezers to investigate the mechanics of force generation by myosin ensembles interacting with multiple actin filaments.

These actomyosin bundles facilitate investigation in a hierarchical and compliant environment that captures motor communication and ensemble force output. The customizable

nature of the assay allows for altering experimental conditions to understand how modification to the myosin ensemble, actin filament bundle, or the surrounding environment result in differing force outputs.

3.2 Introduction

As motor proteins are essential to life, converting chemical energy into mechanical work (Goldstein, *et al.*, 2001; Sweeney, *et al.*, 2018; O'Connell, *et al.*, 2007). Myosin motors interact with actin filaments by taking steps along the filaments similar to a track, and the dynamics of actin-myosin networks carry out muscle contraction, cell motility, the contractile ring during cytokinesis, and movement of cargo inside the cell, among other essential tasks (O'Connell, *et al*., 2007; Kaya, *et al*., 2017; Akhshi, *et al*., 2014; Brawley, *et al*., 2009; Hartman, *et al*., 2012; Spudich, *et al*., 1995). Since myosins have so many essential roles, failure in the functionality of the myosin–actin network can lead to disease development, such as mutations in the myosin heavy chain that cause heart hypercontractility in hypertrophic cardiomyopathy (HCM) (Sommese, *et al*., 2013; Nag, *et al*., 2017; Kawana, *et al*., 2017; Girolami, *et al*., 2014; Debold, *et al*., 2007; Barron, 1999). In muscle contraction, individual myosin motors cooperate with each other by working as an ensemble to provide the required mechanical energy that carries out the relative sliding of Afs (Duke, 1999; Vilfan, *et al*., 2003; Huxley, 1957; Huxley, 2004). Myosin motors form crossbridges between AFs and use conformational changes due to its mechanochemical cycle to

collectively move toward the barbed end of the aligned filaments (Huxley, 1957; Huxley, 2004; Kad, *et al.*, 2005; Veigel, *et al.*, 2003; Spudich, 2001). Development of quantitative *in vitro* motility assays at the SM level using techniques such as optical trapping

has facilitated gathering unprecedented detail of how individual myosin motors function, including measuring SM force generation and step sizes (Simmons, *et al*., 1996; Finer, *et al*., 1994; Kron, *et al*., 1991; Molloy, *et al*., 1995; Ruegg, *et al*., 2002; Nayak, *et al*., 2020; Dupuis, *et al*., 1997; Tyska, *et al*., 1999; Tyska, *et al*., 2002). Finer *et al.* developed the "three-bead" or "dumbbell" optical trapping assay to probe the force-generation mechanics of single myosin II motors (Finer, *et al*., 1994; Finer, *et al*., 1995). As muscle myosin II works in teams to contract AFs but is non-processive at the SM level, the optical trapping assay orientation had to be rearranged from the classic motor-bound bead approach (Finer, *et al*., 1995). To form the dumbbell assay, two optical traps were used to hold an AF over a myosin motor bound to a coverslip-attached bead, and force output by the single motor was measured through movements of the AF within the trap (Finer, *et al*., 1994). However, SM forces and using a single motor/single filament assay orientation do not give a full image about system-level force generation since many motor proteins, including myosin II, do not work in isolation and often do not function as a sum of their parts (Duke, 1999; Vilfan, *et al*., 2003; Huxley, 1957; Al Azzam, *et al*., 2021; Wagoner, *et al*., 2021; Walcott, *et al*., 2012; Stewart, *et al*., 2021; Hilbert, *et al*., 2013). More complex structures that include more than one motor interacting with more than one filament are necessary to better understand the synergy of myosin and actin filaments' networks (Duke, 1999; Al Azzam, *et al.*, 2022). The dumbbell assay orientation has been exploited to investigate small ensemble force generation by having multiple myosins attached to a bead or using a myosin-thick filament attached to a surface and allowing the motors to interact with the suspended AF (Kaya, *et al*., 2017; Finer, *et al*., 1994; Walcott, *et al*., 2012; Debold, *et al*., 2013; Kaya, *et al*., 2010; Pertici, *et al*., 2018; Cheng, *et al*., 2020). Other small ensemble assays include an *in vitro* filament gliding

assay wherein myosin motors are coated onto a coverslip surface, and a bead bound to an AF is used to probe the force generated by the team of motors (Kaya, *et al*., 2017; Stewart, *et al*., 2021; Hilbert, *et al*., 2013; Kaya, *et al*., 2010; Pertici, *et al*., 2018; Cheng, *et al*., 2020; Stam, *et al*., 2015; Rastogi, *et al*., 2016; Debold, *et al*., 2005). In both these cases, the myosins are bound to a rigid surface—bead or coverslip—and utilize one AF. In these cases, the motors are not able to move freely or communicate with each other, nor does having myosins rigidly bound reflect the compliant, hierarchical environment in which the motors would work together in the sarcomere (Al Azzam, *et al*., 2021). Previous studies have suggested that myosin II can sense its environment and adapt accordingly to changing viscoelastic or motor concentration conditions by altering characteristics such as force generation and duty ratio (Stam, *et al*., 2015; Albert, *et al*., 2014; Erdmann, *et al*., 2012).Thus, there is a need to develop an optical trapping assay that fosters and captures motor communication and system compliancy to paint a more realistic picture of the mechanistic underpinnings of myosin II ensemble force generation.

Here, we introduce a novel approach—the first to offer a construct that closely mimics the complex mechanics of an actual sarcomere. This enables the study of myosin II motors within a compliant and hierarchical system that mirrors true biological conditions. Traditional methods, such as single-molecule "dumbbell" optical trapping assays, have provided invaluable insights into the force-generation mechanics of myosin motors. However, they have fallen short in aspects such as motor force coordination and environment sensing. Our novel protocol addresses these limitations by employing a modular assay geometry, where multiple myosin motors are interconnected between two actin filaments. This configuration not only facilitates the direct observation of motor communication and

ensemble force generation but also allows for the examination of how myosin II adapts to changes in viscoelastic conditions and motor concentration. These are crucial for understanding the nuanced force feedback mechanisms that govern muscle contraction and cellular motility (Stam *et al*., 2015; Albert *et al*., 2014). By replicating the hierarchical organization and system compliance characteristic of muscle sarcomeres, our method provides a more physiologically relevant model. This offers profound insights into the molecular foundations of motor protein functionality and their role in larger-scale biological processes. Through these innovative ensemble assays, we aim to bridge the gap between traditional biochemical analysis and biomechanical reality, setting a new standard for the study of actomyosin dynamics.

3.3 Investigating Myosin II Mechanisms: Protocol Steps and Implementation

1. Etching coverslips

1.1. Dissolve 100 g of KOH in 300 mL of 100% ethanol in a 1,000 mL beaker. Stir with a stir bar until the majority of the KOH has dissolved.

CAUTION: Concentrated KOH solution can cause burns and damage to clothing. Wear gloves, eye protection, and a lab coat.

1.2. Place coverslips individually in coverslip cleaning racks.

NOTE: Racks are designed with slits that hold single coverslips spaced apart to allow for etching and rinsing on each face of the coverslip, drain holes in the bottom, and made of material that can withstand the harsh etching conditions. They can be custom-made or purchased commercially.

1.3. Prepare and label three 1,000 mL beakers: one with 300 mL of ethanol and two beakers with 300 mL of reverse osmosis (RO) water.

NOTE: Here, RO water was sourced from a lab water purifier, but it could also be purchased commercially if a local purifier is not available.

1.4. Place each of the four beakers in a bath sonicator to degas for 5 min.

1.5. Submerge a rack of coverslips in the beaker of KOH and ethanol and sonicate for 5 min.

1.6. Transfer the rack of coverslips from the KOH/ethanol beaker to the ethanol-only beaker. Dip rack up and down in the beaker until there is no beading.

NOTE: Take care to not disturb the coverslips or forcefully drop the rack into the beaker. This will cause the coverslips to come out of the rack or cause chemical splashing.

1.7. Carefully transfer the rack of coverslips from the ethanol beaker to a beaker of water, dipping up and down until there is no beading.

1.8. Submerge the rack of coverslips in the beaker of water that has not been used yet and sonicate again for 5 min.

1.9. Use a bottle to spray the rack of coverslips with water until it runs off the coverslips smoothly. Repeat with the ethanol.

1.10. Place the racks to dry in an oven at 90 °C for 20 min. Store the racks of etched coverslips at room temperature in closed containers to prevent contamination before use.

2. Actin filament polymerization

2.1. Make Solution T

2.1.1. In a 50 mL conical tube, add 3.94 g of Tris-HCl and 0.147 g of CaCl2. Add RO water to make a total volume of 50 mL and mix well.

NOTE: The final concentrations of Solution T are 500 mM Tris-HCl and 20 mM CaCl2, respectively.

2.1.2. Label the tube Solution T and store it at 4 °C.

2.2. Make TC Buffer

2.2.1. Mix 40 mL of RO water and 1.5 mL of Solution T in a 50 mL conical tube. Change the pH to 8.0 by adding small amounts of concentrated KOH. Add water to make 50 mL of the solution, and verify the pH. Adjust the pH if needed.

NOTE: The final TC buffer contains 5 mM Tris-HCl and 0.2 mM CaCl2 at pH 8.

2.2.2. Label the tube TC and store it at 4 °C.

2.3. Make FC Buffer

2.3.1. Add 85 mL of RO water, 10 mL of Solution T, 3.73 g of KCl, and 0.041 g of MgCl2 to a 100 mL buffer bottle. Modify the pH to 7.5 by adding small volumes of concentrated KOH. Add water to make a final volume of 100 mL and verify the pH.

NOTE: The final FC buffer contains 500 mM Tris-HCl, 500 mM KCl, 2 mM MgCl2, and 2 mM CaCl2 at pH 7.5.

2.3.2. Label the tube FC and store it at 4 °C.

2.4. Prepare General Actin Buffer (GAB).

2.4.1. Mix 485 µL of TC buffer, 10 µL of 10 mM ATP, and 5 µL of 50 mM DTT in a

microcentrifuge tube.

NOTE: Final buffer conditions are 5 mM Tris-HCl, 0.2 mM CaCl2, 0.5 mM DTT, and 0.2 mM ATP.

2.4.2. Label it as GAB and store it at 4 °C.

2.5. Prepare Actin Polymerization Buffer (APB).

2.5.1. Mix 455 µL of FC buffer, 25 µL of 100 mM ATP, and 20 µL of 50 mM DTT in a microcentrifuge tube.

NOTE: The final buffer conditions are 50 mM Tris-HCl, 500 mM KCl, 2 mM MgCl2, 2 mM CaCl2 2 mM DTT, and 5 mM ATP.

2.5.2. Label the tube as APB and store it at 4 °C.

2.6. Reconstitute actin

2.6.1. Reconstitute rabbit skeletal muscle actin by adding 100 µL of deionized water to a 1 mg vial of lyophilized actin. Mix well by gently pipetting up and down. Aliquot into 5 µL samples, snap-freeze, and store the 10 mg/mL actin aliquots at -80 °C.

2.6.2. Reconstitute biotinylated rabbit skeletal muscle actin by adding 20 µL of RO water. Aliquot into 5 µL samples, snap-freeze, and store the 1 mg/mL biotinylated actin aliquots at -80 °C.

2.7. Non-labeled actin polymerization with rhodamine phalloidin stabilization

2.7.1. Thaw one vial of 10 mg/mL actin and keep it on ice.

2.7.2. Prepare fresh GAB buffer, add 100 µL of GAB to the actin aliquot, and mix by gently

pipetting up and down. Incubate the solution on ice for 1 h.

2.7.3. Prepare fresh APB during the incubation. After incubation, polymerize the actin into filaments by adding 11 µL of APB to the actin solution. Mix well by gently pipetting up and down. Place on ice for 20 min.

2.7.4. Add 5 µL of rhodamine-labeled phalloidin to the freshly polymerized actin filament solution. Leave on ice in the dark for 1 h.

2.7.5. Store the rhodamine actin vial wrapped in aluminum foil in the dark at 4 °C.

NOTE: It is suggested to use these filaments for a maximum period of 1 week. AF quality can be confirmed each day through a quick imaging of a flow cell containing only AFs and viewing consistent filaments day to day.

2.8. Biotinylated actin polymerization with Alexa Fluor 488 phalloidin stabilization

2.8.1. Thaw one vial of 10 mg/mL actin and 1 vial of 1 mg/mL biotinylated actin and keep them on ice.

2.8.2. Make fresh GAB buffer.

2.8.3. Combine the two vials (step 2.8.1) in a 10:1 actin:biotinylated actin ratio. Add 100 µL of GAB to the actin mixture and mix well by gently pipetting up and down. Incubate on ice for 1 h.

2.8.4. Make fresh APB during the incubation.

2.8.5. After the incubation step, polymerize the actin by adding 11 µL of APB to the actin solution. Mix well by pipetting up and down gently. Incubate on ice for 20 min.

2.8.6. Add 5 µL of Alexa Fluor 488-labeled phalloidin and incubate on ice in the dark for 1 h.

2.8.7. Store the biotinylated actin vial wrapped in aluminum foil in the dark at 4 °C.

NOTE: These filaments can be used for a maximum period of 1 week.

3. Myosin and bead preparation

3.1. Reconstitute Myosin II

3.1.1. Briefly spin down (~5 s) lyophilized skeletal myosin II to collect it at the bottom of the tube using a standard minicentrifuge.

3.1.2. Reconstitute the myosin to 10 mg/mL by adding 100 µL of 1 mM DTT prepared in RO water.

3.1.3. Dilute the stock myosin solution 10x by adding 10 µL of 10 mg/mL myosin to 90 µL of 1 mM DTT in RO water. Make small-volume (1–5 µL) aliquots, snap-freeze, and store at -80 °C.

NOTE: Myosin activity can be confirmed by performing a standard gliding filament assay as published previously46,47. See the discussion for a brief description.

3.2. Cleaning streptavidin-coated beads

3.2.1. Dilute 20 µL of 1 µm streptavidin beads into 80 µL of RO water. Wash four times by spinning down at 9,600 × g and reconstituting in 100 µL of RO water.

3.2.2. Sonicate for 2 min at 40% amplitude and store the washed beads on a rotator at 4 µC.

4. Flow cell preparation

4.1. Prepare a poly-l-lysine solution (PLL) by adding 30 mL of 100% ethanol to a 50 mL tube and adding 200 µL of 0.1% w/v poly-l-lysine in water and mix well.

4.2. Add an etched coverslip to the PLL solution and allow it to soak for 15 min. Remove the coverslip with tweezers, taking care to only touch the edge of the coverslip as it is puµLed up from the tube (see Figure 1A–C). Grab the coverslips by their edges with a gloved hand.

4.3. Dry the coverslip with a filtered airline until there is no ethanol left and no residue on the coverslip.

4.4. Apply two pieces of double-sided sticky tape to the middle of a microscope slide, 3–4 mm apart from each other. Tear or cut off the excess tape that hangs off the edge of the slide.

4.5. Add the PLL-coated coverslip on top of the tape perpendicular to the long axis of the microscope slide (forming a T) to form a channel.

4.6. Use a small tube to compress the coverslip onto the tape and microscope slide thoroughly until the tape is transparent (Figure 1A). Ensure there are no bubbles in the tape as this can cause leakage from the flow channel.

NOTE: The flow cell can hold a volume of 10–15 µL.

5. Actomyosin bundle preparation

5.1. In separate tubes, dilute each type of actin filament (rhodamine- and biotinylated 488-labeled) 600x by mixing 0.5 µL of the respective, labeled actin with 300 µL of APB. Add an additional 5 µL of the correspondingly labeled phalloidin to each tube and incubate on ice in the dark for 15 min.

5.2. To the biotinylated actin solution, add an oxygen scavenging system of 1 µL of beta-D-glucose at 500 mg/mL, 1 µL of glucose oxidase at 25 mg/mL, and 1 µL of catalase at 500 units/mL. Add 1 µL of 100 mM ATP and 1 µL of 100x diluted, cleaned streptavidin beads.

Gently stir with a pipette tip. Put the suspension on a rotator at 4 °C while the rest of the actomyosin bundle is being assembled.

5.3. Add 15 µL of the diluted rhodamine actin to the PLL flow cell (Figure 1D). Wick the excess solution through the flow cell but do not allow the flow channel to become dry. Incubate for 10 min in a humidity chamber.

NOTE: Humidity chambers can be made from empty pipette tip boxes with water added to the bottom and the lid covered in aluminum foil to block light.

5.4. Prepare a 1 mg/mL casein solution in APB.

5.5. Add 15 µL of 1 mg/mL casein to prevent non-specific binding of the subsequent components (Figure 1E). Incubate for 5 min in a humidity chamber.

5.6. Add the desired concentration of myosin to the biotinylated actin and bead suspension from step 5.2. Gently stir with the pipette tip, and then immediately add 15 µL of the step 5.2 suspension + the desired myosin concentration to the flow cell (Figure 1F,G). Incubate for 20 min. Seal the open ends of the flow cell with nail polish to prevent evaporation during imaging and optical trapping experiments.

NOTE: A myosin solution concentration of 1 µM yields robust bundling and can be used as a starting point for the desired customization of the assay (see Figure 2).

6. Force measurements using Optical Trap (NT2 Nanotracker2)

NOTE: While the protocol below is specifically for the NT2 system, this assay can be used with other optical trapping systems, including those that are custom-built, that also have fluorescence capabilities. The general workflow remains the same of getting the surface of the slide in focus,

performing bead calibrations, and acquiring data by finding fluorescent actin bundles. For the NT2 system, Supplemental Figure S1, Supplemental Figure S2, Supplemental Figure S3, Supplemental Figure S4, Supplemental Figure S5, Supplemental Figure S6, and Supplemental Figure S7 provide details of the optical trapping system and the software interface.

6.1. Turn on the control box and laser (Supplemental Figure S1).

6.2. Start the optical trap computer software by clicking on the JPK Nanotracker icon on the desktop.

6.3. Wake up the remote controller by clicking on the Logitech button at the center (Supplemental Figure S2).

6.4. Turn on the fluorescence module by toggling the on/off switch (Supplemental Figure S3).

6.5. Turn the filter cube turret for brightfield imaging (Supplemental Figure S4).

6.6. Once the system is ready, turn on the laser using the Laser Power button at the left-bottom corner of the screen to 50 mW and let it stabilize for 30 min (Supplemental Figure S5).

6.7. Sequentially click on the Illumination, Camera, Objective, and Stage Movement buttons 1within the software to bring up those windows for viewing and manipulation during the experiment. Turn the microscope illumination on by clicking on the On/Off button and setting it to maximum power by clicking and dragging the bar all the way to the right (Supplemental Figure S5).

6.8. Open the sample area and remove the sample holder from the microscope stage. Add the flow cell, secure it with the metal sample holders, and make sure that the slide with the coverslip is on the bottom.

6.9. Add 30 µL of RO water to the center of the bottom objective. Do not let the pipette tip touch the lens. Reinsert the sample stage.

NOTE: As the NT2 system uses a water immersion objective as the trapping objective, the immersion media may be different depending on the trapping objective in the user's setup.

6.10. Raise the lower objective using the on-screen control arrows or L2 on the remote controller until the bead of water touches the coverslip (Supplemental Figure S5).

6.11. Lower the top objective until about half the distance to the flow cell is reached using the on-screen arrows or R2 on the remote controller. Add 170 µL of RO water to the top of the flow cell directly under the top objective. Lower the top objective until it breaks the surface tension of the water and forms a meniscus.

6.12. Move the microscope stage using the arrow pad on the remote controller until the edge of the tape adjacent to the flow channel is reached. Close the sample door.

NOTE: A "click" upon closing the sample door indicates that the laser shutter is now open. This is a safety feature that only allows the shutter to open if the door is closed.

6.13. Using the Objective window in the screen, bring the edge of the tape in focus by bringing the bottom objective named Laser Objective up by clicking on the upper arrow using the on-screen controls. Do the same for the top objective by clicking bottom arrow (Supplemental Figure S5).

NOTE: The double arrows move the objective or stage faster. The edge of the tape is used for focusing because it is a large, easy-to-find object that is close to the coverslip surface. Air bubbles within the tape are another option. However, this is not required if the user has an

automated routine to find the surface focus or a preferred in-house method.

6.14. Once the tape is in focus, partially close the iris at the top of the optical trap. Bring the top objective down until the polygon shape of the iris is visible. Bring those edges in focus, reopen the iris, and then couple the objectives using by clicking on the Padlock icon (Supplemental Figure S5).

6.15. Find a floating bead and trap it by clicking on the Trap Shutter button, which will open the shutter and allow the trapping laser to hit the sample. Click on the Trap cursor on the screen and drag it to move the location of the trapping laser. Once trapped, calibrate the bead to correlate voltage measurements to force and displacement.

6.16. Click on the Calibration button. Adjust the calibration routine based on power spectra analysis and fit the corner frequency within the software for the X, Y, and Z directions (Supplementary Figure S6).

6.17. Click on Settings. Type in the diameter of the bead (1,000 nm), and type in the temperature of the stage found in the bottom left of the software window. (see Supplemental Figure S6).

6.18. Click on Trap 1. Click on X Signal. Click on Run to perform the corner frequency fit. Click and drag within the window to optimize the function fit. Click on Use It for sensitivity and stiffness values. Click on Accept Values. Repeat for the Y and Z signals. Close the window. (see Supplemental Figure S6).

NOTE: Bead calibration routines on other optical trapping systems or custom-built systems that have been robustly tested by the user, such as the equipartition method or drag force method, are also acceptable57,58.

6.19. Find an actomyosin bundle by searching for beads bound to AFs on the surface of the coverslip.

6.20. When a bead uncrowded by other floating beads is detected, observe the AFs around it by fluorescence imaging to verify the presence of a bundle.

6.21. Verify that a bundle is present by looking for both fluorescent AFs colocalized. Turn on the white light source and use the appropriate filter cube to image each actin filament by turning the turret (488 nm and 532 nm excitation filter cubes for Alexa Fluor 488 and rhodamine excitation, respectively). See Supplemental Figure S4.

NOTE: A control experiment to verify the fluorescence intensity of single AFs can be useful in identifying bundles that are composed of a single 488- and single rhodamine-labeled filaments, or applicable to whichever set of fluorophores the user chooses to use.

6.22. Once verified, trap the bead attached to the top filament of the bundle by clicking on the Trap Shutter button.

6.23. Use the on-screen controls to record the data by clicking on the Oscilloscope button (Supplemental Figure S7). To visualize measurements without recording the data, click on Start. To save all data, click on Autosave. To record measurements, click on Start Record. Choose which data are to be visualized in real-time (position, force, x-direction, y-direction) by choosing from the drop down menu X signal or Y signal. Remember that xdirection is left to right, and y-direction is up and down on the screen. See Supplemental Figure S7.

NOTE: Data will be saved as .out files and includes time, voltage, displacement, and force for each direction. These files can be exported into other software for visualization and analysis.

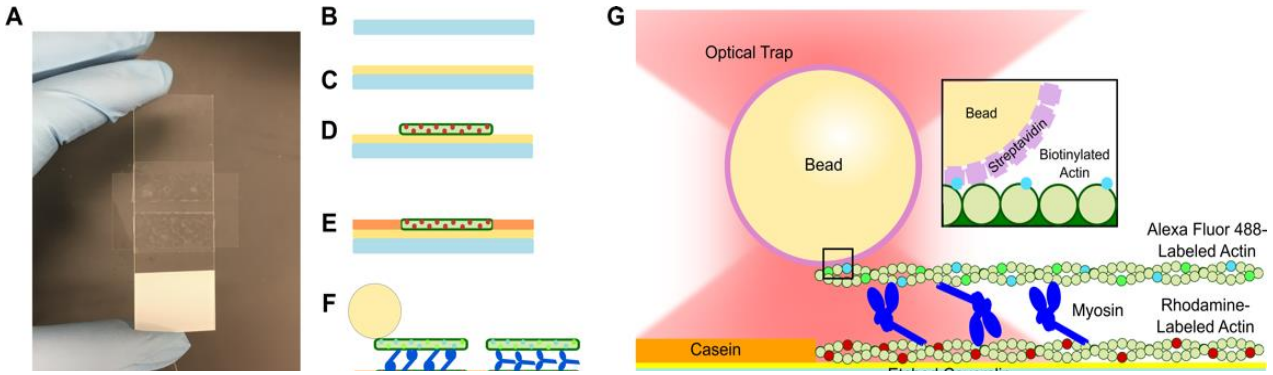

Figure 3.1: Assay Schematic. Etched coverslips are coated in poly-l-lysine and used to form the flow cell by using double-sided tape and a microscope slide (A-C). Timed introductions and incubation steps described in the protocol result in rhodamine phalloidin-stabilized actin as the template or bottom filament (D), followed by casein blocking to prevent non-specific binding (E), and (F) Alexa Fluor 488 phalloidin-stabilized biotinylated actin as the cargo or top filament, and teams of myosin II between that slide the filaments apart and generate force when ATP is introduced. The geometry of the motors and nature of crosslinking within the bundle could vary under different conditions, such as salt concentration. Streptavidin beads are used as the optical handle for the trap and bind solely to the cargo biotinylated actin filament, which aids in validating that proper bundles are formed on the slide (G).

3.1 Results

Flow cells containing the actomyosin bundle systems are of a standard design, consisting of a microscope slide and an etched coverslip separated by a channel made from double-sided sticky tape (Figure 3.1). The assay is then built from the coverslip up using staged introductions as described in the protocol.

The final assay consists of template rhodamine-labeled actin filaments; the desired myosin concentration (1 μM was used for the representative results in Figure 3.2 and Figure 3.3); biotinylated, Alexa Fluor 488-labeled actin filaments; 1 μm streptavidin beads; the oxygen scavenging system; ATP; and APB buffer. Multiple bundles will be formed per flow cell, and the actin concentrations described above give adequate spacing between bundles to ensure no unwanted interactions. This also facilitates obtaining multiple force measurements per flow cell to increase data acquisition efficiency. Force profiles should be reproducible within a flow cell and from flow cell to flow cell.

While the protocol above is geared toward the use of a commercial optical trapping setup, the flow cell and assay presented here could be easily utilized for a different commercial instrument or custom-built optical trapping setup coupled with a microscope or microscope stage and possessing fluorescence imaging capabilities. Once all flow cell additions are complete according to the above protocol, the actomyosin bundles on the slide (Figure 3.1) are ready for immediate measurement. The flow cell is added to the optical trap microscope stage, multiple bead calibration measurements are acquired, and bundles are identified through fluorescence colocalization of the bundle filaments. A bead bound to a bundle is trapped, and the displacement and corresponding force measurement begins. The user

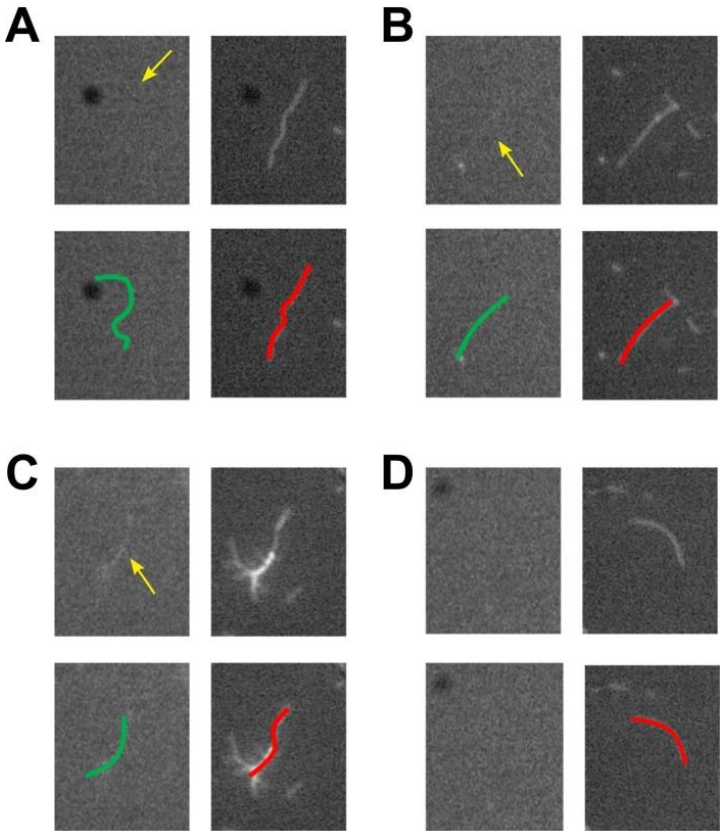

Figure 3.2: Fluorescent actomyosin bundles. Four different encounters of actin filaments and bundles within the bundle assay presented in Figure 3.1. The top cargo biotinylated actin filament with the Alexa Fluor 488 phalloidin channel is shown on the left, and the bottom template actin filament with the rhodamine phalloidin channel is on the right. At the bottom, the same figure is shown with colored lines overlaid to help guide the eye. (A) A top actin filament is found near a bottom actin filament but has an incomplete overlay. This would not be used for bundle experiments. (B) Top and bottom actin filaments are colocalized, and the intensity of each filament confirms that they are each single filaments within the bundle. This would be a good candidate for bundle experiments. (C) A large bundle of self-assembled rhodamine filaments is found on the bottom. While there is a corresponding top actin filament that is colocalized, there are too many bottom filaments present; thus, it would not be used for bundle experiments. This is also an example of how when multiple actin filaments of the same type are bundled, the fluorescence intensity increases. The user can utilize this as a gauge for judging single filaments versus bundles of the same filament type. (D) A bottom filament is present with no corresponding top filament, also confirming no bleedthrough. This would not be used for bundle experiments.

can observe the acquisition of data in real time on the computer monitor. Depending on the concentration of myosin used in the flow cell, the bundle could begin exhibiting substantial movement immediately, or it may take 30 s–1 min to effectively see an increase in displacement/force.

A representative force trace is shown in Figure 3.3A where the myosin motors exhibit a steady ramp in force followed by a plateau. It is typical to see these types of traces develop over 2–5 min. However, it is also possible to measure actomyosin bundles that do not generate any net force (Figure 3.3B). These traces appear as baseline noise or exhibit no substantial net increase in force over 90 s. This is likely due to a low local concentration of motor that does not permit productive sliding, or the bundle is in an unfavorable parallel orientation where the plus and minus ends of the filaments are aligned.

As the contents of the flow cell can be susceptible to degradation from the incident illumination and trapping laser, local heating on the slide over time, and generation of radial oxygen species, it is strongly advised to not use the same flow cell for more than 1 h. For maximum efficiency, it is suggested to have another assay incubating while acquiring data.

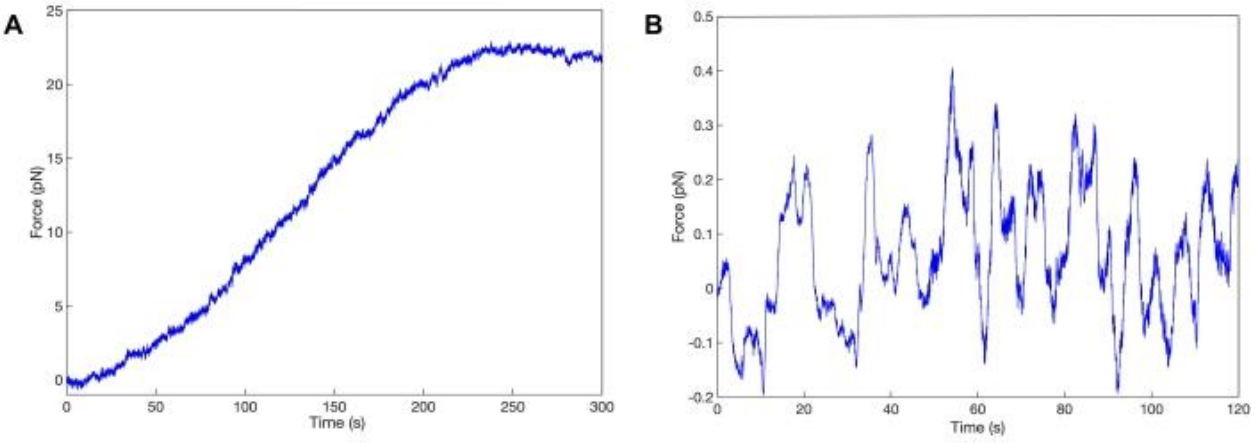

Figure 3.3: Myosin II ensemble force generation. Representative traces of skeletal myosin II motors generating force within the constructed *in vitro* actin structural hierarchy. The myosin motors are working together to collectively and productively generate force until a plateau is reached and force is sustained (A) or experience antagonization near baseline (B).

Displacement/force trace can be exported from the optical trapping software into Excel, Matlab, Igor, or other data management programs for further filtering and analysis. Data that can be extracted from such optical trapping ensemble/bundle experiments include different types of force generation profiles (baseline, ramp/plateau) under varying assay conditions, velocity of force generation, maximum force generation, ensemble kinetic and stepping behavior through step sizes and dwell times between steps or teams of steps, as well as duty ratio. The user can also alter the assay conditions to compare how adding different types of myosin motors, adding actin binding proteins, or changing buffer conditions influence these ensemble force generation characteristics.

3.5 Discussion

An *in vitro* study using optical tweezers combined with fluorescence imaging was performed to investigate the dynamics of myosin ensembles interacting with actin filaments. Actin-myosin-actin bundles were assembled using muscle myosin II, rhodamine actin at the bottom of the bundle and on the coverslip surface, and 488-labeled, biotinylated actin filaments on the top of the bundle. Actin protein from rabbit muscle was polymerized and stabilized using general actin buffers (GAB) and actin polymerizing buffers (APB). GAB and APB must be freshly prepared every day in the lab using ATP, FC buffer, and TC buffer. Muscle myosin II was used to form the actin-myosin-actin sandwiches. Phalloidin was used for fluorescent staining of the actin filaments, as well as stabilization *in vitro*.

Myosin activity can be confirmed by performing a standard gliding filament assay as published previously (Miller-Jaster, *et al*., 2012; Persson, *et al*., 2010). Myosin II and its subfragments can bind to the coverslip surface in a variety of orientations, and the presence of

the tail domain can slow down filament sliding as compared to assays using heavy meromyosin (Miller-Jaster, *et al*., 2012; Kron, *et al*., 1986; Yanagida, *et al*., 1984). However, gliding and surface movement can still be observed. A more apparent demonstration of myosin activity is active actin filament breaking that can be observed where longer actin filaments are broken into smaller fragments that then glide away in multiple directions. This occurs due to the high concentration of active motors on the surface, has been observed by multiple laboratories, and does not occur without active myosin motors present (Rastogi, *et al*., 2016; Tsuda, *et al*., 1996; Stewart, *et al*., 2013; Harada, *et al*., 1990; Fordyce, *et al*., 2008; Ozeki, *et al*., 2009). Further, the bundle assay presented here aids in alleviating motility issues that have primarily been associated with the gliding filament assay, such as the variety of motor binding orientations on a glass coverslip, because the bundle assay involves casein blocking of the glass surface so that motors bind within the bundle (Persson, *et al*., 2010; Neuman, *et al*., 2008; Neuman, *et al*., 2004).

The first step is to add rhodamine actin filaments as the bottom or template filament to a poly-L-lysine coated coverslip in a flow cell. Poly-L-lysine is used to promote actin binding since poly-lysine is positively charged while actin has negative charges and has been used in previous cytoskeletal *in vitro* assay preparations (Thoresen, *et al.,* 2013; Matusovsky, *et al.,* 2021; Reinemann, *et al.,* 2017). Before bundle formation, different actin dilutions were added to a flow cell to optimize the actin concentration. In this case, 600x from the stock was the optimal dilution that yielded a sufficient number of template filaments for bundle formation but with adequate spacing so that bundles were individualized. Dilution was carried out using the APB buffer. Adding rhodamine actin was followed by a layer of casein to block the surface and avoid non-specific binding. The flow cell was incubated for 30 min and washed after incubation with buffer to wash out any unbound actin filaments. Finally, a combination of myosin, 488/biotin

actin, and streptavidin-coated beads were added to the flow cell to facilitate actin–myosin bundle formation. The bead concentration should be such that there are enough to bind surface-bound bundles and enough in suspension to facilitate calibration. However, too high of a bead concentration can cause difficulty during trapping experiments due to neighboring beads falling into the laser trap and disrupting measurement. Myosin motors are added to the combination right before injecting it to the slide so that the myosin motors do not preemptively aggregate with the cargo or top biotinylated actin filament and will thus bind the bottom rhodamine to bundle biotinylated actin filaments.

The NT2 optical trapping system is a commercial optical trap with combined brightfield, differential interference contrast (DIC), and epifluorescence imaging modalities. It is coupled with a Zeiss AxioObserver 3 inverted microscope with 100x/NA 1.46 and 63x/NA 1.0 water immersion trapping and detection objectives. The system is equipped with click and drag trapping capability of one laser trap and can be used while imaging in any of the listed modalities previously. The formed bundles are detected and confirmed by using fluorescence imaging. Having a white light source with appropriate filter cubes (GFP/FITC and TRITC/CY3) allows for rapid switching between filament imaging. Colocalized AFs were verified by visualizing the AFs at the different excitation wavelengths before taking each force measurement using optical tweezers. As the filaments can photobleach quickly even with an oxygen scavenging reagent, it is suggested that researchers optimize visualization parameters such as intensity and exposure time before performing the bundle experiments.

Optical trapping was employed to take the force measurements, using the streptavidin beads in the presence of ATP to bind the biotinylated cargo actin filament and activate myosin force generation as a force transducer. Displacement and force versus time data obtained by

optical trapping were extracted from the trapping software for analysis. However, the commercial trapping software also provides analysis routines that can be utilized, or custom algorithms in other programs can be programmed by the user to visualize and analyze trapping data. On custom optical trapping systems, the user may have excitation lasers instead of a white light source with filters, which are also acceptable to use. Further, fluorescent dyes can be changed to be suited to the existing equipment a user may have if the emission spectra do not overlap and cause bleedthrough. We note that the assay presented is a baseline assay that can be further customized by the user depending on their research question within the realm of actomyosin ensemble mechanics. The general workflow can also be applied to other *in vitro* cytoskeletal ensemble systems that may be of interest, such as microtubule bundle assays that form minimal models of mitotic spindle (Al Azzam, *et al.*, 2021; Thoresen, *et al.*, 2013; Reinemann, *et al.*, 2017; Cordova, *et al.*, 2018; Reinemann, *et al.*, 2018; Shimamoto, *et al.*, 2014). Modifications could include but are not limited to changing the fluorophore labels that are suited to the user's existing setup altering myosin concentration, construct, or isotype; and titrating buffer conditions, among other aspects.

Potential challenges are possible when performing this assay. When forming the actin–myosin bundles, myosin concentration within the actin bundles may not be homogeneous across the slide. To accommodate this, multiple bundles across the entire slide will be measured to ensure that motor distribution and force generation profiles are properly sampled. It is also challenging to know bundle orientation if this is required for interpretation of force data. Thus, multiple trials should be taken for each bundle. One could also incorporate actin filament end labeling through fluorescent gelsolin or gelsolin-coated beads of a smaller size than the optical trapping handle. Fluorescence imaging can also be used to look at x and y component forces to

deduce bundle orientation. Moreover, as myosin aggregation state is highly influenced by the ionic strength of the buffer with formation of thick filaments occurring upon rapid dilution of KCl, buffer salt concentration should be monitored appropriately (Shimamoto, *et al.*, 2018; Shimamoto, *et al.*, 2015).

Previous studies that used other *in vitro* methods such as gliding assays were helpful to identify the role of myosin domains and study the configuration and interactions between myosin and other actin binding proteins. However, these methods have a disadvantage in that binding myosin onto a rigid surface will limit the potential for coordination between myosin motors and thus mechanosensing feedback that occurs to determine whether the motor ensemble is in a high or low duty ratio mode (Wagoner, *et al.*, 2021; Stewart, *et al.*, 2021; Stam, *et al.*, 2015; Thoresen, *et al.*, 2011). Further, optical trapping with single-myosin motor networks does not give a clear understanding of how myosin motors interact with each other and with actin filaments. The protocol developed here allows for the investigation of myosin motor ensemble dynamics within a compliant, hierarchical actin network. It is also customizable in terms of motor-filament ensemble characteristics such as concentration, isoform, and buffer environment, among other aspects, to allow for systematic investigation. The presented protocol is a platform for future studies of more complex actomyosin networks and maintains the precision of displacement and force generation measurements facilitated by optical trapping that has traditionally been used for single-molecule studies.

3.6 Acknowledgments

This work is supported in part by the University of Mississippi Graduate Student Council

Research Fellowship (OA), University of Mississippi Sally McDonnell-Barksdale Honors College (JCW, JER), the Mississippi Space Grant Consortium under grant number NNX15AH78H (JCW, DNR), and the American Heart Association under grant number 848586 (DNR).

BIBLIOGRAPHY

3.7 Bibliography

Akhshi, T. K., Wernike, D., Piekny, A. Microtubules and actin crosstalk in cell migration and division. Cytoskeleton. 71 (1), 1–23 (2014).

Al Azzam, O., Trussell, C. L., Reinemann, D. N. Measuring force generation within reconstituted microtubule bundle assemblies using optical tweezers. Cytoskeleton. 78 (3), 111–125 (2021).

Albert, P. J., Erdmann, T., Schwarz, U. S. Stochastic dynamics and mechanosensitivity of myosin II minifilaments. New Journal of Physics. 16 (2014).

American Journal of Physiology - Heart and Circulatory Physiology. 293 (1), 284–291 (2007).

Brawley, C. M., Rock, R. S. Unconventional myosin traffic in cells reveals a selective actin cytoskeleton. Proceedings of the National Academy of Sciences of the United States of America. 106 (24), 9685–9690 (2009).

Cheng, Y. S., De Souza Leite, F., Rassier, D. E. The load dependence and the force-velocity relation in intact myosin filaments from skeletal and smooth muscles. American Journal of Physiology - Cell Physiology. 318 (1), C103–C110 (2020).

Cordova, J. C. *et al.* Bioconjugated core–shell microparticles for high-force optical trapping. Particle and Particle Systems Characterization. 35 (3), 1–8 (2018).

Debold, E. P. *et al.* Hypertrophic and dilated cardiomyopathy mutations differentially affect the molecular force generation of mouse α-cardiac myosin in the laser trap assay.

Debold, E. P., Patlak, J. B., Warshaw, D. M. Slip sliding away: Load-dependence of velocity generated by skeletal muscle myosin molecules in the laser trap. Biophysical Journal. 89 (5), L34–L36 (2005).

Debold, E. P., Walcott, S., Woodward, M., Turner, M. A. Direct observation of phosphate

inhibiting the Force-generating capacity of a miniensemble of myosin molecules. Biophysical Journal. 105 (10), 2374–2384 (2013).

Duke, T. A. J. Molecular model of muscle contraction. Proceedings of the National Academy of Sciences of the United States of America. 96 (6), 2770–2775 (1999).

Dupuis, D. E., Guilford, W. H., Wu, J., Warshaw, D. M. Actin filament mechanics in the laser trap. Journal of Muscle Research and Cell Motility. 18 (1), 17–30 (1997).

Erdmann, T., Schwarz, U. S. Stochastic force generation by small ensembles of myosin II motors. Physical Review Letters. 108 (18), 1–5 (2012).

Finer, J. T. *et al.* Characterization of single actin-myosin interactions. Biophysical Journal. 68 (4 SUPPL.), 291–296 (1995).

Finer, J. T., Simmons, R. M., Spudich, J. a Single myosin molecule mechanics: piconewton forces and nanometre steps. Nature. 368 (6467), 113–119 (1994).

Fordyce, P. M., Valentine, M. T., Block, S. M. Advances in surface-based assays for single molecules.

Forth, S., Hsia, K. C., Shimamoto, Y., Kapoor, T. M. Asymmetric friction of nonmotor MAPs can lead to their directional motion in active microtubule networks. Cell. 157 (2), 420–432 (2014).

Girolami, F. *et al.* Novel α-actinin 2 variant associated with familial hypertrophic cardiomyopathy and juvenile atrial arrhythmias: A massively parallel sequencing study. Circulation: Cardiovascular Genetics. 7 (6), 741–750 (2014).

Goldstein, L. S. Kinesin molecular motors: transport pathways, receptors, and human disease. Proceedings of the National Academy of Sciences of the United States of America. 98 (13), 6999–7003 (2001).

Guo, B., Guilford, W. H. The tail of myosin reduces actin filament velocity in the in vitro motility assay. Cell Motility and the Cytoskeleton. 59 (4), 264–272 (2004).

Harada, Y., Sakurada, K., Aoki, T., Thomas, D. D., Yanagida, T. Mechanochemical coupling in actomyosin energy transduction by in vitro movement assay. Journal of Molecular Biology. 216 (1), 49–68 (1990).

Hartman, M. A., Spudich, J. A. The myosin superfamily at a glance. Journal of Cell Science. 125 (7), 1627–1632 (2012).

Hilbert, L., Cumarasamy, S., Zitouni, N. B., Mackey, M. C., Lauzon, A. M. The kinetics of mechanically coupled myosins exhibit group size-dependent regimes. Biophysical Journal. 105 (6), 1466–1474 (2013).

HUXLEY, A. F. Muscle structure and theories of contraction. Progress in Biophysics and Biophysical Chemistry. 7, 255–318 (1957).

Huxley, H. E. Fifty years of muscle and the sliding filament hypothesis. European Journal of Biochemistry. 271 (8), 1403–1415 (2004).

John T. Barron Hypertrophic cardiomyopathy. Current Treatment Options in Cardiovascular Medicine. 1 (3), 277–282 (1999).

Kad, N. M., Kim, S., Warshaw, D. M., VanBuren, P., Baker, J. E. Single-myosin crossbridge interactions with actin filaments regulated by troponin-tropomyosin. Proceedings of the National Academy of Sciences of the United States of America. 102 (47), 16990–16995 (2005).

Kawana, M., Sarkar, S. S., Sutton, S., Ruppel, K. M., Spudich, J. A. Biophysical properties of human b-cardiac myosin with converter mutations that cause hypertrophic cardiomyopathy. Science Advances. 3 (2), 1–11 (2017).

Kaya, M., Higuchi, H. Nonlinear elasticity and an 8-nm working stroke of single myosin molecules in myofilaments. Science. 329 (5992), 686–689 (2010).

Kaya, M., Tani, Y., Washio, T., Hisada, T., Higuchi, H. Coordinated force generation of skeletal myosins in myofilaments through motor coupling. Nature Communications. 8 (May), 1–13 (2017).

Kron, S. J., Spudich, J. A. Fluorescent actin filaments move on myosin fixed to a glass surface. Proceedings of the National Academy of Sciences of the United States of America. 83 (17), 6272–6276 (1986).

Kron, S. J., Uyeda, T. Q. P., Warrick, H. M., Spudich, J. A. An approach to reconstituting motility of single myosin molecules. Journal of Cell Science. 98 (SUPPL. 14), 129–133 (1991).

Lee Sweeney, H., Holzbaur, E. L. F. Motor proteins. Cold Spring Harbor Perspectives in Biology. 10 (5), a021931 (2018).

Mansoon, A., Balaz, M., Albet-Torres, N., Rosengren, K. J. In vitro assays of molecular motors –- impact of motor-surface interactions. Frontiers in Bioscience. 13, 5732–5754 (2008).

Matusovsky, O. S. *et al.* Millisecond conformational dynamics of skeletal Myosin II power stroke studied by high-speed atomic force microscopy. ACS Nano. 15 (2), 2229–2239 (2021).

Miller-Jaster, K. N., Petrie Aronin, C. E., Guilford, W. H. A quantitative comparison of blocking agents in the in vitro motility assay. Cellular and Molecular Bioengineering. 5 (1), 44–51 (2012).

Molloy, J. E., Burns, J. E., Kendrick-Jones, B., Tregear, R. T., White, D. C. S. Movement and force produced by a single myosin head. Nature. 378 (6553), 209–212 (1995).

Murrell, M., Thoresen, T., Gardel, M. Reconstitution of contractile actomyosin arrays. Methods in Enzymology. 540 (11), 265–282 (2014).

Nag, S. *et al.* The myosin mesa and the basis of hypercontractility caused by hypertrophic cardiomyopathy mutations. Nature Structural & Molecular Biology. 24 (6), 525–533 (2017).

Nayak, A. *et al.* Single-molecule analysis reveals that regulatory light chains fine-tune skeletal myosin II function. Journal of Biological Chemistry. 295 (20), 7046–7059 (2020).

Neuman, K. C., Block, S. M. Optical trapping. Review of Scientific Instruments. 75 (9), 2787–2809 (2004).

Neuman, K. C., Nagy, A. Single-molecule force spectroscopy: Optical tweezers, magnetic tweezers and atomic force microscopy. Nature Methods. 5 (6), 491–505 (2008)

O'Connell, C. B., Tyska, M. J., Mooseker, M. S. Myosin at work: Motor adaptations for a variety of cellular functions. Biochimica et Biophysica Acta - Molecular Cell Research. 1773 (5), 615–630 (2007).

Ozeki, T. *et al.* Surface-bound casein modulates the adsorption and activity of kinesin on SiO2 surfaces. Biophysical Journal. 96 (8), 3305–3318 (2009).

Persson, M. *et al.* Heavy meromyosin molecules extending more than 50 nm above adsorbing electronegative surfaces. Langmuir. 26 (12), 9927–9936 (2010).

Pertici, I. *et al.* A myosin II nanomachine mimicking the striated muscle. Nature Communications. 9 (1), 1–10 (2018).

Rastogi, K., Puliyakodan, M. S., Pandey, V., Nath, S., Elangovan, R. Maximum limit to the number of myosin II motors participating in processive sliding of actin. Scientific Reports. 6 (August), 1–11 (2016).

Reinemann, D. N. *et al.* Collective force regulation in anti-parallel microtubule gliding by dimeric Kif15 kinesin motors. Current Biology. 27 (18), 2810–2820.e6 (2017).

Reinemann, D. N., Norris, S. R., Ohi, R., Lang, M. J. Processive Kinesin-14 HSET exhibits directional flexibility depending on motor traffic. Current Biology. 28 (14), 2356–2362.e5 (2018).

Ruegg, C. *et al.* Molecular motors: Force and movement generated by single Myosin II molecules. Physiology. 17 (5), 213–218 (2002).

Shimamoto, Y., Forth, S., Kapoor, T. M. Measuring pushing and braking forces generated by ensembles of Kinesin-5 crosslinking two microtubules. Developmental Cell. 34 (6), 669–681 (2015).

Shimamoto, Y., Kapoor, T. M. Analyzing the micromechanics of the cell division apparatus. Methods in Cell Biology. 145, 173–190 (2018).

Simmons, R. M., Finer, J. T., Chu, S., Spudich, J. A. Quantitative measurements of force and displacement using an optical trap. Biophysical Journal. 70 (4), 1813–1822 (1996).

Single-Molecule Techniques: A Laboratory Manual. 431–460, at <https://static1.squarespace.com/static/53aa0662e4b0d4cbb80321fe/t/53b179e2e4b00738d882ec41/1404140002944/FordyceValentineCSHLabManual.pdf> (2008).

Spudich, J. A. *et al.* Myosin structure and function. Cold Spring Harbor Symposium on Quantitative Biology. 60, 783–791 (1995).Sommese, R. F. *et al.* Molecular consequences of the R453C hypertrophic cardiomyopathy mutation on human β-cardiac myosin motor function. Proceedings of the National Academy of Sciences of the United States of America. 110 (31), 12607–12612 (2013).

Spudich, J. A. The myosin swinging cross-bridge model. Nature reviews. Molecular Cell

Biology. 2 (May), 387–392 (2001).

Stam, S., Alberts, J., Gardel, M. L., Munro, E. Isoforms confer characteristic force generation and mechanosensation by myosin II filaments. Biophysical Journal. 108 (8), 1997–2006 (2015).

Stewart, T. J. *et al.* Actin sliding velocities are influenced by the driving forces of actin-myosin binding. Cellular and Molecular Bioengineering. 6 (1), 26–37 (2013).

Stewart, T. J., Murthy, V., Dugan, S. P., Baker, J. E. Velocity of myosin-based actin sliding depends on attachment and detachment kinetics and reaches a maximum when myosin-binding sites on actin saturate. Journal of Biological Chemistry. 297 (5), 101178 (2021).

Thoresen, T., Lenz, M., Gardel, M. L. Reconstitution of contractile actomyosin bundles. Biophysical Journal. 100 (11), 2698–2705 (2011).

Thoresen, T., Lenz, M., Gardel, M. L. Thick filament length and isoform composition determine self-organized contractile units in actomyosin bundles. Biophysical Journal. 104 (3), 655–665 (2013).

Tsuda, Y., Yasutake, H., Ishijima, A., Yanagida, T. Torsional rigidity of single actin filaments and actin-actin bond breaking force under torsion measured directly by in vitro micromanipulation. Proceedings of the National Academy of Sciences of the United States of America. 93 (23), 12937–12942 (1996).

Tyska, M. J. *et al.* Two heads of myosin are better than one for generating force and motion. Proceedings of the National Academy of Sciences of the United States of America. 96 (8), 4402–4407 (1999).

Tyska, M. J., Warshaw, D. M. The myosin power stroke. Cell Motility and the Cytoskeleton. 51 (1), 1–15 (2002).

Veigel, C., Molloy, J. E., Schmitz, S., Kendrick-Jones, J. Load-dependent kinetics of force production by smooth muscle myosin measured with optical tweezers. Nature Cell Biology. 5 (11), 980–986 (2003).

Vilfan, A., Duke, T. Instabilities in the transient response of muscle. Biophysical Journal. 85 (2), 818–827 (2003).

Wagoner, J. A., Dill, K. A. Evolution of mechanical cooperativity among myosin II motors. Proceedings of the National Academy of Sciences of the United States of America. 118 (20), e2101871118 (2021).

Walcott, S., Warshaw, D. M., Debold, E. P. Mechanical coupling between myosin molecules causes differences between ensemble and single-molecule measurements. Biophysical Journal. 103 (3), 501–510 (2012).

Weirich, K. L., Stam, S., Munro, E., Gardel, M. L. Actin bundle architecture and mechanics regulate myosin II force generation. Biophysical Journal. 120 (10), 1957–1970 (2021).

Yanagida, T., Nakase, M., Nishiyama, K., Oosawa, F. Direct observation of motion of single F-actin filaments in the presence of myosin. Nature. 307 (5946), 58–60 (1984).

CHAPTER 4

MYOSIN II ADJUST MOTILITY PROPERTIES AND REGULATES FORCE PRODUCTION BASED ON MOTOR ENVIRONMENT

*This chapter is adapted from Omayma Y. Al Azzam, Janie C. Watts, Justin E. Reynolds, Juliana E. Davis, and Dana N. Reinemann, "Myosin II Adjusts Motility Properties and Regulates Force Production Based on Motor Environment". Cell Mol Bioeng. 2022 Aug 16;15(5):451-465. doi: 10.1007/s12195-022-00731-1. PMID: 36444350; PMCID: PMC9700534. Reproduced with permission from Springer Nature, license number: 575771022641

4.1 Summary

Myosin II has been investigated with optical trapping, but single motor-filament assay arrangements are not reflective of the complex cellular environment. To understand how myosin interactions propagate up in scale to accomplish system force generation, we devised a novel actomyosin ensemble optical trapping assay that reflects the hierarchy and compliancy of a physiological environment and is modular for interrogating force effectors. Hierarchical actomyosin bundles were formed *in vitro*. Fluorescent template and cargo actin filaments (AF) were assembled in a flow cell and bundled by myosin. Beads were added in the presence of ATP to bind the cargo AF and activate myosin force generation to be measured by optical tweezers.

Three force profiles resulted across a range of myosin concentrations: high force with a ramp-plateau, moderate force with sawtooth movement, and baseline. The three force profiles, a well as high force output, were recovered even at low solution concentration, suggesting that myosins self-optimize within AFs. Individual myosin steps were detected in the ensemble traces, indicating motors are taking one step at a time while others remain engaged in order to sustain productive force generation. Motor communication and system compliancy are significant contributors to force output. Environmental conditions, motors taking individual steps to sustain force, the ability to backslip, and non-linear concentration dependence of force indicate that the actomyosin system contains a force-feedback mechanism that senses the local cytoskeletal environment and communicates to the individual motors whether to be in a high or low duty ratio

4.2 Introduction

Myosins are motor proteins that convert chemical energy into mechanical work to step along actin filaments (AFs) (Hartman and Spudich 2012; J. a Spudich *et al.* 1995). The dynamics of myosin–actin net- works facilitate the movement and reorganization necessary for essential large-scale cellular tasks such as cell motility and the contractile ring during cytokine- sis (Akhshi, Wernike, and Piekny 2014; Hartman and Spudich 2012; Pollard 2010; Spudich *et al.* 1995). Skeletal myosin II is responsible for muscle contraction through working as an ensemble to carry out the relative sliding of AFs within a sarcomere (Huxley 2004; Spudich 2001). Myosins within a thick filament form crossbridges between AFs and use conformational change

due to its mechanochemical cycle to collectively move within the aligned filaments to promote overall contraction (Huxley 2004; Kad *et al.,* 2005; Spudich 2001; Spudich *et al.,* 1995). Skeletal myosin II has been studied extensively at the single molecule (SM) level and at the muscle level to better understand the underlying mechanics of muscle contraction (Duke 1999; Finer *et al.,* 1995; Finer, Simmons, and Spudich 1994; Kron *et al.,* 1991; Piazzesi *et al.* 2007; Ruegg *et al.,* 2002; Yanagida *et al.,* 2000). SM studies, such as those using optical trapping (OT), have been essential in evaluating the mechanistic behavior of molecular motors, including myosin, determining properties such as SM force generation and step sizes that can be overshadowed in bulk experiments (Finer *et al.,* 1994; Svoboda and Block 1994). A distinct property of skeletal myosin II is its low duty ratio or non-processive nature as a single molecule, or it does not stay engaged with its AF track for the majority of its mechanochemical cycle (Finer *et al.,* 1994; Howard 2001; O'Connell, Tyska, and Mooseker 2007). Thus, myosin II has been classified as a ''rower'' type motor, or a motor that must work in large arrays in order to facilitate productive movement, instead of a ''porter'' type motor like conventional kinesin-1 that can tote cargo as a SM while remaining engaged with its microtubule track for a considerable distance (Al Azzam, Trussell, and Reinemann 2021; Howard 2001; Leibler and Huse 1993)..

A seminal paper by Finer *et al.,* analyzed the force generation properties of single myosin II motor con- structs using OT through development of the ''three- bead'' or ''dumbbell'' assay (Finer *et al.,* 1995, 1994). As muscle myosin II works in teams to contract AFs and is non-processive as a single molecule, the OT assay orientation needed to be rearranged from the classic motor-bound bead approach with the filament adhered to the coverslip (Al Azzam *et al.,* 2021).Their alternative was to utilize two laser traps to sus- pend an AF bound on each end to the trapped beads (forming the ''dumbbell'') over a myosin motor bound to a bead attached to a

coverslip so that upon AF release, myosin would not be able to diffuse away and thus have the ability to obtain multiple force and step measurements (Finer *et al.,* 1995, 1994).

However, a prevalent challenge still present in the SM biophysics field is reconstituting a motor-filament environment that better reflects physiological function (Elting and Spudich 2012). Many optical trapping motor studies use isolated, reductionist geometries, such as a single motor interacting with a single filament, which does not reflect the structural hierarchy in which some motors, such as myosin II, function (Al Azzam *et al.,* 2021; Elting and Spudich 2012). More complex in vitro structures that contain multiple myosin motors are necessary to better understand the synergy of myosin and AFs networks (O'Connell, *et al*., 2007). The dumbbell assay orientation has been used to probe small motor ensemble force generation by having multiple myosins attached to a third bead or using a myosin thick filament attached to a surface and allowing the motors to interact with the suspended AF (Debold *et al.,* 2013; Kaya *et al.* 2017; Kaya and Higuchi 2010; Walcott, Warshaw, and Debold 2012). Kaya *et al.,* evaluated single myosin mechanics within a myofilament attached to a coverslip and with the AF suspended above, finding that low system stiffness minimizes drag of negatively strained myosins during loaded conditions (Kaya and Higuchi 2010). In addition, myosin's elastic portion is stretched during active force generation, reducing step size with increasing load even though the working stroke remains approximately constant, and step sizes of single myosin heads varied from 7 to 4 nm in a load dependent manner (Kaya and Higuchi 2010). In a subsequent paper using the same assay orientation, Kaya *et al.,* observed ~ 4 nm stepwise actin displacements beyond a load of 30 pN, suggesting that steps cannot be driven exclusively by single myosins but instead by potentially coordinated force generations among multiple myosins, and the probability of coordinated force generation can be enhanced against high loads by using strain-dependent

kinetics between force states, multiple power strokes, and high ATP concentration (Kaya *et al.*, 2017). Walcott *et al.*, observed that mechanical coupling between myosins causes differences between SM and ensemble through employing the three-bead assay orientation but having multiple myosin motors attached to the coverslip-bound bead to form a small myosin ensemble, measuring smooth increase in force as opposed to individual binding events (Walcott *et al.*, 2012). They also employed an AF gliding assay to observe AF length-dependent motility and that the myosin ensembles glide unloaded AFs faster than predictions from SM measurements would indicate (Walcott *et al.*, 2012). Using a similar AF gliding assay, Hilbert *et al*. measured three distinct myosin group size-dependent motility regimes where above a critical AF length, increasing the number of myosins attached to the AF leads to a further increase in gliding velocity, and at lower myosin concentration, the group effect becomes lost, suggesting that a minimal myosin concentration is needed to achieve an inter-myosin communication effect also observed by Stachowiak *et al*., where myosin II self-organizes within reconstituted actomyosin bundles (Hilbert *et al*., 2013). Recently, Stewart *et al*., utilized the AF gliding assay to find that velocity and ATPase activity are both strain-dependent, and gliding velocity maximizes with the saturation of myosin binding sites on actin, which challenges the conventional independent force model of muscle contraction that assumes AF sliding is limited by detachment of individual myosins from actin (Stewart *et al*., 2021). Similarly, Wagoner *et al.*, purported that the amount of force felt by an individual motor will depend on the forces exerted by the other motors, giving rise to a force-mediated motor cooperativity that affects the number of motors bound but also the order in which each motor performs its transitions; further, myosins have evolved to reduced filament backsliding to increase the speed and efficiency of muscle contraction (Wagoner and Dill 2021). Sung *et al.*, demonstrated that human b-cardiac S1 myosin subfragment ADP release

rate depends exponentially on applied load by using harmonic force spectroscopy, and values are in agreement with a previous study by Greenberg *et al.,* who investigated the load-dependent ADP release of porcine b-cardiac myosin at saturating ATP (Greenberg and Moore 2010; Sung *et al.,* 2015). In a subsequent study, Liu *et al.,* determined that load-de- pendent cardiac S1 myosin detachment rates, and thus ensemble duty ratio and force generation, can be altered by cardiomyopathy-causing mutations and small molecule activators and inhibitors of cardiac myosin, suggesting that large-scale cardiac contractility can be controlled by tuning molecular level load-dependent kinetics (Liu *et al.,* 2018).

Altogether, there is overwhelming evidence that myosin motor behavior deviates between the SM level and when working teams, and these motor ensembles are not a sum of the individual parts, which has been attributed to myosin's inherent need to adapt to multiple types of environments and external loads (Debold *et al.,* 2013; O'Connell *et al.,* 2007; Ruegg *et al.,* 2002; Wagoner and Dill 2021; Walcott *et al.,* 2012). Additionally, the feedback loop from the environment to the motor ensemble, such as net- work stiffness, motor compliancy, and detecting number of bound motors, will also dictate force output through altering motor communication and coordination in the form of force generation and duty ratio (Albert, Erdmann, and Schwarz 2014; Ennomani *et al.,* 2016; Erdmann and Schwarz 2012; Hilbert *et al.,* 2013; Kaya *et al.,* 2017; Stam *et al.,* 2015; Stewart *et al.,* 2021; Weirich *et al.,* 2021). However, in ensemble studies to this point, the myosins are bound to a rigid surface, such as a bead or coverslip, and utilize one AF. In these cases, the motors are not able to move or communicate freely with each other, nor does having myosins rigidly bound reflect the physiological com- pliancy and hierarchical environment in which the motors would work together (Al Azzam *et al.,* 2021). As this critical parameter is necessary for force readout, there is a need to develop an

optical trapping assay that fosters and captures motor coordination and system compliancy to paint a more realistic picture of the mechanistic underpinnings of myosin II ensemble force generation. Here, we formulate an approach that combines the precision of OT with in vitro active assembly of cytoskeletal hierarchy and measure ensemble myosin II force generation between two actin filaments using optical tweezers to capture elements of motor communication and cooperativity suggested by previous simulation and AF gliding experiment studies (Albert *et al.*, 2014; Erdmann and Schwarz 2012; Stam *et al.*, 2015; Stewart *et al.*, 2021; Wagoner and Dill 2021; Walcott *et al.*, 2012).

4.3 Methods

4.3.1 Actin Polymerization

Actin polymerization was performed as described previously (Balikov *et al.*, 2017; Cordova *et al.*, 2018). Non-labeled rabbit skeletal muscle actin (Cytoskeleton) was reconstituted by adding 100 µL of reverse osmosis (RO) water to 1 mg of lyophilized actin. The contents were mixed by gently pipetting up and down, aliquoted, and stored at - 80 °C with final actin concentration of 10 mg/mL. To polymerize non-labeled actin into filaments, 5 µL of 10 mg/mL actin were mixed with 100 µL General Actin Buffer (GAB: 5 mM Tris–HCl, 0.2 mM CaCl2, 0.5 mM DTT,0.2 mM ATP). The mixture was kept on ice and allowed to incubate for one hour. Actin was then polymerized into filaments by adding 5.5 µL of Actin Polymerizing Buffer (APB: 50 mM Tris–HCl, 500 mM KCl, 2 mM MgCl2, 2 mM CaCl2 2 mM DTT, 5 mM ATP) to the actin mixture, mixed well by gently pipetting up and down, and allowed to incubate for 20 min on ice. Actin filaments were stabilized and fluorescently labeled by adding 5 µL of rhodamine- labeled phalloidin (Cytoskeleton). The vial was wrapped in aluminum foil to block

light and allowed to incubate on ice for one hour. The mixture was stored at 4 °C to be used for preparing actin myosin bundles for up to one week.

Biotinylated skeletal muscle actin (Cytoskeleton) was reconstituted by adding 20 µL of RO water to 20 lg of lyophilized actin. The contents were mixed well by gently pipetting up and down, aliquoted, and stored at - 80 °C with final biotinylated actin concentration of 1 mg/mL. Biotinylated actin was formed so that actin and biotinylated actin were in a 10:1 ratio by mixing 5 µL of 10 mg/mL actin and 5 µL of 1 mg/ mL biotinylated actin. This solution was mixed with 100 µL GAB and allowed to incubate for one hour on ice. To polymerize the biotinylated actin filaments, 11 µL of APB was added to the actin mixture, mixed well by gently pipetting up and down, and allowed to incubate for 20 min in ice. To stabilize and fluorescently label the biotinylated actin filaments, 5 µL of Alexa Fluor 488 labeled phalloidin (ThermoFisher) were added to the biotinylated actin. The vial was wrapped in aluminum foil to block light and allowed to incubate on ice for one hour. The mixture was stored at 4 °C to be used for preparing actin myosin bundles for up to one week.

4.3.2 Optical Trapping Actomyosin Bundle Assay Preparation

Full length rabbit skeletal muscle myosin II (Cytoskeleton) was reconstituted to 10 mg/mL by adding 100 µL of RO water containing 1 mM DTT. Stock myosin was diluted 10 9 by adding 10 µL of 10 mg/mL myosin to 90 µL of 1 mM DTT in RO water, snap frozen, and stored at -80 °C. 1 µL streptavidin-coated beads (Spherotech) were cleaned by diluting 20 µL of 1 µL streptavidin beads into 80 µL RO water and washing 4 times by spinning down at 10,000 rpm and reconstituting in 100 µL RO water. The beads were sonicated for 2 min at 40% and stored on a rotator at 4 °C. Etched coverslips were soaked in poly-l-lysine solution (PLL: 30 mL of

100% ethanol, 200 µL of 0.1% w/v poly-L-lysine (SigmaAldrich)) for 15 min to allow coating the surface to facilitate actin filament binding. The coverslip was removed from the PLL solution with tweezers, taking care to only touch the edge of the coverslip, and dried with a filtered airline until there was no ethanol left and no residue on the coverslip.

A standard 10–15 µL flow cell was formed using a microscope slide, the PLL coverslip, and double-sided sticky tape. On the microscope slide, two pieces of double-sided sticky tape were applied to the middle of the slide and separated by 3–4 mm. The PLL coated coverslip was then added to the top of the tape perpendicular to the long axis of the microscope slide to form a channel where the liquid will be added. The coverslip was compressed onto the tape and microscope slide thoroughly using a small tube until the tape was transparent.

For formation of actomyosin bundles, both rhodamine and biotinylated 488-labeled actin filament solutions were diluted 600X in APB as this dilution was sufficient for multiple bundles to form per slide but were spread out enough to ensure isolated measurements. To ensure robust labeling of filaments, 5 µL of their respective labeled phalloidin were added to each tube and incubated on ice in the dark for 15 min.

To begin assembling the actomyosin bundles, 15 µL of the diluted rhodamine actin were introduced to the PLL flow cell and allowed to incubate for 10 min in a humidity chamber. During this incubation in a separate tube, 15 µL of the diluted biotinylated actin were mixed with an oxygen scavenging system of 1 µL beta- D-glucose at 500 mg/mL, 1 µL glucose oxidase at 25 mg/mL, and 1 µL catalase at 500 units/mL to stabilize the filaments and reduce photobleaching during fluorescence imaging (Cordova *et al.* 2018; Reinemann *et al.* 2017). In addition, 1 µL of 100 mM ATP and 1 µL of 10 9 diluted cleaned streptavidin beads were added to the mixture. The solution was gently mixed by pipetting up and down, and the mixture was

put in a rotator at 4 °C while the rest of the actomyosin bundle was being assembled.

A 1 mg/mL casein solution (Blotting Grade Blocker, Biorad) was made in APB. After the rhodamine- labeled actin incubation, 15 µL of 1 mg/mL casein was added to the flow cell to prevent non-specific binding of subsequent components and incubated for 5 min in humidity chamber (Appleyard *et al.*, 2007; Cordova *et al.*, 2018; Dong *et al.*, 2010; Fordyce, Valentine, and Block 2008; Miller-Jaster, Petrie Aronin, and Guilford 2012; Reinemann *et al.*, 2017, 2018). Before adding the biotinylated actin mixture to the flow cell, 1 µL of the desired concentration of myosin (10, 1, 0.1, 0.01, 0.002, or 0.0001 µL) was added to the solution, mixed by gently pipetting up and down, immediately added to the flow cell, and allowed to incubate for 20 min. The ends of the flow cell were sealed with nail polish to prevent evaporation during imaging and optical trap- ping experiments.

4.3.3 Optical Trapping Measurements and Analysis

The flow cell was loaded onto the optical trapping instrument (NT2 Nanotracker2 from JPK/ BrukerNano) (Rauch and Jähnke 2014). which contains a single trapping laser and is combined with brightfield, differential interference contrast, and epifluorescence imaging to simultaneously image and measure force generated by actomyosin bundles. Epifluorescence imaging of filaments was achieved by excitation with an ultra- stable metal-halide light source (Photofluor LM-75,89North) and 488 and 532 nm excitation filter cubes. Before force measurement, bead position and trap stiffness were calibrated by trapping a bead in solution above the coverslip surface and running the power spectrum calibration routine within the JPK NT2 software. Bundle formation was investigated by verifying colocalization of single rhodamine and biotinylated 488-labeled actin filaments bundled by myosin motors through fluorescence imaging

(Fig. S1). After verification, the bead bound to the colocalized filament bundle was trapped. Resistance of bead movement from the trap center due to bundle filament sliding was measured as change in bead position and force generation vs. time. Custom MATLAB codes were used to visualize traces and perform position, force, and stepping/dwell analysis (Reinemann *et al.*, 2017, 2018). The step/dwell finding algorithm is based on a student's t-test to determine the edge of each step so that a dwell is defined in between (Brady *et al.*, 2015; Reinemann *et al.*, 2017, 2018). One-way ANOVA was performed on overall step size and detachment time averages, as well as step sizes and detachment times within force profile categories. p values are provided in figure captions and indications of non-significance (n.s.).

4.4 Results

4.4.1 Development of the Actomyosin Bundle Assay

Optical tweezers combined with fluorescence microscopy were employed to probe the mechanics of full-length myosin II motor ensembles interacting with actin filaments. Actomyosin bundles assays were developed with the goal of formulating an assay that incorporates AF structural hierarchy and compliancy, multiple myosin motors, and modular assay conditions to probe how myosin II motors work together to achieve force generation (Fig. 4.1). The bundle assay was constructed by first introducing rhodamine phalloidin actin to a flow cell made with a poly-L-lysine coated coverslip. After subsequent incubation with casein to prevent non-specific binding, myosin II, biotinylated Alexa Fluor 488 phalloidin AF, and streptavidin beads were added to the flow cell in the presence of ATP. Isolated bundles were identified through fluorescence imaging of each actin filament within the bundle, and force generation by the confirmed bundle was measured using the optical trap.

4.4.2 Actomyosin Bundle Measurements Reveal Three Force Profiles

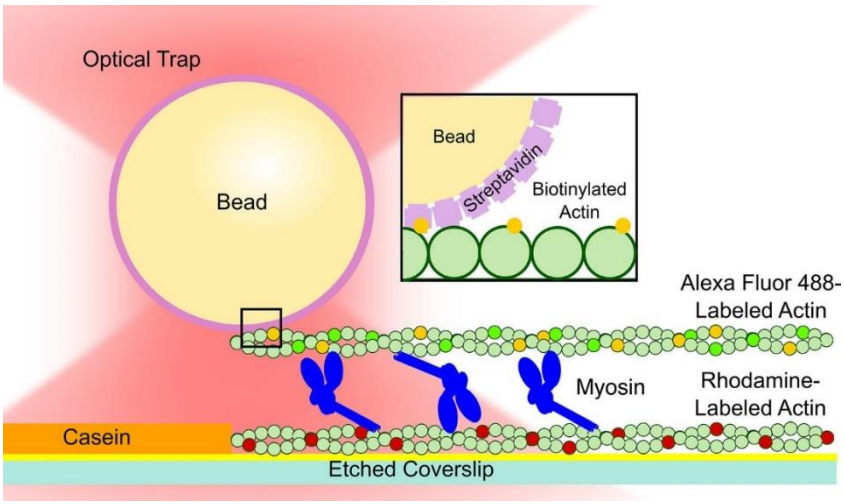

Figure 4.1: Assay schematic. Actin filament–myosin bundles are formed *in vitro*, and force generation by the motor ensemble is probed using optical tweezers. Actin filaments within the bundle are labeled with rhodamine and Alexa Fluor 488 phalloidin to differentiate between filaments and confirm bundle formation. The cargo actin filament is also biotinylated to bind streptavidin beads for optical trapping experiments.

Understanding factors that affect communication between myosin motors within actomyosin ensembles is important for deducing overall mechanisms of force generation at the molecular level. We investigated how the change in myosin concentration affects the inter- actions between myosin II motors and therefore dynamics of actin-myosin bundles, force generation, and motor stepping. Six myosin II solution concetrations were used to develop actin-myosin bundle assays (10, 1, 0.1, 0.01, 0.002, or 0.0001 µL). For myosin concentrations 10, 1, 0.1, 0.01, and 0.002 µL, measuring ensemble force generation by the optical trap yielded three similar force profiles at each con- centration: a smooth force ramp followed by a plateau, a sawtooth-like pattern with antagonistic force generation, and low force generation close to baseline (Fig. 4.2). At 0.0001 µL myosin solution concentration, bundles did not form nor was force generation measured. Force profiles were categorized depending on the number of sequential steps taken in one direction and the overall net force generated. Traces with no net force generation and no consecutive steps taken were classified as baseline traces. races with overall low force generation and multiple back and forth

sequential 4–5 nm steps were classified as sawtooth. Force ramp traces were characterized as having a steady in- crease in force in a primary direction, having multiple sequential steps in the same direction, ultimately plateauing after a substantial period of time (at least > 1 min), and having higher overall net force generation. Each solution concentration yielding three similar force profiles suggests that myosins have the ability to self-optimize within their bundle environment based on the local concentration of myosin, and thus number of occupied binding sites, within the bundle. Interestingly, for the ramping and sawtooth traces at each concentration, patterns that resembled stepping were observed (Fig. 4.2B) at intervals of approximately 4–5 nm, which is similar to previously recorded measurements of single myosin II step sizes (Kad *et al.*, 2005; Kaya *et al.*, 2017; Kaya and Higuchi 2010). Further, across the full concentration range, 51% of the traces were categorized as ramp/plateau, 30% were sawtooth-like, and 19% were baseline, suggesting that the favored orientation during self- assembly is one that permits a substantial level of movement and force generation.

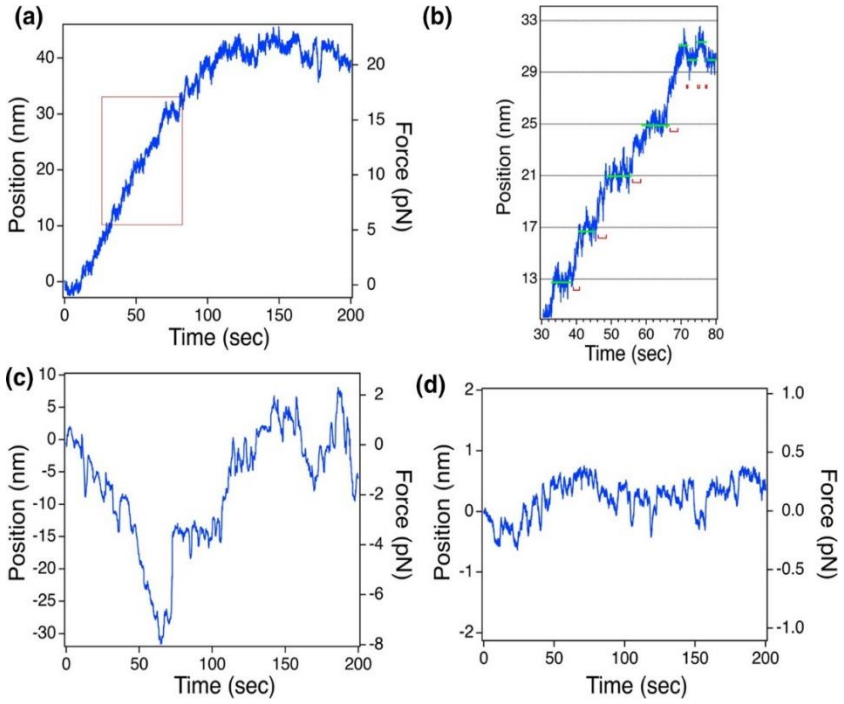

Figure 4.2: Myosin ensemble force profiles. Representative traces of the force profiles measured using the actomyosin bundle assay: (a) smooth force ramp followed by a plateau, (b) expanded box from (a) to emphasize single motor stepping with a 4 nm axis spacing and detachment times between steps, (c) sawtooth-like pattern with antagonistic force generation, and (d) low force generation close to baseline.

4.4.3 Myosin Step Size and Detachment Time Within Ensembles Depends on Local Motor Concentration

The individual interactions between motors within the ensemble and the AF bundle during force generation were quantified using a step/dwell finding algorithm to analyze the dependence of step size and time between steps on motor concentration and force pro- file. As multiple motors are working in each of the measured traces, it is possible that the measured time between steps, or dwells, are due to multiple motor activity and may not be true single molecule dwells; thus, we will refer to the dwell times as detachment times between detected steps. Step sizes and detachment times between detected steps were measured at each myosin solution concentration for the ramp and sawtooth-like traces (Figs. 4.3a–4.3c 10 μM, Figs. 4.3d–4.3f μM, Figs. 4.3g–4.3i 0.1 μM, Figs. 4.3j–4.3k 0.01 μL, and Figs. 4.3l–4.3m 0.002 μL). Forward and backward step sizes were measured and fit to Gaussian functions (Figs. 4.3a, 4.3d, 4.3g, 4.3j, 4.3l). Forward (Fig. 4.3b, 4.3e, 4.3h, 4.3k, 4.3m) and backward (Figs. 4.3c, 4.3f, 4.3i) detachment times were averaged using Gaussian fitting, and decay constants were found through fitting single exponential functions. Figure 4.3n shows that step sizes ranged from ~ 4 to 9 nm across the range of concentrations. At higher myosin solution concentrations, step size decreased and plateaued at ~ 4 nm, suggesting that these myosin bundles may have their actin binding sites

saturated. Also, most of the steps for higher myosin concentrations were forward steps, but backward steps that did not significantly differ in size were also detected, which also supports AF saturation as the step sizes in both directions appear to be restricted. In lower myosin concentrations, the spread of myosin step size increased and no backwards steps were detected. Corresponding forward detachment times for the higher myosin concentrations were very similar, and the detected backward detachment times were shorter than the forward times. At lower myosin concentration, the detachment times between detected steps had a larger spread, were on average longer than for higher concentrations, and significantly

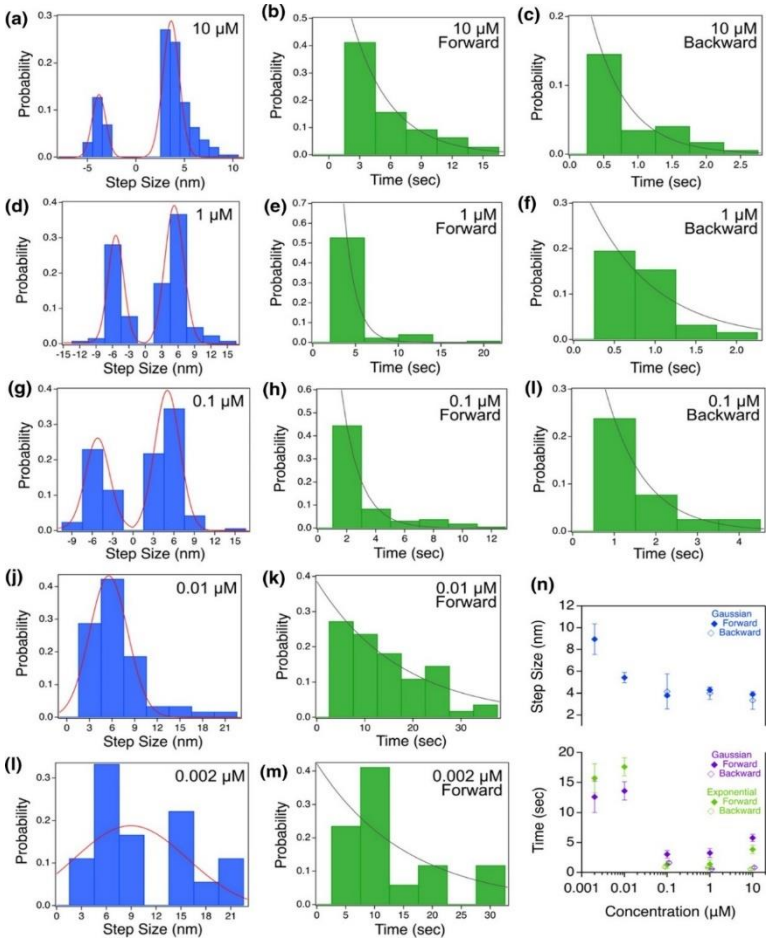

Figure 4.3: Dependence of step size and detachment time on ensemble concentration.(a) Average forward step size at 10 µL myosin is 4.7 6 0.8 nm (N = 145), and average backward step size is 3.8 6 0.7 nm (N = 43). (b–c) Forward and backward detachment times average 5.8 6 0.6 s and 0.8 6 0.2 s, respectively, and decay constants of 3.8 s and 0.5 s, respectively. (d) Average forward step size at 1 µL is 4.3 6 0.2 nm (N = 79), and average backward step size is 4.0 6 0.2 nm (N = 49). (e–f) Forward and backward detachment times average 3.2 6 0.7 s and 0.6 6 0.05 s, respectively, and decay constants of 1.4 s and 0.8 s, respectively. (g) Average forward step size at 0.1 µL is 3.8 6 0.2 nm (N = 101), and average backward step size is 4.2 6 0.3 nm (N = 64). (h–i) Forward and backward detachment times average 3.0 6 0.6 s and 1.6 6 0.3 s, respectively, and decay constants of 1.3 s and 0.9 s, respectively. (j) Average forward step size at 0.01 µL is 5.4 6 0.5 nm (N = 59) with no detected backward steps. (k) Forward detachment times average 13.6 6 1.5 s and decay constant of 17.6 s. (l) Average forward step size at 0.002 µL is 8.9 6 1.4 nm (N = 18) with no detected backward steps. (m) Forward detachment times average 12.6 6 1.4 s and decay constant of 15.7 s. (n) Overall trend of increasing step size and detachment time with decreasing myosin concentration.

different, indicating the start of possible communication breakdown between the motors, especially as at even lower motor concentration (0.0001 μL solution concentration), bundles could not reliably form or generate force.

4.4.4 Step Size, Detachment Time, and Force Dependence on Trace Profile. As the myosin II concentrations investigated were solution concentrations and the three force profiles were observed for each concentration, this suggests that the motors have the ability to self-optimize within their AF bundle based on local concentration of myosin and number of occupied filament binding sites accordingly. As such, we asked whether step size, detachment time, or maximum force generated depended on force profile. In Fig. 4.4a, step size and detachment time are divided into categories of ramp vs. sawtooth-like traces. As observed from Fig. 4.3, backward step sizes and detachment times were not detected at more dilute motor concentrations. However, the significantly larger step sizes and detachment times at these more dilute concentrations were found only in force ramping traces. Forward and backward steps from the sawtooth-like traces did not significantly differ between concentrations but the detachment times were slightly different. Figure 4.4b reveals that maximum force generation at each concentration was significantly higher in the ramp/plateau traces than the sawtooth-like traces. Interestingly, the maximum force of the sawtooth traces remained essentially the same regardless of myosin solution concentration, but at more dilute concentrations, the maximum force of the ramp/plateau traces increased on average and had a larger variation. If the AF binding sites are indeed saturated by myosins in the higher concentration cases, then it is possible that having a concentration slightly less restrictive than saturated can yield higher force generation. However, this trend drops off sharply as no force generation was measured for bundles at a myosin concentration an order of magnitude lower than what is plotted.

4.5 Discussion

We have integrated actomyosin bundles consisting of multiple AFs and myosin motors within an optical trapping assay in order to capture myosin ensemble mechanics that have been shown previously to depend on system compliancy and motor communication. Unlike previous studies that used heavy meromyosin (HMM) or the further truncated S1 construct, full length myosin motors were used here in order to understand the mechanical implications of the full protein and its role in force coordination, net force generation, and motor stepping. By incorporating AF- myosin-AF bundles into the assay, this allows the myosin motors to self-optimize within their more native multi-AF hierarchical environment instead of being rigidly attached to a bead or coverslip surface and allow for more elastic communications to occur between motors directly, as well as through the AFs to more distal motors within the bundle environment (Gittes

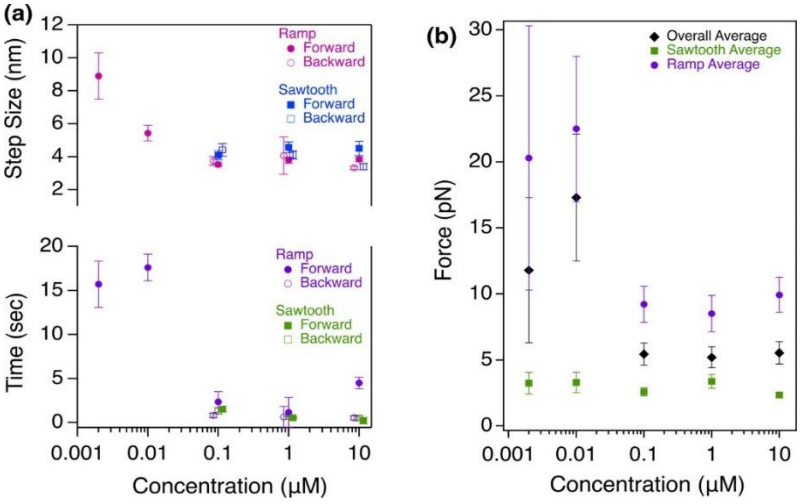

Figure 4.4: Step size, detachment time, and force dependence on trace profile. (a) Step size (top) and detachment decay constant (bottom) dependence trends on concentration separated by trace profile. (A-top) Magenta closed and open circles are average step forward and backward step sizes within force ramping traces compared to blue closed and open squares that are average forward and backward step sizes within sawtooth-like traces. (A-bottom) Purple closed and open circles are decay constants for forward and backward transitions within force ramping traces compared to green closed and open squares that are decay constants within sawtooth-like traces.(b) Average maximum force generation at each myosin bundle concentration (black diamonds: 10 µL 5.5 6 0.8 pN (N = 59), 1 µL 5.2 6 0.8 pN (N = 49), 0.1 µL 5.4 6 0.8 pN (N = 66), 0.01 µL 17.3 6 4.8 pN (N = 11), 0.002 µL 11.8 6 5.5 pN (N = 14)), and average maximum force generation divided by trace profile. Ramp (purple circles): 10 µL 9.9 6 1.3 pN (N = 28), 1 µL 8.5 6 1.4 pN (N = 22), 0.1 µL 9.2 6 1.4 pN (N = 33), 0.01 µL 22.5 6 5.5 pN (N = 8), 0.002 µL 20.3 6 10.0 pN (N = 7). Sawtooth-like (green squares): 10 µL 2.3 6 0.2 pN (N = 16), 1 µL 3.4 6 0.5 pN (N = 17), 0.1 µL 2.6 6 0.3 pN (N = 17), 0.01 µL 3.3 6 0.8 pN (N = 3), 0.002 µL 3.2 6 0.8 pN (N = 7). One-way ANOVA analysis revealed that maximum forces across the concentration range for the ramping traces are significantly different (p = 0.011) while the maximum forces across all tested concentrations for the sawtooth-like traces are n.s. (p = 0.31). Error bars, SEM.

et al., 1996; Lüdecke *et al.,* 2018; Reinemann *et al.,* 2018). We probed a range of myosin concentrations, and bundles at each concentration yielded three force profiles of low to no force generation, middle range force generation with a sawtooth-like pattern, and higher force generation with a smoother force ramp followed by a plateau. The finding of three force regimes aligns with the results presented by Hilbert *et al.* with the exception that their study used an un-loaded gliding filament assay (Hilbert *et al.,* 2013).

Using our loaded OT bundle assay, we observed patterns that resembled individual motor steps, especially in the sawtooth-like and ramp/plateau patterns. Thus, we used a step/dwell finding algorithm to analyze the steps in each force profile. We found step sizes that ranged from 4 to 9 nm, which is consistent with previously measured step sizes of individual myosin II motors and suggests that even though the myosins are in an ensemble, they are taking steps one at a time in order to build and sustain force generation. Further, the step size increases as likely fewer actin binding sites are occupied with myosin motors within the bundles, which resembles the findings of Kaya *et al.,* where in myofilaments, step sizes decreased from 7 to 4 nm with increasing load on the system (Kaya *et al.,* 2017). As myosin concentration within the AF bundles decreases, so does the number of occupied AF binding sites; thus, the stiffness of the overall architecture decreases as well, which would likely not facilitate efficient motor communication or movement (Albert *et al.,* 2014; Erdmann and Schwarz 2012; Galkin, Orlova, and Egelman 2012; Santos A., Shauchuk Y., Cichoń U., Vavra K.C. 2020). A smaller percentage of backward steps were also detected. At higher concentrations, the backward steps were similar in size to the forward steps, but at more dilute concentrations, backsteps were not detected by the algorithm. Stewart *et al.* suggest that AF binding sites can become saturated and yield a maximum AF gliding velocity (Stewart *et al.,* 2021). If AF binding site saturation is the case in

our more concentrated AF bundles, then having backsteps that are essentially the same size as the forward steps makes sense. If a forward step occurred in a saturated environment, it is possible that a cascade of force/tension signals from the end of the AF bundle let the motor know that it has the ability to move forward so that energy is not wasted in a diffusional search for the next binding site. However, the motor could still slip and fall backward a maximum of one step size. This also aligns with the study from Wagoner *et al.,* who suggests that the amount of force felt by an individual motor will depend on the forces exerted by surrounding motors and affect the order in which each motor performs its transitions (Wagoner and Dill 2021). Further, backstepping or backsliding is not detected in more dilute myosin ensembles, suggesting that motor communication begins to break down with fewer motors present. In conjunction, the step size increases with decreased myosin concentration as the bundle environment is not as crowded, giving the motors more freedom to move a larger distance than when the AF binding sites are saturated. Using the same algorithm, we analyzed the dwell times between detected steps. However, as there are multiple motors at play and there are different degrees of motor ensemble coordination due to changes in concentration, these could also be thought of as detachment times or the time between one motor taking a detected step forward or backward and the subsequent step. At higher concentrations, the forward detachment time decreases slightly with decreasing concentration, and the backward detachment time increases with decreasing concentration. At more dilute concentrations, the forward dwell times increase significantly. In these cases, the bundle is not saturated or as crowded and thus it is likely that communication takes longer across longer distances to make sure that space is available to move the longer step size. This also suggests a lower duty ratio state than in the higher concentration bundles. There is more time between each step or time motors are not trying to actively engage with the AF. If the duty ratio

decreases and approaches a more single molecule type state, there will be more time spent detached from the AF and therefore when a motor does release, there is not the propensity for surrounding motors to rapidly reattach and sustain previously built-up force. Change in duty ratio of myosin between single molecules and ensembles has been previously suggested and modeled computationally, (Albert *et al.,* 2014; Erdmann and Schwarz 2012; Kaya *et al.,* 2017; Stam *et al.,* 2015; Wagoner and Dill 2021) and here, we are able to observe the transition of increased duty ratio when moving between smaller and larger concentration ensembles through changes in stepping and force output as facilitated by using a compliant multi-AF architecture.

The interdependence of motor ensemble size and effective force generation has been suggested previously, (Debold *et al.,* 2013; Hilbert *et al.,* 2013; Stam *et al.,* 2015; Stewart *et al.,* 2021; Wagoner and Dill 2021; Walcott *et al.,* 2012; Weirich *et al.,* 2021) but here we also find that under load, ensemble size likely dictates the force generation trace profile of whether there is a sawtooth-like, allost antagonistic back-and-forth tug-of-war or the motors work together to produce a smooth force ramp. Interestingly, these force profiles are similar to the computational results of Erdmann *et al.,* who investigated the mechanics of small myosin ensembles using a parallel cluster model (Albert *et al.,* 2014; Erdmann and Schwarz 2012). They also found sawtooth and ramping force generation profiles that depend on external force, system stiffness, and ensemble size (Albert *et al.,* 2014; Erdmann and Schwarz 2012). In myosin ensembles, they purport that there are two types of mechano-sensitive processes taking place: catch bonding of post-power stroke state motors that directly depends on load, and the transition from the post-power stroke state to the weakly-bound state provides another type of catch bonding due to differing unbinding times that reduces reverse rates (Albert *et al.,* 2014; Erdmann and Schwarz 2012). Additionally, post-power stroke to weakly-bound transitions only occur in elastic

environments and suggest that both internal and external mechanics need to be considered when evaluating myosin ensemble function (Albert *et al.,* 2014; Erdmann and Schwarz 2012). If the dwell or detachment times presented here are analogous to the post-power stroke to weakly-bound transitions and facilitate the second type of catch bonding behavior, it makes sense that there is such a stark difference in stepping/dwell behavior between the more concentrated and more dilute bundles. At higher concentrations, there are more steps and shorter dwell times which matches with a reduction in reverse rates. Further, if these transitions only occur in elastic environments, our assay setup allowed us to observe and measure these changes in stepping behavior.

Interestingly, as solution myosin concentration decreases, we observe a significant increase in maximum force measured in each trace. By separating the force profiles into ramp vs. sawtooth-like, we observe that the substantially higher average force generation occurs in the smoother force ramp traces as well as an increase in step size from 4 to almost 9 nm. This is intriguing because previous studies suggest that saturation of AFs by myosins yields maximum sliding velocity, but these are also referring to unloaded gliding filament assays (Stewart *et al.,* 2021). However, it is possible that when the amount of motors available to bind into actin binding sites within the bundle is slightly lower than saturation, the system yields a bit more flexibility in a mechanical sense but also for self-optimization within the bundle. This has been suggested to occur on larger system scale by Stachowiak *et al.,* and aligns with our observation of an essentially doubled step size (Stewart *et al.,* 2021). The lower maximal force and lack of detection of backslips in the sawtooth-like traces then suggests that there is a lower local concentration of myosin that formed those particular bundle assemblies than in the force ramp cases.

Overall, these results suggest that the local environment of myosin II, including concentration and system stiffness, influence the level of motor cooperativity, communication, and thus force regulation, within AF bundles. Our proposed working mechanism includes when myosin binding sites within the AF bundles are saturated (Fig. 4.5—top), step sizes, both forward and backward, are restricted to the single molecule step size due to the surrounding occupied sites. In order to make forward progress, the saturated bundle has to communicate systematically to know when to move each individual motor efficiently, establishing a method to proceed one step at a time and sustain the already generated force by the system, as in a competitive tug-of-war game. This communication could occur locally between adjacent myosin motors through their individual stiffness that change throughout the mechanochemical system but also within the AF system (Galkin *et al.,* 2012; Santos A., Shauchuk Y., Cichoń U., Vavra K.C. 2020; Uyeda *et al.,* 2011). Having the filaments saturated with bound motors will increase the overall stiffness, allowing for larger scale communication, and as discussed previously, yields maximal unloaded velocity (Stewart *et al.,* 2021). Thus, it is possible that to achieve the maximal unloaded velocity observed by others, the motors use system stiffness to relay a metachronal-like effect, which has been suggested previously for contractile systems using heavy meromyosin (Guérin *et al.,* 2010; Mitsuka, Yamada, and Shimizu 1979; Yasuda, Shindo, and Ishiwata 1996). How- ever, being restricted to ~ 4 nm steps may not yield the highest force generation potential. Once the acto- myosin system becomes slightly less saturated (Fig. 4.5—middle), the inherent increased flexibility of the system due to fewer bound motors allow for self- organization within the bundle, and a slightly less stiff system facilitates communication to increase step sizes and foster higher force generation potential.

Lowering myosin concentration beyond this ‘‘sweet spot’’ begins a communication

breakdown due to lack of nearby motors and changes in flexural rigidity due to fewer motors. Motors begin to act more as single molecules with an inherently low duty ratio and rapid detachment rate that does not facilitate productive ensemble force generation (Fig. 4.5—bottom). Another possible reason for baseline force trace profiles is that myosin ‘‘dead heads’’ may be present and contribute to filament bundles becoming stuck. While we cannot completely rule this out, we believe that dead heads are an issue more inherent to the design of the in vitro motility assay, or gliding filament assay, which we are not using here. In gliding filament assays, myosins (typically HMM or S1) are added to a coverslip surface and can bind in an uncontrolled variety of orientations, including some that are not conducive for stepping or gliding and thus enter a rigor state (Hooijman, Stewart, and Cooke 2011; Rasicci *et al.*, 2022; Stewart *et al.* 2010). Also, myosin tail interactions with actin have been shown to cause significant drag in such assays and may contribute to further sliding degradation if myosin motors are bound to the glass surface in a ‘‘tail up’’ orientation (Rasicci *et al.,* 2022). Other studies have demonstrated that dead head purification (removal of ‘‘dead’’ myosin motors) had very little to no effect on improving actin motility (Hooijman *et al.,* 2011; Rasicci *et al.,* 2022) or even had a detrimental effect on activity of the remaining myosins. However, as we are building actomyosin bundles with a casein-blocked surface, the opportunity to bind anything but the actin filaments is minimized, as are the artifacts that can result from in vitro motility assay preparations. Thus, we believe this is a less likely scenario (Rasicci *et al.,* 2022; Schmid and Toepfer 2021).

In conjunction with local concentration and system stiffness, other environmental and structural factors may also be at play in regulating myosin ensemble dynamics. Myosin is known to form the interacting heads motif (IHM) where the heads fold back on the myosin tail, as well as the autoinhibited, super-relaxed (SRX) state with slow ATP turnover (Hooijman, Stewart, and Cooke 2011; Rasicci *et al.*, 2022; Stewart *et al.*, 2010). Recent studies have demonstrated a direct correlation between the respective structural and biochemical states. As the IHM and SRX states are a form of muscle regulation important for energy conservation and are sensitive to force, these combined actions would certainly downregulate system contractility due to fewer AF-engaged heads (Hooijman *et al.*, 2011; Rasicci *et al.*, 2022). However, instead of SRX

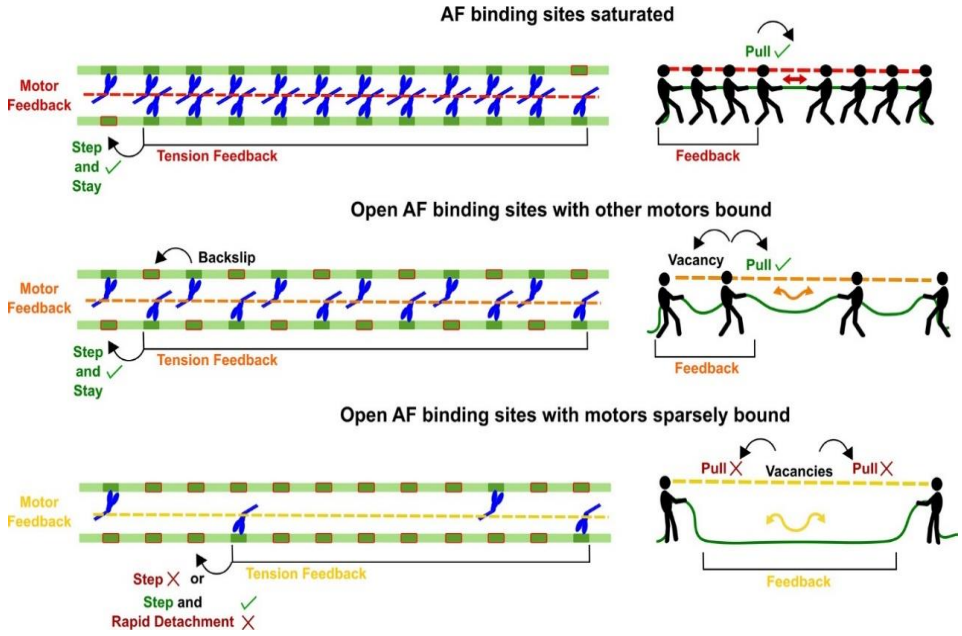

Figure 4.5: Force Dependence on Ensemble Environmental Conditions. Proposed mechanism comparison for how motor number, environment, and system compliancy dictate force-feedback within actomyosin bundles. The top bundle is saturated with only a few available binding sites open (red rectangles), thus the system can only proceed one step at time. In addition, having many motors bound stiffens the filaments and may act as a system-scale force sensor to determine motor ensemble speed and force generation. In the middle bundle, there are more binding sites available, thus myosins within the system have the opportunity to self-organize into an optimal arrangement that facilitates larger step sizes and higher force generation than the saturated case because the system is not as limited by availability of the next open AF binding site. Fewer motors bound result in a more compliant AF system that may communicate to the myosins' catch bonding ability and thus regulate motor organization within the bundle. However, motility and force generation efficiency drop off when motor number reduces further, as in the bottom bundle. Lack of nearby motors and increased AF compliancy signal back to the motors to reduce their duty ratio and act more similarly to single molecule behavior where myosins remain detached from AFs for the majority of their mechanochemical cycle.

engagement being a strict ‘‘on’’ and ‘‘off’’ type of regulation, these states provide a more gradual recruitment or withdrawal of myosin heads and force production, providing a downstream, metachronal- like communication effect of increasingly higher or lower filament stiffness and thus telling more heads to enter such a state, which aligns with our hypothesis above (Rasicci *et al.,* 2022; Schmid and Toepfer 2021).

Another factor to consider is the structure of the actin filament bundle, including overlap length and filament polarity. Size of the overlap length between two filaments would determine the amount of intra- bundle space and AF binding sites available for myo- sins to step and generate collective force. Previous studies have demonstrated that a critical AF length is needed to increase velocity in a gliding filament assay, and myosin II has the ability to self-organize within reconstituted actomyosin bundles where myosin spontaneously reorganized into discrete clusters during contraction (Hilbert *et al.,* 2013; Stachowiak *et al.,* 2012). Other studies have indicated that diffusible motors and filament crosslinkers exhibit entropic behavior in the self-assembly of large cytoskeletal structures like the mitotic spindle and contractile ring partly through maximizing the overlap length of overlapping filaments (Braun *et al.,* 2011, 2016; Lansky *et al.,* 2015). Perhaps there is a level of entropic contribution to the self-optimization observed previously and, in this study, due to myosin’s ability to exhibit both diffusional and processive properties depending on its local environment. Further, as the time to reach plateau in the force ramping traces were all similar, it is possible that finding the optimal position within the bundle for system force generation is found first before substantial collective work is performed by the motor ensemble to ensure that energy is not wasted in a non-ideal environment. This would likely put actin filament overlap lengths at a similar starting geometry; however, further study should be pursued to clarify the mechanism.

Then what drives actomyosin bundles to enter a force ramp vs. sawtooth-like force generation state? Perhaps actin filament polarity contributes. As depicted in Fig. S2, myosins step toward the barbed or plus end of the AF, so it makes sense that track directionality would affect overall force generation. We assume that myosins in our experiments are not aggregated into thick filaments due to the ionic strength of the buffer. In addition, myosin tail inter- actions with AFs have shown to induce significant drag in gliding filament assays (Guo and Guilford 2004). Thus, in an anti-parallel oriented bundle (plus and minus ends of each filament are opposite of each other), a motor with heads step- ping along the bottom filament and tail interacting with the top filament would work in concert with a motor stepping on the top filament in the opposite direction to collectively move the top AF in the same direction. In a parallel bundle, where the plus and minus ends of both filaments are aligned, there could be a degree of antagonization from tail drag and could lead to a ramp or sawtooth-like force generation state depending on the number of tail interactions vs. bound/stepping motors. So, collective force generation could occur in either orientation. However, going back to Fig. 4.5, if a bundle is saturated with motors, it is likely that weaker tail interactions will not have the opportunity to interact with the AF due to steric hinderance. This then leads to the metachronal-like communication wave of myosin force generation that experiences feedback due to the stiffness of the AF environment. When fewer motors are present and bound, there are more opportunities for tail interactions that may also entropically drive motors to separate and create the larger steps sizes observed above. The nature of these interactions would be of interest in future study. Taken together, we propose that main contributors for force generation in self-optimized actomyosin bundles are local motor concentration within the bundle and concomitantly how many motors are bound, leading to a force-feedback mechanism driven by system stiffness and compliancy.

4.6 Conclusions

By using a novel actomyosin assay design consisting of multiple myosin motors within an AF bundle, we were able to capture elements such as structural hierarchy, system compliancy, and motor self-optimization that have been previously alluded to be critical to elucidate how myosin behavior evolves from the single molecule to ensemble level but have not been investigated collectively using optical tweezers. The results above indicate that motor number, environment, and system stiffness are likely significant contributors to dictating motor duty ratio and overall force output in small myosin ensembles, as suggested by the changes in motor ensemble motility and force generation between saturated and less concentrated actomyosin bundles. Experimental and mechanistic details of the force- feedback mechanism between neighboring myosin motors through high resolution motor imaging within these environments, changes in system compliancy, entropic contributions, and cues from the local cytoskeletal environment are interesting subjects for further investigation in order to better understand how force propagates throughout motor-filament systems and specifically the molecular basis of mechanosensation in actomyosin systems that facilitate larger-scale muscle contraction.

4.7 Acknowledgments

This work is supported in part by the University of Mississippi Graduate Student Council Research Fellowship (OA), University of Mississippi Sally McDonnell-Barksdale Honors College (JCW, JER), the Mississippi Space Grant Consortium under Grant Number NNX15AH78H (JCW, DNR), and the American Heart Association under Grant Number 848586 (DNR).

BIBLIOGRAPHY

4.8 Bibliography

Akhshi, T. K., D. Wernike, and A. Piekny. Microtubules and actin crosstalk in cell migration and division. Cytoskeleton. 71:1–23, 2014.

Al Azzam, O., C. L. Trussell, and D. N. Reinemann. Measuring force generation within reconstituted micro- tubule bundle assemblies using optical tweezers. Cytoskeleton. 78:111–125, 2021.

Albert, P. J., T. Erdmann, and U. S. Schwarz. Stochastic dynamics and mechanosensitivity of myosin II minifila- ments. New J. Phys. 16:093019, 2014.

Appleyard, D. C., K. Y. Vandermeulen, H. Lee, and M. J. Lang. Optical trapping for undergraduates. Am. J. Phys. 75:5–14, 2007. https://doi.org/10.1119/1.2366734.

Balikov, D. A., *et al.* The nesprin-cytoskeleton interface probed directly on single nuclei is a mechanically rich system. Nucleus. 1034:1–14, 2017. https://doi.org/10.1080/19491034.2017.1322237.

Brady, S. K., S. Sreelatha, Y. Feng, S. P. S. Chundawat, and M. J. Lang. Cellobiohydrolase from Trichoderma reesei degrades cellulose in single cellobiose steps. Nat. Commun. 6:1–9, 2015.

Braun, M., Z. Lansky, G. Fink, F. Ruhnow, S. Diez, and M. E. Janson. Adaptive braking by Ase1 prevents over- lapping microtubules from sliding completely apart. Nat. Cell Biol. 13:1259–1264, 2011.

Braun, M., Z. Lansky, F. Hilitski, Z. Dogic, and S. Diez. Entropic forces drive contraction in cytoskeletal networks. BioEssays. 38:474–481, 2016.

Cordova, J. C., *et al.* Bioconjugated coreshell microparticles for high-force optical trapping. Part. Part. Syst. Charact. 35:1–8, 2018.

Debold, E. P., S. Walcott, M. Woodward, and M. A. Turner. Direct observation of phosphate inhibiting the force-generating capacity of a miniensemble of myosin molecules. Biophys. J. 105:2374–2384, 2013. https://doi.org/10.1016/j.bpj.2013.09.046.

Dong, J., C. E. Castro, M. C. Boyce, M. J. Lang, and S. Lindquist. Optical trapping with high forces reveals unexpected behaviors of prion fibrils. Nat. Struct. Mol. Biol. 17:1422–1430, 2010. https://doi.org/10.1038/nsmb.1954.

Duke, T. A. J. Molecular model of muscle contraction. Proc. Natl. Acad. Sci. U.S.A. 96:2770–2775, 1999.

Elting, M. W., and J. A. Spudich. Future challenges in single-molecule fluorescence and laser trap approaches to studies of molecular motors. Dev. Cell. 23:1084–1091, 2012. https://doi.org/10.1016/j.devcel.2012.10.002.

Ennomani, H., *et al.* Architecture and connectivity govern actin network contractility. Curr. Biol. 26:616–626, 2016.

Erdmann, T., and U. S. Schwarz. Stochastic force generation by small ensembles of myosin II motors. Phys. Rev. Lett. 108:1–5, 2012.

Finer, J. T., *et al.* Characterization of single actin-myosin interactions. Biophys. J. 68:291–296, 1995.

Finer, J. T., R. M. Simmons, and J. A. Spudich. Single myosin molecule mechanics: piconewton forces and nanometre steps. Nature. 368:113–119, 1994.

Fordyce, P. M., M. T. Valentine, and S. M. Block. Ad- vances in surface-based assays for single molecules. Single- Mol. Tech. A. 17:431–460, 2008.

Galkin, V. E., A. Orlova, and E. H. Egellan. Actin filaments as tension sensors. Curr. Biol.

22:R96–R101, 2012. h ttps://doi.org/10.1016/j.cub.2011.12.010.

Gittes, F., E. Meyho¨fer, S. Baek, and J. Howard. Directional loading of the kinesin motor molecule as it buckles a microtubule. Biophys. J. 70:418–429, 1996.

Greenberg, M. J., and J. R. Moore. The molecular basis of frictional loads in the in vitro motility assay with applications to the study of the loaded mechanochemistry of molecular motors. Cytoskeleton. 67:273–285, 2010.

Gue´rin, T., J. Prost, P. Martin, and J. F. Joanny. Coordination and collective properties of molecular motors: theory. Curr. Opin. Cell Biol. 22:14–20, 2010.

Guo, B., and W. H. Guilford. The tail of myosin reduces actin filament velocity in the in vitro motility assay. Cell Motil. Cytoskeleton. 59:264–272, 2004.

Hartman, M. A., and J. A. Spudich. The myosin super- family at a glance. J. Cell Sci. 125:1627–1632, 2012. http s://doi.org/10.1242/jcs.094300.

Hilbert, L., S. Cumarasamy, N. B. Zitouni, M. C. Mackey, and A. M. Lauzon. The kinetics of mechanically coupled myosins exhibit group size-dependent regimes. Biophys. J. 105:1466–1474, 2013. https://doi.org/10.1016/j.bpj.2013.07.054.

Hooft, A. M., E. J. Maki, K. K. Cox, and J. E. Baker. An accelerated state of myosin-based actin motility. Biochemistry. 46:3513–3520, 2007.

Hooijman, P., M. A. Stewart, and R. Cooke. A new state of cardiac myosin with very slow ATP turnover: a potential cardioprotective mechanism in the heart. Biophys. J. 100:1969–1976, 2011.

Howard, J. Mechanics of Motor Proteins and the Cytosksleton. Appl. Mech. Rev. 55(2):B39–B39, 2001.

Huxley, H. E. Fifty years of muscle and the sliding filament hypothesis. Eur. J. Biochem.

271:1403–1415, 2004.

Jackson, D. R., and J. E. Baker. The energetics of allosteric regulation of ADP release from myosin heads. Phys. Chem. Chem. Phys. 11:4808–4814, 2009.

Kad, N. M., S. Kim, D. M. Warshaw, P. VanBuren, and J.E. Baker. Single-myosin crossbridge interactions with actin filaments regulated by troponin-tropomyosin. Proc. Natl. Acad. Sci. U.S.A. 102:16990–16995, 2005.

Kaya, M., and H. Higuchi. Nonlinear elasticity and an 8- nm working stroke of single myosin molecules in myofilaments. Science (80-). 329:686–689, 2010.

Kaya, M., Y. Tani, T. Washio, T. Hisada, and H. Higuchi. Coordinated force generation of skeletal myosins in myofilaments through motor coupling. Nat. Commun. 8:1– 13, 2017. https://doi.org/10.1038/ncomms16036.

Kron, S. J., T. Q. P. Uyeda, H. M. Warrick, and J. A. Spudich. An approach to reconstituting motility of single myosin molecules. J. Cell Sci. 98:129–133, 1991.

Lansky, Z., *et al.* Diffusible crosslinkers generate directed forces in microtubule networks. Cell. 160:1159–1168, 2015. 36Leibler, S., and D. A. Huse. Porters versus rowers: a unified stochastic model of motor proteins. J. Cell Biol. 121:1357–1368, 1993.

Liu, C., M. Kawana, D. Song, K. M. Ruppel, and J. A. Spudich. ControμLing load-dependent kinetics of b-cardiac myosin at the single-molecule level. Nat. Struct. Mol. Biol. 25:505–514, 2018. https://doi.org/10.1038/s41594-018-0069-x.

Lu¨decke, A., A. Seidel, M. Braun, and S. Diez. Diffusive tail anchorage determines velocity and force produced by kinesin-14 between crosslinked microtubules. Nat. Com- mun. 9:2214, 2018.

Mansoon, A., M. Balaz, N. Albet-Torres, and K. J. Rosengren. In vitro assays of molecular motors—impact of motor-surface interactions. Front. Biosci. 13:5732–5754, 2008.

Miller-Jaster, K. N., C. E. Petrie Aronin, and W. H. Guilford. A quantitative comparison of blocking agents in the in vitro motility assay. Cell. Mol. Bioeng. 5:44–51, 2012.

Mitsuka, M., T. Yamada, and H. Shimizu. On the con- traction of myosin- extracted skinned single fibers with active myosin fragments. J. Biochem. 85:559–565, 1979.

O'Connell, C. B., M. J. Tyska, and M. S. Mooseker. Myosin at work: Motor adaptations for a variety of cellular functions. Biochim. Biophys. Acta - Mol. Cell Res. 1773:615–630, 2007.

Persson, M., *et al.* Heavy meromyosin molecules extending more than 50 nm above adsorbing electronegative surfaces. Langmuir. 26:9927–9936, 2010.

Piazzesi, G., *et al.* Skeletal muscle performance determined by modulation of number of myosin motors rather than motor force or stroke size. Cell. 131:784–795, 2007.

Pollard, T. D. Mechanics of cytokinesis in eukaryotes. Curr. Opin. Cell Biol. 22:50–56, 2010. https://doi.org/10. 1016/j.ceb.2009.11.010.

Rahman, M. A., A. Salhotra, and A. Ma˚ nsson. Comparative analysis of widely used methods to remove nonfunctional myosin heads for the in vitro motility assay. J. Muscle Res. Cell Motil. 39:175–187, 2018. https://doi.org/ 10.1007/s10974-019-09505-1.

Rasicci, D. V., *et al.* Dilated cardiomyopathy mutation E525K in human beta-cardiac myosin stabilizes the inter- acting heads motif and super-relaxed state of myosin. BioRxiv. 10:1465, 2022.

Rauch, P., and T. Ja¨hnke. Optical tweezers for quantitative force measurements and live cell

experiments. Micros. To- day. 22:24–31, 2014.

Reinemann, D. N., *et al.* Collective force regulation in anti- parallel microtubule gliding by dimeric Kif15 kinesin motors. Curr. Biol. 27:2810-2820.e6, 2017.

Reinemann, D. N., S. R. Norris, R. Ohi, and M. J. Lang. Processive kinesin-14 HSET exhibits directional flexibility depending on motor traffic. Curr. Biol. 28:2356-2362.e5, 2018. https://doi.org/10.1016/j.cub.2018.06.055.

Ruegg, C., C. Veigel, J. E. Molloy, S. Schmitz, J. C. Sparrow, and R. H. A. Fink. Molecular motors: Force and movement generated by single myosin II molecules. Phys- iology. 17:213–218, 2002. https://doi.org/10.1152/nips.01389.2002.

Santos, A., Y. Shauchuk, U. Cichon´, and K. C. Vavra. How actin tracks affect myosin motors. In: Myosins, edited by L. M. Coluccio. Cham: Springer, 2020, pp. 183–197.

Schmid, M., and C. N. Toepfer. Cardiac myosin super relaxation (SRX): a perspective on fundamental biology, human disease and therapeutics. Biol. Open. 10:1–11, 2021.

Spudich, J. A. The myosin swinging cross-bridge model.Nat. Rev. Mol. Cell Biol. 2:387–392, 2001.

Spudich, J. A., J. Finer, B. Simmons, K. Ruppel, B. Patterson, and T. Uyeda. Myosin structure and function. Cold Spring Harb. Symp. Quant. Biol. LX:783–791, 1995.

Stachowiak, M. R., *et al.* Self-organization of myosin II in reconstituted actomyosin bundles. Biophys. J. 103:1265– 1274, 2012. https://doi.org/10.1016/j.bpj.2012.08.028.

Stam, S., J. Alberts, M. L. Gardel, and E. Munro. Isoforms confer characteristic force generation and mechanosensation by myosin II filaments. Biophys. J. 108:1997–2006, 2015. https://doi.org/10.1016/j.bpj.2015.03.030.

Stewart, M. A., K. Franks-Skiba, S. Chen, and R. Cooke. Myosin ATP turnover rate is a

mechanism involved in thermogenesis in resting skeletal muscle fibers. Proc. Natl. Acad. Sci. U.S.A. 107:430–435, 2010.

Stewart, T. J., V. Murthy, S. P. Dugan, and J. E. Baker. Velocity of myosin-based actin sliding depends on attachment and detachment kinetics and reaches a maximum when myosin-binding sites on actin saturate. J. Biol. Chem. 297:101178, 2021. https://doi.org/10.1016/j.jbc.2021.101178

Sung, J., *et al.* Harmonic force spectroscopy measures load- dependent kinetics of individual human b-cardiac myosin molecules. Nat. Commun. 6:1–9, 2015.

Svoboda, K., and S. M. Block. Force and velocity measured for single kinesin molecules. Cell. 77:773–784, 1994. 62Uyeda, T. Q. P., Y. Iwadate, N. Umeki, A. Nagasaki, and S Yumura. Stretching actin filaments within cells enhances their affinity for the myosin ii motor domain. PLoS ONE. 6:e26200, 2011.

Wagoner, J. A., and K. A. Dill. Evolution of mechanical cooperativity among myosin II motors. Proc. Natl. Acad. Sci. U.S.A. 118:20, 2021.

Walcott, S., D. M. Warshaw, and E. P. Debold. Mechanical coupling between myosin molecules causes differences between ensemble and single-molecule measurements. Biophys. J. 103:501–510, 2012. https://doi.org/10.1016/j.b pj.2012.06.031.

Weirich, K. L., S. Stam, E. Munro, and M. L. Gardel. Actin bundle architecture and mechanics regulate myosin II force generation. Biophys. J. 120:1957–1970, 2021. https://d oi.org/10.1016/j.bpj.2021.03.026.

Yanagida, T., *et al.* Single-motor mechanics and models of the myosin motor. Philos. Trans. R. Soc. B. 355:441–447, 2000.

Yasuda, K., Y. Shindo, and S. Ishiwata. Synchronous behavior of spontaneous oscillations of

sarcomeres in skeletal myofibrils under isotonic conditions. Biophys. J. 70:1823–1829, 1996.

CHAPTER 5

DISSECTING MYOSIN II DYNAMICS: INVESTIGATING THE ROLE OF THE TAIL DOMAIN AND IONIC STRENGTH IN MOTOR ENSEMBLE COORDINATION AND FORCE PRODUCTION

5.1 Summary

While the head domain of myosin II plays a central role in ATP hydrolysis and stepping along actin filaments, other factors significantly influence myosin dynamics and muscle function. The tail domain contributes to the organization and stability of myosin in muscle fibers, affecting motor protein interactions and contractile strength. Additionally, the ionic strength of the surrounding environment critically impacts myosin-actin interactions and motor coordination. In this chapter, an in-depth investigation is conducted to elucidate how the tail domain and ionic strength influence myosin II dynamics within motor ensembles, focusing on their impact on motor coordination and overall force generation. This analysis aims to deepen our understanding of the intricate mechanisms governing myosin II activity in muscle sarcomeres, particularly how these factors contribute to the collective behavior and efficiency of myosin motors during the complex process of muscle contraction.

5.2 Introduction

5.2.1 Influence of Ionic Strength on Myosin Motor Ensemble Dynamics and Force Generation

The dynamic interactions between actin and myosin II, fundamental to processes such as muscle contraction and cell movement, are considerably influenced by environmental elements like ionic strength. This parameter, which quantifies the concentration of dissolved ions in a solution, subtly modifies the electrostatic interactions pivotal to the organization of the actin-myosin network. Consequently, variations in ionic strength can lead to significant changes in the structural and functional characteristics of these protein networks (K. Clark *et al*., 2007). Ionic strength affects the assembly and stability of thick filaments through electrostatic interactions and the solubility of myosin molecules. High ionic strengths tend to shield the electrostatic repulsion between charged myosin molecules, promoting their aggregation into thick filaments. Conversely, low ionic conditions can lead to disassembly or prevent the formation of these filaments due to increased electrostatic repulsion (Guhathakurta *et al*., 2018). Thick filament length and isoform composition are critical determinants of the contractile units' self-organization within actomyosin bundles. Myosin II isoforms, varying in tail length and motor domain properties, contribute to the diversity of actomyosin bundle architectures observed in different physiological contexts. For instance, non-muscle myosin II forms shorter thick filaments compared to those in skeletal muscle, influencing the contractile unit's organization and function within the bundle (R. A. Murphy *et al*., 1997; Pette & Staron, 2000; Thomas & Roopnarine, 2002).

Studies have shown that variations in myosin II isoforms and the controlled assembly of thick filaments can regulate actomyosin contractility. The self-organization of contractile units within in vitro actomyosin bundles demonstrates that both the mechanochemical properties of

myosin II and the thick filaments' physical dimensions are crucial for determining the bundles' contractile behavior (Thoresen *et al*., 2013). Ionic strength directly influences the electrostatic interactions between actin and myosin heads. At low ionic strength, weakened electrostatic repulsion promotes actomyosin binding, potentially leading to a higher fraction of myosin heads attached to actin filaments. However, excessive actomyosin binding at low ionic strength can hinder force generation due to steric hindrance and limitations in filament flexibility. In contrast, high ionic strength can decrease actomyosin binding affinity due to increased electrostatic repulsion. This may reduce the number of attached myosin heads, potentially limiting contractile force. However, optimal spacing between bound myosin heads at high ionic strength can favor efficient force generation through cooperative power strokes Beyond actomyosin binding, ionic strength also modulates myosin head dynamics and crosslinking activity. At low ionic strength, weakened electrostatic repulsion can lead to increased myosin head flexibility and processivity, as heads encounter fewer electrostatic barriers during filament translocation. This can enhance actin filament sliding velocity but may compromise network stability due to weakened crosslinking (Irving *et al*., 2000). Conversely, high ionic strength can restrict myosin head flexibility due to enhanced electrostatic interactions. This can decrease filament sliding velocity but potentially strengthen crosslinking within the network, promoting network stability and potentially enhancing force generation (Ishikawa, 2007; Kad *et al*., 2005; *Sliding Filament Theory, Sarcomere, Muscle Contraction, Myosin | Learn Science at Scitable*, n.d.; Stewart *et al*., 2021a). The regulatory light chains associated with myosin II possess critical binding sites for regulatory proteins like calmodulin. Ionic strength can influence the binding affinity of these regulatory proteins to myosin, thereby modulating myosin activation and ATPase activity. At low ionic strength, weakened electrostatic interactions may favor calmodulin binding, potentially

inhibiting myosin activation and ATPase activity (Means, 1988, 1988; Yang & Tsai, 2021). On the other hand, high ionic strength may reduce calmodulin binding, promoting myosin activation and potentially increasing ATPase activity. This intricate interplay between ionic strength, regulatory proteins, and myosin activity adds another layer of complexity to the regulation of contractile function within actin-myosin networks (Doran & Lehman, 2021; Viswanathan *et al*., 2020). Understanding the multifaceted effects of ionic strength on myosin II dynamics in actin-myosin networks is crucial for deciphering cellular contractility and motility. By fine-tuning ionic environments, cells can delicately regulate network architecture, actomyosin interactions, myosin head dynamics, and contractile function to adapt to diverse physiological demands. Further research into the interplay between ionic strength, regulatory proteins, and post-translational modifications of actin and myosin promises to unveil even deeper layers of control within these contractile machineries (Guhathakurta *et al*., 2018; Kad *et al*., 2005; Spudich, 2001; Thomas & Roopnarine, 2002; Wegner, 1976). In the dynamic interplay of the actomyosin network, the role of specific ions like Potassium (K^+), Calcium (Ca^{2+}), and Magnesium (Mg^{2+}) is multifaceted and critical. K^+ influences actomyosin binding, with its concentration affecting the degree of electrostatic interactions and thus binding efficiency. It also indirectly impacts myosin head flexibility and directly interacts with the ATP binding pocket of the myosin head, modulating ATPase activity (Ishikawa, 2007; Ojima, 2019; Zhang *et al*., 2024). Ca^{2+}, known for its regulatory role, interacts with myosin's regulatory light chains, affecting activation and ATPase activity as illustrated in Figure 5.1.

It also influences actin-binding proteins, impacting network crosslinking. Mg^{2+}, essential as a cofactor in ATP binding and hydrolysis, plays a key role in maintaining actin filament stability and network integrity. The concentration of these ions thus has a profound impact on various aspects of the actomyosin network, including contractile function and stability (Beeler *et al.*, 1985; Houdusse & Sweeney, 2016; KOHAMA, 2016; Moraczewska *et al.*, 2012; *(PDF) Molecular Mechanism of Mg-ATPase Activity*, n.d.). It is important to remember that these ions don't work in isolation. Their combined effects and interplay determine the overall impact on myosin II dynamics and network function. For example, K^+ and Ca^{2+} can synergistically influence actomyosin binding and activation through their combined influence on electrostatic interactions and regulatory pathways. Similarly, Mg^{2+} plays a crucial role in both ATPase activity and actin filament stability, contributing to the overall contractile efficiency of the network. By understanding the specific roles of different ions in modulating the actomyosin ATP cycle and network assembly, researchers can gain valuable insights into cellular contractility and motility. This knowledge can then be applied to develop new therapeutic strategies or biomimetic materials that harness the power of the actin-myosin machinery. Ultimately, the interplay between ionic strength, myosin coordination, and force generation is a

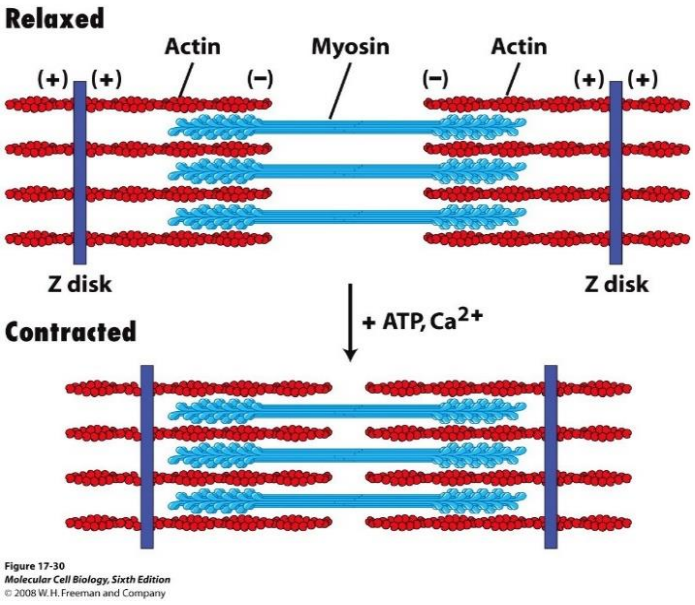

Figure 5.1: Calcium's Role in Actin-Myosin Interaction. The figure shows a sarcomere's transition from relaxation to contraction, emphasizing calcium's role in facilitating actin-myosin interactions. Calcium binding initiates the sliding of myosin heads along actin filaments, causing sarcomere contraction. Adapted from 'Molecular Cell Biology,' Sixth Edition, 2008, published by W.H. Freeman and Company

complex interplay. Carefully designed in vitro assays can help unravel this intricate motility, providing valuable insights into cellular contractility and informing the development of new therapeutic strategies or biomimetic materials harnessing the power of actomyosin machinery (Beeler *et al*., 1985; KOHAMA, 2016; Moraczewska *et al*., 2012; Myung *et al*., 2021; *(PDF) Molecular Mechanism of Mg-ATPase Activity*, n.d.; Tu *et al*., 2016; Wakabayashi & Ebashi, 1968).

5.2.2 Investigating the Impact of Myosin II's Tail Domain on Motor Behavior and Force Production

Myosin II is composed of three major parts: the head, neck, and tail domains, each contributing uniquely to the protein's function. The two heads contain the motor domains responsible for ATP hydrolysis and actin binding, the neck serves as a lever arm that amplifies small changes in the motor domain into larger movements, and the tail is crucial for filament formation and regulation of myosin activity. The head domain of myosin II is the primary site for ATP hydrolysis and actin interaction. This ATPase activity is essential for the myosin's ability to generate force and movement along actin filaments (Baldo *et al*., 2020b; Kad *et al*., 2005; Korn, 2000; Spudich *et al*., 1995). Studies on the structure of myosin II have provided detailed insights into the atomic arrangement of the actin-myosin complex, revealing how ATP binding and hydrolysis induce conformational changes necessary for the power stroke mechanism (Baldo *et al*., 2020b; Rayment *et al*., 1993; Squire, 2019). The neck region, composed of light chain-binding IQ motifs, acts as a lever arm, translating the conformational changes in the head domain into displacement of the myosin along the actin filament. The length and composition of the neck are thought to influence the stroke size and, consequently, the speed of movement. highlighting

the variability in myosin performance based on neck region modifications (*Unconventional Myosins: How Regulation Meets Function - PMC*, n.d.), (Altman, 2013). The tail domain is instrumental in the assembly of myosin into thick filaments , a process critical for the generation of contractile force in muscle fibers and the organization of myosin in non-muscle cells. The coiled-coil structure of the tail promotes dimerization and filament formation, enabling the myosin molecules to work cooperatively (Ojima, 2019; *The Myosin II Coiled-Coil Domain Atomic Structure in Its Native Environment | PNAS*, n.d.; Thoresen *et al*., 2013). However, the tail can also apply a drag force on actin, potentially slowing the speed of actin filament sliding , especially under conditions where filament saturation or the cellular environment imposes physical constraints (Houdusse & Sweeney, 2016; Korn, 2000). This aspect of tail function suggests a regulatory role in modulating the efficiency of force generation and the speed of movement (Stewart *et al*., 2021b).

Proteolytic cleavage of myosin II can produce two significant fragments: Heavy Meromyosin (HMM) and Subfragment 1 (S1). HMM, which includes the heads and a portion of the tail (S2), can still generate force and bind to actin, albeit without the full-length tail (Dulyaninova & Bresnick, 2013). This capacity of HMM to produce movement demonstrates that the essential elements for force generation reside within the head and the proximal tail region. S1, consisting solely of the head domain, retains the ability to bind actin and hydrolyze ATP, underscoring the head's central role in the motor activity of myosin (Wagner & Giniger, 1981) (Burghardt *et al*., 2007; Itakura *et al*., 1993; Walcott *et al*., 2009).

Previous studies on myosin II have often focused on analyzing single molecule components, and rigid ensemble constructs and investigated myosin motor fragments in isolation (Finer *et al*., 1994; Kaya & Higuchi, 2010). While these investigations have provided invaluable insights into

the individual functionalities and mechanisms of these parts, they do not fully capture the complexity and hierarchy of interactions within the actual system. The singular molecule approach overlooks the compliance and synergy that allow for comprehensive interactions among the myosin domains themselves and with actin filaments (O. Y. Al Azzam *et al*., 2022). This limitation hampers a thorough understanding of the tail's role in force generation, motor coordination, and the resultant force output. Specifically, the impact of the presence or absence of the tail domain on the overall dynamics of myosin function remains inadequately elucidated. To bridge this gap, more physiological constructs or assays that mimic the real hierarchical environment are necessary.

Our approach, as outlined in Alazzam *et al*., addresses this challenge by introducing an optical trapping assay designed to reflect the system's compliance and hierarchical organization accurately. This innovative method allows for the observation and analysis of myosin II molecules in conditions that closely resemble their natural biological context as ensemble of motors interacting with multiple actin filaments. By employing optical trapping, we can dissect the nuanced interactions between the myosin domains and actin, particularly focusing on how the tail domain contributes to force generation and the coordination of multiple motors. This assay provides a platform for exploring how the structural integrity and interactions of myosin II influence its motility and force-producing capabilities within a more physiologically relevant framework.

5.3 Methods

Building upon the approach developed by Alazzam *et al.*, this study investigates the dynamics of myosin II motors, focusing on the structural variations and the effects of changing

ionic strengths. The experimental setup involved the preparation of a microscopic slide designed to create a sandwich-like construct of actin and myosin within the assay. This construct was pivotal for closely mimicking the natural interaction between these proteins, thereby facilitating a realistic observation of their dynamics under varying conditions. Two significant modifications were introduced to the ionic environment of the solution to probe their effects on motor coordination and force generation:

1. Ionic Composition Adjustment: The study utilized GAB buffer in lieu of the traditional APB buffer to alter the ionic composition of the solution. Notably, GAB buffer is characterized by the absence of KCl, in contrast to APB buffer, which contains 500 mM KCl. This deliberate modification aimed to assess the role of KCl in modulating actin-myosin interactions and motor activity.

2. Buffer Concentration Modification: In pursuit of exploring the effects of reduced ionic strength, the study proposed preparing the APB buffer with a reduced salt concentration. Specifically, the APB buffer was modified to contain 250 mM KCl, achieved by halving the salt content in the FC buffer used for its preparation. This adjustment provided a unique opportunity to investigate the impact of decreased ionic strength on myosin motor coordination and force generation.

Parallel to these modifications, the study focused on the impact of the absence of the tail domain by employing a myosin II ensemble of the S1 segment. This approach facilitated an investigation into how the structural absence affects overall force output and motor coordination within the ensemble, thus influencing overall muscle dynamics. Different concentrations of the S1 motor segment from both skeletal and cardiac myosin were tested, including 1 mg/ml, 0.1, 0.01, 0.02, and 0.001 mg/ml, to cover a broad range of motor activities. Subsequent analyses

involved the use of MATLAB for the calculation of maximum force generation and motor step size.

5.4 Results and Discussion

5.4.1 Dynamics and Force Generation in Myosin II S1: Exploring the Effect of the Tail Domain's Absence

The approach developed by Al Azzam *et al.* . was utilized in the examination of myosin ensembles. This methodology, adapted to explore the dynamics of S1 skeletal myosin, facilitated the observation of the collective behavior of myosin motors. The focus on ensembles, as opposed to individual motors, allowed for a deeper investigation into how the absence of the tail domain impacts motor coordination and force generation within these complex systems. To further understand how the dynamics of S1 skeletal myosin is impacted by varying motor concentrations or the density of motors engaging with actin filaments, investigations were conducted across three specific concentrations of S1 myosin: 1 µM, 0.01 µM, and 0.05 µM. Like in full- length experiments, regardless of the concentration of myosin motors, three distinct force profiles were observed: ramp-plateau, sawtooth-like, and base line as shown in **Figure 5.2**. The distribution of

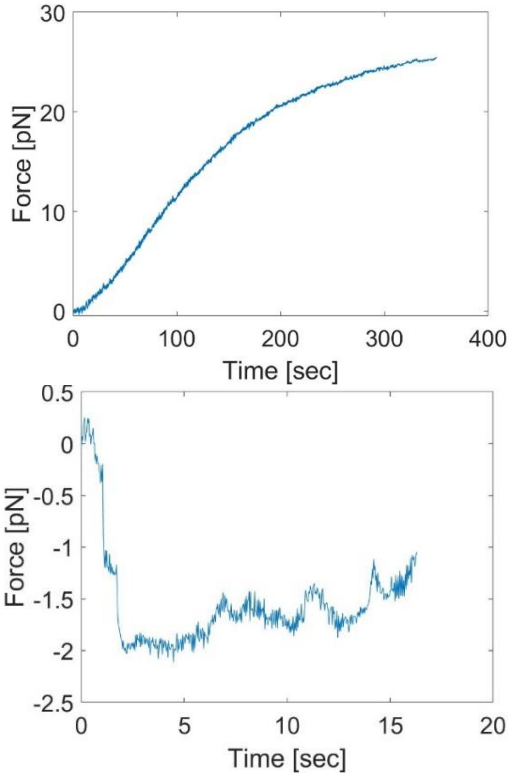

Figure 5.2: Variation in Force Profiles with S1 Skeletal Myosin Under Different Concentrations. Profile A exhibits a ramp-plateau pattern reaching a maximum force of 26pN, while Profile B displays a sawtooth-like pattern with a peak force of 2 pN.

maximum force generation spanned across low (0 to 10 pN) with mostly sawtooth-like force traces , medium (11 to 20 pN) with ramp-plateau force traces, and high (21 to approximately 60 pN) with ramp -plateau ranges. Figure 5.3 illustrates the percentage distribution of maximum force generated by S1 skeletal myosin under different motor concentrations. At the highest concentration of 1 µM S1 myosin, (N=10), the occurrence of generating high forces (20.0+ pN) with highest value of 60 pN was the highest.

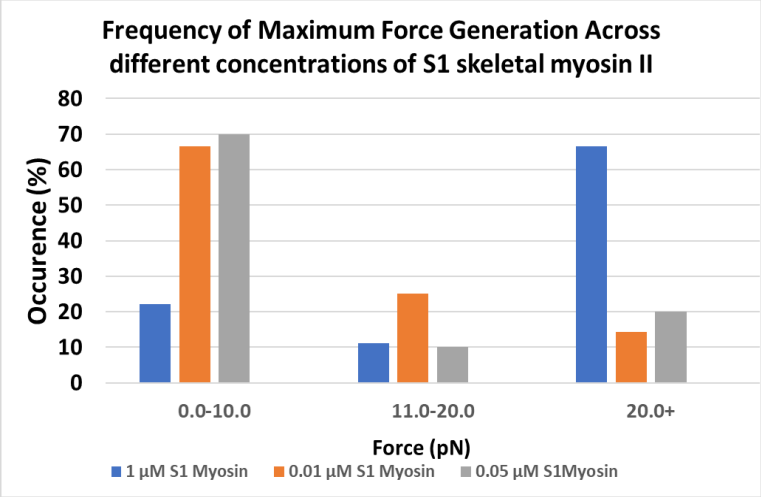

Figure 5.3: Percentage Distribution of Maximum Force Generation Ranges with S1 Skeletal Myosin at different motor Concentration.

All force generation patterns observed were ramp-plateau, suggesting a consistent and robust interaction between S1 myosin and actin. The uniform presence of ramp-plateau patterns at this concentration underscores a stable and efficient mechanism of myosin-actin cross-linking and force generation. This could be due to an increased likelihood of cross-bridge formation between myosin and actin, resulting in greater force production. For the intermediate concentration of 0.05 µM, the data shows a significant occurrence in the medium force range (11.0-20.0 pN), but not as high as the 1 µM concentration in the highest force range. A 70% of the force traces (N=10) were ramp-plateau patterns, indicative of a moderate, consistent force generation with forces starting at +5 pN and peaking at 30 pN. This concentration also presented a few sawtooth-like patterns with forces below 4 pN which is 20% of the overall experiments, and a single instance where no force was generated, which is 10 %of the experiments. This could reflect a

balance between myosin density and available space for effective cross-bridge cycling, leading to substantial force production but not reaching the peak efficiency seen at 1 µM. For the lowest concentration of 0.01 µM, results show a dominant frequency in the low force range, but also notable occurrences in the medium force range. The more variable interaction between S1 myosin heads and actin observed at this concentration might also possibly be due to decreased stability in their cross-linking and bundling. Among twelve experiments (N=12) , five exhibited ramp-plateau patterns with forces over 10 pN with reaching highest of 50 pN (41.7%) , while seven displayed sawtooth-like patterns with forces below 10 pN (58.3%). This variation in force generation patterns among the three different concentrations suggests a critical role of concentration in determining the nature of force generation, reflecting a suboptimal concentration for force production where there are not enough myosin heads to consistently generate higher forces, but still sufficient to contribute to a moderate level of force generation. With having higher maximum force generation at the highest motor concentration, our hypothesis suggests that the absence of the tail region in S1 myosin II could mitigate the issues that typically arise with higher concentrations of full-length myosin. The tail portion of the myosin molecule is known to be involved in the assembly of myosin into thick filaments and can contribute to the aggregation of myosin molecules. When the tail is removed, as in the case of S1 myosin fragments, the aggregation that impairs force generation at high concentrations may indeed be reduced or absent. The statistical analysis of S1 skeletal myosin across three concentrations—1µM, 0.01µM, and 0.05µM—demonstrated variability in force generation as shown in **Figure 5.4**. At 1µM, an average force of 25±5.7 pN was recorded. At 0.01µM, the data revealed an average force of 12.3±4.7 pN. At 0.05µM, the average force was slightly lower at 11±3.0 pN. The parallels in force generation capabilities between S1 and full-length skeletal

myosin underscores the head domain's essential role in myosin's motor function, suggesting the tail domain's contribution lies more in structural organization and filament assembly than in direct force production. Additionally, the observation of predominantly smooth ramp-plateau patterns with S1 motor indicates that the tail might play a role in introducing some level of friction which has been seen in previous studies (Houdusse & Sweeney, 2016) so with the absence of tail domain, force generation becomes smoother. Another factor that could explain the deviation in force patterns is how myosin motors are arranged when forming bundles in the absence of the tail. In full-length myosin, the tail aids the bundling process, enabling more efficient crosslinking with actin filaments through induced drag. However, without the tail, the mechanism by which S1 myosin forms bundles and achieves crosslinking could involve each of the two heads attaching to separate actin filaments. This configuration could lead to tighter bundles, due to the closer proximity of the myosin heads as compared to the arrangement in full-length myosin, where the tail is present on one side. Such a compact bundling strategy sheds light on how S1 myosin maintains effective interactions with actin filaments and continues to generate force. To fully grasp the implications of the tail domain's absence on motor coordination and force production, further research is crucial. Investigating different assay geometries might reveal more about the tail's role in force generation. Additionally, studying the cooperative interactions among myosin molecules without

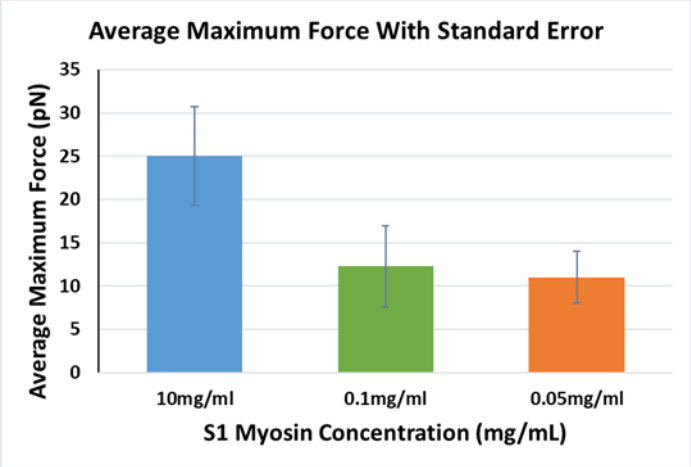

Figure 5.4: Variations in Maximum Force Generation at Different Concentrations of S1 Skeletal Myosin

the tail domain under a broad range of conditions, including ionic strength and motor concentration, could shed light on its influence on the collective behavior of myosin motors within actomyosin complexes, underlining the importance of studying the adaptability of myosin's interaction mechanisms and the capability of motors to coordinate binding and interacting with actin filaments even without traditionally essential structural components.

5.4.2 Investigating Ionic Strength Effects on Full-Length Skeletal Myosin II: Implications for Motor Coordination and Force Dynamics

In the exploration of ionic strength effects on skeletal myosin II dynamics, our study employed skeletal myosin at 1mg/ml, adapting the Al Azzam *et al.* approach with a focus on ionic environments. The main buffer originally used in the solution covering the actin-myosin bundles is the APB buffer. This buffer's composition is critical for providing the ionic environment necessary for the proper functioning of the actin-myosin interactions, thereby facilitating a realistic assessment of the myosin motor's behavior and force dynamics in a controlled experimental setup. The original APB buffer, containing 500 mM KCl, was modified in two key ways:

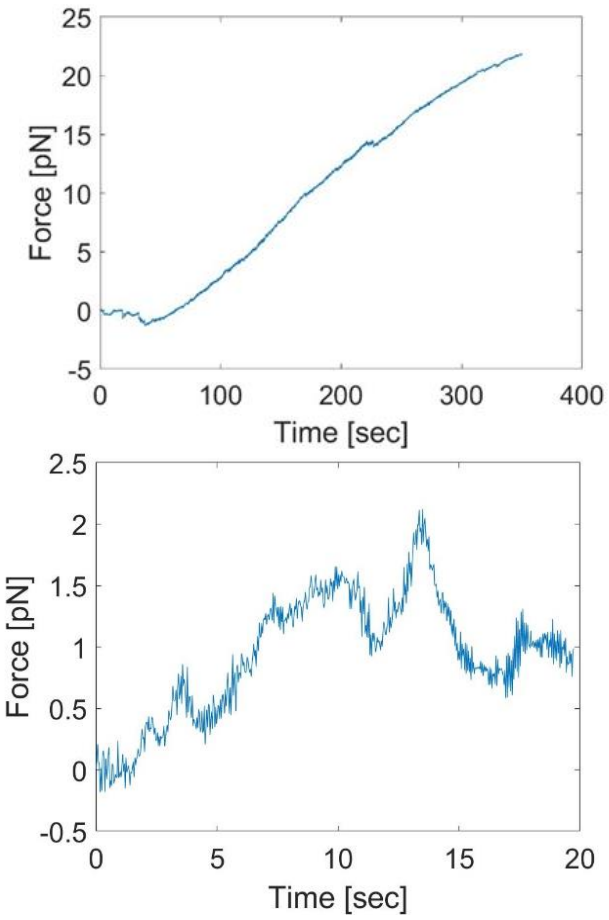

Figure 5.5: Variation in Force Profiles with Skeletal Myosin at Half Buffer Concentration. Profile A exhibits a ramp-plateau pattern reaching a maximum force of 23pN, while Profile B displays a sawtooth-like pattern with a peak force of 2.1pN.

Ionic Composition Adjustment: The replacement of the traditional APB buffer with GAB buffer, which lacks KCl, aimed to explore the role of potassium chloride in facilitating actin-myosin interactions. The absence of KCl in the GAB buffer led to no formation of actomyosin bundles or filament visualization under fluorescence imaging, emphasizing KCl's essential role in actin-myosin binding and motor activity.

Buffer Concentration Modification: By reducing the salt content in the APB buffer to 250 mM KCl, we aimed to study the impact of lower ionic strength on myosin motor function. Bundles formation was confirmed using fluorescence imaging. Force measurements were taken for the bundles with the reduced buffer concentration. It was shown that, despite this reduction in buffer ionic strength, maximum force averages were similar to the ones resulted from the regular APB buffer concentration. Maximum forces observed were in three ranges, low, medium, and high maximum forces. Averages range between 1 and 60 pN. The distribution of maximum force generation under half buffer condition is shown in Figure 5.3. The fundamental force generation profiles—Sawtooth-like, ramp plateau, and baseline remained the same as well. Figure 5.6 shows two different force profiles observed for 1mg/ml skeletal myosin bundles with half buffer concentration. The distribution of these patterns among 12 experiments (N=12) revealed 7 instances of ramp plateau (58.3%) , indicating a predominant occurrence of this pattern, 4 instances of sawtooth-like patterns (33.3%), characterized by lower force values, and 1 instance of a baseline or no force observed. The ramp plateau patterns exhibited maximum force values exceeding +15 pN, reaching up to a remarkable 70 pN, suggesting strong and sustained force generation. On the other hand, sawtooth-like patterns demonstrated maximum force values below 10 pN, with 1.5 pN being the most frequently observed value, indicating more variable and less potent force generation.

The single baseline observation underscores instances where no significant force was generated, highlighting the variability in force generation capacity under the given experimental conditions.

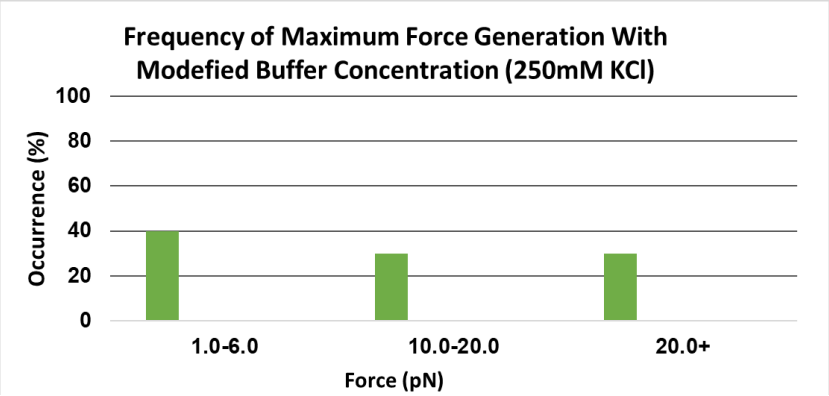

Figure 5.6: Percentage Distribution of Maximum Force Generation Ranges with Skeletal Myosin at Half Buffer Concentration.

From a statistical standpoint, across all observed patterns and force values (N=12), findings include values such as 23, 25.5, 70, 40, 80, 16, 1.5, 0.25, 1.5, 10, and 1.5), the average force generated was approximately 24.48 pN. The standard deviation, a measure of the dispersion of these values, was calculated to be around 26.72 pN, while the standard error, providing an estimate of the precision of the mean, was approximately 8.06 pN. These statistical measures reflect the range and variability of force generation observed in this set of experiments. This indicates that a decrease in ionic strength, to this extent, does not significantly affect myosin's force generation capabilities.

These results underscore the nuanced role of ionic strength, with particular emphasis on KCl concentration, in the modulation of myosin II motor coordination and force generation. The absence of KCl disrupts actomyosin interactions , while moderate reductions in ionic strength, as achieved by halving the KCl concentration in APB buffer, do not significantly alter the fundamental force generation dynamics of myosin II. Further studies are warranted to comprehensively investigate the collective impact of all ions involved in myosin dynamics, including magnesium (Mg), chloride (Cl), potassium (K), and calcium (Ca), to gain a more

comprehensive understanding of the intricate interplay within the myosin motor ensemble.

5.5 Conclusion

In conclusion, our exploration into the dynamics of S1 myosin and the impact of ionic strength on myosin motor behavior has shed light on the remarkable adaptability of myosin motor ensembles. Our investigation has reaffirmed that S1 myosin, despite lacking the tail domain, can generate forces across three distinct ranges, like in full-length myosin, underscoring the remarkable adaptability of motor proteins in the absence of their tail domains. This adaptation suggests a compelling mechanism wherein the two heads of a single S1 myosin motor are capable of simultaneously engaging with two actin filaments. This configuration likely results in the formation of more compact bundles, with the filaments drawn closer together, thereby enhancing the stability of the entire structure. Observations indicate that all force profiles transition to a smooth ramp-plateau pattern at higher myosin concentrations, which suggests that force generation by S1 myosin is facilitated more readily than in its full-length myosin. This phenomenon is likely attributable to the elimination of friction and drag forces that are typically introduced by the tail domain in full-length myosin. Furthermore, our investigation into ionic strength variations has revealed the nuanced role of KCl concentration in modulating myosin II motor coordination and force generation. As we move forward, further studies should aim to reveal the comprehensive effect of all ions involved in myosin dynamics, this holistic understanding of ion-mediated modulation of myosin behavior will deepen our knowledge of motor coordination and force generation in cellular processes. By building upon the foundations laid by Alazzam *et al.*, future research can continue to unveil the intricacies of myosin motor ensembles.

BIBLIOGRAPHY

5.6 Bibliography

Akhshi, T. K., Wernike, D., & Piekny, A. (2014). Microtubules and actin crosstalk in cell migration and division. *Cytoskeleton*, *71*(1), 1–23.

Al Azzam, O., Trussell, C. L., & Reinemann, D. N. (2021). Measuring force generation within reconstituted microtubule bundle assemblies using optical tweezers. *Cytoskeleton*, *78*(3), 111–125. https://doi.org/10.1002/cm.21678

Al Azzam, O. Y., Watts, J. C., Reynolds, J. E., Davis, J. E., & Reinemann, D. N. (2022). Myosin II Adjusts Motility Properties and Regulates Force Production Based on Motor Environment. *Cellular and Molecular Bioengineering*, *15*(5), 451–465. https://doi.org/10.1007/s12195-022-00731-1

Albert, P. J., Erdmann, T., & Schwarz, U. S. (2014). Stochastic dynamics and mechanosensitivity of myosin II minifilaments. *New Journal of Physics*, *16*(9), 093019. https://doi.org/10.1088/1367-2630/16/9/093019

Alberts, B., Johnson, A., Lewis, J., Raff, M., Roberts, K., & Walter, P. (2002). Molecular Motors. In *Molecular Biology of the Cell. 4th edition*. Garland Science. https://www.ncbi.nlm.nih.gov/books/NBK26888/

Altman, D. (2013). Myosin Work and Motility: Mechanism. In G. C. K. Roberts (Ed.), *Encyclopedia of Biophysics* (pp. 1671–1679). Springer. https://doi.org/10.1007/978-3-642-16712-6_754

Andrei, S., & Iorgoveanu, C. (2014). New perspective in heart failure management: Could myosin activators be the answer? *Discoveries (Craiova, Romania)*, *2*(4), e33. https://doi.org/10.15190/d.2014.25

Ashkin, A. (1997). Optical trapping and manipulation of neutral particles using lasers. *Proceedings of the National Academy of Sciences of the United States of America*, *94*(10), 4853–4860. https://doi.org/10.1073/pnas.94.10.4853

Ashkin, A., Dziedzic, J. M., Bjorkholm, J. E., & Chu, S. (1986). Observation of a single-beam gradient

force optical trap for dielectric particles. *Optics Letters*, *11*(5), 288. https://doi.org/10.1364/ol.11.000288

Ashkin, A., & Laboratories, B. (n.d.). *Optical Tweezers and their Application to Biological Systems*.

Auguin, D., Robert-Paganin, J., Réty, S., Kikuti, C., David, A., Theumer, G., Schmidt, A. W., Knölker, H.-J., & Houdusse, A. (2023). Omecamtiv mecarbil and Mavacamten target the same myosin pocket despite antagonistic effects in heart contraction. *bioRxiv*, 2023.11.15.567213. https://doi.org/10.1101/2023.11.15.567213

Azzam, O. A., Watts, J. C., Reynolds, J. E., Davis, J. E., & Reinemann, D. N. (2022). Probing Myosin Ensemble Mechanics in Actin Filament Bundles Using Optical Tweezers. *JoVE (Journal of Visualized Experiments)*, *183*, e63672. https://doi.org/10.3791/63672

Baldo, A. P., Tardiff, J. C., & Schwartz, S. D. (2020a). Mechanochemical Function of Myosin II: Investigation into the Recovery Stroke and ATP Hydrolysis. *The Journal of Physical Chemistry. B*, *124*(45), 10014–10023. https://doi.org/10.1021/acs.jpcb.0c05762

Baldo, A. P., Tardiff, J. C., & Schwartz, S. D. (2020b). Mechanochemical Function of Myosin II: Investigation into the Recovery Stroke and ATP Hydrolysis. *The Journal of Physical Chemistry. B*, *124*(45), 10014–10023. https://doi.org/10.1021/acs.jpcb.0c05762

Barrick, S. K., & Greenberg, M. J. (2021). Cardiac myosin contraction and mechanotransduction in health and disease. *The Journal of Biological Chemistry*, *297*(5), 101297. https://doi.org/10.1016/j.jbc.2021.101297

Beeler, T. J., Wang, T., Gable, K., & Lee, S. (1985). Comparison of the rat microsomal Mg-ATPase of various tissues. *Archives of Biochemistry and Biophysics*, *243*(2), 644–654. https://doi.org/10.1016/0003-9861(85)90542-9

Brunello, E., Fusi, L., Ghisleni, A., Park-Holohan, S.-J., Ovejero, J. G., Narayanan, T., & Irving, M. (2020). Myosin filament-based regulation of the dynamics of contraction in heart muscle. *Proceedings of the National Academy of Sciences*, *117*(14), 8177–8186. https://doi.org/10.1073/pnas.1920632117

Burghardt, T. P., Yan Hu, J., & Ajtai, K. (2007). Myosin Dynamics on the Millisecond Time Scale. *Biophysical Chemistry*, *131*(1–3), 15–28. https://doi.org/10.1016/j.bpc.2007.08.008

Chakraborti, A., Baldo, A. P., Tardiff, J. C., & Schwartz, S. D. (2021). Investigation of the Recovery Stroke and ATP Hydrolysis and Changes Caused Due to the Cardiomyopathic Point Mutations in Human Cardiac β Myosin. *The Journal of Physical Chemistry. B*, *125*(24), 6513–6521. https://doi.org/10.1021/acs.jpcb.1c03144

Chakraborti, A., Tardiff, J. C., & Schwartz, S. D. (2022a). Insights into the Mechanism of the Cardiac Drug Omecamtiv Mecarbil─A Computational Study. *The Journal of Physical Chemistry. B*, *126*(48), 10069–10082. https://doi.org/10.1021/acs.jpcb.2c06679

Chakraborti, A., Tardiff, J. C., & Schwartz, S. D. (2022b). Insights into the Mechanism of the Cardiac Drug Omecamtiv Mecarbil—A Computational Study. *The Journal of Physical Chemistry. B*, *126*(48), 10069–10082. https://doi.org/10.1021/acs.jpcb.2c06679

Chakraborti, A., Tardiff, J. C., & Schwartz, S. D. (2023). Exploring the effect of myosin modulators on the ATP hydrolysis step of human cardiac beta myosin using transition path sampling. *Biophysical Journal*, *122*(3), 259a. https://doi.org/10.1016/j.bpj.2022.11.1491

Chou, C., & Chin, M. T. (2021). Pathogenic Mechanisms of Hypertrophic Cardiomyopathy beyond Sarcomere Dysfunction. *International Journal of Molecular Sciences*, *22*(16), 8933. https://doi.org/10.3390/ijms22168933

Chowdhury, D. (2014). Michaelis-Menten at 100 and allosterism at 50: Driving molecular motors in a hailstorm with noisy ATPase engines and allosteric transmission. *The FEBS Journal*, *281*(2), 601–611. https://doi.org/10.1111/febs.12596

Clark, K., Langeslag, M., Figdor, C. G., & van Leeuwen, F. N. (2007). Myosin II and mechanotransduction: A balancing act. *Trends in Cell Biology*, *17*(4), 178–186. https://doi.org/10.1016/j.tcb.2007.02.002

Cleland, J. G., Teerlink, J. R., Senior, R., Nifontov, E. M., Mc Murray, J. J., Lang, C. C., Tsyrlin, V. A., Greenberg, B. H., Mayet, J., Francis, D. P., Shaburishvili, T., Monaghan, M., Saltzberg, M.,

Neyses, L., Wasserman, S. M., Lee, J. H., Saikali, K. G., Clarke, C. P., Goldman, J. H., … Malik, F. I. (2011). The effects of the cardiac myosin activator, omecamtiv mecarbil, on cardiac function in systolic heart failure: A double-blind, placebo-controlled, crossover, dose-ranging phase 2 trial. *The Lancet*, *378*(9792), 676–683. https://doi.org/10.1016/S0140-6736(11)61126-4

Cooper, G. M., & Hausman, R. (2000). A molecular approach. *The Cell. 2nd Ed. Sunderland, MA: Sinauer Associates*.

Create new possibilities with Pearson. Start learning today. (n.d.). Retrieved March 22, 2024, from https://www.pearson.com/en-us.html

Cytokinetics' heart failure drug gets a thumbs-down from FDA. (n.d.). Retrieved March 26, 2024, from https://www.fiercepharma.com/pharma/fda-turns-down-cytokinetics-once-promising-heart-failure-drug-omecamtiv

Daniels, M. J., Fusi, L., Semsarian, C., & Naidu, S. S. (2021). Myosin Modulation in Hypertrophic Cardiomyopathy and Systolic Heart Failure: Getting Inside the Engine. *Circulation*, *144*(10), 759–762. https://doi.org/10.1161/CIRCULATIONAHA.121.056324

Day, S. M., Tardiff, J. C., & Ostap, E. M. (2022). Myosin modulators: Emerging approaches for the treatment of cardiomyopathies and heart failure. *The Journal of Clinical Investigation*, *132*(5). https://doi.org/10.1172/JCI148557

Debold, E. P., Walcott, S., Woodward, M., & Turner, M. A. (2013). Direct observation of phosphate inhibiting the force-generating capacity of a miniensemble of Myosin molecules. *Biophysical Journal*, *105*(10), 2374–2384. https://doi.org/10.1016/j.bpj.2013.09.046

Doenst, T., Nguyen, T. D., & Abel, E. D. (2013). Cardiac Metabolism in Heart Failure—Implications beyond ATP production. *Circulation Research*, *113*(6), 709–724. https://doi.org/10.1161/CIRCRESAHA.113.300376

Doran, M. H., & Lehman, W. (2021). The Central Role of the F-Actin Surface in Myosin Force Generation. *Biology*, *10*(12), 1221. https://doi.org/10.3390/biology10121221

Dulyaninova, N. G., & Bresnick, A. R. (2013). The heavy chain has its day. *Bioarchitecture*, *3*(4), 77–85.

https://doi.org/10.4161/bioa.26133

El Hadi, H., Freund, A., Desch, S., Thiele, H., & Majunke, N. (2023). Hypertrophic, Dilated, and Arrhythmogenic Cardiomyopathy: Where Are We? *Biomedicines*, *11*(2), 524. https://doi.org/10.3390/biomedicines11020524

Elliott, P., & McKenna, W. (2008). Hypertrophic cardiomyopathy: A 50th anniversary. *Heart*, *94*(10), 1247–1248. https://doi.org/10.1136/hrt.2008.154344

Felker, G. M., Solomon, S. D., Claggett, B., Diaz, R., McMurray, J. J. V., Metra, M., Anand, I., Crespo-Leiro, M. G., Dahlström, U., Goncalvesova, E., Howlett, J. G., MacDonald, P., Parkhomenko, A., Tomcsányi, J., Abbasi, S. A., Heitner, S. B., Hucko, T., Kupfer, S., Malik, F. I., & Teerlink, J. R. (2022). Assessment of Omecamtiv Mecarbil for the Treatment of Patients With Severe Heart Failure. *JAMA Cardiology*, *7*(1), 26–34. https://doi.org/10.1001/jamacardio.2021.4027

Finer, J. T., Mehta, A. D., & Spudich, J. A. (1995). Characterization of single actin-myosin interactions. *Biophysical Journal*, *68*(4 Suppl), 291S-296S; discussion 296S-297S.

Finer, J. T., Simmons, R. M., & Spudich, J. A. (1994). Single myosin molecule mechanics: Piconewton forces and nanometre steps. *Nature*, *368*(6467), 113–119. https://doi.org/10.1038/368113a0

Fujita, K., Ohmachi, M., Ikezaki, K., Yanagida, T., & Iwaki, M. (2019). Direct visualization of human myosin II force generation using DNA origami-based thick filaments. *Communications Biology*, *2*(1), 1–11. https://doi.org/10.1038/s42003-019-0683-0

Furuta, K., & Toyoshima, Y. Y. (2008). Minus-end-directed motor Ncd exhibits processive movement that is enhanced by microtubule bundling in vitro. *Current Biology: CB*, *18*(2), 152–157. https://doi.org/10.1016/j.cub.2007.12.056

Glynn, P., Ning, H., Bavishi, A., Mehta, P. P., Shah, S., Yancy, C., Lloyd-Jones, D. M., & Khan, S. S. (2021). Heart Failure Risk Distribution and Trends in the United States Population, NHANES 1999–2016. *The American Journal of Medicine*, *134*(3), e153–e164. https://doi.org/10.1016/j.amjmed.2020.07.025

Gordon, A. M., Regnier, M., & Homsher, E. (2001). Skeletal and Cardiac Muscle Contractile Activation:

Tropomyosin “Rocks and Rolls.” *Physiology*, *16*(2), 49–55. https://doi.org/10.1152/physiologyonline.2001.16.2.49

Greenberg, M. J., & Moore, J. R. (2010). The molecular basis of frictional loads in the in vitro motility assay with applications to the study of the loaded mechanochemistry of molecular motors. *Cytoskeleton (Hoboken, N.J.)*, *67*(5), 273–285. https://doi.org/10.1002/cm.20441

Guhathakurta, P., Prochniewicz, E., & Thomas, D. D. (2018). Actin-Myosin Interaction: Structure, Function and Drug Discovery. *International Journal of Molecular Sciences*, *19*(9), 2628. https://doi.org/10.3390/ijms19092628

Hancock, W. O., & Howard, J. (1998). Processivity of the motor protein kinesin requires two heads. *The Journal of Cell Biology*, *140*(6), 1395–1405.

Hartman, M. A., & Spudich, J. A. (2012). The myosin superfamily at a glance. *Journal of Cell Science*, *125*(7), 1627–1632.

Hashem, S., Tiberti, M., & Fornili, A. (2017). Allosteric modulation of cardiac myosin dynamics by omecamtiv mecarbil. *PLOS Computational Biology*, *13*(11), e1005826. https://doi.org/10.1371/journal.pcbi.1005826

Heart Disease and Stroke Statistics—2023 Update: A Report From the American Heart Association | Circulation. (n.d.). Retrieved March 25, 2024, from https://www.ahajournals.org/doi/10.1161/CIR.0000000000001123

Heart Disease: Types, Causes, and Symptoms. (n.d.). Retrieved March 25, 2024, from https://www.webmd.com/heart-disease/heart-disease-types-causes-symptoms

Heart failure: Symptoms, causes, diagnosis and treatments. (n.d.). Retrieved March 25, 2024, from https://www.msn.com/en-us/health/condition/in-heart-failure/in-heart-failure

Heart Failure—Are you at risk?: Just Heart Cardiovascular Group Inc.: Cardiologists. (n.d.). Retrieved March 25, 2024, from https://www.myjustheart.com/blog/heart-failure-are-you-at-risk

Heart failure—Symptoms and causes. (n.d.). Mayo Clinic. Retrieved March 25, 2024, from https://www.mayoclinic.org/diseases-conditions/heart-failure/symptoms-causes/syc-20373142

Hilbert, L., Cumarasamy, S., Zitouni, N. B., Mackey, M. C., & Lauzon, A.-M. (2013). The kinetics of mechanically coupled myosins exhibit group size-dependent regimes. *Biophysical Journal*, *105*(6), 1466–1474.

Houdusse, A., & Sweeney, H. L. (2016). How myosin generates force on actin filaments. *Trends in Biochemical Sciences*, *41*(12), 989–997. https://doi.org/10.1016/j.tibs.2016.09.006

Https://www.aasavariclinic.com/latest-update/heart-failure-is-a-m/15. (n.d.). Retrieved March 25, 2024, from https://www.aasavariclinic.com/latest-update/heart-failure-is-a-m/15

Hypertrophic Cardiomyopathy Center | Cleveland Clinic. (n.d.). Retrieved March 25, 2024, from https://my.clevelandclinic.org/departments/heart/depts/hypertrophic-cardiomyopathy

Hypertrophic cardiomyopathy: Who has an inherited risk? (2016, July 12). Harvard Health. https://www.health.harvard.edu/heart-health/hypertrophic-cardiomyopathy-who-has-an-inherited-risk

Ireland, C. G., & Ho, C. Y. (2024). Genetic Testing in Hypertrophic Cardiomyopathy. *American Journal of Cardiology*, *212*, S4–S13. https://doi.org/10.1016/j.amjcard.2023.10.032

Irving, M., Piazzesi, G., Lucii, L., Sun, Y.-B., Harford, J. J., Dobbie, I. M., Ferenczi, M. A., Reconditi, M., & Lombardi, V. (2000). Conformation of the myosin motor during force generation in skeletal muscle. *Nature Structural Biology*, *7*(6), 482–485. https://doi.org/10.1038/75890

Ishikawa, R. (2007). Actin, Actin-binding Proteins and Myosins in Nervous System. In A. Lajtha & N. Banik (Eds.), *Handbook of Neurochemistry and Molecular Neurobiology: Neural Protein Metabolism and Function* (pp. 223–242). Springer US. https://doi.org/10.1007/978-0-387-30379-6_6

Itakura, S., Yamakawa, H., Toyoshima, Y. Y., Ishijima, A., Kojima, T., Harada, Y., Yanagida, T., Wakabayashi, T., & Sutoh, K. (1993). Force-Generating Domain of Myosin Motor. *Biochemical and Biophysical Research Communications*, *196*(3), 1504–1510. https://doi.org/10.1006/bbrc.1993.2422

Johnson, C. A., Walklate, J., Svicevic, M., Mijailovich, S. M., Vera, C., Karabina, A., Leinwand, L. A., &

Geeves, M. A. (2019). The ATPase cycle of human muscle myosin II isoforms: Adaptation of a single mechanochemical cycle for different physiological roles. *The Journal of Biological Chemistry*, *294*(39), 14267–14278. https://doi.org/10.1074/jbc.RA119.009825

Kad, N. M., Kim, S., Warshaw, D. M., VanBuren, P., & Baker, J. E. (2005). Single-myosin crossbridge interactions with actin filaments regulated by troponin-tropomyosin. *Proceedings of the National Academy of Sciences*, *102*(47), 16990–16995.

Kawana, M., Spudich, J. A., & Ruppel, K. M. (2022). Hypertrophic cardiomyopathy: Mutations to mechanisms to therapies. *Frontiers in Physiology*, *13*. https://doi.org/10.3389/fphys.2022.975076

Kaya, M., & Higuchi, H. (2010). Nonlinear elasticity and an 8-nm working stroke of single myosin molecules in myofilaments. *Science (New York, N.Y.)*, *329*(5992), 686–689. https://doi.org/10.1126/science.1191484

Kaya, M., Tani, Y., Washio, T., Hisada, T., & Higuchi, H. (2017). Coordinated force generation of skeletal myosins in myofilaments through motor coupling. *Nature Communications*, *8*, 16036. https://doi.org/10.1038/ncomms16036

Kitamura, K., Tokunaga, M., Iwane, A. H., & Yanagida, T. (1999). A single myosin head moves along an actin filament with regular steps of 5.3 nanometres. *Nature*, *397*(6715), 129–134. https://doi.org/10.1038/16403

KOHAMA, K. (2016). Calcium inhibition as an intracellular signal for actin–myosin interaction. *Proceedings of the Japan Academy. Series B, Physical and Biological Sciences*, *92*(10), 478–498. https://doi.org/10.2183/pjab.92.478

Korn, E. D. (2000). Coevolution of head, neck, and tail domains of myosin heavy chains. *Proceedings of the National Academy of Sciences of the United States of America*, *97*(23), 12559–12564.

Kruppa, A. J., & Buss, F. (2021). Motor proteins at the mitochondria–cytoskeleton interface. *Journal of Cell Science*, *134*(7), jcs226084. https://doi.org/10.1242/jcs.226084

Kuo, S. C., & Sheetz, M. P. (1993). Force of single kinesin molecules measured with optical tweezers. *Science (New York, N.Y.)*, *260*(5105), 232–234. https://doi.org/10.1126/science.8469975

Liew, C.-C., & Dzau, V. J. (2004). Molecular genetics and genomics of heart failure. *Nature Reviews Genetics*, *5*(11), 811–825. https://doi.org/10.1038/nrg1470

Liu, L. C. Y. (n.d.). *Novel Therapies in Heart Failure*.

Lőrinczy, D., & Belagyi, J. (2000). Functional and structural differences in skeletal and cardiac myosins. A molecular dynamic approach. *Thermochimica Acta*, *343*(1), 27–33. https://doi.org/10.1016/S0040-6031(99)00361-5

Malik, F. I., Hartman, J. J., Elias, K. A., Morgan, B. P., Rodriguez, H., Brejc, K., Anderson, R. L., Sueoka, S. H., Lee, K. H., Finer, J. T., Sakowicz, R., Baliga, R., Cox, D. R., Garard, M., Godinez, G., Kawas, R., Kraynack, E., Lenzi, D., Lu, P. P., … Morgans, D. J. (2011). Cardiac myosin activation: A potential therapeutic approach for systolic heart failure. *Science (New York, N.Y.)*, *331*(6023), 1439–1443. https://doi.org/10.1126/science.1200113

Maron, B. J., & Maron, M. S. (2013). Hypertrophic cardiomyopathy. *Lancet (London, England)*, *381*(9862), 242–255. https://doi.org/10.1016/S0140-6736(12)60397-3

Matusovsky, O. S., Månsson, A., & Rassier, D. E. (2023). Cooperativity of myosin II motors in the non-regulated and regulated thin filaments investigated with high-speed AFM. *Journal of General Physiology*, *155*(3), e202213190. https://doi.org/10.1085/jgp.202213190

McNamara, J. W., Li, A., dos Remedios, C. G., & Cooke, R. (2014). The role of super-relaxed myosin in skeletal and cardiac muscle. *Biophysical Reviews*, *7*(1), 5–14. https://doi.org/10.1007/s12551-014-0151-5

Means, A. R. (1988). Molecular Mechanisms of Action of Calmodulin. In J. H. Clark (Ed.), *Proceedings of the 1987 Laurentian Hormone Conference* (Vol. 44, pp. 223–262). Academic Press. https://doi.org/10.1016/B978-0-12-571144-9.50012-0

Mogilner, A. (2002). Mechanics of Motor Proteins and the Cytoskeleton. *Physics Today*, *55*(3), 63–64. https://doi.org/10.1063/1.1472396

Moraczewska, J., Sliwińska, M., & Redowicz, M. J. (2012). [Calcium ions in the regulation of acto-myosin interactions]. *Postepy Biochemii*, *58*(4), 437–451.

Morgan, B. P., Muci, A., Lu, P.-P., Qian, X., Tochimoto, T., Smith, W. W., Garard, M., Kraynack, E., Collibee, S., Suehiro, I., Tomasi, A., Valdez, S. C., Wang, W., Jiang, H., Hartman, J., Rodriguez, H. M., Kawas, R., Sylvester, S., Elias, K. A., … Morgans, D. J. (2010). Discovery of omecamtiv mecarbil the first, selective, small molecule activator of cardiac Myosin. *ACS Medicinal Chemistry Letters*, *1*(9), 472–477. https://doi.org/10.1021/ml100138q

Murphy, C. T., Rock, R. S., & Spudich, J. A. (2001). A myosin II mutation uncouples ATPase activity from motility and shortens step size. *Nature Cell Biology*, *3*(3), 311–315. https://doi.org/10.1038/35060110

Murphy, R. A., Walker, J. S., & Strauss, J. D. (1997). Myosin Isoforms and Functional Diversity in Vertebrate Smooth Muscle. *Comparative Biochemistry and Physiology Part B: Biochemistry and Molecular Biology*, *117*(1), 51–60. https://doi.org/10.1016/S0305-0491(96)00314-8

Myung, S.-K., Kim, H.-B., Lee, Y.-J., Choi, Y.-J., & Oh, S.-W. (2021). Calcium Supplements and Risk of Cardiovascular Disease: A Meta-Analysis of Clinical Trials. *Nutrients*, *13*(2), 368. https://doi.org/10.3390/nu13020368

Nagy, L., Kovács, Á., Bódi, B., Pásztor, E. T., Fülöp, G. Á., Tóth, A., Édes, I., & Papp, Z. (2015). The novel cardiac myosin activator omecamtiv mecarbil increases the calcium sensitivity of force production in isolated cardiomyocytes and skeletal muscle fibres of the rat. *British Journal of Pharmacology*, *172*(18), 4506–4518. https://doi.org/10.1111/bph.13235

Neuman, K. C., & Block, S. M. (2004). Optical trapping. *The Review of Scientific Instruments*, *75*(9), 2787–2809. https://doi.org/10.1063/1.1785844

Nikitina, L. V., Kopylova, G. V., Shchepkin, D. V., Nabiev, S. R., & Bershitsky, S. Y. (2015). Investigations of Molecular Mechanisms of Actin-Myosin Interactions in Cardiac Muscle. *Biochemistry. Biokhimiia*, *80*(13), 1748–1763. https://doi.org/10.1134/S0006297915130106

O'Connell, C. B., Tyska, M. J., & Mooseker, M. S. (2007). Myosin at work: Motor adaptations for a variety of cellular functions. *Biochimica et Biophysica Acta (BBA) - Molecular Cell Research*, *1773*(5), 615–630. https://doi.org/10.1016/j.bbamcr.2006.06.012

Ojima, K. (2019). Myosin: Formation and maintenance of thick filaments. *Animal Science Journal = Nihon Chikusan Gakkaiho*, *90*(7), 801–807. https://doi.org/10.1111/asj.13226

Optical Trapping. (n.d.). Retrieved March 25, 2024, from https://advlabs.aapt.org/items/detail.cfm?ID=13735

Parker, F., & Peckham, M. (2020). Disease mutations in striated muscle myosins. *Biophysical Reviews*, *12*(4), 887–894. https://doi.org/10.1007/s12551-020-00721-5

(PDF) Molecular Mechanism of Mg-ATPase Activity. (n.d.). Retrieved March 26, 2024, from https://www.researchgate.net/publication/270650202_Molecular_Mechanism_of_Mg-ATPase_Activity

Pérez-García, L., Selin, M., Ciarlo, A., Magazzù, A., Pesce, G., Sasso, A., Volpe, G., Pérez Castillo, I., & Arzola, A. V. (2023). Optimal calibration of optical tweezers with arbitrary integration time and sampling frequencies: A general framework [Invited]. *Biomedical Optics Express*, *14*(12), 6442–6469. https://doi.org/10.1364/BOE.495468

Pette, D., & Staron, R. S. (2000). Myosin isoforms, muscle fiber types, and transitions. *Microscopy Research and Technique*, *50*(6), 500–509. https://doi.org/10.1002/1097-0029(20000915)50:6<500::AID-JEMT7>3.0.CO;2-7

Piazzesi, G., Reconditi, M., Linari, M., Lucii, L., Bianco, P., Brunello, E., Decostre, V., Stewart, A., Gore, D. B., Irving, T. C., Irving, M., & Lombardi, V. (2007). Skeletal muscle performance determined by modulation of number of myosin motors rather than motor force or stroke size. *Cell*, *131*(4), 784–795. https://doi.org/10.1016/j.cell.2007.09.045

Planelles-Herrero, V. J., Hartman, J. J., Robert-Paganin, J., Malik, F. I., & Houdusse, A. (2017). Mechanistic and structural basis for activation of cardiac myosin force production by omecamtiv mecarbil. *Nature Communications*, *8*(1), 190. https://doi.org/10.1038/s41467-017-00176-5

Pollard, T. D. (2010). Mechanics of cytokinesis in eukaryotes. *Current Opinion in Cell Biology*, *22*(1), 50–56.

Porters versus rowers: A unified stochastic model of motor proteins. (1993). *The Journal of Cell Biology*,

121(6), 1357–1368.

Rayment, I., Rypniewski, W. R., Schmidt-Bäse, K., Smith, R., Tomchick, D. R., Benning, M. M., Winkelmann, D. A., Wesenberg, G., & Holden, H. M. (1993). Three-dimensional structure of myosin subfragment-1: A molecular motor. *Science (New York, N.Y.)*, *261*(5117), 50–58. https://doi.org/10.1126/science.8316857

Reinemann, D. N., Norris, S. R., Ohi, R., & Lang, M. J. (2018). Processive Kinesin-14 HSET Exhibits Directional Flexibility Depending on Motor Traffic. *Current Biology*, *28*(14), 2356-2362.e5. https://doi.org/10.1016/j.cub.2018.06.055

Rice, A., & Fischer, R. (n.d.). *Calibration of Optical Tweezers*.

Roth, G. A., Mensah, G. A., Johnson, C. O., Addolorato, G., Ammirati, E., Baddour, L. M., Barengo, N. C., Beaton, A. Z., Benjamin, E. J., Benziger, C. P., Bonny, A., Brauer, M., Brodmann, M., Cahill, T. J., Carapetis, J., Catapano, A. L., Chugh, S. S., Cooper, L. T., Coresh, J., … Fuster, V. (2020). Global Burden of Cardiovascular Diseases and Risk Factors, 1990–2019. *Journal of the American College of Cardiology*, *76*(25), 2982–3021. https://doi.org/10.1016/j.jacc.2020.11.010

Ruegg, C., Veigel, C., Molloy, J. E., Schmitz, S., Sparrow, J. C., & Fink, R. H. A. (2002). Molecular motors: Force and movement generated by single myosin II molecules. *News in Physiological Sciences*, *17*, 213–218. https://doi.org/10.1152/nips.01389.2002

Rüegg, C., Veigel, C., Molloy, J. E., Schmitz, S., Sparrow, J. C., & Fink, R. H. A. (2002). Molecular motors: Force and movement generated by single myosin II molecules. *News in Physiological Sciences: An International Journal of Physiology Produced Jointly by the International Union of Physiological Sciences and the American Physiological Society*, *17*, 213–218. https://doi.org/10.1152/nips.01389.2002

Schirber, M. (2018). Nobel Prize—Lasers as Tools. *Physics*, *11*, 100. https://doi.org/10.1103/PhysRevLett.24.156

Shaevitz, J. (2006). *A Practical Guide to Optical Trapping*. https://www.semanticscholar.org/paper/A-Practical-Guide-to-Optical-Trapping-Shaevitz/d28a1af8ba1550ed69c28a13a385be58765bb867

Sitbon, Y. H., Yadav, S., Kazmierczak, K., & Cordary, D. S. (2020). Insights into myosin regulatory and essential light chains: A focus on their roles in cardiac and skeletal muscle function, development and disease. *Journal of Muscle Research and Cell Motility*, *41*(4), 313–327. https://doi.org/10.1007/s10974-019-09517-x

Sliding Filament Theory, Sarcomere, Muscle Contraction, Myosin | Learn Science at Scitable. (n.d.). Retrieved March 26, 2024, from https://www.nature.com/scitable/topicpage/the-sliding-filament-theory-of-muscle-contraction-14567666/

Spirito, P., Seidman, C. E., McKenna, W. J., & Maron, B. J. (1997). The management of hypertrophic cardiomyopathy. *The New England Journal of Medicine*, *336*(11), 775–785. https://doi.org/10.1056/NEJM199703133361107

Spudich, J. A. (2001). The myosin swinging cross-bridge model. *Nature Reviews Molecular Cell Biology*, *2*(5), 387–392.

Spudich, J. A., Finer, J., Simmons, B., Ruppel, K., Patterson, B., & Uyeda, T. (1995). Myosin structure and function. *Cold Spring Harbor Symposia on Quantitative Biology*, *60*, 783–791.

Spudich, J. A., Rice, S. E., Rock, R. S., Purcell, T. J., & Warrick, H. M. (2011). Optical Traps to Study Properties of Molecular Motors. *Cold Spring Harbor Protocols*, *2011*(11), 1305–1318. https://doi.org/10.1101/pdb.top066662

Squire, J. (2019). Special Issue: The Actin-Myosin Interaction in Muscle: Background and Overview. *International Journal of Molecular Sciences*, *20*(22), 5715. https://doi.org/10.3390/ijms20225715

Stevens, H. M., Azzam, O. A., & Reinemann, D. N. (2024). Effects of a cardiac myosin activator on actin-myosin ensemble coordination. *Biophysical Journal*, *123*(3), 540a. https://doi.org/10.1016/j.bpj.2023.11.3268

Stewart, T. J., Jackson, D. R., Smith, R. D., Shannon, S. F., Cremo, C. R., & Baker, J. E. (2013). Actin Sliding Velocities are Influenced by the Driving Forces of Actin-Myosin Binding. *Cellular and Molecular Bioengineering*, *6*(1), 26–37. https://doi.org/10.1007/s12195-013-0274-y

Stewart, T. J., Murthy, V., Dugan, S. P., & Baker, J. E. (2021a). Velocity of myosin-based actin sliding

depends on attachment and detachment kinetics and reaches a maximum when myosin-binding sites on actin saturate. *The Journal of Biological Chemistry*, *297*(5), 101178. https://doi.org/10.1016/j.jbc.2021.101178

Stewart, T. J., Murthy, V., Dugan, S. P., & Baker, J. E. (2021b). Velocity of myosin-based actin sliding depends on attachment and detachment kinetics and reaches a maximum when myosin-binding sites on actin saturate. *The Journal of Biological Chemistry*, *297*(5), 101178. https://doi.org/10.1016/j.jbc.2021.101178

Stilgoe, A. B., Armstrong, D. J., & Rubinsztein-Dunlop, H. (2021). Enhanced Signal-to-Noise and Fast Calibration of Optical Tweezers Using Single Trapping Events. *Micromachines*, *12*(5), 570. https://doi.org/10.3390/mi12050570

Sudden death in young people: Heart problems often blamed—Mayo Clinic. (n.d.). Retrieved March 25, 2024, from https://www.mayoclinic.org/diseases-conditions/sudden-cardiac-arrest/in-depth/sudden-death/art-20047571

Sung, J., Nag, S., Mortensen, K. I., Vestergaard, C. L., Sutton, S., Ruppel, K., Flyvbjerg, H., & Spudich, J. A. (2015). Harmonic force spectroscopy measures load-dependent kinetics of individual human β-cardiac myosin molecules. *Nature Communications*, *6*, 7931. https://doi.org/10.1038/ncomms8931

Svoboda, K., & Block, S. M. (1994a). Biological applications of optical forces. *Annual Review of Biophysics and Biomolecular Structure*, *23*, 247–285. https://doi.org/10.1146/annurev.bb.23.060194.001335

Svoboda, K., & Block, S. M. (1994b). Force and velocity measured for single kinesin molecules. *Cell*, *77*(5), 773–784. https://doi.org/10.1016/0092-8674(94)90060-4

Swenson, A. M., Tang, W., Blair, C. A., Fetrow, C. M., Unrath, W. C., Previs, M. J., Campbell, K. S., & Yengo, C. M. (2017). Omecamtiv Mecarbil Enhances the Duty Ratio of Human β-Cardiac Myosin Resulting in Increased Calcium Sensitivity and Slowed Force Development in Cardiac Muscle*. *Journal of Biological Chemistry*, *292*(9), 3768–3778.

https://doi.org/10.1074/jbc.M116.748780

Syamaladevi, D. P., Spudich, J. A., & Sowdhamini, R. (2012). Structural and Functional Insights on the Myosin Superfamily. *Bioinformatics and Biology Insights*, *6*, 11–21. https://doi.org/10.4137/BBI.S8451

Tang, W., Ge, J., Unrath, W. C., Desetty, R., & Yengo, C. M. (2021). Cardiomyopathy mutations impact the actin-activated power stroke of human cardiac myosin. *Biophysical Journal*, *120*(11), 2222–2236. https://doi.org/10.1016/j.bpj.2021.04.007

Teekakirikul, P., Zhu, W., Huang, H. C., & Fung, E. (2019). Hypertrophic Cardiomyopathy: An Overview of Genetics and Management. *Biomolecules*, *9*(12), 878. https://doi.org/10.3390/biom9120878

Teerlink, J. R., Diaz, R., Felker, G. M., McMurray, J. J. V., Metra, M., Solomon, S. D., Adams, K. F., Anand, I., Arias-Mendoza, A., Biering-Sørensen, T., Böhm, M., Bonderman, D., Cleland, J. G. F., Corbalan, R., Crespo-Leiro, M. G., Dahlström, U., Echeverria Correa, L. E., Fang, J. C., Filippatos, G., … GALACTIC-HF Investigators. (2020). Omecamtiv mecarbil in chronic heart failure with reduced ejection fraction: GALACTIC-HF baseline characteristics and comparison with contemporary clinical trials. *European Journal of Heart Failure*, *22*(11), 2160–2171. https://doi.org/10.1002/ejhf.2015

Teerlink, J. R., Diaz, R., Felker, G. M., McMurray, J. J. V., Metra, M., Solomon, S. D., Adams, K. F., Anand, I., Arias-Mendoza, A., Biering-Sørensen, T., Böhm, M., Bonderman, D., Cleland, J. G. F., Corbalan, R., Crespo-Leiro, M. G., Dahlström, U., Echeverria, L. E., Fang, J. C., Filippatos, G., … Kurtz, C. E. (2021). Cardiac Myosin Activation with Omecamtiv Mecarbil in Systolic Heart Failure. *New England Journal of Medicine*, *384*(2), 105–116. https://doi.org/10.1056/NEJMoa2025797

Teerlink, J. R., Metra, M., Zacà, V., Sabbah, H. N., Cotter, G., Gheorghiade, M., & Cas, L. D. (2009). Agents with inotropic properties for the management of acute heart failure syndromes. Traditional agents and beyond. *Heart Failure Reviews*, *14*(4), 243–253.

https://doi.org/10.1007/s10741-009-9153-y

The myosin II coiled-coil domain atomic structure in its native environment | PNAS. (n.d.). Retrieved March 26, 2024, from https://www.pnas.org/doi/10.1073/pnas.2024151118

Thomas, D. D., & Roopnarine, O. (2002). An Overview of the Actin-Myosin Interaction. *Results and Problems in Cell Differentiation*, *36*, 1–5. https://doi.org/10.1007/978-3-540-46558-4_1

Thoresen, T., Lenz, M., & Gardel, M. L. (2013). Thick filament length and isoform composition determine self-organized contractile units in actomyosin bundles. *Biophysical Journal*, *104*(3), 655–665. https://doi.org/10.1016/j.bpj.2012.12.042

Tsutsui, H., Kinugawa, S., & Matsushima, S. (2011). Oxidative stress and heart failure. *American Journal of Physiology. Heart and Circulatory Physiology*, *301*(6), H2181-2190. https://doi.org/10.1152/ajpheart.00554.2011

Tu, M. K., Levin, J. B., Hamilton, A. M., & Borodinsky, L. N. (2016). Calcium signaling in skeletal muscle development, maintenance and regeneration. *Cell Calcium*, *59*(2–3), 91–97. https://doi.org/10.1016/j.ceca.2016.02.005

Types of heart failure. (2018). In *InformedHealth.org [Internet]*. Institute for Quality and Efficiency in Health Care (IQWiG). https://www.ncbi.nlm.nih.gov/books/NBK481485/

Unconventional Myosins: How Regulation Meets Function—PMC. (n.d.). Retrieved March 26, 2024, from https://www.ncbi.nlm.nih.gov/pmc/articles/PMC6981383/

Viswanathan, M. C., Schmidt, W., Franz, P., Rynkiewicz, M. J., Newhard, C. S., Madan, A., Lehman, W., Swank, D. M., Preller, M., & Cammarato, A. (2020). A role for actin flexibility in thin filament-mediated contractile regulation and myopathy. *Nature Communications*, *11*(1), 2417. https://doi.org/10.1038/s41467-020-15922-5

Wagner, P. D., & Giniger, E. (1981). Calcium-sensitive binding of heavy meromyosin to regulated actin in the presence of ATP. *Journal of Biological Chemistry*, *256*(24), 12647–12650. https://doi.org/10.1016/S0021-9258(18)42941-9

Wagoner, J. A., & Dill, K. A. (2021). Evolution of mechanical cooperativity among myosin II motors.

Proceedings of the National Academy of Sciences of the United States of America, *118*(20), e2101871118. https://doi.org/10.1073/pnas.2101871118

Wakabayashi, T., & Ebashi, S. (1968). Reversible change in physical state of troponin induced by calcium ion. *Journal of Biochemistry*, *64*(5), 731–732. https://doi.org/10.1093/oxfordjournals.jbchem.a128955

Walcott, S., Fagnant, P. M., Trybus, K. M., & Warshaw, D. M. (2009). Smooth Muscle Heavy Meromyosin Phosphorylated on One of Its Two Heads Supports Force and Motion *. *Journal of Biological Chemistry*, *284*(27), 18244–18251. https://doi.org/10.1074/jbc.M109.003293

Walcott, S., Warshaw, D. M., & Debold, E. P. (2012). Mechanical coupling between myosin molecules causes differences between ensemble and single-molecule measurements. *Biophysical Journal*, *103*(3), 501–510. https://doi.org/10.1016/j.bpj.2012.06.031

Watanabe, S., Watanabe, T. M., Sato, O., Awata, J., Homma, K., Umeki, N., Higuchi, H., Ikebe, R., & Ikebe, M. (2008). Human Myosin Vc Is a Low Duty Ratio Nonprocessive Motor. *The Journal of Biological Chemistry*, *283*(16), 10581–10592. https://doi.org/10.1074/jbc.M707657200

Wegner, A. (1976). Head to tail polymerization of actin. *Journal of Molecular Biology*, *108*(1), 139–150. https://doi.org/10.1016/S0022-2836(76)80100-3

Winkelmann, E. R., Dallazen, F., Bronzatti, A. B. S., Lorenzoni, J. C. W., & Windmöller, P. (2015). Analysis of steps adapted protocol in cardiac rehabilitation in the hospital phase. *Revista Brasileira De Cirurgia Cardiovascular: Orgao Oficial Da Sociedade Brasileira De Cirurgia Cardiovascular*, *30*(1), 40–48. https://doi.org/10.5935/1678-9741.20140048

Woerdemann, M. (2012). Introduction to Optical Trapping. In M. Wördemann (Ed.), *Structured Light Fields: Applications in Optical Trapping, Manipulation, and Organisation* (pp. 5–26). Springer. https://doi.org/10.1007/978-3-642-29323-8_2

Woo, A., Rakowski, H., Liew, J. C., Zhao, M.-S., Liew, C.-C., Parker, T. G., Zeller, M., Wigle, E. D., & Sole, M. J. (2003). Mutations of the β myosin heavy chain gene in hypertrophic cardiomyopathy: Critical functional sites determine prognosis. *Heart*, *89*(10), 1179–1185.

Woody, M. S., Greenberg, M. J., Barua, B., Winkelmann, D. A., Goldman, Y. E., & Ostap, E. M. (2018). Positive cardiac inotrope omecamtiv mecarbil activates muscle despite suppressing the myosin working stroke. *Nature Communications*, *9*(1), 3838. https://doi.org/10.1038/s41467-018-06193-2

Yanagida, T., Esaki, S., Iwane, A. H., Inoue, Y., Ishijima, A., Kitamura, K., Tanaka, H., & Tokunaga, M. (2000). Single-motor mechanics and models of the myosin motor. *Philosophical Transactions of the Royal Society of London. Series B, Biological Sciences*, *355*(1396), 441–447. https://doi.org/10.1098/rstb.2000.0585

Yang, C.-F., & Tsai, W.-C. (2021). Calmodulin: The switch button of calcium signaling. *Tzu-Chi Medical Journal*, *34*(1), 15–22. https://doi.org/10.4103/tcmj.tcmj_285_20

Zaiser, E., Sehnert, A. J., Duenas, A., Saberi, S., Brookes, E., & Reaney, M. (2020). Patient experiences with hypertrophic cardiomyopathy: A conceptual model of symptoms and impacts on quality of life. *Journal of Patient-Reported Outcomes*, *4*(1), 102. https://doi.org/10.1186/s41687-020-00269-8

Zhang, Y., Fu, W., Liu, D., Chen, X., & Zhou, P. (2024). Deciphering the thick filaments assembly behavior of myosin as affected by enzymatic deamidation. *Food Chemistry*, *433*, 137385. https://doi.org/10.1016/j.foodchem.2023.137385

β-Cardiac myosin hypertrophic cardiomyopathy mutations release sequestered heads and increase enzymatic activity | Nature Communications. (n.d.). Retrieved March 25, 2024.

CHAPTER 6

INVESTIGATING THE ENSEMBLE DYNAMICS CARDIAC MYOSIN II IN THE PRESENCE OF OMECAMTIV MECARBIL

6.1 Summary

This study adopts the approach designed by Al Azzam *et al.*, which combines an ensemble of cardiac myosin II motors interacting with multiple actin filaments, integrated with optical tweezers, to investigate the dynamics of cardiac myosin II and its modulation by Omecamtiv Mecarbil (OM), a contractility-enhancing drug. The focus is on understanding how OM influences the force generation and coordination of myosin motors within this ensemble, reflecting a more physiologically relevant model of cardiac muscle function than single molecule level measurements. Central to the study is the examination of cardiac myosin's interaction dynamics with OM, drawing on insights from various significant research works. Our bundle assay approach allows for a systematic investigation into how different OM concentrations and other motor environment conditions impact motor coordination and force production in the cardiac myosin ensemble.

6.2 Introduction

6.2.1 Cardiac Myosin II Structural and Function

Cardiac myosin, a close relative of skeletal myosin, shares a common structural blueprint, yet it has evolved to fulfill its unique role in powering the pumping action that sustains blood circulation. Structurally, both cardiac and skeletal myosin consist of essential components: a head, neck, and tail region, accompanied by associated light chains. The head, the epicenter of ATPase activity and actin binding, plays a pivotal role in the power stroke of muscle contraction. The neck region acts as a lever arm, transmitting force from the head to the tail, and is stabilized by light chains, which also modulate myosin's dynamic functionality. Meanwhile, the tail region is instrumental in filament assembly and structural organization within the muscle fiber (Hartman & Spudich, 2012; Syamaladevi *et al*., 2012).

Despite their shared structural framework, cardiac and skeletal myosin exhibit striking differences reflective of their distinct functional roles. Notably, the isoforms of heavy and light chains in cardiac myosin are uniquely tailored to meet the continuous, rhythmic demands of the heart, in contrast to the rapid and forceful contractions required by skeletal muscle myosin isoforms for body movement and posture maintenance. Significantly, the kinetic properties of the myosin head vary considerably between cardiac and skeletal myosin. Cardiac myosin has a slower ATPase activity, aligning with the heart's need for sustained contractions and energy efficiency. Conversely, skeletal myosin exhibits a faster ATPase activity, enabling rapid and powerful muscle contractions, essential for voluntary movements. Furthermore, the interaction between the neck region and light chains in cardiac myosin is finely tuned to provide the endurance and resilience necessary for continuous heartbeats. In contrast, skeletal myosin is optimized for generating greater force and speed, catering to the varied and intermittent demands of skeletal muscle activities (El Hadi *et al*., 2023; Lőrinczy & Belagyi, 2000, 2000; Sitbon *et al*., 2020).

6.2.2 Molecular Basis of Heart Diseases

Heart diseases, encompassing a range of conditions including cardiomyopathies and heart failure, represent a formidable global health challenge, contributing significantly to morbidity and mortality worldwide. Among these conditions, heart failure, characterized by the heart's inability to effectively pump blood, stands as a prominent concern, giving rise to debilitating symptoms such as shortness of breath, fatigue, and fluid retention (*Heart Failure*, n.d.). In the United States, the prevalence of heart failure has witnessed a concerning upward trajectory, with approximately 6.2 million Americans affected between 2013 and 2016, marking an 8.77% increase from previous years. If present trends persist, projections indicate a staggering 46% rise in prevalence by 2030, potentially impacting over 8 million Americans (Glynn *et al.*, 2021). Figure 6.1 (adapted from SimpleMed, 2020) illustrates two types of heart failure, each with distinct structural changes to the heart muscle. On the left side of the image, we have "Heart failure with preserved ejection fraction (Diastolic heart failure)." In this condition, the walls of the heart are depicted as thickened and stiff. This thickening can impede the heart's ability to fill properly, as the stiffened walls do not relax normally during diastole (the phase of the heartbeat when the heart muscle relaxes and allows the chambers to fill with blood). As a result, the heart struggles to fill with blood, which can lead to inadequate blood flow to the rest of the body. On the right side, the image shows "Heart failure with reduced ejection fraction (Systolic heart failure)." This condition is characterized by thin and dilated walls of the heart. The dilation and thinning of the walls are indicative of the heart's reduced ability to pump blood effectively. In systolic heart failure, the heart's contraction is weakened, and it cannot generate enough force to eject a sufficient volume of blood into the circulation during systole (the phase of the heartbeat

when the heart muscle contracts and pumps blood from the chambers into the arteries) (“Types of Heart Failure,” 2018).

The conventional management of heart conditions, including Hypertrophic Cardiomyopathy (HCM), Dilated Cardiomyopathy (DCM), and heart failure (HF), has predominantly revolved around symptom alleviation and the deceleration of disease progression. While these strategies remain crucial, they do not target the fundamental mechanisms underpinning these conditions. Cardiomyopathies, fundamentally disorders of abnormal cardiac contractility, demand therapeutic approaches that directly intervene with the cardiac muscle's contractile apparatus and its regulatory mechanisms. Current research endeavors are thus focused on the development of precise therapeutic strategies aimed at circumventing the side effects associated with existing treatments (El Hadi *et al*., 2023; *Heart Disease: Types, Causes, and Symptoms*, n.d.; Roth *et al*., 2020). The ATP cycle, governed by the binding, hydrolysis, and release of ATP, orchestrates the contractions necessary for blood propulsion. However, disruptions in this cycle, stemming from genetic mutations affecting motor proteins, alterations in myosin isoform expression, or dysregulation of myosin ATPase activity, can precipitate serious cardiac issues (Chakraborti *et al*., 2021; Johnson *et al*., 2019; C. T. Murphy *et al*., 2001). Additionally, molecular-level factors contributing to heart diseases including imbalances in calcium handling, oxidative stress, and perturbations in signaling pathways governing cardiac muscle contraction (Chakraborti *et al*., 2021; C. T. Murphy *et al*., 2001; Myung *et al*., 2021; Tsutsui *et al*., 2011). Notably, heart failure is closely intertwined with disturbances in cardiac myosin function, particularly within the ATP cycle critical for effective myosin-actin interactions

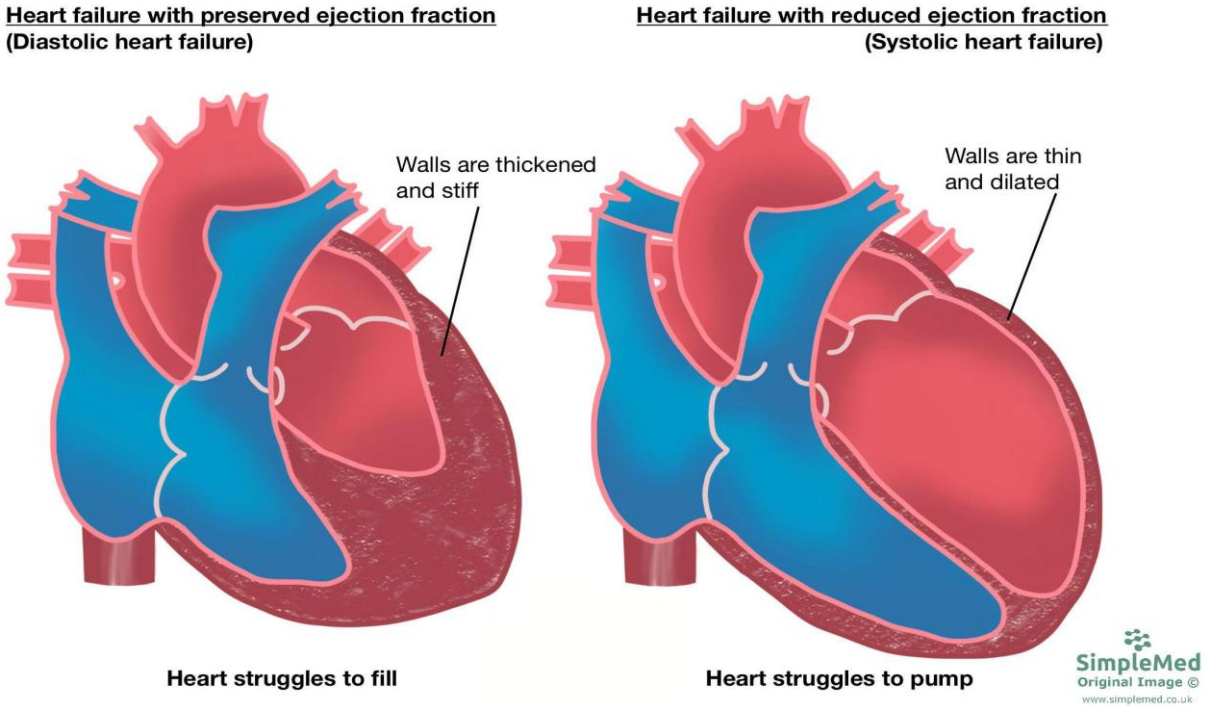

Figure 6.1: Comparative Illustration of Heart Failure Types: Left: Diastolic Heart Failure - Characterized by thickened and stiff heart walls, leading to difficulties with heart filling. Right: Systolic Heart Failure - Characterized by thin, dilated heart walls, resulting in compromised pumping efficacy. Adapted from "Cardiovascular System Overview," by SimpleMed, 2020, [https://www.simplemed.co.uk/cardiovascular-system-overview

and muscle contractions. In heart failure, disruptions in this cycle can manifest as inefficiencies in ATP utilization, resulting in suboptimal force generation during the power stroke of cardiac myosin. These inefficiencies may arise from genetic mutations affecting the myosin molecule, shifts in myosin isoform expression, or dysregulated myosin ATPase activity. Consequently, heart muscle's capacity to contract forcefully and efficiently is compromised, often leading to a scenario where the heart expends energy without generating commensurate contractile force, culminating in energy depletion within cardiac muscle cells (Day *et al*., 2022),(Barrick & Greenberg, 2021; Chakraborti *et al*., 2023; Daniels *et al*., 2021).

6.2.3 Omecamtiv Mecarbil (OM) Molecular Mechanisms and Therapeutic Potential in Cardiac Myosin Dynamics

Studies at the molecular level, particularly those testing the effects of cardiac drugs such as Omecamtiv Mecarbil (OM) on cardiac myosin dynamics, are pivotal for advancing our understanding of heart disease treatment. OM, a notable cardiac inotropic agent, demonstrates efficacy in enhancing cardiac functionality, particularly in hearts compromised by failure, and has garnered significant attention for its unique mechanism of action and potential benefits in treating heart failure (Morgan *et al*., 2010; Teerlink *et al*., 2021). OM is a small molecule that acts allosterically on cardiac myosin, the motor protein responsible for muscle contraction in the heart. Unlike traditional heart failure drugs, OM's mechanism of action does not primarily involve the neurohormonal pathways or the excitation–contraction coupling process. Instead, it binds to an allosteric site on the myosin protein, distinct from the active site of ATP interaction, inducing a conformational change in the protein. This allosteric modulation results in enhanced force production and prolongation of cardiac muscle contraction, addressing the underlying contractile dysfunction seen in heart failure (Cleland *et al*., 2011; Hashem *et al*., 2017; Woody *et al*., 2018).

OM was first discovered by Bradley P. Morgan and his team. Their research at Cytokinetics, Inc., aimed to discover selective activators of cardiac myosin to treat systolic heart failure (Morgan *et al*., 2010). The team's approach was unique in targeting cardiac myosin directly, OM does not work like traditional heart medications that increase calcium levels to boost contraction. Instead, it takes a more targeted approach, interacting directly with the myosin motor domain, specifically at an allosteric site, thereby influencing the ATPase cycle integral to muscle contraction. By doing so, OM increases the duration of the myosin-actin cross-bridge cycle, resulting in more effective and prolonged contractions of the heart muscle without substantially increasing energy consumption. This method was expected to avoid the toxicities

associated with current inotropes. They identified compounds that activate the cardiac sarcomere by measuring increases in myosin ATPase activity in a high-throughput, fully soluble, calcium-responsive, reconstituted sarcomere or myofibril assay.

Another study performed by Hashim *et al.* illustrated that OM binds to an allosteric site on the cardiac myosin motor domain. This binding typically occurs during the recovery stroke phase, a transitional stage where the myosin head moves from a post-rigor state to a pre-powerstroke state. In this phase, myosin is bound to ATP, but ATP hydrolysis has not yet occurred. OM's interaction with myosin during this phase is critical as it influences the subsequent steps in the ATPase cycle. Upon binding, OM induces a shift in the equilibrium of the recovery stroke towards the pre-powerstroke state. This shift is significant because it stabilizes the myosin in a configuration that is primed for efficient interaction with actin. By doing so, OM prolongs the duration of the myosin-actin cross-bridge cycle, enhancing the force production without significantly increasing energy consumption (Hashem *et al*., 2017).

More specifically, during ATP hydrolysis, OM alters the arrangement of active site residues. This modification affects the transition state of ATP hydrolysis, shifting the equilibrium towards the hydrolysis products (ADP and inorganic phosphate). As a result, OM influences the timing and efficiency of the ATP hydrolysis step, which is a crucial determinant of the overall contractile cycle. This alteration in the ATPase cycle has a cascade of effects on cardiac muscle contraction. By affecting the ATP hydrolysis step, OM enhances the force generation capabilities of cardiac myosin. This leads to prolonged and more effective heart muscle contractions, which are particularly beneficial in the context of heart failure where the heart's ability to contract efficiently is compromised. Moreover, the prolonged actin-myosin attachment duration induced by OM contributes to the increased force sustainability. By extending the period during which

myosin remains bound to actin, OM ensures that each contraction cycle is more effective in pumping blood, crucial for heart failure patients who suffer from reduced cardiac output. The findings highlighted OM's ability to enhance the duty ratio of myosin within the sarcomere, thereby increasing the number of myosin molecules strongly bound to actin. This interaction results in an elevated force production and an overall improvement in cardiac function, offering substantial benefits in heart failure conditions (Chakraborti *et al*., 2022a, 2023; Swenson *et al*., 2017; Woody *et al*., 2018).

The molecular-level analysis conducted by Hashim *et al.* uncovered that OM induces a more efficient allosteric communication within the myosin molecule. The study brought to light a reorganization in the network of dynamic correlations within myosin, enhancing effective communication pathways between OM's binding site and distant functional regions. This observation suggests that OM binding facilitates a more direct connection between its binding site and critical functional areas near the ATP binding site, such as the G helix and Switch 2 (Hashem *et al*., 2017).

In a study conducted by Nagy *et al.*, (Nagy *et al*., 2015), OM was investigated in the context of its effects on calcium sensitivity in rat cardiomyocytes and skeletal muscle fibers. This research was pivotal in understanding the potential of OM as a therapeutic agent in the treatment of systolic heart failure. The study aimed to meticulously analyze the mechanical effects of OM in a concentration-dependent manner. To achieve this, Nagy *et al.* utilized permeabilized cardiomyocyte-sized preparations and single skeletal muscle fibers derived from Wistar-Kyoto rats. The methodology involved monitoring active force production, calcium sensitivity, and the kinetics of activation and relaxation, in addition to passive force, both in the presence and absence of OM. The findings indicated that OM increased the calcium sensitivity of force

production in permeabilized cardiomyocytes, exhibiting a bell-shaped effect with maximal impacts observed at concentrations between 0.3–1 μM. Notably, as OM concentrations increased, the kinetics of force development and relaxation were progressively slowed. Furthermore, an increase in passive force in cardiomyocytes was observed under the influence of OM. These effects, while also present in diaphragm muscle fibers, varied in extent depending on the intrinsic kinetics of these muscle fibers.

From a mechanistic standpoint, OM was identified as a Ca^{2+}-sensitizing agent, influencing both cardiomyocytes and skeletal muscle fibers. This finding indicates a direct modulation of actin-myosin interactions by OM, altering the mechanics and kinetics of activation-relaxation cycles during calcium-induced contractions. The study also highlighted the selectivity of OM's effects, primarily targeting the myocardium. This specificity is noteworthy, considering that the cardiac myosin β-heavy chain, which OM targets, is also expressed in certain types of skeletal muscle fibers. In a comprehensive in vitro study conducted by Woody *et al.*, (Woody *et al*., 2018) the effects of Omecamtiv Mecarbil (OM) on cardiac myosin were meticulously examined using advanced single-molecule optical trapping techniques. They discovered that OM dramatically reduces the working stroke of myosin to less than 0.4 nm, a significant decrease from the usual range of about 5.4 nm. Additionally, OM extends the myosin-actin attachment duration fivefold at physiological ATP levels, with detachment becoming independent of both ATP concentration and the applied force. Crucially, the study found that the effect of OM on myosin's working stroke is dose-dependent, as evidenced by an EC50 of approximately 100 nM. This EC50 value indicates the concentration of OM required to achieve half of its maximum effect in suppressing myosin's working stroke. The simulations conducted in the study suggest that the prolonged attachment induced by OM leads to increased muscle

force production, attributable to thin-filament activation by OM-inhibited myosin molecules. These insights are pivotal in understanding how OM can enhance cardiac muscle contractility despite its inhibition of myosin's mechanical activity, offering valuable guidance for future therapeutic drug development targeting heart muscle function. In a study performed by Day *et al.*, (Day *et al*., 2022) the study delves into the dual effects of OM on cardiac myosin dynamics Initially, OM was developed to bind β-cardiac myosin and activate Ca^{2+}-regulated actin-activated myosin ATPase activity. This activation was thought to increase the duty ratio of myosin, resulting in higher force production from a group of myosins without changing the rate of muscle shortening. The drug was shown to increase the rate of phosphate release from the myosin-actin complex, a key step in the actomyosin ATPase cycle, fulfilling its intended role as a muscle activator without disturbing calcium release kinetics. Omecamtiv Mecarbil demonstrated a profound effect on cardiac muscle contraction by specifically targeting the S1 domain of the cardiac β-myosin heavy chain. This targeted interaction leads to enhanced ATPase activity, altering the myosin head's mechanical properties. Consequently, there is an increased rate of inorganic phosphate production, which is crucial in accelerating the actomyosin cycle. The drug's influence extends to augmenting the number of active force-generating cross-bridges, which significantly amplifies and prolongs the contractions of the cardiac muscle.

To study the effect of OM on cardiac muscle mechanics, a comprehensive research study was conducted by Swenson, Tang *et al.*, (Swenson *et al.*, 2017). They utilized a variety of experimental approaches including the purification and analysis of human β-cardiac myosin S1, transient kinetic analysis, and in vitro motility assays. The study revealed that OM dramatically altered the myosin ATPase kinetics, leading to enhanced drag forces and contributing to the slowing of actin filament sliding velocity. In human myocardium, OM increased calcium

sensitivity and slowed force generation, while not affecting the maximally activated force. These findings highlight OM's unique mechanism of action, distinct from traditional inotropic drugs, and its potential as a therapeutic agent in the treatment of heart failure. The comprehensive nature of this study, encompassing both in vitro and muscle mechanics analysis, provides significant insights into the mechanistic basis of OM's effects on cardiac muscle function. Further analysis of these results suggests that OM affects myosin ATPase cycle kinetics, leading to enhanced drag forces, which contribute to the slowing of actin filament sliding. OM alters the duty ratio of myosin, the fraction of the ATPase cycle during which myosin is bound to actin, which is a critical factor in muscle contraction. Specifically, OM seems to increase the duration of strong binding states of myosin to actin during the filament sliding process. Interestingly, OM also induces a population of myosin heads to remain in a weakly bound state with slow product release. These weakly bound states are thought to contribute to the overall drag forces that slow the actin filament sliding velocity. The unique ionic strength dependence of the in vitro motility assay in the presence of OM suggests that the inhibition of sliding velocity can be partially attributed to the drag forces from these weakly attached myosin heads. The study further explored the density dependence of in vitro motility, revealing that the sliding velocity increases at lower densities in the presence of OM, especially at low ionic strength. This observation supports the notion that fewer myosin heads available to interact with actin filaments reduce the drag forces, thereby increasing the velocity (Stewart *et al*., 2013, 2021a; Sung *et al*., 2015).

Exploring the role of OM further, we delve into the regulatory mechanisms of the thin filament as influenced by calcium and OM, as depicted in Figure 6.2 (Day *et al*., 2022). Here, the regulated thin filament is diagrammed, with the myosin binding sites blocked by tropomyosin (blue line) in the absence of calcium. Calcium shifts the position of tropomyosin from a

"blocked" state to a "closed" state. While in the closed state, the tropomyosin occasionally shifts to reveal the "open" state of the thin filament. Rapid actin binding and P_i release by OM-bound myosin stabilize the open state of the thin filament. Figure 6.2 shows the mechanism of action of OM enhancing interactions between actin and myosin in sarcomeres. Although OM-bound myosin has an inhibited working stroke, its prolonged time of actin attachment keeps the thin filament in the open state, allowing non-OM-bound myosins to attach and undergo uninhibited working strokes. For clarity, myosin molecules are illustrated with single motor domains.

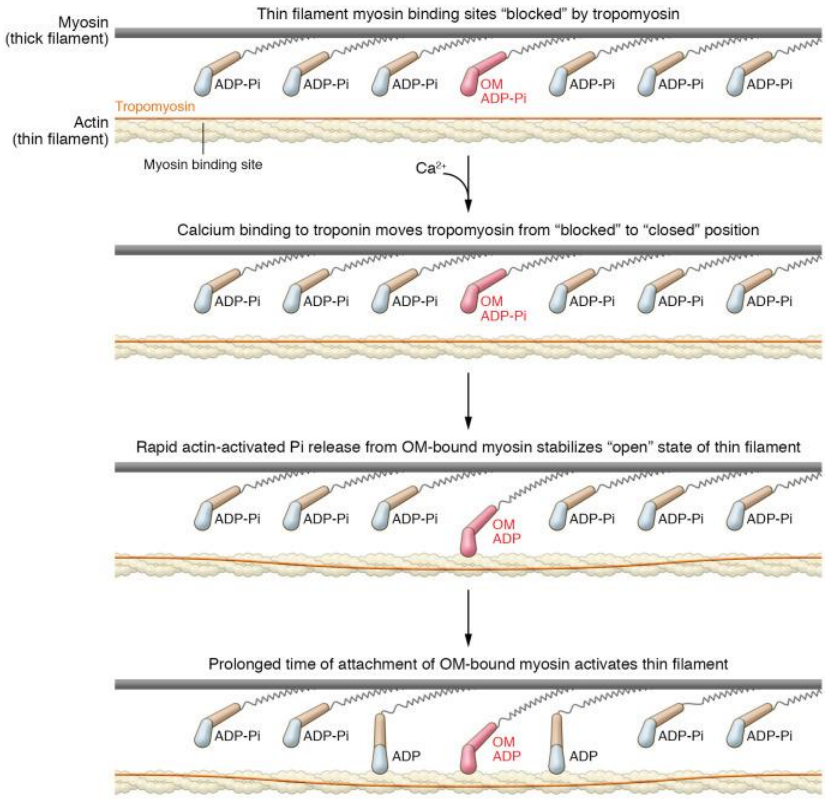

Figure 6.2: Enhancement of Myosin-Actin Interaction by OM Drug During ATP Hydrolysis: This diagram illustrates the molecular mechanism by which the drug OM facilitates muscle contraction. Initially, the myosin binding sites on actin are obscured by tropomyosin. Upon calcium binding to troponin, tropomyosin is repositioned, revealing the binding sites. OM drug-bound myosin (highlighted in pink) then attaches to actin, and the rapid release of inorganic phosphate (Pi) from the OM-bound myosin complex stabilizes actin's "open" state. Prolonged binding of OM-modified myosin to actin leads to sustained activation of the thin filament, thereby enhancing muscle contractility. This figure is adapted from Day SM, *et, al* 2022 American Society for Clinical Investigation. Copyright © 2024 American Society for Clinical Investigation ISSN: 0021-9738 (print), 1558-8238 (online)

This dual nature of OM as both an inhibitor and activator can be understood by considering its impact on the myosin ATPase cycle. While OM inhibits certain aspects of myosin's mechanical function (such as reducing the working stroke size), it also increases the time myosin spends in force-

generating states when bound to actin. This prolonged force-bearing state could potentially enhance the overall force generation of cardiac muscle despite the inhibition of individual myosin heads' mechanical activity (Planelles-Herrero *et al*., 2017; Woody *et al*., 2018). Clinical trials further substantiated the efficacy of OM. In the COSMIC-HF phase II study, patients with systolic heart failure receiving OM exhibited improved cardiac function, as evidenced by longer systolic ejection times, higher stroke volumes, smaller left ventricular dimensions, and lower levels of NT-proBNP.

These benefits were most pronounced in the group receiving pharmacokinetic-titrated OM. The subsequent GALACTIC-HF phase III trial, involving over 8000 patients, demonstrated that OM significantly reduced heart failure events or death compared to placebo. Notably, OM was particularly beneficial for patients with lower ejection fractions and those with severe heart failure, highlighting its potential as a treatment for patients with limited options due to intolerance of standard heart failure medications. Despite these promising results, OM faced a setback when it was denied approval by the FDA (*Cytokinetics' Heart Failure Drug Gets a Thumbs-down from FDA*, n.d.). The denial was rooted in concerns over its overall benefit-risk profile, with specific attention to the adequacy of evidence supporting its effectiveness and safety for a broad patient population. This decision underscores the complexities and challenges in translating clinical trial outcomes into widespread clinical practice, especially for drugs with novel mechanisms of action. Nevertheless, the interest among researchers in OM remains high, driven by its unique mechanism that targets allosteric sites rather than the ATP-binding pocket in myosins. This distinction suggests that OM could offer a fundamentally different approach to modulating heart muscle function, potentially sidestepping some of the limitations and side effects associated with more traditional therapies. The call for further investigation into OM is

not just about overcoming regulatory hurdles but also about deepening our understanding of its action in more physiologically relevant contexts. Studying OM in environments that closely mimic the natural ensemble of myosin motors in cardiac tissue could provide valuable insights into its mechanisms and therapeutic potential, offering hope for future interventions in heart failure treatment (Felker *et al*., 2022; *Https://Www.Aasavariclinic.Com/Latest-Update/Heart-Failure-Is-a-m/15*, n.d.).

In "Mechanistic and Structural Basis for Activation of Cardiac Myosin Force Production by Omecamtiv Mecarbil," researchers delve into the unique dual role of Omecamtiv Mecarbil (OM) as both a myosin inhibitor and a cardiac muscle activator, OM's mechanism of action is grounded in its selective binding to cardiac myosin. Contrary to altering the motor mechanism or the myosin structure, OM binds to an allosteric site that stabilizes the myosin lever arm in a 'primed' position. This stabilization leads to an increased number of myosin heads in the primed pre-powerstroke (PPS) state, ready for efficient binding to the actin filament, thereby enhancing the force production during cardiac contractions. Kinetic studies reveal that OM shifts the equilibrium of the recovery stroke and the myosin ATP hydrolysis step towards the ADP.Pi-bound state. This shift increases the population of myosin heads in the PPS state, which are then ready to engage in forceful contractions with actin filaments. Despite this inhibitory action on certain kinetic steps, OM does not significantly slow down essential processes like hydrolysis, or myosin attachment and detachment from F-actin, thus preserving the overall functionality of the motor (Baldo *et al*., 2020a),(Planelles-Herrero *et al*., 2017).

Small-angle X-ray scattering (SAXS) studies provided further confirmation of OM's influence, demonstrating that OM-bound cardiac S1 fragments adopt a conformation similar to the myosin motor in the PPS state. This finding supports the notion that OM binding stabilizes

the PPS state, tilting the balance towards a primed lever arm conformation. Moreover, the binding affinity of OM to cardiac myosin is notably high (0.29 μM) when the motor is in states favoring the PPS state, suggesting a precise and efficient mechanism of action. Interestingly, OM adopts a specific crescent shape upon binding, which aids in its function. One of the most significant revelations of the study is how OM increases contractile force. It does so not by accelerating the motor cycle but by increasing the number of myosin heads that engage the actin filament during cardiac contraction. This strategy effectively boosts contractile force without impairing the motor's cycle progression (Daniels *et al*., 2021; Hashem *et al*., 2017).

6.2.4 Omecamtiv Mecarbil ’s Influence on Ensemble Cardiac Myosin II Dynamics

Omecamtiv Mecarbil (OM) has shown promising outcomes in clinical trials as a potential treatment for heart failure, but the exact molecular mechanisms governing its mode of action remain enigmatic. While it was initially described as a straightforward “myosin activator,” recent research suggests a more complex picture. OM’s interaction with myosin might extend the “pre-powerstroke” state, influence myosin’s ATPase activity, and interact with regulatory proteins. However, the true impact of OM likely extends beyond direct myosin activation, and further research is needed to clarify the exact binding site(s) and their functional consequences, decipher how OM’s effects translate to changes in whole-muscle mechanics, and explore potential off-target interactions and potential side effects.

While numerous in vitro studies have explored the impact of Omecamtiv Mecarbil (OM) on the dynamics of myosin II and the activation of heart muscles, these investigations have predominantly been confined to single-molecule (SM) analyses or environments that fail to replicate the compliant systems where myosin motors operate dynamically. While invaluable,

these studies primarily focus on the molecular level, which, although insightful, may not fully capture the complex dynamics of myosin motors within the cardiac muscle's hierarchical and compliant systems. In the cardiac muscle, myosin motors do not operate in isolation; they function as part of a dynamic ensemble, engaging in cooperative interactions and responding to mechanical feedback from the environment, such as changes in local stiffness and occupancy of actin binding sites. These interactions are thought to contribute to the emergent properties of muscle contraction that cannot be observed in single-molecule scenarios (Azzam *et al*., 2022; Finer *et al*., 1994; Rüegg *et al*., 2002; Stevens *et al*., 2024; Wagoner & Dill, 2021; Walcott *et al*., 2012). Understanding the effects of OM within the context of an ensemble of myosin motors can provide a more physiologically relevant picture of how this drug enhances cardiac contractility. This approach can shed light on how OM-induced prolongation of myosin-actin attachment influences not just the individual myosin heads but also the collective behavior of myosin ensembles. Such a perspective is essential because it accounts for the force feedback between motors, which could lead to a nuanced understanding of how OM affects the heart's pumping efficiency. Moreover, studying OM in an ensemble context can reveal how the prolonged attachment of myosin to actin, as induced by OM, affects the force generation and movement of adjacent myosin motors. This is particularly relevant in therapeutic scenarios where the goal is to improve cardiac output in a failing heart. The compliant system of the cardiac muscle allows for the sensing of the mechanical environment, where a stiffer actin filament due to more bound myosin could signal other myosin heads to adjust their activity, potentially leading to a more coordinated and efficient contraction.

In the quest to bridge the knowledge gap surrounding Omecamtiv Mecarbil (OM) and its molecular mechanisms in heart failure treatment, the approach developed by Al Azzam *et al.*

extends beyond traditional single molecule *in vitro* studies that often focus on cardiac myosin motors in isolation or under rigid conditions, which fail to capture the dynamic environment of the human heart. The strategy employed here integrates optical tweezers with fluorescence imaging to closely examine the ensemble behavior of cardiac myosin motors interacting with multiple actin filaments. This approach is pivotal in understanding how OM modulates the cooperative behavior of myosin motors and their interaction with actin filaments. It is especially relevant in the context of heart failure, where myosin's coordinated activity is crucial.

6.3 Materials and Methods

In order to unravel the dynamics of Omecamtiv Mecarbil (OM) in cardiac myosin ensemble assays, an *in vitro* assay was developed, which was subsequently combined with optical microscopy and fluorescence imaging techniques. Initially, the assay was prepared by incubating rhodamine-labeled actin filaments on coverslips that had been coated with poly-L-lysine. This preparatory step was followed by the addition of myosin beads solution, comprising fluorescent actin, microbeads, ATP, and an oxygen scavenging system, to facilitate motor activity.

Concentrations of S1 cardiac myosin, ranging from 10 mg/ml to 0.001 mg/ml, were used in the assays to elucidate the motor coordination within the ensemble. MATLAB was employed to analyze the force generation, step size of motor molecules, as well as their collective performance, providing a quantitative assessment of the ensemble dynamics. Subsequently, different concentrations of OM were incorporated into the assay to discern its impact on myosin's functionality and coordination. These concentrations were selected, especially focusing on ensembles with a myosin concentration of 10 mg/ml, to observe the modifications in force output and the coordination among individual motor molecules.

Following the determination of an optimal concentration of OM (0.8 mg/ml) for the 10 mg/ml myosin ensembles, the investigation was extended to assess how OM influenced myosin behavior across a spectrum of lower myosin concentrations (0.02 mg/ml, 0.001 mg/ml, and 0.0001 mg/ml). This part of the study was crucial in understanding the broader implications of OM's interaction with myosin under varied conditions. Moreover, the study was further enhanced by integrating analysis with S1 cardiac myosin ensembles across the aforementioned range of concentrations. Through the utilization of MATLAB for the detailed examination of force, step size, and the durations of attachment and detachment, a comprehensive understanding of the ensemble dynamics was achieved.

6.4 Results and Discussion

This study revealed that the force generated by cardiac myosin is substantially lower than that produced by skeletal muscle as was illustrated by previous studies (Gordon *et al*., 2001; McNamara *et al*., 2014). The initial experiments were conducted on cardiac full-length myosin. Results revealed very low to neglected force production., which could be resulted from the intrinsic self-inhibition properties and the folded state induced by the tail portion of the molecule. Given these findings, the focus of this research shifted towards S1 myosin. In general, Analysis of the force traces indicated that, in the case of cardiac myosin, the traces were not smooth, suggesting a more variable and less consistent force generation pattern.

Furthermore, the average force generated by cardiac myosin was observed to be less than 2.0 pN, underscoring a fundamental difference in the efficiency and capacity of force production when compared to skeletal myosin. Figure 6.3 presents two distinct force traces obtained from experiments involving cardiac and skeletal myosin bundles. The trace on the lower (left) side of

the figure represents data from a cardiac myosin bundle experiment. This trace typically exhibits lower force generation, which is reflective of the inherent mechanical properties and contractile behavior of cardiac myosin. Cardiac myosin, which is adapted for endurance and continuous activity, generally generates less force than skeletal myosin, as it operates under different physiological conditions within the heart muscle. This discrepancy in force generation between S1 cardiac and skeletal myosin can be attributed to the inherent differences in their physiological roles and the biochemical pathways that regulate their activity. While skeletal muscle is designed for strength, speed, and adaptability to varying loads, cardiac muscle prioritizes endurance and consistency, operating within a narrower range of force generation to ensure reliable heart function (Gordon *et al*., 2001; McNamara *et al*., 2014).

Force generation and motor step analysis were conducted using S1 cardiac myosin at various concentrations, namely 10, 0.02, 0.01, and 0.001 mg/ml. It was observed that at the minimal motor concentration of 0.0001 mg/ml, actin filament bundles were not visible under fluorescence imaging, suggesting an insufficient number of motors to form bundles. As depicted in Figure 6.4 , data indicates that a motor concentration of 10 mg/ml resulted in an average force

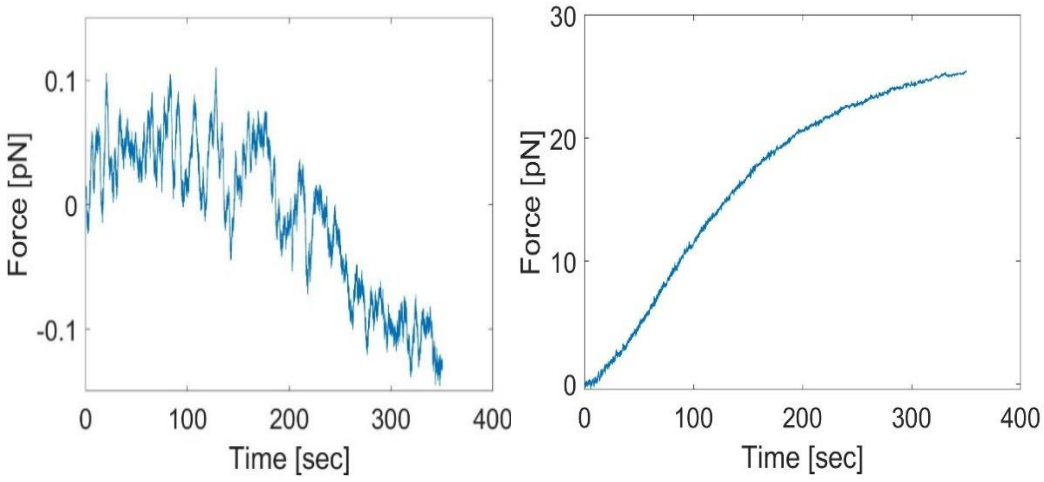

Figure 6.3: Examples of Force Traces Generated by Cardiac and Skeletal Myosin: Left Trace: Cardiac Myosin Force Generation. Right Trace: Skeletal Myosin Force Generation

output of 0.96 pN with SEM of ±0.25. In contrast, at a motor concentration of 0.02 mg/ml, the average force output was slightly higher, registering at 0.99 pN with SEM of ±0.22. A further decrease in motor concentration to 0.01 mg/ml led to an average force output of 0.73 pN wit SEM of ± 0.0.19. In Figure 6.5, which shows the frequency of maximum force generation across different S1 concentrations, the force is categorized into three ranges: 0.0-0.5 pN, 0.5-1.0 pN, and 1.0+ pN. The data indicates that at the lowest concentration of 0.01mg/ml S1 Myosin, there is a predominant occurrence in the lowest force range (0.0-0.5 pN), suggesting that at this dilute concentration, myosin's capacity for force generation is compromised. This could be due to diminished motor binding opportunities, leading to less efficient force production. In contrast, the concentration of 0.02mg/ml shows a more balanced distribution of force generation across all three force ranges, with the greatest occurrence noted in the mid-range (0.5-1.0 pN). This might imply an optimal myosin arrangement that facilitates effective

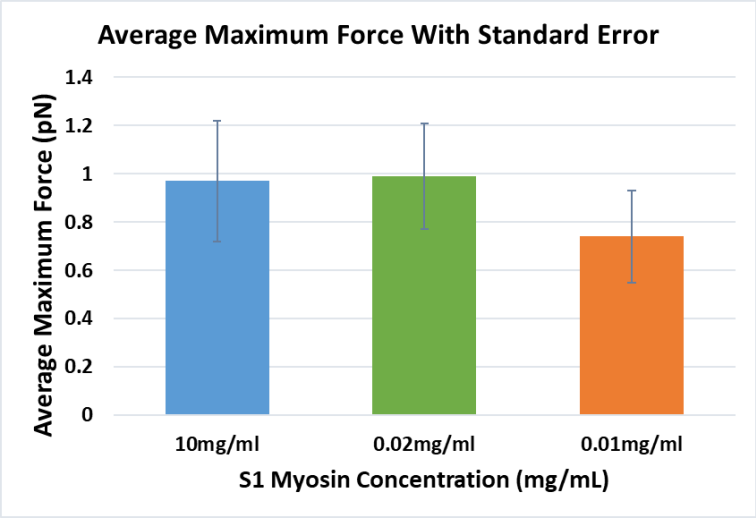

Figure 6.4 Variations in Maximum Force Generation at Different Concentrations of S1 Cardiac Myosin

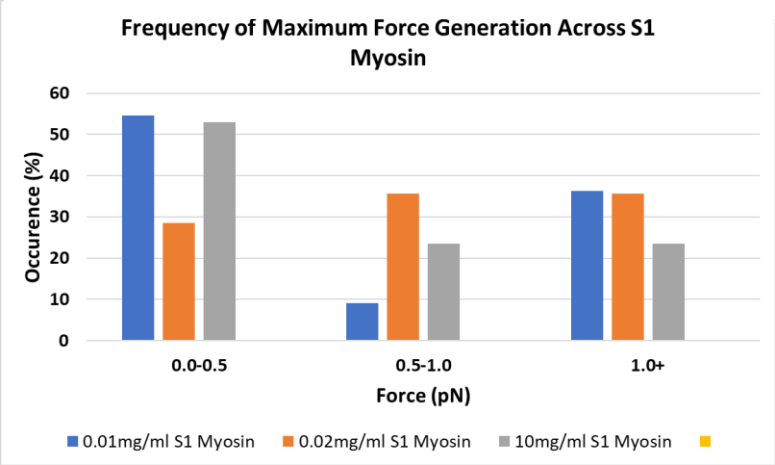

Figure 6.5: Percentage Distribution of Maximum Force Generation Ranges with S1 cardiac Myosin at different motor Concentration.

force generation due to a more compliant system allowing for better myosin head alignment and distribution. At the highest concentration of 10mg/ml, there is a notable shift toward the 0.0-0.5 pN and 1.0+ pN force ranges. The slight decrease in average force generation compared to 0.02mg/ml could suggest that an overly saturated motor environment leads to increased system stiffness, potentially hindering the coordination and movement of myosin motors necessary for generating force. These findings corroborate the conclusions drawn by Alazzam *et al*., reinforcing the understanding of motor environment's impact on force generation and the dynamic behavior within actin-myosin networks for cardiac myosin as previously documented for skeletal myosin.

To investigate the impact of Omecamtiv Mecarbil (OM) on full-length and S1 cardiac myosin II ensembles, experiments were conducted utilizing the same actin-myosin bundles assays but with the presence of OM in myosin solution. To titrate a proper concentration of OM to the bundle assay, OM stock was diluted using DMSO. The solvent mixture of distilled water and DMSO (50/50) used to dilute OM significantly hindered the formation of actin-myosin bundles, corroborating literature that highlights myosin II's susceptibility to environmental conditions, particularly solvent composition and ionic strength. A transition to utilizing solely DMSO for OM dissolution markedly enhanced the stability of the bundles. Concentrations of OM at 0.8 mg/ml, 0.4 mg/ml, and 0.2 m/ml were titrated to the bundles solutions, with S1 myosin concentration of 10mg/ml used. The first indication was that the addition of OM in general has facilitated the formation of distinct bundles visible and verified by fluorescence imaging compared to S1 myosin bundles without OM. Among the variety of OM concentrations used, for 0.8 mg/mL OM, the average value of maximum force was 0.84 with SEM of ±0.25 pN for N=10 indicating some variability in the measurements. As the concentration of OM

decreased to 0.4 mg/mL OM, the average maximum force slightly decreased to 0.82 pN with SEM of ±0.22 for N=22 which implies less spread in the data compared to the 0.8 mg/mL OM concentration. Further reduction in concentration to 0.2 mg/mL OM showed a more substantial decrease in the average maximum force to 0.53 pN with SEM of ±0.16 for N=29 suggesting a tighter grouping of the force measurements around the mean. Figure 6.6 bellow illustrates the frequency of maximum force generation across different OM concentrations compared to maximum force generated by S1 cardiac myosin without OM. The data is categorized into three force ranges: 0.0-0.5 pN, 0.5-1.0 pN, and 1.0+ pN. Most of the force traces where still in sawtooth-like pattern, however, it became smoother and less noisy. A discernible trend is that the frequency of higher force generation (1.0+ pN) is greatest without the addition of OM (10mg/ml S1 without OM), suggesting that the presence of OM may actually inhibit the force generation capability of S1 cardiac myosin. In contrast, with increasing concentrations of OM (0.8mg/ml, 0.4mg/ml, and 0.2mg/ml OM), there is a notable decline in occurrences of force generation in the higher force category. Furthermore, the highest concentration of OM (0.8mg/ml) demonstrates a higher occurrence of force generation in the lowest range (0.0-0.5 pN), which could imply that the addition of OM could be negatively impacting the myosin's ability to generate force. This is in line with the hypothesis that OM inhibits cardiac myosin II dynamics, as higher

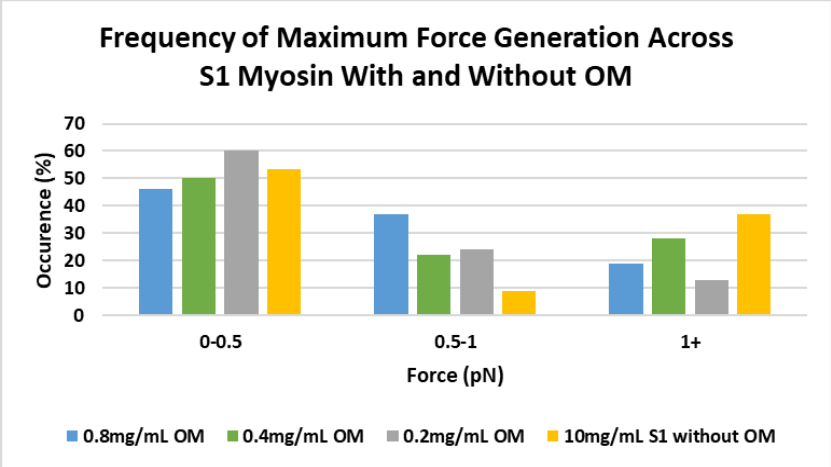

Figure 6.6: Percentage Distribution of Maximum Force Generation Ranges with10 mg/ml S1 cardiac Myosin Compared to Bundles With Different OM Concentrations.

concentrations of OM correlate with a decrease in higher force generation events.

For motor step analysis for experiments conducted on S1 cardiac myosin treated with 0.8 mg/ml OM, the motor step analysis yielded the following statistics: an average step size of 1.7 nm with a standard deviation of ±2.6 nm, across 281 observations, resulting in a standard error of the mean (SEM) of 0.16 nm. The dwell time analysis for the same sample revealed an average of 8.2 seconds, a standard deviation of ± 11.9seconds, with the same number of observations (N=281) and an SEM of± 0.71 seconds. Conversely, for S1 cardiac myosin without OM treatment, the step analysis results were as follows: an average step size of 0.66 nm with a standard deviation of ±0.91 nm, based on 154 observations, and an SEM of ±0.074 nm. The dwell time analysis for this untreated group presented an average of 13.9 seconds, a standard deviation of ±21.4 seconds, again with 154 observations, and an SEM of ±1.72 seconds. These results suggest that the presence of OM may have a considerable impact on the mechanical properties of S1 cardiac myosin, as evidenced by the differences in step size and dwell times when compared to the untreated myosin samples. Figure 6.7 shows force traces for bundles with OM and bundles without OM. The ones with OM seem to be smoother. This was the case for the majority of traces of force generated by bundles with OM. The smoothness observed in force traces in assays involving OM can infer several physiological implications. A smooth force trace may suggest a more synchronized transition between the states of the myosin ATPase cycle. If the steps between the attachment, power stroke, and detachment phases are occurring in a more coordinated manner, it could lead to a force generation that appears steadier and more consistent over time. Alternatively, this smoothness could be indicative of slower cross-bridge cycling, possibly resulting from OM's effect on prolonging the myosin-actin attachment. When myosin heads remain bound to actin for extended periods, the abrupt changes in force typically seen

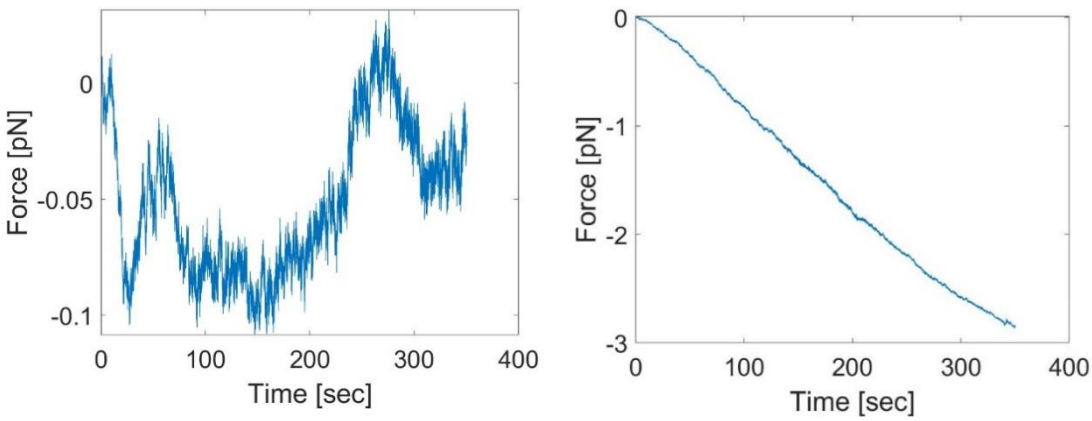

Figure 6.7: Force Traces of Bundles of S1 Cardiac Myosin Without OM (left) and With OM (right). Here, the force generated by bundles with OM seems to be in smother pattern than those without OM.

during rapid attachment and detachment cycles could be diminished, leading to a smoother trace. In addition to these interpretations, the observed smoothness may also be related to the cooperative interactions among multiple myosin heads within the sarcomere. The previous work of Alazzam *et al.* mentioned earlier in this dissertation underscore that within the sarcomere, the myosin motors are finely attuned to the biochemical and mechanical environment of the actin-myosin network. Applying this concept here, the introduction of Omecamtiv Mecarbil (OM) into this microenvironment by prolonging the attachment of myosin to actin, plays a pivotal role in modulating the dynamics of force generation at this more granular level. This prolongation effect of OM on the myosin-actin interaction serves as a feedback mechanism, enabling myosin motors to adapt their binding and cycling behavior based on the altered conditions. Specifically, by extending the duration of the myosin-actin cross-bridge, OM may increase the local stiffness of the actin filament. This mechanical change can act as a signal to surrounding myosin motors, influencing their decision on whether to engage in another contraction cycle based on the presence of OM and the resultant environmental conditions. Such a feedback loop within the sarcomere highlights a sophisticated regulatory system, where myosin motors are not merely passive participants in force generation but actively respond to the physicochemical cues in their

vicinity.

6.5 Conclusions

This study explored the role of Omecamtiv Mecarbil (OM) in modulating the dynamics of cardiac myosin motor within ensembles of motors, adopting a more realistic and physiologically relevant approach. This study aimed to transcend the limitations of single-molecule analyses by exploring the effects of OM in a system that closely mimics the complex environment of the cardiac sarcomere, including aspects such as system compliance, motor coordination, and the intrinsic feedback mechanisms between motors that govern actin myosin dynamics. The findings shed light on OM dual nature as both an inhibitor of myosin II and an activator of the actin-myosin interaction. Our findings, supported by detailed analyses of force generation and kinetic behaviors in the presence of OM, provide significant insights into the complex mechanisms underlying cardiac muscle dynamics and the therapeutic potential of OM in treating heart failure. OM's role as an inhibitor of myosin II is govern with its function as an activator of the actin-myosin interaction. The observed decrease in force generation with OM highlights its inhibitory effect on myosin II's mechanical activity. However, the smoother steps in force traces with OM underscore its role in facilitating a more coordinated and efficient actin-myosin interaction. This is central to understanding OM's unique therapeutic action—enhancing cardiac contractility without the deleterious effects associated with conventional inotropic agents.

Building upon our comprehensive investigation into the role of Omecamtiv Mecarbil (OM) on the dynamics of cardiac myosin within ensembles of motors, our study has laid a foundational understanding of OM's impact on cardiac function. However, to fully harness the therapeutic potential of OM and to refine our understanding of cardiac muscle physiology,

further investigation into a wider range of OM concentrations, cardiac myosin concentrations, and ionic strengths is imperative.

Future research should aim to explore the effects of OM across a broader spectrum of concentrations to delineate the dose-response relationship more precisely. This will enable us to identify the optimal concentration of OM that maximizes therapeutic efficacy while minimizing potential side effects. Similarly, varying the concentration of cardiac myosin in these assays will provide deeper insights into the drug's mechanism of action and its influence on the sarcomere's contractile dynamics under conditions that mimic different physiological and pathological states. Additionally, investigating the role of ionic strength on the interaction between OM and cardiac myosin is crucial. Ionic strength affects the electrostatic interactions within the actin-myosin complex and could significantly influence the efficacy of OM. Understanding how changes in ionic conditions alter OM's effects on myosin dynamics will contribute to a more nuanced comprehension of its pharmacological action and its potential impact on cardiac muscle contractility under varying physiological conditions.

BIBLIOGRAPHY

6.6 Bibliography

Akhshi, T. K., Wernike, D., & Piekny, A. (2014). Microtubules and actin crosstalk in cell migration and division. *Cytoskeleton*, *71*(1), 1–23.

Al Azzam, O., Trussell, C. L., & Reinemann, D. N. (2021). Measuring force generation within reconstituted microtubule bundle assemblies using optical tweezers. *Cytoskeleton*, *78*(3), 111–125. https://doi.org/10.1002/cm.21678

Al Azzam, O. Y., Watts, J. C., Reynolds, J. E., Davis, J. E., & Reinemann, D. N. (2022). Myosin II Adjusts Motility Properties and Regulates Force Production Based on Motor Environment. *Cellular and Molecular Bioengineering*, *15*(5), 451–465. https://doi.org/10.1007/s12195-022-00731-1

Albert, P. J., Erdmann, T., & Schwarz, U. S. (2014). Stochastic dynamics and mechanosensitivity of myosin II minifilaments. *New Journal of Physics*, *16*(9), 093019. https://doi.org/10.1088/1367-2630/16/9/093019

Alberts, B., Johnson, A., Lewis, J., Raff, M., Roberts, K., & Walter, P. (2002). Molecular Motors. In *Molecular Biology of the Cell. 4th edition*. Garland Science. https://www.ncbi.nlm.nih.gov/books/NBK26888/

Altman, D. (2013). Myosin Work and Motility: Mechanism. In G. C. K. Roberts (Ed.), *Encyclopedia of Biophysics* (pp. 1671–1679). Springer. https://doi.org/10.1007/978-3-642-16712-6_754

Andrei, S., & Iorgoveanu, C. (2014). New perspective in heart failure management: Could myosin activators be the answer? *Discoveries (Craiova, Romania)*, *2*(4), e33. https://doi.org/10.15190/d.2014.25

Ashkin, A. (1997). Optical trapping and manipulation of neutral particles using lasers.

Proceedings of the National Academy of Sciences of the United States of America, *94*(10), 4853–4860. https://doi.org/10.1073/pnas.94.10.4853

Ashkin, A., Dziedzic, J. M., Bjorkholm, J. E., & Chu, S. (1986). Observation of a single-beam gradient force optical trap for dielectric particles. *Optics Letters*, *11*(5), 288. https://doi.org/10.1364/ol.11.000288

Ashkin, A., & Laboratories, B. (n.d.). *Optical Tweezers and their Application to Biological Systems*.

Auguin, D., Robert-Paganin, J., Réty, S., Kikuti, C., David, A., Theumer, G., Schmidt, A. W., Knölker, H.-J., & Houdusse, A. (2023). Omecamtiv mecarbil and Mavacamten target the same myosin pocket despite antagonistic effects in heart contraction. *bioRxiv*, 2023.11.15.567213. https://doi.org/10.1101/2023.11.15.567213

Azzam, O. A., Watts, J. C., Reynolds, J. E., Davis, J. E., & Reinemann, D. N. (2022). Probing Myosin Ensemble Mechanics in Actin Filament Bundles Using Optical Tweezers. *JoVE (Journal of Visualized Experiments)*, *183*, e63672. https://doi.org/10.3791/63672

Baldo, A. P., Tardiff, J. C., & Schwartz, S. D. (2020a). Mechanochemical Function of Myosin II: Investigation into the Recovery Stroke and ATP Hydrolysis. *The Journal of Physical Chemistry. B*, *124*(45), 10014–10023. https://doi.org/10.1021/acs.jpcb.0c05762

Baldo, A. P., Tardiff, J. C., & Schwartz, S. D. (2020b). Mechanochemical Function of Myosin II: Investigation into the Recovery Stroke and ATP Hydrolysis. *The Journal of Physical Chemistry. B*, *124*(45), 10014–10023. https://doi.org/10.1021/acs.jpcb.0c05762

Barrick, S. K., & Greenberg, M. J. (2021). Cardiac myosin contraction and mechanotransduction in health and disease. *The Journal of Biological Chemistry*, *297*(5), 101297. https://doi.org/10.1016/j.jbc.2021.101297

Beeler, T. J., Wang, T., Gable, K., & Lee, S. (1985). Comparison of the rat microsomal Mg-ATPase of various tissues. *Archives of Biochemistry and Biophysics*, *243*(2), 644–654. https://doi.org/10.1016/0003-9861(85)90542-9

Brunello, E., Fusi, L., Ghisleni, A., Park-Holohan, S.-J., Ovejero, J. G., Narayanan, T., & Irving, M. (2020). Myosin filament-based regulation of the dynamics of contraction in heart muscle. *Proceedings of the National Academy of Sciences*, *117*(14), 8177–8186. https://doi.org/10.1073/pnas.1920632117

Burghardt, T. P., Yan Hu, J., & Ajtai, K. (2007). Myosin Dynamics on the Millisecond Time Scale. *Biophysical Chemistry*, *131*(1–3), 15–28. https://doi.org/10.1016/j.bpc.2007.08.008

Chakraborti, A., Baldo, A. P., Tardiff, J. C., & Schwartz, S. D. (2021). Investigation of the Recovery Stroke and ATP Hydrolysis and Changes Caused Due to the Cardiomyopathic Point Mutations in Human Cardiac β Myosin. *The Journal of Physical Chemistry. B*, *125*(24), 6513–6521. https://doi.org/10.1021/acs.jpcb.1c03144

Chakraborti, A., Tardiff, J. C., & Schwartz, S. D. (2022a). Insights into the Mechanism of the Cardiac Drug Omecamtiv Mecarbil─A Computational Study. *The Journal of Physical Chemistry. B*, *126*(48), 10069–10082. https://doi.org/10.1021/acs.jpcb.2c06679

Chakraborti, A., Tardiff, J. C., & Schwartz, S. D. (2022b). Insights into the Mechanism of the Cardiac Drug Omecamtiv Mecarbil—A Computational Study. *The Journal of Physical Chemistry. B*, *126*(48), 10069–10082. https://doi.org/10.1021/acs.jpcb.2c06679

Chakraborti, A., Tardiff, J. C., & Schwartz, S. D. (2023). Exploring the effect of myosin modulators on the ATP hydrolysis step of human cardiac beta myosin using transition path sampling. *Biophysical Journal*, *122*(3), 259a.

https://doi.org/10.1016/j.bpj.2022.11.1491

Chou, C., & Chin, M. T. (2021). Pathogenic Mechanisms of Hypertrophic Cardiomyopathy beyond Sarcomere Dysfunction. *International Journal of Molecular Sciences*, *22*(16), 8933. https://doi.org/10.3390/ijms22168933

Chowdhury, D. (2014). Michaelis-Menten at 100 and allosterism at 50: Driving molecular motors in a hailstorm with noisy ATPase engines and allosteric transmission. *The FEBS Journal*, *281*(2), 601–611. https://doi.org/10.1111/febs.12596

Clark, K., Langeslag, M., Figdor, C. G., & van Leeuwen, F. N. (2007). Myosin II and mechanotransduction: A balancing act. *Trends in Cell Biology*, *17*(4), 178–186. https://doi.org/10.1016/j.tcb.2007.02.002

Cleland, J. G., Teerlink, J. R., Senior, R., Nifontov, E. M., Mc Murray, J. J., Lang, C. C., Tsyrlin, V. A., Greenberg, B. H., Mayet, J., Francis, D. P., Shaburishvili, T., Monaghan, M., Saltzberg, M., Neyses, L., Wasserman, S. M., Lee, J. H., Saikali, K. G., Clarke, C. P., Goldman, J. H., … Malik, F. I. (2011). The effects of the cardiac myosin activator, omecamtiv mecarbil, on cardiac function in systolic heart failure: A double-blind, placebo-controlled, crossover, dose-ranging phase 2 trial. *The Lancet*, *378*(9792), 676–683. https://doi.org/10.1016/S0140-6736(11)61126-4

Cooper, G. M., & Hausman, R. (2000). A molecular approach. *The Cell. 2nd Ed. Sunderland, MA: Sinauer Associates*.

Create new possibilities with Pearson. Start learning today. (n.d.). Retrieved March 22, 2024, from https://www.pearson.com/en-us.html

Cytokinetics' heart failure drug gets a thumbs-down from FDA. (n.d.). Retrieved March 26, 2024, from https://www.fiercepharma.com/pharma/fda-turns-down-cytokinetics-once-

promising-heart-failure-drug-omecamtiv

Daniels, M. J., Fusi, L., Semsarian, C., & Naidu, S. S. (2021). Myosin Modulation in Hypertrophic Cardiomyopathy and Systolic Heart Failure: Getting Inside the Engine. *Circulation*, *144*(10), 759–762. https://doi.org/10.1161/CIRCULATIONAHA.121.056324

Day, S. M., Tardiff, J. C., & Ostap, E. M. (2022). Myosin modulators: Emerging approaches for the treatment of cardiomyopathies and heart failure. *The Journal of Clinical Investigation*, *132*(5). https://doi.org/10.1172/JCI148557

Debold, E. P., Walcott, S., Woodward, M., & Turner, M. A. (2013). Direct observation of phosphate inhibiting the force-generating capacity of a miniensemble of Myosin molecules. *Biophysical Journal*, *105*(10), 2374–2384. https://doi.org/10.1016/j.bpj.2013.09.046

Doenst, T., Nguyen, T. D., & Abel, E. D. (2013). Cardiac Metabolism in Heart Failure—Implications beyond ATP production. *Circulation Research*, *113*(6), 709–724. https://doi.org/10.1161/CIRCRESAHA.113.300376

Doran, M. H., & Lehman, W. (2021). The Central Role of the F-Actin Surface in Myosin Force Generation. *Biology*, *10*(12), 1221. https://doi.org/10.3390/biology10121221

Dulyaninova, N. G., & Bresnick, A. R. (2013). The heavy chain has its day. *Bioarchitecture*, *3*(4), 77–85. https://doi.org/10.4161/bioa.26133

El Hadi, H., Freund, A., Desch, S., Thiele, H., & Majunke, N. (2023). Hypertrophic, Dilated, and Arrhythmogenic Cardiomyopathy: Where Are We? *Biomedicines*, *11*(2), 524. https://doi.org/10.3390/biomedicines11020524

Elliott, P., & McKenna, W. (2008). Hypertrophic cardiomyopathy: A 50th anniversary. *Heart*,

94(10), 1247–1248. https://doi.org/10.1136/hrt.2008.154344

Felker, G. M., Solomon, S. D., Claggett, B., Diaz, R., McMurray, J. J. V., Metra, M., Anand, I., Crespo-Leiro, M. G., Dahlström, U., Goncalvesova, E., Howlett, J. G., MacDonald, P., Parkhomenko, A., Tomcsányi, J., Abbasi, S. A., Heitner, S. B., Hucko, T., Kupfer, S., Malik, F. I., & Teerlink, J. R. (2022). Assessment of Omecamtiv Mecarbil for the Treatment of Patients With Severe Heart Failure. *JAMA Cardiology*, *7*(1), 26–34. https://doi.org/10.1001/jamacardio.2021.4027

Finer, J. T., Mehta, A. D., & Spudich, J. A. (1995). Characterization of single actin-myosin interactions. *Biophysical Journal*, *68*(4 Suppl), 291S-296S; discussion 296S-297S.

Finer, J. T., Simmons, R. M., & Spudich, J. A. (1994). Single myosin molecule mechanics: Piconewton forces and nanometre steps. *Nature*, *368*(6467), 113–119. https://doi.org/10.1038/368113a0

Fujita, K., Ohmachi, M., Ikezaki, K., Yanagida, T., & Iwaki, M. (2019). Direct visualization of human myosin II force generation using DNA origami-based thick filaments. *Communications Biology*, *2*(1), 1–11. https://doi.org/10.1038/s42003-019-0683-0

Furuta, K., & Toyoshima, Y. Y. (2008). Minus-end-directed motor Ncd exhibits processive movement that is enhanced by microtubule bundling in vitro. *Current Biology: CB*, *18*(2), 152–157. https://doi.org/10.1016/j.cub.2007.12.056

Glynn, P., Ning, H., Bavishi, A., Mehta, P. P., Shah, S., Yancy, C., Lloyd-Jones, D. M., & Khan, S. S. (2021). Heart Failure Risk Distribution and Trends in the United States Population, NHANES 1999–2016. *The American Journal of Medicine*, *134*(3), e153–e164. https://doi.org/10.1016/j.amjmed.2020.07.025

Gordon, A. M., Regnier, M., & Homsher, E. (2001). Skeletal and Cardiac Muscle Contractile

Activation: Tropomyosin “Rocks and Rolls.” *Physiology*, *16*(2), 49–55. https://doi.org/10.1152/physiologyonline.2001.16.2.49

Greenberg, M. J., & Moore, J. R. (2010). The molecular basis of frictional loads in the in vitro motility assay with applications to the study of the loaded mechanochemistry of molecular motors. *Cytoskeleton (Hoboken, N.J.)*, *67*(5), 273–285. https://doi.org/10.1002/cm.20441

Guhathakurta, P., Prochniewicz, E., & Thomas, D. D. (2018). Actin-Myosin Interaction: Structure, Function and Drug Discovery. *International Journal of Molecular Sciences*, *19*(9), 2628. https://doi.org/10.3390/ijms19092628

Hancock, W. O., & Howard, J. (1998). Processivity of the motor protein kinesin requires two heads. *The Journal of Cell Biology*, *140*(6), 1395–1405.

Hartman, M. A., & Spudich, J. A. (2012). The myosin superfamily at a glance. *Journal of Cell Science*, *125*(7), 1627–1632.

Hashem, S., Tiberti, M., & Fornili, A. (2017). Allosteric modulation of cardiac myosin dynamics by omecamtiv mecarbil. *PLOS Computational Biology*, *13*(11), e1005826. https://doi.org/10.1371/journal.pcbi.1005826

Heart Disease and Stroke Statistics—2023 Update: A Report From the American Heart Association | Circulation. (n.d.). Retrieved March 25, 2024, from https://www.ahajournals.org/doi/10.1161/CIR.0000000000001123

Heart Disease: Types, Causes, and Symptoms. (n.d.). Retrieved March 25, 2024, from https://www.webmd.com/heart-disease/heart-disease-types-causes-symptoms

Heart failure: Symptoms, causes, diagnosis and treatments. (n.d.). Retrieved March 25, 2024, from https://www.msn.com/en-us/health/condition/in-heart-failure/in-heart-failure

Heart Failure—Are you at risk?: Just Heart Cardiovascular Group Inc.: Cardiologists. (n.d.). Retrieved March 25, 2024, from https://www.myjustheart.com/blog/heart-failure-are-you-at-risk

Heart failure—Symptoms and causes. (n.d.). Mayo Clinic. Retrieved March 25, 2024, from https://www.mayoclinic.org/diseases-conditions/heart-failure/symptoms-causes/syc-20373142

Hilbert, L., Cumarasamy, S., Zitouni, N. B., Mackey, M. C., & Lauzon, A.-M. (2013). The kinetics of mechanically coupled myosins exhibit group size-dependent regimes. *Biophysical Journal*, *105*(6), 1466–1474.

Houdusse, A., & Sweeney, H. L. (2016). How myosin generates force on actin filaments. *Trends in Biochemical Sciences*, *41*(12), 989–997. https://doi.org/10.1016/j.tibs.2016.09.006

Https://www.aasavariclinic.com/latest-update/heart-failure-is-a-m/15. (n.d.). Retrieved March 25, 2024, from https://www.aasavariclinic.com/latest-update/heart-failure-is-a-m/15

Hypertrophic Cardiomyopathy Center | Cleveland Clinic. (n.d.). Retrieved March 25, 2024, from https://my.clevelandclinic.org/departments/heart/depts/hypertrophic-cardiomyopathy

Hypertrophic cardiomyopathy: Who has an inherited risk? (2016, July 12). Harvard Health. https://www.health.harvard.edu/heart-health/hypertrophic-cardiomyopathy-who-has-an-inherited-risk

Ireland, C. G., & Ho, C. Y. (2024). Genetic Testing in Hypertrophic Cardiomyopathy. *American Journal of Cardiology*, *212*, S4–S13. https://doi.org/10.1016/j.amjcard.2023.10.032

Irving, M., Piazzesi, G., Lucii, L., Sun, Y.-B., Harford, J. J., Dobbie, I. M., Ferenczi, M. A., Reconditi, M., & Lombardi, V. (2000). Conformation of the myosin motor during force generation in skeletal muscle. *Nature Structural Biology*, *7*(6), 482–485.

https://doi.org/10.1038/75890

Ishikawa, R. (2007). Actin, Actin-binding Proteins and Myosins in Nervous System. In A. Lajtha & N. Banik (Eds.), *Handbook of Neurochemistry and Molecular Neurobiology: Neural Protein Metabolism and Function* (pp. 223–242). Springer US. https://doi.org/10.1007/978-0-387-30379-6_6

Itakura, S., Yamakawa, H., Toyoshima, Y. Y., Ishijima, A., Kojima, T., Harada, Y., Yanagida, T., Wakabayashi, T., & Sutoh, K. (1993). Force-Generating Domain of Myosin Motor. *Biochemical and Biophysical Research Communications*, *196*(3), 1504–1510. https://doi.org/10.1006/bbrc.1993.2422

Johnson, C. A., Walklate, J., Svicevic, M., Mijailovich, S. M., Vera, C., Karabina, A., Leinwand, L. A., & Geeves, M. A. (2019). The ATPase cycle of human muscle myosin II isoforms: Adaptation of a single mechanochemical cycle for different physiological roles. *The Journal of Biological Chemistry*, *294*(39), 14267–14278. https://doi.org/10.1074/jbc.RA119.009825

Kad, N. M., Kim, S., Warshaw, D. M., VanBuren, P., & Baker, J. E. (2005). Single-myosin crossbridge interactions with actin filaments regulated by troponin-tropomyosin. *Proceedings of the National Academy of Sciences*, *102*(47), 16990–16995.

Kawana, M., Spudich, J. A., & Ruppel, K. M. (2022). Hypertrophic cardiomyopathy: Mutations to mechanisms to therapies. *Frontiers in Physiology*, *13*. https://doi.org/10.3389/fphys.2022.975076

Kaya, M., & Higuchi, H. (2010). Nonlinear elasticity and an 8-nm working stroke of single myosin molecules in myofilaments. *Science (New York, N.Y.)*, *329*(5992), 686–689. https://doi.org/10.1126/science.1191484

Kaya, M., Tani, Y., Washio, T., Hisada, T., & Higuchi, H. (2017). Coordinated force generation of skeletal myosins in myofilaments through motor coupling. *Nature Communications*, *8*, 16036. https://doi.org/10.1038/ncomms16036

Kitamura, K., Tokunaga, M., Iwane, A. H., & Yanagida, T. (1999). A single myosin head moves along an actin filament with regular steps of 5.3 nanometres. *Nature*, *397*(6715), 129–134. https://doi.org/10.1038/16403

KOHAMA, K. (2016). Calcium inhibition as an intracellular signal for actin–myosin interaction. *Proceedings of the Japan Academy. Series B, Physical and Biological Sciences*, *92*(10), 478–498. https://doi.org/10.2183/pjab.92.478

Korn, E. D. (2000). Coevolution of head, neck, and tail domains of myosin heavy chains. *Proceedings of the National Academy of Sciences of the United States of America*, *97*(23), 12559–12564.

Kruppa, A. J., & Buss, F. (2021). Motor proteins at the mitochondria–cytoskeleton interface. *Journal of Cell Science*, *134*(7), jcs226084. https://doi.org/10.1242/jcs.226084

Kuo, S. C., & Sheetz, M. P. (1993). Force of single kinesin molecules measured with optical tweezers. *Science (New York, N.Y.)*, *260*(5105), 232–234. https://doi.org/10.1126/science.8469975

Liew, C.-C., & Dzau, V. J. (2004). Molecular genetics and genomics of heart failure. *Nature Reviews Genetics*, *5*(11), 811–825. https://doi.org/10.1038/nrg1470

Liu, L. C. Y. (n.d.). *Novel Therapies in Heart Failure*.

Lőrinczy, D., & Belagyi, J. (2000). Functional and structural differences in skeletal and cardiac myosins. A molecular dynamic approach. *Thermochimica Acta*, *343*(1), 27–33. https://doi.org/10.1016/S0040-6031(99)00361-5

Malik, F. I., Hartman, J. J., Elias, K. A., Morgan, B. P., Rodriguez, H., Brejc, K., Anderson, R. L., Sueoka, S. H., Lee, K. H., Finer, J. T., Sakowicz, R., Baliga, R., Cox, D. R., Garard, M., Godinez, G., Kawas, R., Kraynack, E., Lenzi, D., Lu, P. P., … Morgans, D. J. (2011). Cardiac myosin activation: A potential therapeutic approach for systolic heart failure. *Science (New York, N.Y.)*, *331*(6023), 1439–1443. https://doi.org/10.1126/science.1200113

Maron, B. J., & Maron, M. S. (2013). Hypertrophic cardiomyopathy. *Lancet (London, England)*, *381*(9862), 242–255. https://doi.org/10.1016/S0140-6736(12)60397-3

Matusovsky, O. S., Månsson, A., & Rassier, D. E. (2023). Cooperativity of myosin II motors in the non-regulated and regulated thin filaments investigated with high-speed AFM. *Journal of General Physiology*, *155*(3), e202213190. https://doi.org/10.1085/jgp.202213190

McNamara, J. W., Li, A., dos Remedios, C. G., & Cooke, R. (2014). The role of super-relaxed myosin in skeletal and cardiac muscle. *Biophysical Reviews*, *7*(1), 5–14. https://doi.org/10.1007/s12551-014-0151-5

Means, A. R. (1988). Molecular Mechanisms of Action of Calmodulin. In J. H. Clark (Ed.), *Proceedings of the 1987 Laurentian Hormone Conference* (Vol. 44, pp. 223–262). Academic Press. https://doi.org/10.1016/B978-0-12-571144-9.50012-0

Mogilner, A. (2002). Mechanics of Motor Proteins and the Cytoskeleton. *Physics Today*, *55*(3), 63–64. https://doi.org/10.1063/1.1472396

Moraczewska, J., Sliwińska, M., & Redowicz, M. J. (2012). [Calcium ions in the regulation of acto-myosin interactions]. *Postepy Biochemii*, *58*(4), 437–451.

Morgan, B. P., Muci, A., Lu, P.-P., Qian, X., Tochimoto, T., Smith, W. W., Garard, M.,

Kraynack, E., Collibee, S., Suehiro, I., Tomasi, A., Valdez, S. C., Wang, W., Jiang, H., Hartman, J., Rodriguez, H. M., Kawas, R., Sylvester, S., Elias, K. A., … Morgans, D. J. (2010). Discovery of omecamtiv mecarbil the first, selective, small molecule activator of cardiac Myosin. *ACS Medicinal Chemistry Letters*, *1*(9), 472–477. https://doi.org/10.1021/ml100138q

Murphy, C. T., Rock, R. S., & Spudich, J. A. (2001). A myosin II mutation uncouples ATPase activity from motility and shortens step size. *Nature Cell Biology*, *3*(3), 311–315. https://doi.org/10.1038/35060110

Murphy, R. A., Walker, J. S., & Strauss, J. D. (1997). Myosin Isoforms and Functional Diversity in Vertebrate Smooth Muscle. *Comparative Biochemistry and Physiology Part B: Biochemistry and Molecular Biology*, *117*(1), 51–60. https://doi.org/10.1016/S0305-0491(96)00314-8

Myung, S.-K., Kim, H.-B., Lee, Y.-J., Choi, Y.-J., & Oh, S.-W. (2021). Calcium Supplements and Risk of Cardiovascular Disease: A Meta-Analysis of Clinical Trials. *Nutrients*, *13*(2), 368. https://doi.org/10.3390/nu13020368

Nagy, L., Kovács, Á., Bódi, B., Pásztor, E. T., Fülöp, G. Á., Tóth, A., Édes, I., & Papp, Z. (2015). The novel cardiac myosin activator omecamtiv mecarbil increases the calcium sensitivity of force production in isolated cardiomyocytes and skeletal muscle fibres of the rat. *British Journal of Pharmacology*, *172*(18), 4506–4518. https://doi.org/10.1111/bph.13235

Neuman, K. C., & Block, S. M. (2004). Optical trapping. *The Review of Scientific Instruments*, *75*(9), 2787–2809. https://doi.org/10.1063/1.1785844

Nikitina, L. V., Kopylova, G. V., Shchepkin, D. V., Nabiev, S. R., & Bershitsky, S. Y. (2015).

Investigations of Molecular Mechanisms of Actin-Myosin Interactions in Cardiac Muscle. *Biochemistry. Biokhimiia*, *80*(13), 1748–1763. https://doi.org/10.1134/S0006297915130106

O'Connell, C. B., Tyska, M. J., & Mooseker, M. S. (2007). Myosin at work: Motor adaptations for a variety of cellular functions. *Biochimica et Biophysica Acta (BBA) - Molecular Cell Research*, *1773*(5), 615–630. https://doi.org/10.1016/j.bbamcr.2006.06.012

Ojima, K. (2019). Myosin: Formation and maintenance of thick filaments. *Animal Science Journal = Nihon Chikusan Gakkaiho*, *90*(7), 801–807. https://doi.org/10.1111/asj.13226

Optical Trapping. (n.d.). Retrieved March 25, 2024, from https://advlabs.aapt.org/items/detail.cfm?ID=13735

Parker, F., & Peckham, M. (2020). Disease mutations in striated muscle myosins. *Biophysical Reviews*, *12*(4), 887–894. https://doi.org/10.1007/s12551-020-00721-5

(PDF) Molecular Mechanism of Mg-ATPase Activity. (n.d.). Retrieved March 26, 2024, from https://www.researchgate.net/publication/270650202_Molecular_Mechanism_of_Mg-ATPase_Activity

Pérez-García, L., Selin, M., Ciarlo, A., Magazzù, A., Pesce, G., Sasso, A., Volpe, G., Pérez Castillo, I., & Arzola, A. V. (2023). Optimal calibration of optical tweezers with arbitrary integration time and sampling frequencies: A general framework [Invited]. *Biomedical Optics Express*, *14*(12), 6442–6469. https://doi.org/10.1364/BOE.495468

Pette, D., & Staron, R. S. (2000). Myosin isoforms, muscle fiber types, and transitions. *Microscopy Research and Technique*, *50*(6), 500–509. https://doi.org/10.1002/1097-0029(20000915)50:6<500::AID-JEMT7>3.0.CO;2-7

Piazzesi, G., Reconditi, M., Linari, M., Lucii, L., Bianco, P., Brunello, E., Decostre, V., Stewart,

A., Gore, D. B., Irving, T. C., Irving, M., & Lombardi, V. (2007). Skeletal muscle performance determined by modulation of number of myosin motors rather than motor force or stroke size. *Cell*, *131*(4), 784–795. https://doi.org/10.1016/j.cell.2007.09.045

Planelles-Herrero, V. J., Hartman, J. J., Robert-Paganin, J., Malik, F. I., & Houdusse, A. (2017). Mechanistic and structural basis for activation of cardiac myosin force production by omecamtiv mecarbil. *Nature Communications*, *8*(1), 190. https://doi.org/10.1038/s41467-017-00176-5

Pollard, T. D. (2010). Mechanics of cytokinesis in eukaryotes. *Current Opinion in Cell Biology*, *22*(1), 50–56.

Porters versus rowers: A unified stochastic model of motor proteins. (1993). *The Journal of Cell Biology*, *121*(6), 1357–1368.

Rayment, I., Rypniewski, W. R., Schmidt-Bäse, K., Smith, R., Tomchick, D. R., Benning, M. M., Winkelmann, D. A., Wesenberg, G., & Holden, H. M. (1993). Three-dimensional structure of myosin subfragment-1: A molecular motor. *Science (New York, N.Y.)*, *261*(5117), 50–58. https://doi.org/10.1126/science.8316857

Reinemann, D. N., Norris, S. R., Ohi, R., & Lang, M. J. (2018). Processive Kinesin-14 HSET Exhibits Directional Flexibility Depending on Motor Traffic. *Current Biology*, *28*(14), 2356-2362.e5. https://doi.org/10.1016/j.cub.2018.06.055

Rice, A., & Fischer, R. (n.d.). *Calibration of Optical Tweezers*.

Roth, G. A., Mensah, G. A., Johnson, C. O., Addolorato, G., Ammirati, E., Baddour, L. M., Barengo, N. C., Beaton, A. Z., Benjamin, E. J., Benziger, C. P., Bonny, A., Brauer, M., Brodmann, M., Cahill, T. J., Carapetis, J., Catapano, A. L., Chugh, S. S., Cooper, L. T., Coresh, J., … Fuster, V. (2020). Global Burden of Cardiovascular Diseases and Risk

Factors, 1990–2019. *Journal of the American College of Cardiology*, *76*(25), 2982–3021. https://doi.org/10.1016/j.jacc.2020.11.010

Ruegg, C., Veigel, C., Molloy, J. E., Schmitz, S., Sparrow, J. C., & Fink, R. H. A. (2002). Molecular motors: Force and movement generated by single myosin II molecules. *News in Physiological Sciences*, *17*, 213–218. https://doi.org/10.1152/nips.01389.2002

Rüegg, C., Veigel, C., Molloy, J. E., Schmitz, S., Sparrow, J. C., & Fink, R. H. A. (2002). Molecular motors: Force and movement generated by single myosin II molecules. *News in Physiological Sciences: An International Journal of Physiology Produced Jointly by the International Union of Physiological Sciences and the American Physiological Society*, *17*, 213–218. https://doi.org/10.1152/nips.01389.2002

Schirber, M. (2018). Nobel Prize—Lasers as Tools. *Physics*, *11*, 100. https://doi.org/10.1103/PhysRevLett.24.156

Shaevitz, J. (2006). *A Practical Guide to Optical Trapping*. https://www.semanticscholar.org/paper/A-Practical-Guide-to-Optical-Trapping-Shaevitz/d28a1af8ba1550ed69c28a13a385be58765bb867

Sitbon, Y. H., Yadav, S., Kazmierczak, K., & Cordary, D. S. (2020). Insights into myosin regulatory and essential light chains: A focus on their roles in cardiac and skeletal muscle function, development and disease. *Journal of Muscle Research and Cell Motility*, *41*(4), 313–327. https://doi.org/10.1007/s10974-019-09517-x

Sliding Filament Theory, Sarcomere, Muscle Contraction, Myosin | Learn Science at Scitable. (n.d.). Retrieved March 26, 2024, from https://www.nature.com/scitable/topicpage/the-sliding-filament-theory-of-muscle-contraction-14567666/

Spirito, P., Seidman, C. E., McKenna, W. J., & Maron, B. J. (1997). The management of

hypertrophic cardiomyopathy. *The New England Journal of Medicine*, *336*(11), 775–785. https://doi.org/10.1056/NEJM199703133361107

Spudich, J. A. (2001). The myosin swinging cross-bridge model. *Nature Reviews Molecular Cell Biology*, *2*(5), 387–392.

Spudich, J. A., Finer, J., Simmons, B., Ruppel, K., Patterson, B., & Uyeda, T. (1995). Myosin structure and function. *Cold Spring Harbor Symposia on Quantitative Biology*, *60*, 783–791.

Spudich, J. A., Rice, S. E., Rock, R. S., Purcell, T. J., & Warrick, H. M. (2011). Optical Traps to Study Properties of Molecular Motors. *Cold Spring Harbor Protocols*, *2011*(11), 1305–1318. https://doi.org/10.1101/pdb.top066662

Squire, J. (2019). Special Issue: The Actin-Myosin Interaction in Muscle: Background and Overview. *International Journal of Molecular Sciences*, *20*(22), 5715. https://doi.org/10.3390/ijms20225715

Stevens, H. M., Azzam, O. A., & Reinemann, D. N. (2024). Effects of a cardiac myosin activator on actin-myosin ensemble coordination. *Biophysical Journal*, *123*(3), 540a. https://doi.org/10.1016/j.bpj.2023.11.3268

Stewart, T. J., Jackson, D. R., Smith, R. D., Shannon, S. F., Cremo, C. R., & Baker, J. E. (2013). Actin Sliding Velocities are Influenced by the Driving Forces of Actin-Myosin Binding. *Cellular and Molecular Bioengineering*, *6*(1), 26–37. https://doi.org/10.1007/s12195-013-0274-y

Stewart, T. J., Murthy, V., Dugan, S. P., & Baker, J. E. (2021a). Velocity of myosin-based actin sliding depends on attachment and detachment kinetics and reaches a maximum when myosin-binding sites on actin saturate. *The Journal of Biological Chemistry*, *297*(5),

101178. https://doi.org/10.1016/j.jbc.2021.101178

Stewart, T. J., Murthy, V., Dugan, S. P., & Baker, J. E. (2021b). Velocity of myosin-based actin sliding depends on attachment and detachment kinetics and reaches a maximum when myosin-binding sites on actin saturate. *The Journal of Biological Chemistry*, *297*(5), 101178. https://doi.org/10.1016/j.jbc.2021.101178

Stilgoe, A. B., Armstrong, D. J., & Rubinsztein-Dunlop, H. (2021). Enhanced Signal-to-Noise and Fast Calibration of Optical Tweezers Using Single Trapping Events. *Micromachines*, *12*(5), 570. https://doi.org/10.3390/mi12050570

Sudden death in young people: Heart problems often blamed—Mayo Clinic. (n.d.). Retrieved March 25, 2024, from https://www.mayoclinic.org/diseases-conditions/sudden-cardiac-arrest/in-depth/sudden-death/art-20047571

Sung, J., Nag, S., Mortensen, K. I., Vestergaard, C. L., Sutton, S., Ruppel, K., Flyvbjerg, H., & Spudich, J. A. (2015). Harmonic force spectroscopy measures load-dependent kinetics of individual human β-cardiac myosin molecules. *Nature Communications*, *6*, 7931. https://doi.org/10.1038/ncomms8931

Svoboda, K., & Block, S. M. (1994a). Biological applications of optical forces. *Annual Review of Biophysics and Biomolecular Structure*, *23*, 247–285. https://doi.org/10.1146/annurev.bb.23.060194.001335

Svoboda, K., & Block, S. M. (1994b). Force and velocity measured for single kinesin molecules. *Cell*, *77*(5), 773–784. https://doi.org/10.1016/0092-8674(94)90060-4

Swenson, A. M., Tang, W., Blair, C. A., Fetrow, C. M., Unrath, W. C., Previs, M. J., Campbell, K. S., & Yengo, C. M. (2017). Omecamtiv Mecarbil Enhances the Duty Ratio of Human β-Cardiac Myosin Resulting in Increased Calcium Sensitivity and Slowed Force

Development in Cardiac Muscle*. *Journal of Biological Chemistry*, *292*(9), 3768–3778. https://doi.org/10.1074/jbc.M116.748780

Syamaladevi, D. P., Spudich, J. A., & Sowdhamini, R. (2012). Structural and Functional Insights on the Myosin Superfamily. *Bioinformatics and Biology Insights*, *6*, 11–21. https://doi.org/10.4137/BBI.S8451

Tang, W., Ge, J., Unrath, W. C., Desetty, R., & Yengo, C. M. (2021). Cardiomyopathy mutations impact the actin-activated power stroke of human cardiac myosin. *Biophysical Journal*, *120*(11), 2222–2236. https://doi.org/10.1016/j.bpj.2021.04.007

Teekakirikul, P., Zhu, W., Huang, H. C., & Fung, E. (2019). Hypertrophic Cardiomyopathy: An Overview of Genetics and Management. *Biomolecules*, *9*(12), 878. https://doi.org/10.3390/biom9120878

Teerlink, J. R., Diaz, R., Felker, G. M., McMurray, J. J. V., Metra, M., Solomon, S. D., Adams, K. F., Anand, I., Arias-Mendoza, A., Biering-Sørensen, T., Böhm, M., Bonderman, D., Cleland, J. G. F., Corbalan, R., Crespo-Leiro, M. G., Dahlström, U., Echeverria Correa, L. E., Fang, J. C., Filippatos, G., … GALACTIC-HF Investigators. (2020). Omecamtiv mecarbil in chronic heart failure with reduced ejection fraction: GALACTIC-HF baseline characteristics and comparison with contemporary clinical trials. *European Journal of Heart Failure*, *22*(11), 2160–2171. https://doi.org/10.1002/ejhf.2015

Teerlink, J. R., Diaz, R., Felker, G. M., McMurray, J. J. V., Metra, M., Solomon, S. D., Adams, K. F., Anand, I., Arias-Mendoza, A., Biering-Sørensen, T., Böhm, M., Bonderman, D., Cleland, J. G. F., Corbalan, R., Crespo-Leiro, M. G., Dahlström, U., Echeverria, L. E., Fang, J. C., Filippatos, G., … Kurtz, C. E. (2021). Cardiac Myosin Activation with Omecamtiv Mecarbil in Systolic Heart Failure. *New England Journal of Medicine*,

384(2), 105–116. https://doi.org/10.1056/NEJMoa2025797

Teerlink, J. R., Metra, M., Zacà, V., Sabbah, H. N., Cotter, G., Gheorghiade, M., & Cas, L. D. (2009). Agents with inotropic properties for the management of acute heart failure syndromes. Traditional agents and beyond. *Heart Failure Reviews*, *14*(4), 243–253. https://doi.org/10.1007/s10741-009-9153-y

The myosin II coiled-coil domain atomic structure in its native environment | PNAS. (n.d.). Retrieved March 26, 2024, from https://www.pnas.org/doi/10.1073/pnas.2024151118

Thomas, D. D., & Roopnarine, O. (2002). An Overview of the Actin-Myosin Interaction. *Results and Problems in Cell Differentiation*, *36*, 1–5. https://doi.org/10.1007/978-3-540-46558-4_1

Thoresen, T., Lenz, M., & Gardel, M. L. (2013). Thick filament length and isoform composition determine self-organized contractile units in actomyosin bundles. *Biophysical Journal*, *104*(3), 655–665. https://doi.org/10.1016/j.bpj.2012.12.042

Tsutsui, H., Kinugawa, S., & Matsushima, S. (2011). Oxidative stress and heart failure. *American Journal of Physiology. Heart and Circulatory Physiology*, *301*(6), H2181-2190. https://doi.org/10.1152/ajpheart.00554.2011

Tu, M. K., Levin, J. B., Hamilton, A. M., & Borodinsky, L. N. (2016). Calcium signaling in skeletal muscle development, maintenance and regeneration. *Cell Calcium*, *59*(2–3), 91–97. https://doi.org/10.1016/j.ceca.2016.02.005

Types of heart failure. (2018). In *InformedHealth.org [Internet]*. Institute for Quality and Efficiency in Health Care (IQWiG). https://www.ncbi.nlm.nih.gov/books/NBK481485/

Unconventional Myosins: How Regulation Meets Function—PMC. (n.d.). Retrieved March 26, 2024, from https://www.ncbi.nlm.nih.gov/pmc/articles/PMC6981383/

Viswanathan, M. C., Schmidt, W., Franz, P., Rynkiewicz, M. J., Newhard, C. S., Madan, A., Lehman, W., Swank, D. M., Preller, M., & Cammarato, A. (2020). A role for actin flexibility in thin filament-mediated contractile regulation and myopathy. *Nature Communications*, *11*(1), 2417. https://doi.org/10.1038/s41467-020-15922-5

Wagner, P. D., & Giniger, E. (1981). Calcium-sensitive binding of heavy meromyosin to regulated actin in the presence of ATP. *Journal of Biological Chemistry*, *256*(24), 12647–12650. https://doi.org/10.1016/S0021-9258(18)42941-9

Wagoner, J. A., & Dill, K. A. (2021). Evolution of mechanical cooperativity among myosin II motors. *Proceedings of the National Academy of Sciences of the United States of America*, *118*(20), e2101871118. https://doi.org/10.1073/pnas.2101871118

Wakabayashi, T., & Ebashi, S. (1968). Reversible change in physical state of troponin induced by calcium ion. *Journal of Biochemistry*, *64*(5), 731–732. https://doi.org/10.1093/oxfordjournals.jbchem.a128955

Walcott, S., Fagnant, P. M., Trybus, K. M., & Warshaw, D. M. (2009). Smooth Muscle Heavy Meromyosin Phosphorylated on One of Its Two Heads Supports Force and Motion *. *Journal of Biological Chemistry*, *284*(27), 18244–18251. https://doi.org/10.1074/jbc.M109.003293

Walcott, S., Warshaw, D. M., & Debold, E. P. (2012). Mechanical coupling between myosin molecules causes differences between ensemble and single-molecule measurements. *Biophysical Journal*, *103*(3), 501–510. https://doi.org/10.1016/j.bpj.2012.06.031

Watanabe, S., Watanabe, T. M., Sato, O., Awata, J., Homma, K., Umeki, N., Higuchi, H., Ikebe, R., & Ikebe, M. (2008). Human Myosin Vc Is a Low Duty Ratio Nonprocessive Motor. *The Journal of Biological Chemistry*, *283*(16), 10581–10592.

https://doi.org/10.1074/jbc.M707657200

Wegner, A. (1976). Head to tail polymerization of actin. *Journal of Molecular Biology*, *108*(1), 139–150. https://doi.org/10.1016/S0022-2836(76)80100-3

Winkelmann, E. R., Dallazen, F., Bronzatti, A. B. S., Lorenzoni, J. C. W., & Windmöller, P. (2015). Analysis of steps adapted protocol in cardiac rehabilitation in the hospital phase. *Revista Brasileira De Cirurgia Cardiovascular: Orgao Oficial Da Sociedade Brasileira De Cirurgia Cardiovascular*, *30*(1), 40–48. https://doi.org/10.5935/1678-9741.20140048

Woerdemann, M. (2012). Introduction to Optical Trapping. In M. Wördemann (Ed.), *Structured Light Fields: Applications in Optical Trapping, Manipulation, and Organisation* (pp. 5–26). Springer. https://doi.org/10.1007/978-3-642-29323-8_2

Woo, A., Rakowski, H., Liew, J. C., Zhao, M.-S., Liew, C.-C., Parker, T. G., Zeller, M., Wigle, E. D., & Sole, M. J. (2003). Mutations of the β myosin heavy chain gene in hypertrophic cardiomyopathy: Critical functional sites determine prognosis. *Heart*, *89*(10), 1179–1185.

Woody, M. S., Greenberg, M. J., Barua, B., Winkelmann, D. A., Goldman, Y. E., & Ostap, E. M. (2018). Positive cardiac inotrope omecamtiv mecarbil activates muscle despite suppressing the myosin working stroke. *Nature Communications*, *9*(1), 3838. https://doi.org/10.1038/s41467-018-06193-2

Yanagida, T., Esaki, S., Iwane, A. H., Inoue, Y., Ishijima, A., Kitamura, K., Tanaka, H., & Tokunaga, M. (2000). Single-motor mechanics and models of the myosin motor. *Philosophical Transactions of the Royal Society of London. Series B, Biological Sciences*, *355*(1396), 441–447. https://doi.org/10.1098/rstb.2000.0585

Yang, C.-F., & Tsai, W.-C. (2021). Calmodulin: The switch button of calcium signaling. *Tzu-Chi Medical Journal*, *34*(1), 15–22. https://doi.org/10.4103/tcmj.tcmj_285_20

Zaiser, E., Sehnert, A. J., Duenas, A., Saberi, S., Brookes, E., & Reaney, M. (2020). Patient experiences with hypertrophic cardiomyopathy: A conceptual model of symptoms and impacts on quality of life. *Journal of Patient-Reported Outcomes*, *4*(1), 102. https://doi.org/10.1186/s41687-020-00269-8

Zhang, Y., Fu, W., Liu, D., Chen, X., & Zhou, P. (2024). Deciphering the thick filaments assembly behavior of myosin as affected by enzymatic deamidation. *Food Chemistry*, *433*, 137385. https://doi.org/10.1016/j.foodchem.2023.137385

β-Cardiac myosin hypertrophic cardiomyopathy mutations release sequestered heads and increase enzymatic activity | Nature Communications. (n.d.). Retrieved March 25, 2024, from https://www.nature.com/articles/s41467-019-10555-9

CHAPTER 7

CONCLUSIONS AND FUTURE WORK

7.1 Conclusions

This dissertation unveils a novel approach to studying actomyosin dynamics, transcending the limitations of single-molecule investigations. A novel assay, mimicking biological system compliance and hierarchy, was engineered, featuring multiple myosin motors embedded within an actin filament bundle. This assay design captured crucial elements key for understanding how myosin behavior evolves from single-molecule to ensemble level: structural hierarchy, system compliance, and motor self-optimization. These factors had not previously been collectively investigated using optical tweezers, allowing us to explore the intricate interplay between key environmental factors and myosin force regulation.

Four critical areas were investigated. First, the impact of myosin concentration on actin-myosin bundle cooperativity was delved into by varying motor density within the bundles and measuring system force generation using optical tweezers. Both skeletal and cardiac myosin II isoforms were employed, shedding light on ensemble dynamics at different motor concentrations for each. Next, the influence of environment on bundle performance was examined. Force generation was measured with varying salt concentrations to understand how ionic strength affects overall dynamics. The same protein constructs as in the previous investigation were utilized, as ionic strength can influence both myosin aggregation and binding kinetics through

screening effects.

To illuminate the role of myosin tails in motor coordination and force production, S1 myosin (containing only the head) was employed in bundles. This allowed for dissection of how the absence of tails impacts force generation and ensemble communication compared to their full-length counterparts. Finally, the effects of drugs used to control cardiac contractility were probed by examining force generation in cardiac myosin bundles subjected to Omecamtiv Mecarbil. These investigations provided valuable insights into how these drugs influence motor cooperation and force generation.

Our findings suggest that motor number, environment, and system stiffness play a significant role in dictating motor duty ratio and overall force output in small myosin ensembles. This is evidenced by the observed changes in motor ensemble motility and force generation between saturated and less concentrated actomyosin bundles. Further exploration into the force-feedback mechanism between neighboring myosin motors, high-resolution motor imaging within these environments, changes in system compliance, entropic contributions, and cues from the local cytoskeletal environment are considered crucial for a deeper understanding of force propagation throughout motor-filament systems and the molecular basis of mechanosensation in actomyosin systems that underlie large-scale muscle contraction.

Ionic strength, while affecting overall dynamics through alterations in electrostatic interactions and binding affinities, requires further study to elucidate the specific mechanisms involved. Interestingly, cardiac myosin displayed similar dynamics and results compared to its S1 fragment in terms of force generation, motor stepping, and overall force output, suggesting that the tail may not play a crucial role within myosin ensembles interacting with actin filaments in the same bundle. However, further investigation is needed to fully understand the tail's

influence on inter-bundle interactions and force transmission. Cardiac myosin also exhibited distinct dynamics compared to skeletal myosin, characterized by lower force generation, less stable bundles, and reduced cooperativity. These findings warrant further exploration of the unique properties of cardiac myosin and its role in the contractile behavior of heart muscle. Finally, Omecamtiv Mecarbil drug titration in cardiac myosin bundles indicated an overall increase in force generation and bundle stability, suggesting its potential as a therapeutic strategy for improving cardiac function.

By harnessing the power of this novel actomyosin assay, we have gained valuable insights into the intricate interplay between myosin motors, their environment, and force generation at the ensemble level. This knowledge lays the foundation for future investigations into the complex dynamics of muscle contraction and opens exciting avenues for the development of therapeutic strategies targeting specific aspects of myosin function in diseases like hypertrophic cardiomyopathy.

7.2 Future work

Building upon the knowledge elucidated within this dissertation, the future invites further exploration of myosin dynamics, with the potential to illuminate both mechanisms and therapeutic avenue, promising advancements in both mechanistic understanding and therapeutic potential. Actin crosslinkers like actinin will be incorporated into the actomyosin bundle assay, shedding light on their influence on network stability and force transmission. Understanding how they impact motor cooperativity, force generation, and bundle stability in the presence and absence of Omecamtiv Mecarbil could yield insights into regulating cardiac contractility. Moreover, the research framework developed in this dissertation is ideally positioned to facilitate

studies on additional drugs that affect contractility, notably Mavacamten. Designed to target hypertrophic cardiomyopathy (HCM) by altering cardiac muscle contractility, the exploration of Mavacamten's effects within the cardiac system is crucial. The innovative methodology introduced in this dissertation is particularly well-suited for detailed analysis of Mavacamten's mechanism of action in myosin ensembles and its broader implications for heart muscle function.

Mechanistically, the interplay between ionic strength and myosin behavior will be further investigated. Deciphering the specific mechanisms by which varying salt concentrations affect crosslinking, motor cooperation, and force generation across a wider range of ionic conditions will significantly advance our understanding of actomyosin regulation. While the tail domain's role within single actomyosin bundles might be limited, its influence on inter-bundle interactions and force transmission remains unclear. Employing assays with multiple, interconnected actomyosin bundles will illuminate the tail's impact on inter-bundle cooperativity and force propagation, revealing a more nuanced picture of its functional significance. Unraveling the intricate force-feedback mechanism between neighboring myosin motors will be another endeavor. High-resolution imaging within the actomyosin network, combined with advanced computational modeling, will hold the key to unlocking this mystery, revealing the interplay of forces and conformational changes within motor clusters and how information exchange and coordinated function occur at the ensemble level.

Bridging the gap between single-molecule dynamics and ensemble behavior remains a fundamental challenge. Integrating existing single-molecule data with our ensemble-level findings through biophysical modeling and theoretical frameworks will yield a holistic understanding of how individual motor properties translate into emergent cooperative phenomena within the actomyosin network. Deciphering how cellular environment cues, such as

calcium signaling and mechanical stresses, influence actomyosin dynamics within intact muscle cells presents a significant hurdle. Developing sophisticated microscale platforms that mimic complex in vivo environments holds promise for unraveling how external signals modulate myosin function and force generation in a tissue-specific context.

By pursuing these diverse and interconnected avenues, there are many remaining open questions regarding myosin dynamics at the ensemble level. Understanding how environmental factors, internal signaling pathways, and inter-motor communication orchestrate coordinated force generation promises not only to illuminate fundamental biophysical principles but also to translate into the development of more targeted and effective therapeutic strategies for cardiac and other contractile disorders

APPENDIX

APPENDIX A

PROTOCOLS

A.1 Buffer Recipes

1. Solution T

   To be used in TC and FC buffer preparation (Chapter 2,3,4,5, and 6)

   Materials:

   Tris-HCl

   $CaCl_2$

   Reverse osmosis water

   Procedure:

   (a) In a 50 mL falcon tube, add::

   3.940 g Tris-HCL

   0.147 g $CaCl_2$

   (b) Add reverse osmosis water to the 50 mL total volume and mix well. (500 mM Tris-HCl and 20 mM $CaCl_{2)}$

   (c) Label solution T and store at 4°C

2. TC Buffer

   To be used in preparation of GAB buffer (Chapter 2,3,4,5,and 6)

   Materials:

   T solution

Reverse osmosis water

Procedure:

(a) Add 40 mL of reverse osmosis water and 1.5 mL of T solution to a 50 falcon tube and mix well.

(b) Adjust the pH to 8.0 by adding small volumes of concentrated KOH

(c) 4-5 pellets of KOH to a 50 mL falcon tube, fill with reverse osmosis water and use to adjust pH)

(d) Add water to a final volume of 50 mL and verify the pH, adjust pH if necessary.

3. Label the tube TC and store at 4°C (5 mM tris-HCl (pH 8.0) and 0.2 mM $CaCl_2$

4. FC Buffer

To be used in preparation of APB buffer and beads solution (Chapter 2,3,4,5,and 6)

Materials:

Solution T

KCl

$MgCl_2$

Procedure:

(a) Mix:

85 mL of reverse osmosis water

10 mL of solution T

3.728 g KCl

0.0406 g $MgCl_2$

(b) Adjust the pH to 7.5 by adding small volumes of concentrated KOH

(c) Add reverse osmosis water to a final volume of 100mL and verify pH, adjust if necessary.

(d) Label the tube FC and store at 4°C. (50 mM Tris-HCl (pH 7.5), 500 mM KCl, 2 mM $MgCl_2$ and 2 mM $CaCl_2$).

5. GAB (General Actin Buffer)

To be used for stabilizing actin filaments (Chapter 2,3,4,5,and 6)

Materials:

TC buffer

ATP

DTT

Procedure:

(a) Prepare by

mixing:

495 µL of TC

buffer

1 µL of 10mM

ATP

2.5 µL of 100mM

DTT

(b) Label the tube GAB and store at 4°C. (5mM Tris-HCl, 0.2 mM $CaCl_2$, 0.5 mM DTT, 0.2 mM ATP)

3. APB (Actin Polymerization Buffer)

To be used for polymerizing actin filaments, and in actin-myosin assays solution (Chapter 2,3,4,5, and 6)

Materials:

FC buffer

ATP

DTT

Procedure:

a. Prepare by mixing:

470 µL of FC buffer

25 µL of 10mM ATP

1 µL of 100mM DTT

b. Label the tube APB and store at 4°C. (50 mM Tris-HCl, 500mM KCl, 2 mM $MgCl_2$, 2 mM DTT, 5 mM ATP

4. 100 mM ATP stock in FC buffer

   To be used in the preparation of GAB and APB buffers and in actin-myosin assays. (Chapter 2,3,4,5, and 6)

   Materials:

   Solid ATP

   FC buffer

   KOH solution

   Procedure:

   - Prepare by mixing:

     0.061 g ATP with 1 mL FC buffer

     Dissolve completely

   - Adjust pH to 7 (likely by adding a few drops of 10 M KOH)
   - Make 25 μL aliquots and store at -80°C

5. 1 M DTT stock in FC buffer

   To be used in the preparation of GAB and APB buffers

   Materials:

   DTT

   Reverse osmosis water

   Procedure:

   - Prepare by mixing:

     0.154 g DTT with 1 mL reverse osmosis water

Dissolve completely

- Make 10 μL and store at -80°C

6. Oxygen scavenging system stock

To be used in actin-myosin assays. (Chapter 2,3,4,5, and 6)

Materials:

Glucose oxidase

Beta-D-glucose

Catalase

FC buffer

Procedure:

- Glucose oxidase: mix 25 mg of glucose oxidase with 1 mL of FC buffer.

Beta-D-glucose: mix 500mg Beta-D-glucose with 1 µLFC buffer.

Catalase: dilute 500 µL catalase into 500 µL FC buffer.

- Aliquot into 5 µLsamples. Store at -80C.

A.2 Actin Filament Preparation

These procedures are used to prepare and reconstitute non-labeled and biotinylated actin filaments. To be used in (Chapter 2,3,4,5, and 6).

A.2.1 Non-labeled Actin

Materials:

Lyophilized actin

Deionized water

Fresh GAB buffer

Fresh APB buffer

Rhodamine-labeled phalloidin

Ice

Procedure:

Reconstituting non-labeled actin:

- Reconstitute rabbit skeletal muscle actin by adding 100 μL of deionized water to a 1 mg vial of lyophilized actin
- Mix well by gently pipetting up and down
- Aliquot into 5 μL samples, snap-freeze, and store the 10 mg/mL actin aliquots at -80 °C.

Polymerizing non-labeled actin:

(a) Thaw one vial of 10 mg/mL actin and keep it on ice.

(b) Prepare fresh GAB and APB buffers following A.1-4 and A.1-5 procedures

(c) Add 50 μL GAB to the actin aliquot, and mix by gently pipetting up and down

(d) Incubate the solution on ice for 1 h.

(e) Polymerize the actin into filaments by adding 5.5 μL APB to the actin solution, mix well by gently pipetting up and down

(f) Place on ice for 20 min

(g) Add 5 μL of rhodamine-labeled phalloidin to the freshly polymerized actin filament solution.

(h) Leave on ice in the dark for 1 h.

(i) Store the rhodamine actin vial wrapped in aluminum foil in the dark at 4 °C.

NOTE: It is suggested to use these filaments for a maximum period of 1 week. AF quality can be confirmed each day through a quick imaging of a flow cell containing only AFs and viewing consistent filaments day to day.

A.3 Biotinylated Actin

Materials:

Lyophilized biotinylated actin

Reverse osmosis water

Fresh GAB buffer

Fresh APB buffer

Alexa Fluor 488 phalloidin

Ice

Procedure:

Reconstituting biotinylated actin:

- Reconstitute biotinylated actin by adding 100 μL of reverse osmosis water to a 1 mg vial of lyophilized biotinylated actin
- Mix well by gently pipetting up and down
- Aliquot into 5 μL samples, snap-freeze, and store the 10 mg/mL biotinylated actin aliquots at -80 °C.
- Thaw one vial of 10 mg/mL biotinylated actin and reconstitute it by adding 20 μL of reverse osmosis water
- Take 5 μL of the actin solution and add to a separate vial, label it ABP solution
- Label the rest (final concentration of biotinylated actin), store at -80 °C.

Polymerizing non-labeled actin:

- Thaw one vial of 10 mg/mL actin and keep it on ice.
- Combine the 10 mg/mL actin with the one labeled ABP.
- Prepare fresh GAB and APB buffers following A.1-4 and A.1-5 procedures

- Add 100 µL GAB to the actin solution labeled ABP, and mix by gently pipetting up and down
- Incubate the solution on ice for 1 h.
- Polymerize the biotinylated actin into filaments by adding 11 μL APB to the actin solution, mix well by gently pipetting up and down
- Place on ice for 20 min
- Add 5 μL of Alexa Fluor-labeled 488 phalloidin to the freshly polymerized biotinylated actin filaments solution.
- Leave on ice in the dark for 1 h.
- Store the biotinylated actin vial wrapped in aluminum foil in the dark at 4 °C.

NOTE: These filaments can be used for a maximum period of 1 week.

A.4 Reconstituting Rhodamine and 488 Alexa Fluor Phalloidin

Reconstituting Rhodamine Phalloidin:

Note: Phalloidin and methanol are toxic. Handle with care.

Materials:

Rhodamine phalloidin

100% methanol

Procedure:

- Briefly centrifuge tube of phalloidin to collect the product at the bottom of the tube using minicentrifuge.
- Reconstitute with 500 μL of 100% methanol to create 14 μM solution. Keep wrapped with aluminum foil to avoid photobleaching caused by light and keep inside ice bucket
- Aliquot into 5 μL samples. Store in the dark at -80C

Reconstituting Alexa Fluor 488 Phalloidin:

Materials:

Rhodamine phalloidin

100% methanol

Procedure:

- Briefly centrifuge tube of phalloidin to collect the product at the bottom of the tube using minicentrifuge.
- Reconstitute with 500 μL of 100% methanol to create 14 μM solution. Keep wrapped with aluminum foil to avoid photobleaching caused by light and keep

inside ice bucket

- Aliquot into 5 μL samples. Store in the dark at -80C

A.5 Reconstituting Myosin Motor Protein

To be used for preparing actin myosin bundle assay (chapter 2,3,4,5, and 6)

Materials:

Lyophilized myosin II DTT

Reverse osmotic water

Procedure:

1. Briefly centrifuge to collect the product at the bottom of the tube.
2. Make 1mM DTT by dissolving 0.01542 g DTT in 1 mL reverse osmosis water
3. Reconstitute to 10 mg/mL by the addition of 100 µL of reverse osmosis water mixed with 100 µL of 1 mM DTT
4. The protein will be in the following buffer: 25 mM PIPES, pH 7, 1.25 M KCl, 2.5% w/v sucrose and 0.5% w/v dextran.
5. Dilute stock myosin 10x by adding 10 µL of stock myosin to 90 µL of 1 mM DTT in reverse osmosis water
6. Make 3 µL aliquots. Snap freeze aliquots in liquid nitrogen
7. Store at -80˚C

A.6 Washing Streptavidin Coated Beads

Washed beads are used for making motility assays. To be used in (chapter 2,3,4,5, and 6)

Materials:

Streptavidin coated beads

FC buffer

Sonicator

Procedure:

1. Dilute 20 μL 0.44 μm streptavidin-coated beads into 80 μL FC.
2. Wash 4 times at 10,000 rpm for 6 minutes, reconstituting in 100 μL FC.
3. Sonicate for 2 minutes at 40%.
4. Store washed beads on a rotator at 4˚C

A.7 Actin Myosin Bundle Assay

This protocol is to prepare actin myosin bundle assay. To be used in (chapter 2,3,4,5, and 6)

Materials:

Alexa Fluor Biotinylated actin

Alexa Fluor phalloidin

Rhodamine actin

Rhodamine phalloidin

APB buffer

10x casein

100mM ATP

Clean beads solution

Oxygen scavenging system

Procedure:

1. Dilute the Alexa Fluor 488 biotinylated actin 500x in APB. Add 5 μL 488 phalloidin to the mixture
2. Dilute the rhodamine actin 500x in APB. Add 5 μL rhodamine phalloidin to the mixture
3. Combine 15 μL of Alexa Fluor 488 biotinylated actin, 1 μL of diluted and cleaned streptavidin beads, 1 μL of 100mM ATP, and the oxygen scavenging system. Put in the

rotator at 4˚C and let sit while the bundle is assembled.

4. Add 15 μL of the 500x dilute rhodamine actin to the flow cell. Let incubate for 15 minutes in humidity chamber.
5. Wash flow cell with 30 μL of APB. Pull through with a Kim wipe.
6. Add 20 μL of the 10x 1 mg/mL casein (blocks binding to the glass coverslip and ensures that only rhodamine actin is bound to the glass) to the flow cell. Let incubate for 5 minutes in humidity chamber.
7. Add 1 μL of 1 M myosin to combination in the rotator from step 3.
8. Add the combination from step 7 to the flow cell. Pull through with a Kim wipe.
9. Incubate flow cell in humidity chamber for 15 minutes.
10. Wash flow cell with 30 μL APB combined with 1 μL clean beads and 1 μL of 1 mg/mL casein
11. Seal the channel of the flow cell with nail polish so it does not dry out
12. Start analysis using optical tweezers and fluorescence imaging

A.8 Bead Slides – Free and Stuck

These bead slides can be used to practice trapping and calibration techniques.

Stuck Bead Slide:

Materials:

Etched coverslip

Microscope slide

Double stick tape

FC buffer (or buffer of choice),

Polystyrene beads

Procedure:

1. Construct a flow cell using an etched coverslip, microscope slide, and double stick tape

2. Make diluted bead solution, dilute stock beads (any functionalization is fine) 5x (i.e. 5 μL bead stock into 20 μL of buffer)

3. Sonicate beads for 4 minutes at 40%

4. Take 1 μL of the sonicated beads and add to 99 μL of buffer (dilute 100x more)

5. Sonicate diluted bead solution 4 minutes at 40%

6. Add 20 μL of diluted bead solution to the flow cell and allow to incubate for ~5 minutes in a humidity chamber

7. Seal slide with grease or nail polish and begin practicing calibration

Free Bead Slide:

Materials:

Etched coverslip

Microscope slide

Double stick tape

FC buffer (or buffer of choice)

Polystyrene beads

Poly-l-lysine (PLL)

Ethanol

Procedure:

1. Blotting grade blocker (BGB, casein), aliquots in -80 ˚C or make fresh from shelf 10 mg/mL

2. Make PLL coated coverslip

3. Add 100 μL PLL into 30 mL ethanol in a 50 mL Falcon tube, vortex

4. Add etched coverslip and allow to coat for 15 minutes

5. Remove coverslip from solution and dry with air line

6. Construct a flow cell using an etched coverslip, microscope slide, and double stick tape

7. Make casein solution

8. Dilute 10 mg/mL BGB aliquot by taking 8 μL and adding to 72 μL of buffer (dilute 10x)

9. Add 20 μL of casein solution to flow cell and allow to incubate for 5 minutes

10. Wash out the flow cell with 20 μL of buffer

11. Make diluted bead solution , dilute stock beads (any functionalization is fine) 5x (i.e. 5 μL bead stock into 20 μL of buffer)

12. Sonicate beads for 4 minutes at 40%

13. Take 1 μL of the sonicated beads and add to 99 μLof buffer (dilute 100x more)

14. Sonicate diluted bead solution 4 minutes at 40%

15. Add 20 μL of diluted bead solution to the flow cell and allow to incubate for ~5 minutes in a humidity chamber

16. Seal slide with grease or nail polish and begin practicing calibration and trapping

A.9 Protocol for Cleaning Coverslips

To be used for making assays (chapter 2,3,4,5 and 6).

Materials:

Reverse osmosis water

Ethanol

KOH pellets

Coverslips

Procedure:

1. Dissolve 100g of KOH in 300 mL of ethanol in a beaker. Stir with a stir bar until the KOH is completely dissolved.
2. Put coverslips in Teflon racks.
3. Fill one beaker with 300 mL of ethanol and two more beakers with 300 mL of RO H2O. Degas all four beakers (KOH in ethanol, ethanol, two beakers with water) for 5 minutes in the bath sonicator on the degas setting.
4. Submerge the rack of coverslips in the beaker with the KOH, and sonicate for 5 Minutes.
5. Dip the rack of coverslips up and down in the beaker with ethanol until the ethanol runs off the coverslips smoothly (no beading).
6. Dip the rack of coverslips up and down in a beaker of water until the water runs

off the coverslips smoothly (no beading).

7. Submerge the rack of coverslips in the other beaker of water and sonicate for 5 minutes.

8. Spritz with water until the water flows off the coverslips smoothly. Don't be afraid to use a little force when it comes to the spritzing steps.

9. Spritz with ethanol until the ethanol flows off the coverslips smoothly.

10. Dry the rack in the oven for at least 15 minutes

B. Supplemental Figures

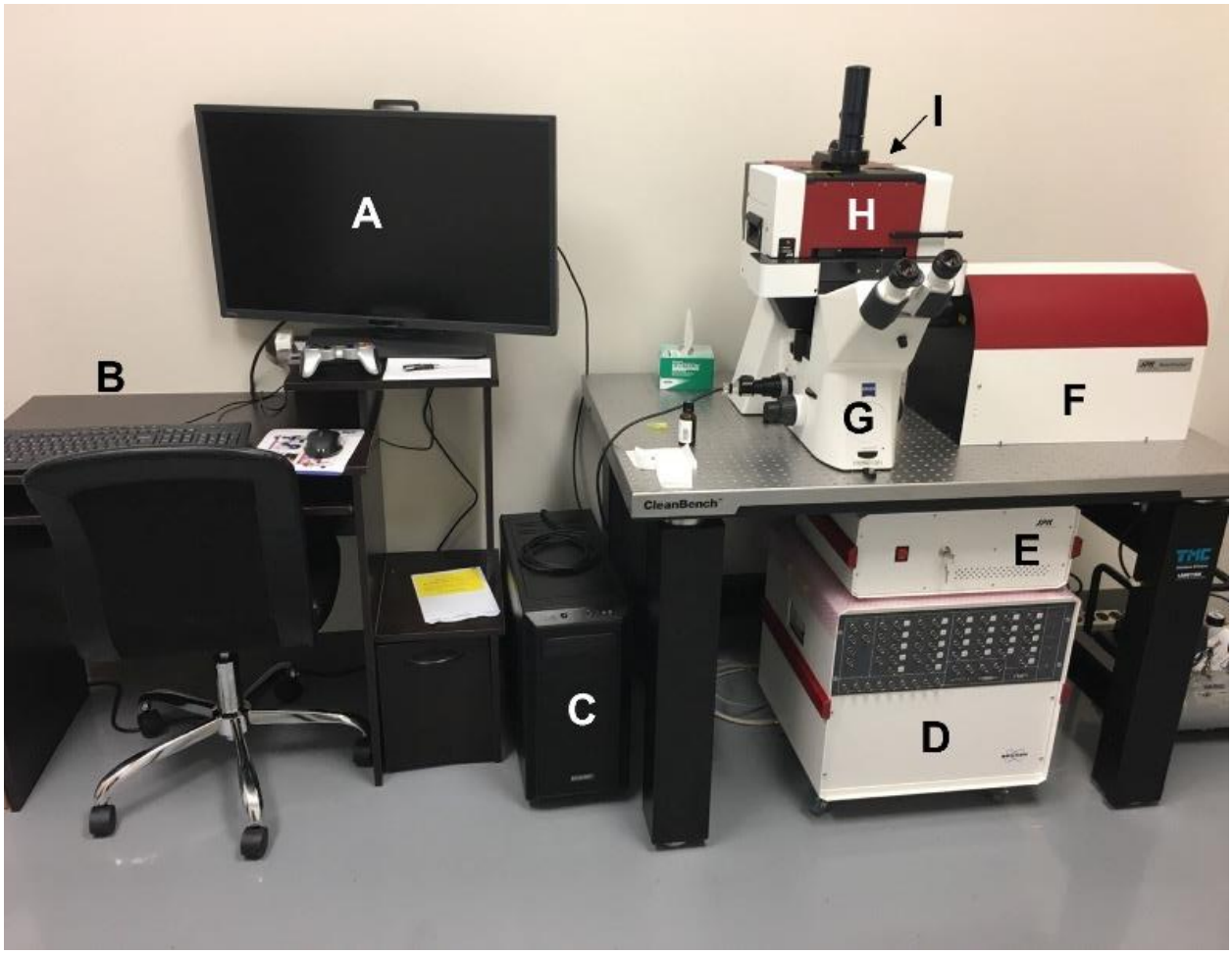

SUPPLEMENATRY FIGURE S1: Bruker/JPK Nanotracker2 Optical Trap. (**A**) Computer monitor. (**B**) Computer keyboard. (**C**) Computer tower. (**D**) Controller box. (**E**) Laser power supply. (**F**) Optical trap optics box. (**G**) Inverted microscope. (**H**) Door to microscope stage. (**I**) Polarizer slider to switch between brightfield and differential interference contrast imaging.

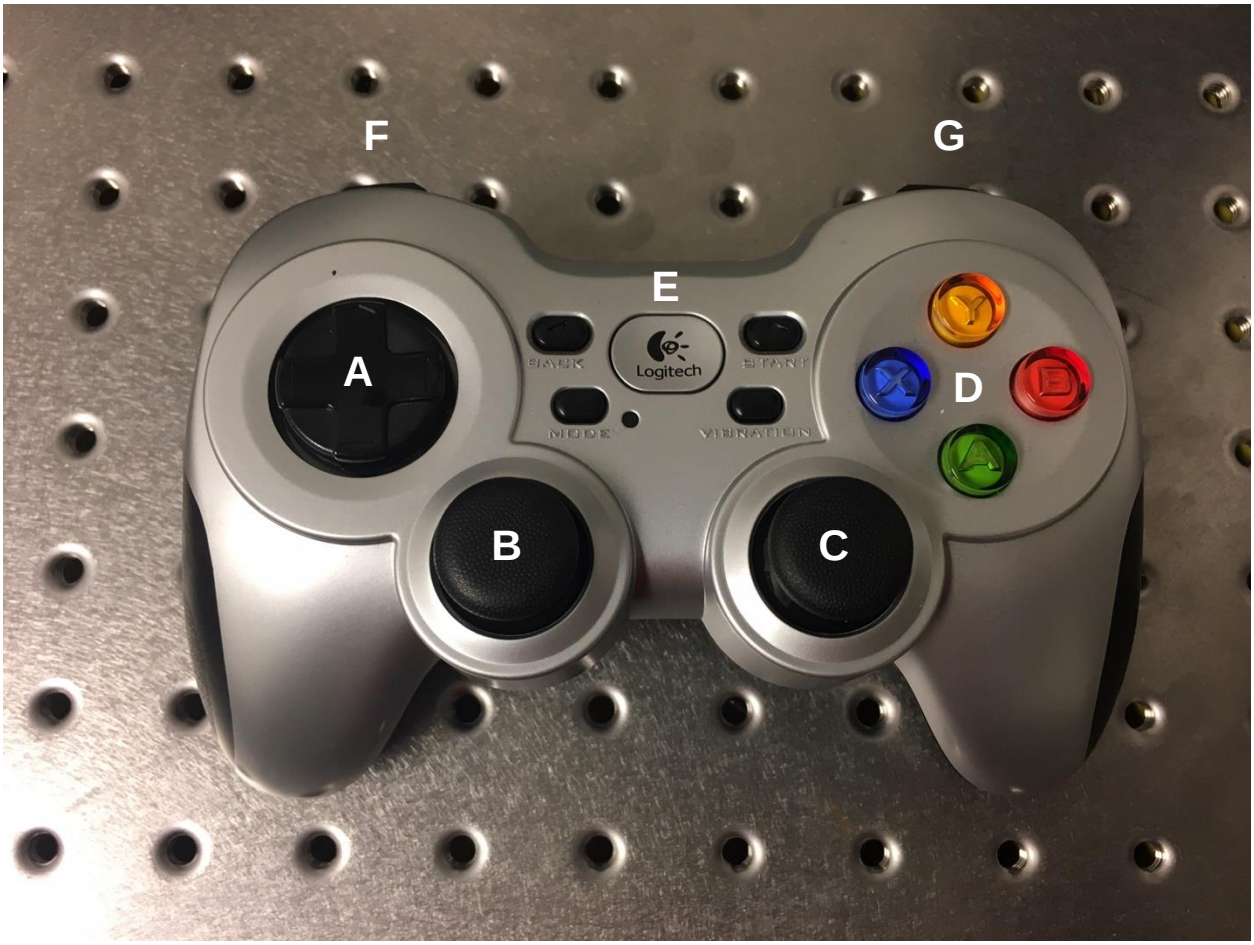

SUPPLEMENATRY FIGURE S2: Remote Control for Optical Trap. (**A**) Keypad to position the motorized stage. (**B-C**) Adjust trap position. (**D**) A, X, and B switch on and off the main shutter, trap 1 shutter, and trap 2 shutter, respectively. (**E**) Logitech button is used to wake up the controller. (**F**) Up and down buttons used to position the trapping objective. (**G**) Up and down buttons used to position the detection objective. Note that the remote control is not required, and all of these manipulations can be accomplished in the software. However, it is convenient to be able to control the objectives and stage position while looking into the microscope stage environment

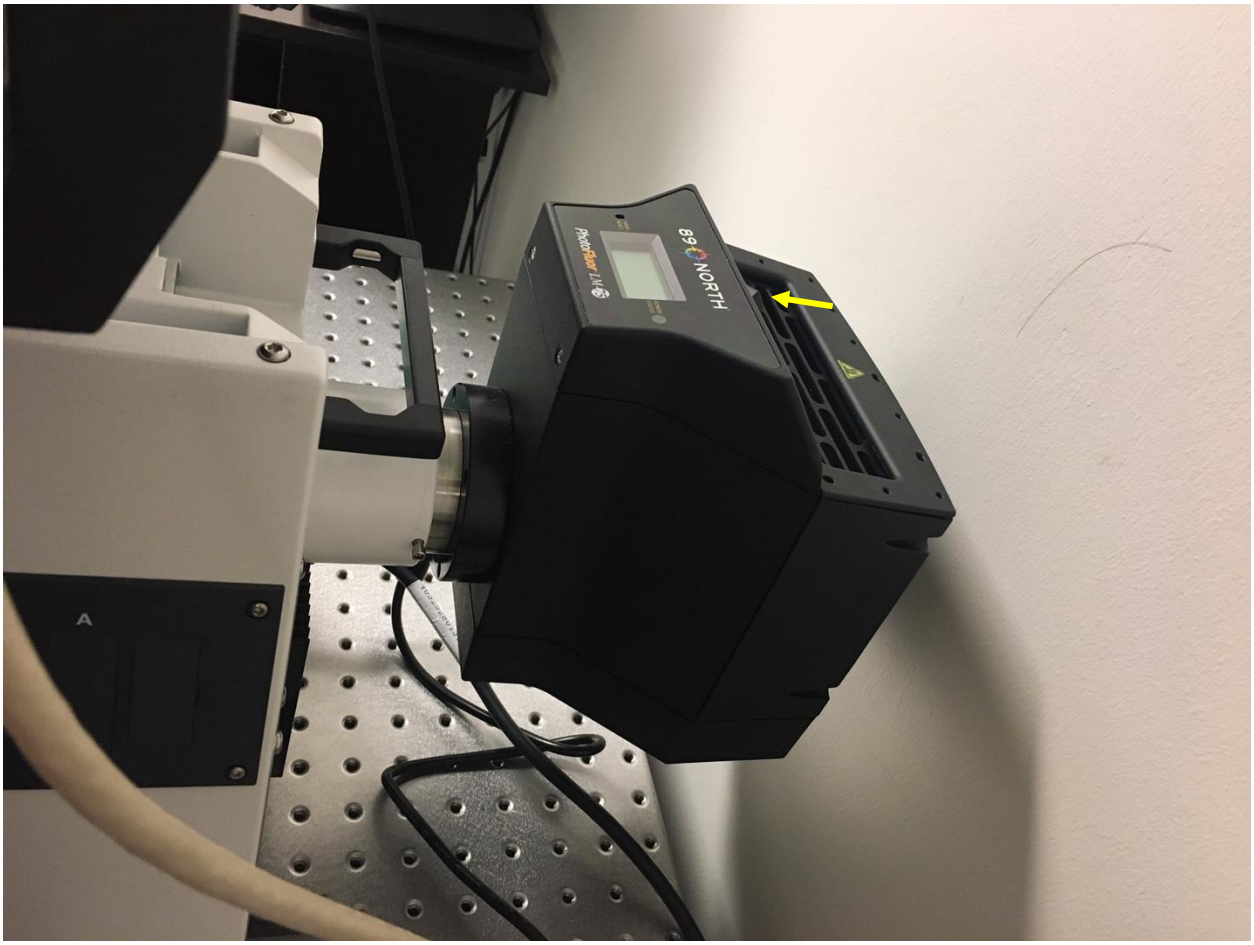

SUPPLEMENATRY FIGURE S3: Fluorescence Module for Optical Trap. The 89North PhotoFluor fluorescence white light source is coupled to the back of the inverted microscope. It is turned on and off with a toggle switch (arrow).

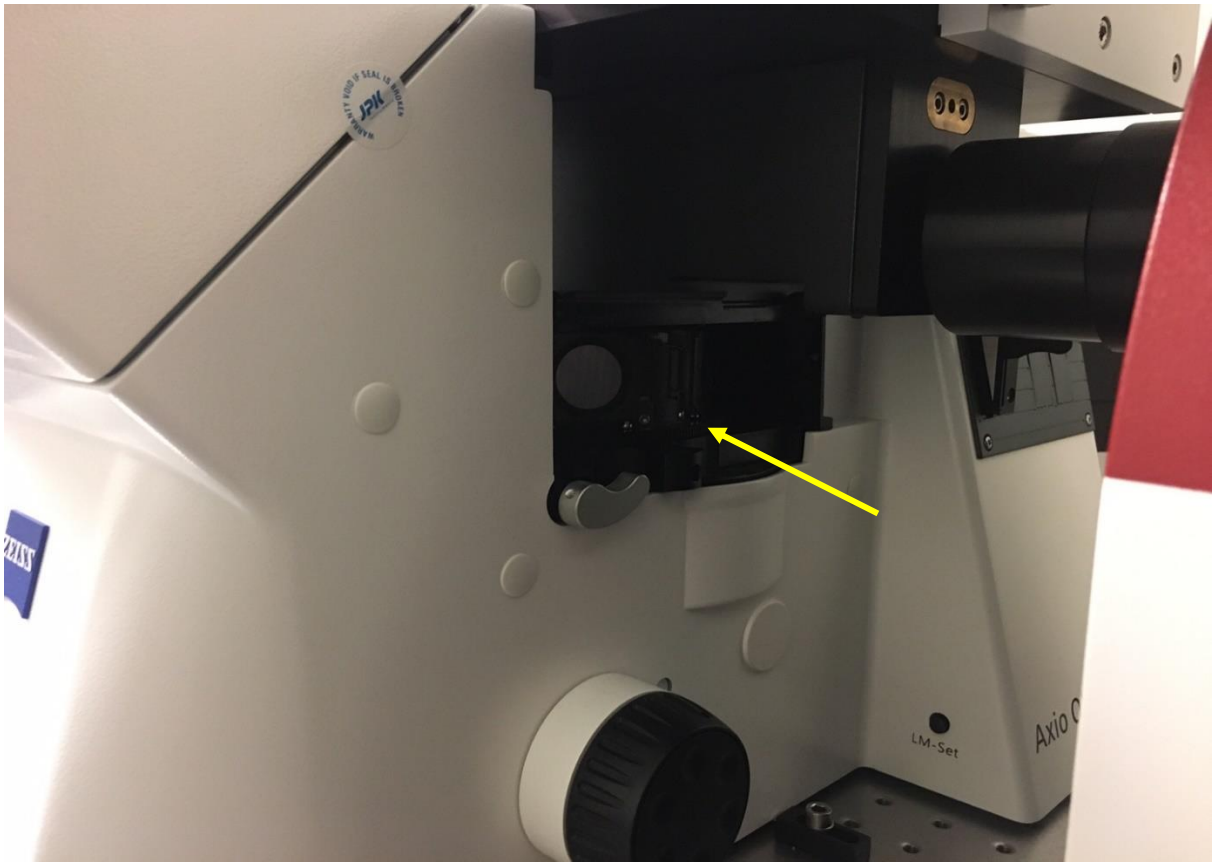

SUPPLEMENATRY FIGURE S4: Fluorescence Filter Cube Turret. The turret (arrow) can be turned to use the filter cube necessary for imaging in DIC, rhodamine, or Alexa Fluor 488 dyes. Note that filter cubes can be switched out to customize the setup for using different fluorophores.

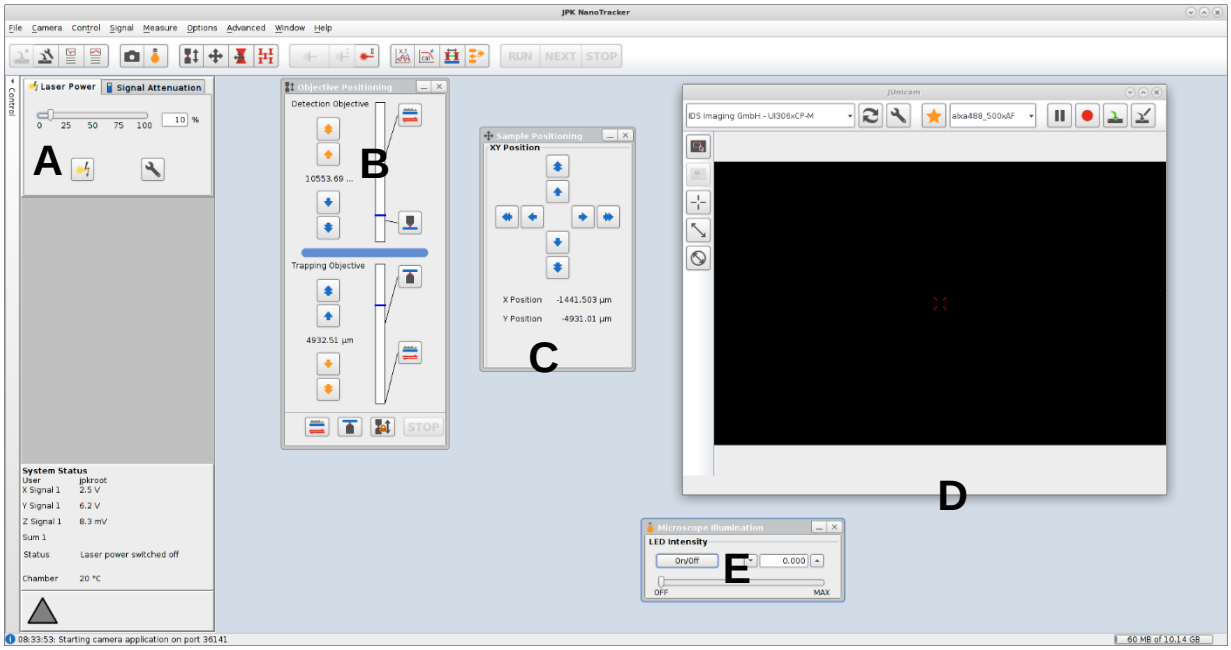

SUPPLEMENATRY FIGURE S5: Nanotracker2 Software. (**A**) Laser power button and control. (**B**) Objective positioning window. Directional arrows are used to move the detection (top) and trapping (bottom) objectives. Double arrows move the objectives at a higher speed. The blue and red button at the bottom left uncouples the objectives and retracts them back to their original position. This is necessary for when taking samples in and out of the microscope stage. The third button from the left with the objectives and padlock icon "couples" the objectives so that when they are both in focus and achieve Kohler illumination, the user can move both the trapping and detection objectives up and down in the z-axis. (**C**) Sample positioning window used to move the microscope stage in the x- and y-axis. Double arrows move the stage at a higher speed. This window is activated by clicking the up/down and left/right arrow icon at the top menu. (**D**) Camera visualization window. The wrench icon can be used to set customized imaging conditions. This window is activated by clicking the camera icon at the top menu. (**E**) Microscope illumination window. This window is activated by clicking the light bulb icon at the top menu.

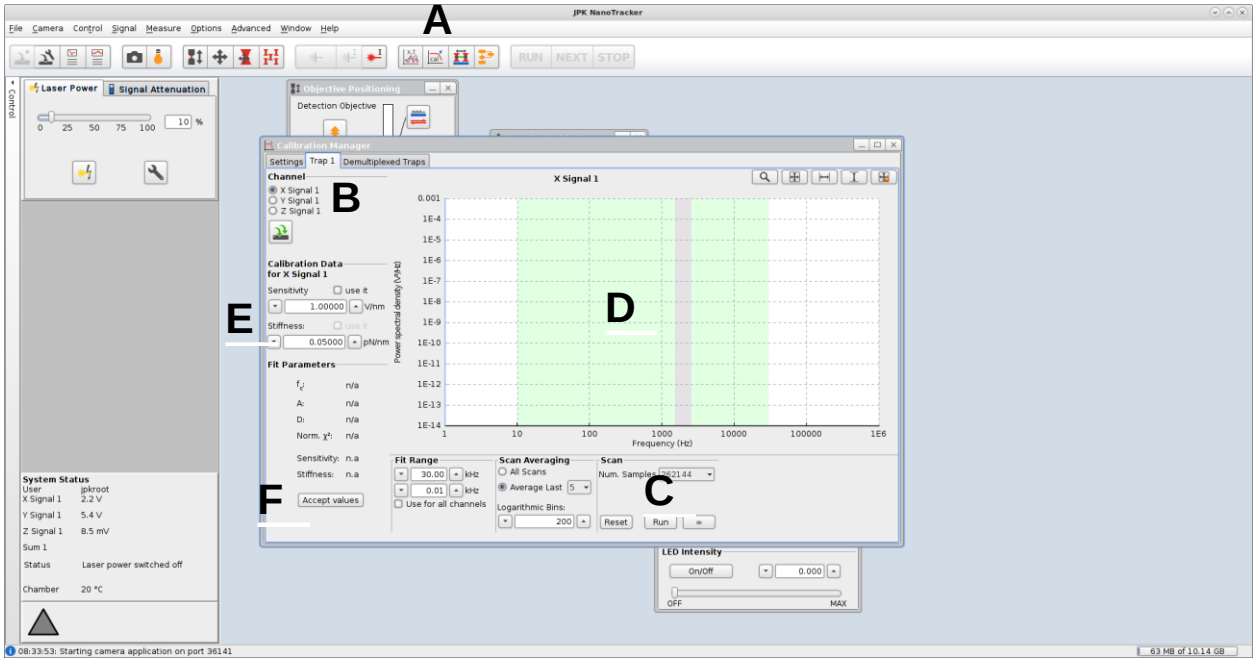

SUPPLEMENATRY FIGURE S6: Calibration Window. (**A**)This window is used for bead calibration and is activated by clicking the "cal" icon at the top menu. To calibrate a bead, a best fit of the corner frequency is accomplished in the x, y, and z signals. (**B**) For each signal, choose the appropriate signal button in the top left. (**C**) Click "run" and optimize the fit by clicking and dragging within the green window (**D**). (**E**) Once satisfied with the fit, click "use it" for sensitivity and stiffness. This will allow for recording displacement in nanometers and force in piconewtons. (**F**) Then click "accept values" at the bottom left. Repeat for the y and z directions.

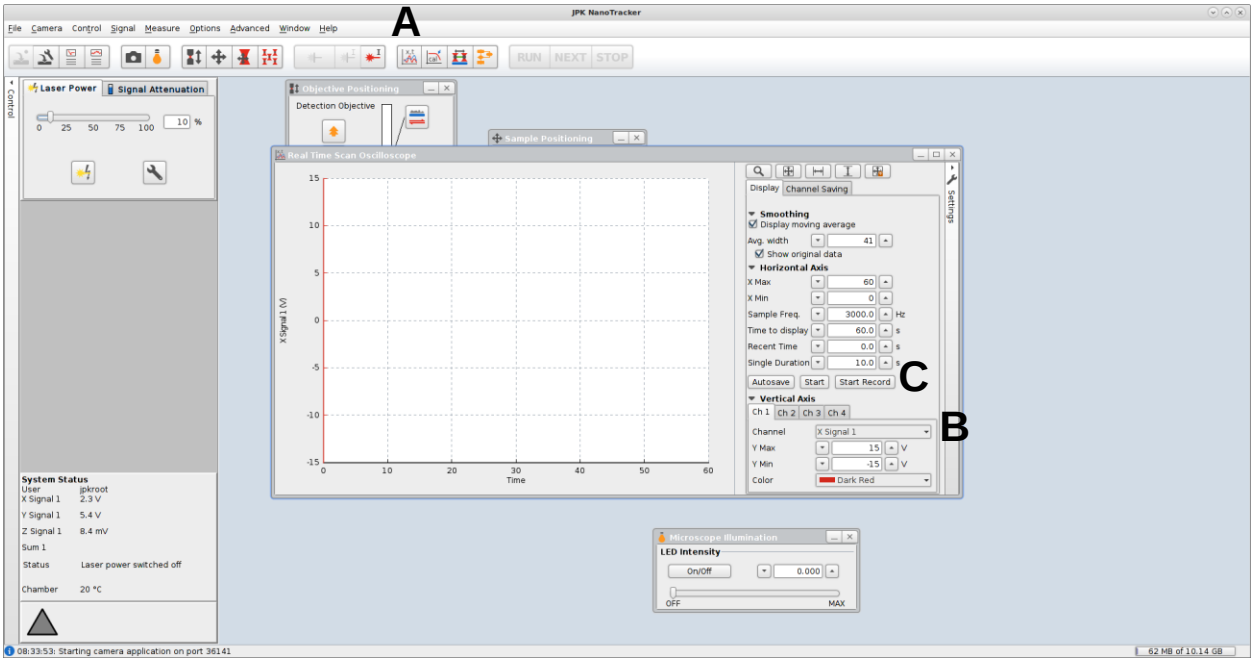

SUPPLEMENATRY FIGURE S7: Data Acquisition Window. This window is used to acquire position and force data and allows the user to see the measurements in real time. (**A**) This window is activated by clicking the "x,t" icon at the top menu. (**B**) The user can switch between viewing the x and y signals. (**C**) Click "start" to begin visualizing data. Click "autosave" to save data. Click "start record" to begin recording and saving data.

VITA
Omayma Y. Alazzam

EDUCATION

Ph.D. in Engineering Science, Emphasis: Chemical Engineering — May 2024 (anticipated)
University of Mississippi, University, MS, USA

M.S. in Engineering Science, Emphasis: Chemical Engineering — 2018
University of Mississippi, University, MS, USA

B.S. in Chemical Engineering — 2015
Jordan University of Science and Technology, Ar-Ramtha, Jordan

EXPERIENCE and APPOINTMENTS

Doctoral Research Assistant, University of Mississippi, University, MS — 2020 – present
Molecular Biophysics and Engineering Lab
Departments of Chemical Engineering and Biomedical Engineering
Dissertation: "Elucidating the Mechanisms of Myosin II Force Feedback and Coordination in Actomyosin Ensembles"
Advisor: Dr. Nikki Reinemann

Master's Research Assistant, University of Mississippi, University, MS — 2016 – 2018
Sustainable Nanomaterials Lab
Department of Chemical Engineering
Thesis: "Cellulose Nanocrystals as 'Green' Emulsifiers Stabilize Crude Oil in Water Emulsions"
Advisor: Dr. Esteban Urena-Benavides

Intern, El Sohly Laboratories, Inc., Oxford, MS — 2018
Project: "Analysis of Urine Samples for Drug Composition"

Undergraduate Research Assistant, Jordan University of Science and Technology — 2014 – 2015
Department of Chemical Engineering
Project: "Aluminum Extraction and Manufacturing Process Design"
Advisor: Dr. Mohammad Harahsheh

PUBLICATIONS

7. **Omayma Al Azzam**, Heath M. Stevens, Isabella Strockbine, Dana N. Reinemann, "Cardiac Myosin Ensemble Coordination in the Prescence of Activating and Inhibiting Drugs," *Biophysical Journal, in preparation.*
6. Emily Kerivan, Victoria N. Amari, William B. Weeks, Leigh H. Hardin, Lyle Tobin, **Omayma Al Azzam**, Dana N. Reinemann, "Deciphering Mechanochemical Influences of Emergent Actomyosin Crosstalk using QCM-D," *under review.* bioRxiv preprint DOI: 10.1101/2024.02.26.582155.

5. **Omayma Al Azzam**, Janie Watts, Justin E. Reynolds, Juliana E. Davis, and Dana N. Reinemann, "Myosin II Adjusts Motility Properties and Regulates Force Production Based on Motor Environment," *Cellular and Molecular Bioengineering** 15 (5), 451-465 (2022). DOI: 10.1007/s12195-022-00731-1.
4. **Omayma Al Azzam***, Janie Watts*, Justin E. Reynolds, Juliana E. Davis, and Dana N. Reinemann, "Probing Myosin Ensemble Mechanics in Actin Filament Bundles using Optical Tweezers," *Journal of Visualized Experiments*, 183, e63672, (2022). DOI: 10.3791/63672. *Co-first authors
3. **Omayma Al Azzam**, Cameron Lee Trussell, and Dana N. Reinemann, "Measuring Force Generation within Reconstituted Microtubule Bundle Assemblies using Optical Tweezers," *Cytoskeleton*, 78, 3, 111-125, (2021). DOI: 10.1002/cm.21678.
2. Sanjiv Parajuli, **Omayma Alazaam**, Mei Wang, Linda C. Mota, Sangeet Adhikari, Dariel Wicks, Esteban E. Urena-Benavides, "Surface properties of cellulose nanocrystal stabilized crude oil emulsions and their effect on petroleum biodegradation," *Colloids and Surfaces A: Physiochemical and Engineering Aspects* 596 (5), 124705, (2020). DOI: 10.1016/j.colsurfa.2020.124705.
1. **Omayma Alazzam**, "Cellulose Nanocrystals as 'Green' Emulsifiers Stabilize Crude Oil in Water Emulsions," Master's thesis, University of Mississippi, (2019).

PROFESSIONAL PRESENTATIONS

3. **Omayma Alazzam** and Dana N. Reinemann, "Deciphering Myosin Ensembles Force Generation and Coordination Crosstalk in Diverse Motor Environments," 2023 Mid-South Biophysics Symposium, Biophysical Society, Oxford, MS, May 2023 (oral)
2. **Omayma Al Azzam**, Janie C. Watts, Dana N. Reinemann, "Interrogation of Myosin II Ensemble Synergy using Optical Tweezers," 2022 Annual Meeting of the Mississippi Academy of Sciences, Biloxi, MS, March 2022 (oral)
1. **Omayma Al Azzam** and Dana N. Reinemann, "Myosin II Adjusts Motility and Regulates Force Production Based on Motor Environment," 2021 Annual Meeting of the Biomedical Engineering Society, Orlando, FL, October 2021 (poster)

SELECT RESEARCH SKILLS

- Scientific communication
- Protocol development
- Data analysis
- Optical microscopy
- Optical tweezers

- Fluorescence microscopy
- Electron microscopy
- High performance liquid chromatography
- Column chromatography
- Bioseparations

FUNDING

University of Mississippi Graduate Student Council Research Grant, 2021
"Investigation of Nanoscale Cell Dynamics that Generate Forces for Muscle Contraction"
Role: Applicant, Budget Proposed: $1,000
Status: Awarded

American Heart Association Predoctoral Fellowship, 2021
"Myosin II Adjusts Motility and Regulates Force Production Based on Motor Environment"
Role: Applicant; Budget Proposed: $65,106
Status: Reviewed, Not Funded

AWARDS and HONORS

2024	Outstanding Doctoral Student, University of Mississippi School of Engineering
2023	Outstanding Graduate Research Student, Ole Miss Local Section of the American Chemical Society
2021	Graduate Student Council Research Fellowship, University of Mississippi

PROFESSIONAL MEMBERSHIPS

2021 – present	American Heart Association
2021 – present	Biomedical Engineering Society
2021 – present	Mississippi Academy of Sciences

TEACHING EXPERIENCE

2023 BME/Ch E 520 Biochemical Process Engineering, Guest Lecturer
2023 BME/Ch E 524 Microscopy for Engineers, Guest Lecturer and Lab Instructor

OUTREACH and SERVICE

Search Committee Member, University of Mississippi (2022)
Served in the hiring process for a postdoctoral position within the Molecular Biophysics and Engineering Lab

Nanoengineering Research Day, University of Mississippi (2021– present)
Led lab tours, presentations, and demonstrations for middle and high school students from diverse backgrounds. Event held multiple times each year.

UM Student Parent Association (2021)
Participated in focus groups for the University to better understand the resources and support available to student parents

Women in STEM, University of Mississippi (2020 – present)
Mentor to undergraduate STEM students, including women, minority, and international students